Interface Electronic Structure

Colin Pirie Farquhar

Thesis submitted for the degree of Doctor of Philosophy

at the

University of Edinburgh

July 1988

Abstract

There are many applications of materials science which involve the interface between two bulk media. Such junctions play an important part in the operation of electronic devices, and in electrical contacts. With new crystal growth techniques such as molecular beam epitaxy, it is possible to grow almost perfect epitaxial interfaces. The properties of these interfaces are different from the bulk due to the variation in potential across the interface, which can lead to states which are localised at the interface being formed. These states can pin the Fermi level, and play an important part in the transport properties of the interface.

This work deals with the development of a new method of calculating interface electronic structure. The loss of periodicity in the z direction means that the usual methods of bulk electronic structure calculations cannot be used directly, unless the interface is repeated periodically. This is the basis of superlattice calculations, where the unit cell has finite length, meaning that the states obtained are discrete, and that states localised on different interfaces can interfere, giving rise to energy bands. It is often difficult to distinguish between interface states and the bulk band structure in these calculations. The method presented in this thesis treats a single isolated interface, by representing each substrate properly via an embedding potential term which is added to the slab Hamiltonian for the first few layers of atoms around the interface. The embedding potentials are derived from the Green functions for the bulk substrates. The effect of the embedding potentials is to ensure that the interface wavefunction is correctly broadened, and that its logarithmic derivatives match correctly onto the substrate continuum. Thus interface states can be easily identified, and their energy determined.

The interface Hamiltonian is solved self consistently using the LAPW method. One problem in the case of insulator and semiconductor systems is that the potential shift across the interface has to be included at the outset, but apart from this the calculation is done entirely from first principles. The method has been tested on bulk aluminium and nickel systems, where each substrate is the same. Good agreement with the known band structure of these materials is obtained. Next an Al-Ni (001) interface is used as an example of a simple metallic system. Interface states are found to exist at certain points of the two dimensional Brillouin zone. Finally, an Al-Si junction is used as an example of a Schottky barrier. Interface states and other departures from bulk behaviour are noted.

Contents

Declaration

This thesis is presented in accordance with the regulations for the degree of Doctor of Philosophy. It has been composed by myself and has not been submitted previously for a higher degree. All sources of information have been specifically acknowledged.

Acknowledgements

The work for this thesis has been done in the Physics department of Edinburgh University, and the Theory and Computational Science (TCS) division of Daresbury Laboratory. I wish to specifically thank the following individuals:

- Dr. John Inglesfield of TCS for introducing me to the embedding potential method, and subsequently providing much help, including a copy of his surface program.
- Prof. David Wallace, my supervisor, for his encouragement and support.
- Dr. Richard Blake of TCS for allowing me to use his program for generating the embedding potentials, and also providing numerous helpful discussions during my visits to Daresbury.
- Donald Macleod, a fellow postgraduate, for listening and commenting on some of the more abstract parts of this work.

For financial support I also wish to thank the Carnegie Trust for the Universities of Scotland, and the Science and Engineering Research Council.

Introduction

This thesis deals with the electronic properties at the interface between two crystals. The changes in bulk electronic structure which occur at interfaces are important for the detailed operation of electronic devices, and for bonding between materials. Examples of the former are semiconductor-semiconductor junctions, and metal-semiconductor Schottky barriers. The latter may be a metallic contact for example. The potential change from the bulk which occurs across such junctions can cause states to form which are localised at the interface, and decay exponentially into each substrate. These states can exist either in a direct gap or a symmetry gap in each material. In the case of the latter, the localised state is superimposed on the continuum of bulk states which leaks across the interface into the opposite substrate.

Interface states may be important in determining the position of the Fermi level in insulator or semiconductor systems. The position of the Fermi energy determines the potential barrier across the junction. For example, the potential shift across an Al-Si Schottky barrier diode is typically around 0.6V. Clearly the transport properties of such interfaces will also be affected, as charge will become trapped in these localised states. There has also been much recent interest in heterostructure systems, which consist of alternating layers of two materials. Each substrate may not have the same lattice constant, but can often still be grown to form an epitaxial interface with the same lattice constant on either side. In such systems the lattice mismatch is accommodated by strain, forming the so called strained layer superlattices, an example being the Si-Ge superlattice. Changing the interface orientation or substrate parameters in such systems can alter the potential shift and detailed electronic structure in

the interface region.

Despite the technological importance of these junctions, not much is known about even the most common examples, such as the aluminium-silicon Schottky barrier. In order to gain insight into the problem there has recently been increased interest in performing *ab initio* interface calculations using new computational techniques. The most common method is the so called superlattice scheme, where the interface is periodically repeated in space, forming a large unit cell, and thus allowing bulk band structure methods to be used. This is useful for studying thin layer superlattices, but for thicker systems or an isolated interface, computational restrictions limit the size of unit cell which can be considered. The finite unit cell length means that all the calculated states are discrete, and also states localised at each interface may interfere, giving rise to energy bands. Now, it is not desirable to have to explicitly include substrates which are several layers of atoms thick in any computational scheme. There are two good reasons for this. Firstly, the electronic structure usually varies over a few layers on either side of the junction, after which it becomes like the bulk. Secondly, the computer time required is much reduced if only those layers of interest are included.

A technique which allows us to concentrate on the local region of interest is described in this thesis. Each substrate is assumed to have the properties of the bulk, and is included in the interface Hamiltonian via an embedding potential term (Chapter 1) which can be calculated once and for all. These embedding potentials are derived from the Green functions for the bulk substrates. Only a few layers on either side of the interface are explicitly considered in the interface region. The effect of the embedding potentials is to ensure that the interface wavefunction matches correctly in value and gradient onto the substrate wavefunctions, and that it is correctly broadened, thus allowing localised states to be easily distinguished from the bulk continuum. The interface Hamiltonian is reduced to the problem of a single electron moving in the mean field of all the others (Chapter 2), as is usually the case in band structure calculations. Having developed a suitable one electron Hamiltonian,

it is then solved to obtain the interface Green function (Chapter 3). This is a useful quantity to evaluate, as the density of states and charge density are easily obtained via integration of the Green function. The method of solution is the linearised augmented plane wave (LAPW) method, which is applicable to a wide range of materials. No spatial separation of states into core and valence electrons is required with this method. Thus elements with d-electrons, such as the transition metals can be easily handled. Such elements are often a problem in band structure calculations using the pseudopotential technique, as d-electrons may have energies in the valence band region, but be localised near the core states, thus making this technique less valid. In order to solve the interface Hamiltonian one must have some starting potential in the interface region. The true potential is obtained by using a self consistent field procedure, using the local density approximation for the exchange-correlation potential. This involves constructing a new potential from the charge density (Chapter 4), which is then used as the input potential for the next iteration, and so on, until input and output potentials are in good agreement.

The method is implemented in the form of a somewhat large (5000 line) FORTRAN 77 computer program which runs on the FPS-164 attached processor at Daresbury laboratory. The program is loosely based on one which is used to study surface electronic structure using the embedding potential formalism, derived by Dr. J. Inglesfield of Daresbury Laboratory, and Dr. G. Benesh of Baylor University, Texas. The present work involved rewriting most of the surface code, except for the treatment of the core states. Bulk aluminium and nickel systems are used as program tests, by considering the same material for each substrate as is embedded in the interface. The results are in good agreement with the known band structures of Al and Ni. Next an Al-Ni (001) interface is considered as an example of a simple metallic system. Interface states are identified within symmetry gaps in the Ni at certain points in the Brillouin zone, which decay into Al band gaps. Finally, an Al-Si (001) junction is used as an example of a Schottky barrier. Interface states are again found, confirming that the interface electronic structure plays an important

role in such junctions.

Note that atomic units are used throughout this work. These are such that $\hbar = m_e = e = 1$. The unit of length is the radius of the first Bohr orbit in the Hydrogen atom (0.5292Å), and the unit of energy is the Hartree (27.2eV).

Some of the work of this thesis has been submitted for publication. This consists of the application of the embedding method to interfaces, and the Al-Ni results.

Chapter 1

The Embedding Potential Method

This chapter deals with the basic principles of the embedding potential method, and how it is applied to the case of an interface. To date, only surfaces and impurities have been treated by other workers using this method. An expression for the total energy is derived in terms of a trial wavefunction in the interface. This variational expression is then minimised to obtain the Hamiltonian, which is then used to construct the interface Green function. Finally, a brief description of how the embedding potentials are constructed is given. This is unchanged from the case of embedding potentials at surfaces, but has been included for completeness, and to justify the use of such embedding potentials at both sides of the interface.

1.1 Background to the Embedding Potential Method

The embedding potential technique was first developed by Inglesfield [1], and has been successfully applied to the case of surface electronic structure [2]. Here it is extended to the case of an isolated interface. Previous interface calculations have been based on the superlattice method, where the interface is periodically repeated to produce a three dimensional crystal with a very large

unit cell [3]. These calculations describe the properties of a real thin layer superlattice, where typically about four to ten layers of each bulk material are included in the calculations, but they are not suitable for either thick layer superlattices, or for an isolated interface, due to the large unit cell required. This superlattice method has also been used for the study of surfaces [4], where a supercell consisting of the bulk material and vacuum is periodically repeated. There are however problems with this technique, which first prompted the development of the embedding potential method for use at surfaces. Firstly, the computation involved is very large due to the large unit cell used. Secondly, there is no distinction between localised and bulk band states as both are discrete in these systems, due to the finite unit cell length, which also leads to interference between localised states on different interfaces. Using the embedding potential technique, one only has to consider a few layers of material on either side of the interface, since in practice the electronic properties are usually found to be as in the bulk within one or two atomic layers of the interface [3]. This reduces the amount of computation to be done relative to the superlattice method. Each embedding potential is derived from the Green function for the relevant bulk substrate. Also, as the substrates are properly represented via the embedding potentials, the wavefunctions calculated in the interface region are correctly broadened, so that the confusion between bulk states and interface states does not arise.

1.2 The Embedding Potential Method at an Interface

The embedding potential formalism has been generalised to the case of an interface between two bulk media. The relevant analytic work and its interpretation is presented in this section.

Consider the interface between two media, regions 2 and 3. The interface

is region 1 in the following diagram.

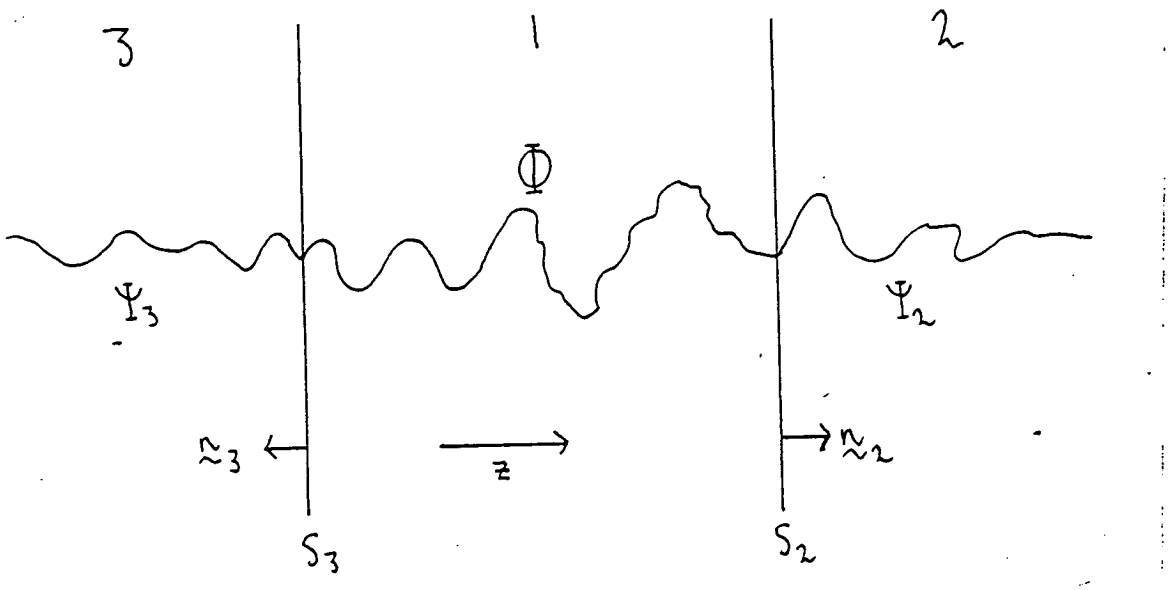

In regions 2 and 3, the potential is that of a perfect crystal.

Initially we derive a variational principle for the whole of regions 1,2, and 3, in terms of an arbitrary trial wavefunction Φ defined explicitly only in the interface region 1. In the two substrates (2 and 3) the trial functions Ψ_2 and Ψ_3 are exact solutions of the Schrödinger equation at some trial energy ϵ. Ψ_2 matches in amplitude onto Φ over S_2, and Ψ_3 matches onto Φ over S_3. Note that the first derivative with respect to z of the total trial wavefunction is in general discontinuous across S_2 and S_3.

The expectation value for the energy is

$$E = \frac{\langle \Psi \,|H|\, \Psi \rangle}{\langle \Psi | \Psi \rangle}$$

Ψ is the total wavefunction, and H is the total Hamiltonian.

Hence

$$E = \frac{\int_1 \Phi^* H \Phi \, d^3r + \epsilon \int_2 \Psi_2^* \Psi_2 \, d^3r + \epsilon \int_3 \Psi_3^* \Psi_3 \, d^3r - \frac{1}{2}[I_{S_2} + I_{S_3}]}{\int_1 \Phi^* \Phi \, d^3r + \int_2 \Psi_2^* \Psi_2 \, d^3r + \int_3 \Psi_3^* \Psi_3 \, d^3r} \qquad (1.1)$$

where

$$I_{S_2} = \int_{S_2} \left(\Phi^* \frac{\partial \Psi_2}{\partial z} - \Phi^* \frac{\partial \Phi}{\partial z} \right) d^2 r_{S_2}$$

and

$$I_{S_3} = \int_{S_3} \left(\Phi^* \frac{\partial \Phi}{\partial z} - \Phi^* \frac{\partial \Psi_3}{\partial z} \right) d^2 r_{S_3}$$

The 4^{th} and 5^{th} terms in 1.1 arise due to the discontinuity in the gradient of the wavefunction at S_2 and S_3. Note the sign change in the 5^{th} term to account for the opposite direction of $\mathbf{n_3}$ to $\mathbf{n_2}$ and the positive z-axis.

We require a relationship between the solutions of the Schrödinger equation in the three regions, which we will then use to eliminate Ψ_2 and Ψ_3 from the expression for the energy (equaton 1.1).

In region 2

$$\left(-\frac{1}{2}\nabla_r^2 + V(\mathbf{r}) - E \right) G_2^\circ(\mathbf{r}, \mathbf{r}') = \delta(\mathbf{r} - \mathbf{r}') \quad (1.2)$$

$$\left(-\frac{1}{2}\nabla_r^2 + V(\mathbf{r}) - E \right) \Psi_2(\mathbf{r}) = 0 \quad (1.3)$$

$G_2^\circ(\mathbf{r}, \mathbf{r}')$ is the Green function in substrate 2, having zero derivative with respect to z on S_2.

Multiplying 1.2 by $\Psi_2(\mathbf{r})$, 1.3 by $G_2^\circ(\mathbf{r}, \mathbf{r}')$ and subtracting gives

$$\Psi_2(\mathbf{r})\delta(\mathbf{r} - \mathbf{r}') = \frac{1}{2}\left[G_2^\circ(\mathbf{r}, \mathbf{r}')\nabla_r^2 \Psi_2(\mathbf{r}) - \Psi_2(\mathbf{r})\nabla_r^2 G_2^\circ(\mathbf{r}, \mathbf{r}') \right]$$

$$\Rightarrow \Psi_2(\mathbf{r}') = \frac{1}{2}\int_2 d^3 r [G_2^\circ(\mathbf{r}, \mathbf{r}')\nabla_r^2 \Psi_2(\mathbf{r}) - \Psi_2(\mathbf{r})\nabla_r^2 G_2^\circ(\mathbf{r}, \mathbf{r}')]$$

Now use Green's theorem, and impose the boundary condition $\frac{\partial G_2^\circ}{\partial z}\Big|_{S_2} = 0$, to give

$$\Psi_2(\mathbf{r}) = -\frac{1}{2}\int_{S_2} d^2 r_{S_2} G_2^\circ(\mathbf{r}, \mathbf{r}_{S_2}) \frac{\partial \Psi_2(\mathbf{r}_{S_2})}{\partial n_2} \quad (1.4)$$

Invert 1.4 to obtain $\frac{\partial \Psi_2(\mathbf{r}_{S_2})}{\partial n_2}$

$$\frac{\partial \Psi_2(\mathbf{r}_{S_2})}{\partial n_2} = -2\int_{S_2} d^2 r'_{S_2} G_2^{\circ -1}(\mathbf{r}_{S_2}, \mathbf{r}'_{S_2}) \Psi_2(\mathbf{r}'_{S_2}) \quad (1.5)$$

Now, $\Phi = \Psi_2$ over S_2, so

$$\frac{\partial \Psi_2(\mathbf{r}_{S_2})}{\partial n_2} = -2\int_{S_2} d^2 r'_{S_2} G_2^{\circ -1}(\mathbf{r}_{S_2}, \mathbf{r}'_{S_2}) \Phi(\mathbf{r}'_{S_2}) \quad (1.6)$$

We now require the normalisation of Ψ_2.

$$H\Psi_2 = E\Psi_2$$

$$\Rightarrow H\delta\Psi_2 = E\delta\Psi_2 + \delta E\Psi_2$$

$$\Rightarrow \Psi_2^* H\delta\Psi_2 = E\Psi_2^*\delta\Psi_2 + \delta E\Psi_2^*\Psi_2$$

$$\Rightarrow \delta E\,|\Psi_2|^2 = \Psi_2^* H\delta\Psi_2 - \delta\Psi_2 H\Psi_2^*$$

$$\Rightarrow |\Psi_2|^2 = \Psi_2^* H\frac{\partial\Psi_2}{\partial E} - \frac{\partial\Psi_2}{\partial E}H\Psi_2^*$$

$$= \frac{1}{2}\left(\frac{\partial\Psi_2}{\partial E}\nabla^2\Psi_2^* - \Psi_2^*\nabla^2\left(\frac{\partial\Psi_2}{\partial E}\right)\right)$$

Hence

$$\begin{aligned}\int_2 d^3r\,|\Psi_2|^2 &= \frac{1}{2}\int_{S_2} d^2r_{S_2}\left(\Psi_2^*\frac{\partial}{\partial n_2}\left(\frac{\partial\Psi_2}{\partial E}\right) - \frac{\partial\Psi_2}{\partial E}\frac{\partial\Psi_2^*}{\partial n_2}\right)\\ &= \frac{1}{2}\int_{S_2} d^2r_{S_2}\left(\Psi_2^*\frac{\partial}{\partial E}\left(\frac{\partial\Psi_2}{\partial n_2}\right) - \frac{\partial\Psi_2}{\partial E}\frac{\partial\Psi_2^*}{\partial n_2}\right)\end{aligned}$$

Using 1.5 for $\frac{\partial\Psi_2}{\partial n_2}$ and $\frac{\partial\Psi_2^*}{\partial n_2}$, gives

$$\begin{aligned}\int_2 d^3r\,|\Psi_2|^2 &= -\int_{S_2} d^2r_{S_2}\int_{S_2} d^2r'_{S_2}\left[\Psi_2^*\frac{\partial}{\partial E}(G_2^{\circ\,-1}\Psi_2) - \frac{\partial\Psi_2}{\partial E}G_2^{\circ\,-1}\Psi_2^*\right]\\ &= -\int_{S_2} d^2r_{S_2}\int_{S_2} d^2r'_{S_2}\left[\Psi_2^*\frac{\partial G_2^{\circ\,-1}}{\partial E}\Psi_2 + \Psi_2^* G_2^{\circ\,-1}\frac{\partial\Psi_2}{\partial E} - \frac{\partial\Psi_2}{\partial E}G_2^{\circ\,-1}\Psi_2^*\right] \quad (1.7)\end{aligned}$$

$G_2^{\circ\,-1}$ is a symmetric function of $\mathbf{r}_{S_2}$, $\mathbf{r}'_{S_2}$, so the final two terms in 1.7 cancel, leaving

$$\int_2 d^3r\,|\Psi_2|^2 = -\int_{S_2} d^2r_{S_2}\int_{S_2} d^2r'_{S_2}\Psi_2(\mathbf{r}_{S_2})\frac{\partial G_2^{\circ\,-1}(\mathbf{r}_{S_2},\mathbf{r}'_{S_2})}{\partial E}\Psi_2(\mathbf{r}'_{S_2}) \quad (1.8)$$

The results we require for region 2 are given by equations 1.6 and 1.8. For region 3, the equivalent results are the same as for region 2. These are

$$\frac{\partial\Psi_3(\mathbf{r}_{S_3})}{\partial n_3} = -2\int_{S_3} d^2r_{S_3}G_3^{\circ\,-1}(\mathbf{r}_{S_3},\mathbf{r}'_{S_3})\Phi(\mathbf{r}'_{S_3}) \quad (1.9)$$

$$\int_3 d^3r\,|\Psi_3|^2 = -\int_{S_3} d^2r_{S_3}\int_{S_3} d^2r'_{S_3}\Psi_3^*(\mathbf{r}_{S_3})\frac{\partial G_3^{\circ\,-1}(\mathbf{r}_{S_3},\mathbf{r}'_{S_3})}{\partial E}\Psi_3(\mathbf{r}'_{S_3}) \quad (1.10)$$

Finally note that Ψ_2 and Ψ_3 can be replaced by Φ in equations 1.7 and 1.10.

Using 1.6, 1.8, 1.9, 1.10 in 1.1 gives

$$
\begin{aligned}
E = \Bigg[& \int_1 \Phi^* H \Phi \, d^3r - \epsilon \int_{S_2} d^2 r_{S_2} \int_{S_2} d^2 r'_{S_2} \Phi^*(\mathbf{r}_{S_2}) \frac{\partial G_2^{o^{-1}}(\mathbf{r}_{S_2}, \mathbf{r}'_{S_2})}{\partial E} \Phi(\mathbf{r}'_{S_2}) \\
& - \epsilon \int_{S_3} d^2 r_{S_3} \int_{S_3} d^2 r'_{S_3} \Phi^*(\mathbf{r}_{S_3}) \frac{\partial G_3^{o^{-1}}(\mathbf{r}_{S_3}, \mathbf{r}'_{S_3})}{\partial E} \Phi(\mathbf{r}'_{S_3}) \\
& + \frac{1}{2} \int_{S_2} \Phi^* \frac{\partial \Phi}{\partial z} \, d^2 r_{S_2} - \frac{1}{2} \int_{S_3} \Phi^* \frac{\partial \Phi}{\partial z} \, d^2 r_{S_3} \\
& + \int_{S_2} d^2 r_{S_2} \int_{S_2} d^2 r'_{S_2} \Phi^*(\mathbf{r}_{S_2}) G_2^{o^{-1}}(\mathbf{r}_{S_2}, \mathbf{r}'_{S_2}) \Phi(\mathbf{r}'_{S_2}) \\
& + \int_{S_3} d^2 r_{S_3} \int_{S_3} d^2 r'_{S_3} \Phi^*(\mathbf{r}_{S_3}) G_3^{o^{-1}}(\mathbf{r}_{S_3}, \mathbf{r}'_{S_3}) \Phi(\mathbf{r}'_{S_3}) \Bigg] \\
\Bigg/ \Bigg[& \int_1 |\Phi|^2 \, d^3r - \int_{S_2} d^2 r_{S_2} \int_{S_2} d^2 r'_{S_2} \Phi^*(\mathbf{r}_{S_2}) \frac{\partial G_2^{o^{-1}}(\mathbf{r}_{S_2}, \mathbf{r}'_{S_2})}{\partial E} \Phi(\mathbf{r}'_{S_2}) \\
& - \int_{S_3} d^2 r_{S_3} \int_{S_3} d^2 r'_{S_3} \Phi^*(\mathbf{r}_{S_3}) \frac{\partial G_3^{o^{-1}}(\mathbf{r}_{S_3}, \mathbf{r}'_{S_3})}{\partial E} \Phi(\mathbf{r}'_{S_3}) \Bigg]
\end{aligned}
\tag{1.11}
$$

where

$$H = -\frac{1}{2}\nabla_r^2 + V(\mathbf{r})$$

The energy is now purely in terms of Φ, our trial wavefunction in the interface. $G^{o^{-1}}$ plays the role of an effective surface potential, and is the embedding potential. Also, from 1.6 and 1.9, we see that $G^{o^{-1}}$ can be interpreted as being a generalised logarithmic derivative.

Now we derive a Schrödinger equation from 1.11. For compactness, an abbreviated notation is used in the following derivation

$$
\begin{aligned}
E \Bigg[& \int_1 \Phi^* \Phi - \int_{S_2} \int_{S_2} \Phi^* \frac{\partial G_2^{o^{-1}}}{\partial E} \Phi - \int_{S_3} \int_{S_3} \Phi^* \frac{\partial G_3^{o^{-1}}}{\partial E} \Phi \Bigg] \\
& = \int_1 \Phi^* H \Phi + \frac{1}{2} \int_{S_2} \Phi^* \frac{\partial \Phi}{\partial z} - \frac{1}{2} \int_{S_3} \Phi^* \frac{\partial \Phi}{\partial z} \\
& + \int_{S_2} \int_{S_2} \Phi^* G_2^{o^{-1}} \Phi + \int_{S_3} \int_{S_3} \Phi^* G_3^{o^{-1}} \Phi \\
& - \epsilon \int_{S_2} \int_{S_2} \Phi^* \frac{\partial G_2^{o^{-1}}}{\partial E} \Phi - \epsilon \int_{S_3} \int_{S_3} \Phi^* \frac{\partial G_3^{o^{-1}}}{\partial E} \Phi
\end{aligned}
$$

So, to first order

$$\begin{aligned}
&\delta E\left[\int_1 \Phi^*\Phi - \int_{S_2}\int_{S_2} \Phi^* \frac{\partial G_2^{o^{-1}}}{\partial E}\Phi - \int_{S_3}\int_{S_3} \Phi^* \frac{\partial G_3^{o^{-1}}}{\partial E}\Phi\right] \\
&+E\left[\int_1 \delta\Phi^*\Phi - \int_{S_2}\int_{S_2} \delta\Phi^* \frac{\partial G_2^{o^{-1}}}{\partial E}\Phi - \int_{S_3}\int_{S_3} \delta\Phi^* \frac{\partial G_3^{o^{-1}}}{\partial E}\Phi\right] \\
&= \int_1 \delta\Phi^* H\Phi + \frac{1}{2}\int_{S_2} \delta\Phi^* \frac{\partial\Phi}{\partial z} - \frac{1}{2}\int_{S_3} \delta\Phi^* \frac{\partial\Phi}{\partial z} \\
&+ \int_{S_2}\int_{S_2} \delta\Phi^* G_2^{o^{-1}}\Phi + \int_{S_3}\int_{S_3} \delta\Phi^* G_3^{o^{-1}}\Phi \\
&-\epsilon\int_{S_2}\int_{S_2} \delta\Phi^* \frac{\partial G_2^{o^{-1}}}{\partial E}\Phi - \epsilon\int_{S_3}\int_{S_3} \delta\Phi^* \frac{\partial G_3^{o^{-1}}}{\partial E}\Phi \\
&+ \text{similar terms involving } \delta\Phi
\end{aligned} \tag{1.12}$$

If E is stationary with respect to small changes in Φ, then

$$\begin{aligned}
&E\Phi - E\int_{S_2} \frac{\partial G_2^{o^{-1}}}{\partial E}\Phi\delta(\mathbf{r}-\mathbf{r}_{S_2}) - E\int_{S_3} \frac{\partial G_3^{o^{-1}}}{\partial E}\Phi\delta(\mathbf{r}-\mathbf{r}_{S_3}) \\
&= H\Phi + \frac{1}{2}\frac{\partial\Phi}{\partial z}\delta(\mathbf{r}-\mathbf{r}_{S_2}) - \frac{1}{2}\frac{\partial\Phi}{\partial z}\delta(\mathbf{r}-\mathbf{r}_{S_3}) \\
&+ \int_{S_2} G_2^{o^{-1}}\Phi\delta(\mathbf{r}-\mathbf{r}_{S_2}) + \int_{S_3} G_3^{o^{-1}}\Phi\delta(\mathbf{r}-\mathbf{r}_{S_3}) \\
&-\epsilon\int_{S_2} \frac{\partial G_2^{o^{-1}}}{\partial E}\Phi\delta(\mathbf{r}-\mathbf{r}_{S_2}) - \epsilon\int_{S_3} \frac{\partial G_3^{o^{-1}}}{\partial E}\Phi\delta(\mathbf{r}-\mathbf{r}_{S_3})
\end{aligned}$$

Rearranging this gives

$$\begin{aligned}
&\left\{H + \frac{1}{2}\delta(\mathbf{r}-\mathbf{r}_{S_2})\frac{\partial}{\partial z} - \frac{1}{2}\delta(\mathbf{r}-\mathbf{r}_{S_3})\frac{\partial}{\partial z}\right\}\Phi(\mathbf{r}) \\
&+\delta(\mathbf{r}-\mathbf{r}_{S_2})\left\{\int_{S_2} d^2r'_{S_2}\left[G_2^{o^{-1}}(\mathbf{r}_{S_2},\mathbf{r}'_{S_2},\epsilon) + (E-\epsilon)\left.\frac{\partial G_2^{o^{-1}}(\mathbf{r}_{S_2},\mathbf{r}'_{S_2})}{\partial E}\right|_{E=\epsilon}\right]\Phi(\mathbf{r}'_{S_2})\right\} \\
&+\delta(\mathbf{r}-\mathbf{r}_{S_3})\left\{\int_{S_3} d^2r_{S_3}\left[G_3^{o^{-1}}(\mathbf{r}_{S_3},\mathbf{r}'_{S_3},\epsilon) + (E-\epsilon)\left.\frac{\partial G_3^{o^{-1}}(\mathbf{r}_{S_3},\mathbf{r}'_{S_3})}{\partial E}\right|_{E=\epsilon}\right]\Phi(\mathbf{r}'_{S_3})\right\} \\
&= E\Phi(\mathbf{r})
\end{aligned} \tag{1.13}$$

The energy derivatives of $G^{o^{-1}}$ in 1.13 correct the effective surface potential $G^{o^{-1}}(\mathbf{r}_S,\mathbf{r}'_S,\epsilon)$ to the value appropriate for the energy E.

We choose to calculate the Green function in the interface region, evaluated at the same energies as the substrate embedding potentials. Hence, E=ϵ in 1.13, thus removing the energy derivatives of the embedding potentials. This leaves us with the following Schrödinger equation for the Green function, G, in the interface

$$\begin{aligned}
&\left\{H + \frac{1}{2}\delta(\mathbf{r}-\mathbf{r}_{S_2})\frac{\partial}{\partial z} - \frac{1}{2}\delta(\mathbf{r}-\mathbf{r}_{S_3})\frac{\partial}{\partial z}\right\} G(\mathbf{r},\mathbf{r}',E) \\
&\quad +\delta(\mathbf{r}-\mathbf{r}_{S_2})\int_{S_2} d^2r'_{S_2} G_2^{o^{-1}}(\mathbf{r}_{S_2},\mathbf{r}'_{S_2},E)G(\mathbf{r}'_{S_2},\mathbf{r}',E) \\
&\quad +\delta(\mathbf{r}-\mathbf{r}_{S_3})\int_{S_3} d^2r'_{S_3} G_3^{o^{-1}}(\mathbf{r}_{S_3},\mathbf{r}'_{S_3},E)G(\mathbf{r}'_{S_3},\mathbf{r}',E) \\
&\quad -EG(\mathbf{r},\mathbf{r}',E) \\
&\quad = \delta(\mathbf{r}-\mathbf{r}')
\end{aligned}$$

$\mathbf{r}$, $\mathbf{r}'$ are in region 1.

In future the energy E at which the embedding potentials and Green function are evaluated will be dropped from the notation.

$G(\mathbf{r},\mathbf{r}')$ is expanded as

$$G(\mathbf{r},\mathbf{r}') = \sum_{i,j} G_{ij}\Phi_i(\mathbf{r})\Phi_j^*(\mathbf{r}') \tag{1.14}$$

Hence

$$\begin{aligned}
\sum_{i,j} G_{ij} \Bigg[&\left\{H + \frac{1}{2}\delta(\mathbf{r}-\mathbf{r}_{S_2})\frac{\partial}{\partial z} + \frac{1}{2}\delta(\mathbf{r}-\mathbf{r}_{S_3})\frac{\partial}{\partial z}\right\}\Phi_i(\mathbf{r}) \\
&+\delta(\mathbf{r}-\mathbf{r}_{S_2})\int_{S_2} d^2r'_{S_2} G_2^{o^{-1}}(\mathbf{r}_{S_2},\mathbf{r}'_{S_2})\Phi_i(\mathbf{r}'_{S_2}) \\
&+\delta(\mathbf{r}-\mathbf{r}_{S_3})\int_{S_3} d^2r'_{S_3} G_3^{o^{-1}}(\mathbf{r}_{S_3},\mathbf{r}'_{S_3})\Phi_i(\mathbf{r}'_{S_3}) \\
&-E\Phi_i(\mathbf{r}) \Bigg] \Phi_j^*(\mathbf{r}') = \delta(\mathbf{r}-\mathbf{r}')
\end{aligned} \tag{1.15}$$

Multiplying equation 1.15 by $\Phi_k^*(\mathbf{r})\Phi_l^*(\mathbf{r}')$, and integrating over region 1, gives

$$\sum_{i,j} G_{ij}(H_{ki} - ES_{ki})\delta_{jl} = \delta_{kl}$$

where

$$
\begin{aligned}
H_{ki} = & \int_1 d^3r \Phi_k^\star(\mathbf{r}) \left(-\frac{1}{2}\nabla_r^2 + V(\mathbf{r}) \right) \Phi_i(\mathbf{r}) \\
& + \frac{1}{2} \int_{S_2} d^2r_{S_2} \Phi_k^\star(\mathbf{r}_{S_2}) \frac{\partial}{\partial z} \Phi_i(\mathbf{r}_{S_2}) - \frac{1}{2} \int_{S_3} d^2r_{S_3} \Phi_k^\star(\mathbf{r}_{S_3}) \frac{\partial}{\partial z} \Phi_i(\mathbf{r}_{S_3}) \\
& + \int_{S_2} d^2r_{S_2} \int_{S_2} d^2r'_{S_2} \Phi_k^\star(\mathbf{r}_{S_2}) G_2^{\circ^{-1}}(\mathbf{r}_{S_2}, \mathbf{r}'_{S_2}) \Phi_i(\mathbf{r}'_{S_2}) \\
& + \int_{S_3} d^2r_{S_3} \int_{S_3} d^2r'_{S_3} \Phi_k^\star(\mathbf{r}_{S_3}) G_3^{\circ^{-1}}(\mathbf{r}_{S_3}, \mathbf{r}'_{S_3}) \Phi_i(\mathbf{r}'_{S_3})
\end{aligned} \tag{1.16}
$$

and

$$
S_{ki} = \int_1 d^3r \Phi_k^\star(\mathbf{r}) \Phi_i(\mathbf{r})
$$

where $\left(-\frac{1}{2}\nabla_r^2 + V(\mathbf{r}) \right)$ has been written explicitly for H in equation 1.16. Hence

$$
G_{ij} = (H - ES)^{-1}_{ij}
$$

As we have two dimensional periodicity in planes parallel to the interface, we can define a two dimensional Bloch wavevector $\mathbf{K}$. The Bloch embedding potential is now given by the inverse over S_2 and S_3 repectively, of

$$
G^\circ_{\mathbf{K}}(\mathbf{r}, \mathbf{r}') = \sum_j G^\circ(\mathbf{r}, \mathbf{r}' - \mathbf{R}_j) \exp(-i\mathbf{K}.\mathbf{R}_j)
$$

The $\{\mathbf{R}_j\}$ run over the direct two dimensional lattice vectors. We can therefore reduce the matrix elements of the Hamiltonian to be over a single two dimensional unit cell.

The next step is to consider the surfaces on which the embedding potentials are defined. Consider the case of the right side of the interface. The embedding

potential is defined over the surface shown in the following diagram.

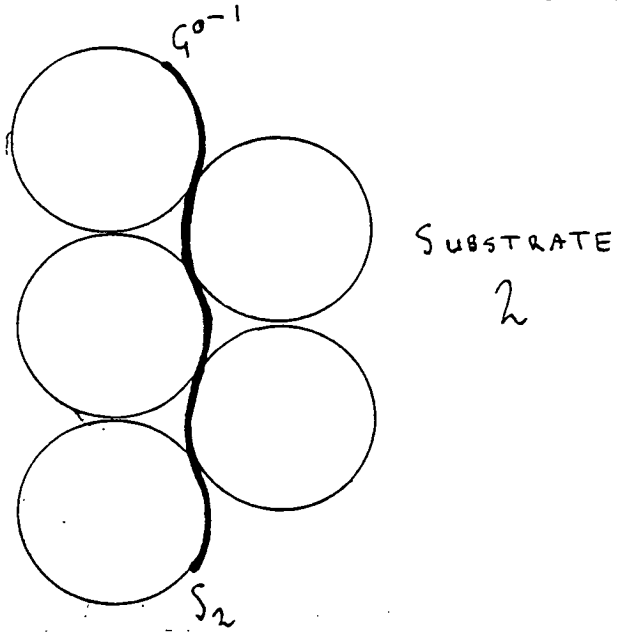

S_2 is obviously not a convenient surface to use, so we shift the embedding surface to S_2' which is flat.

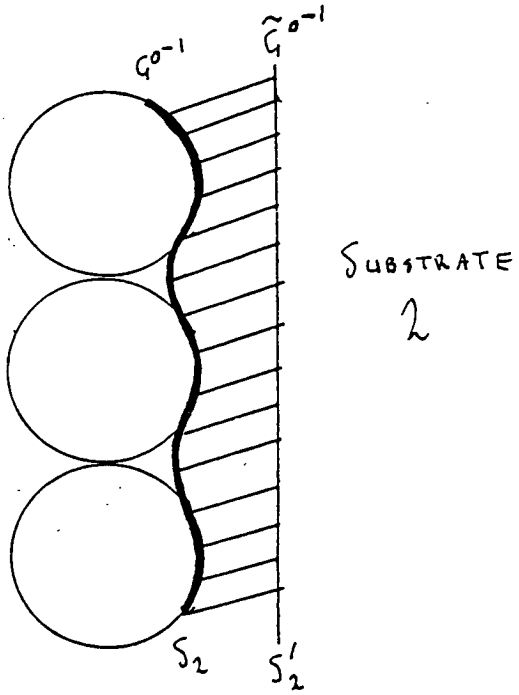

We must justify this shift of embedding surface. To do this we consider the physical interpretation of 1.12. Rearrange this equation into the form

$$\begin{aligned}\delta E \propto & \int_1 d^3r \delta\Phi^*[H\Phi - E\Phi] \\ & + \int_{S_2} d^2r_{S_2} \delta\Phi^* \left[\frac{1}{2}\frac{\partial\Phi}{\partial z} + \int_{S_2} d^2r'_{S_2} \left\{ G_2^{o^{-1}} + (E-\epsilon)\frac{\partial G_2^{o^{-1}}}{\partial E} \right\} \Phi \right] \\ & + \int_{S_3} d^2r_{S_3} \delta\Phi^* \left[-\frac{1}{2}\frac{\partial\Phi}{\partial z} + \int_{S_3} d^2r'_{S_3} \left\{ G_3^{o^{-1}} + (E-\epsilon)\frac{\partial G_3^{o^{-1}}}{\partial E} \right\} \Phi \right] \\ & + \text{similar terms involving } \delta\Phi\end{aligned}$$

So $\delta E = 0$, i.e. the functional is stationary when

$$H\Phi = E\Phi$$

and

$$\frac{\partial\Phi}{\partial z} = -2\int_{S_2} d^2r'_{S_2} \left\{ G_2^{o^{-1}} + (E-\epsilon)\frac{\partial G_2^{o^{-1}}}{\partial E} \right\} \Phi(\mathbf{r}'_{S_2}) \qquad (1.17)$$

There is a similar result to equation 1.17 for S_3.

So it is apparent that the solution of the Schrödinger equation in region 1 must have the correct logarithmic derivatives on S_2 and S_3 . To move to the new embedding planes S'_2 and S'_3, we integrate the Schrödinger equation over a flat potential between S_2 and S'_2, and also between S_3 and S'_3. In practice, the embedding potentials are calculated on S'_2 and S'_3, so the procedure is as before, but S_2 is replaced by S'_2, and S_3 by S'_3. This forces the interface wavefunction to have the correct logarithmic derivatives on S'_2 and S'_3, and thus also on S_2 and S_3, as required.

In future $G^{o^{-1}}$ will refer to the embedding potentials on the flat surfaces. i.e. the tilde on the new embedding surface, $\tilde{G}^{o^{-1}}$, is dropped.

In summary, we use equation 1.16 to solve for the matrix elements of the Hamiltonian, H, then construct the matrix $(H - ES)$ and invert it to obtain the interface Green function matrix, G. We have assumed that a point of two dimensional inversion symmetry exists, so the $G^{o^{-1}}$ are symmetric. The Hamiltonian is also symmetric.

1.3 Construction of the Embedding Potentials

The computer program to calculate the embedding potentials was supplied by Daresbury Laboratory. The exact details of the calculation are not therefore considered here, but a summary of the method of construction is given.

Consider the embedding potential for the right substrate (substrate 2). This is constructed for the following geometry.

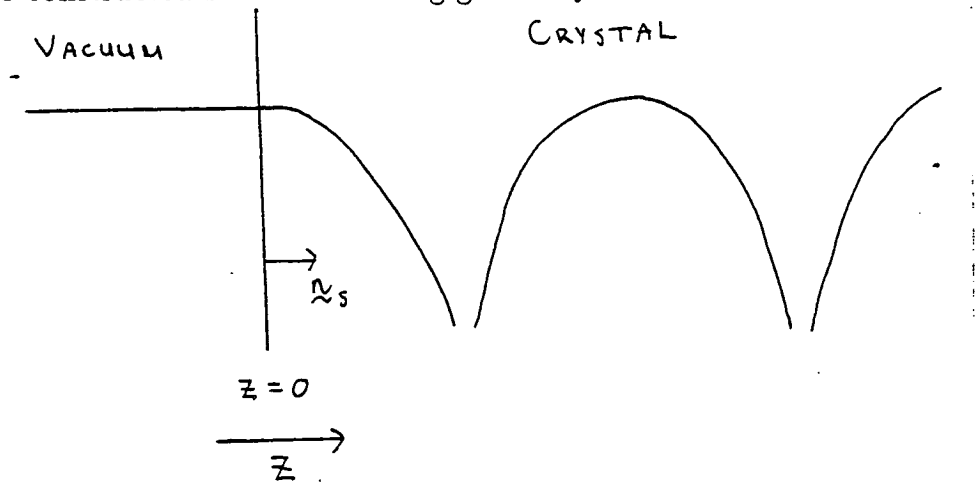

Consider a plane wave incident on the crystal from the left. The total wavefunction in vacuum is

$$\Psi = \exp\left(i\left[\mathbf{K}+\mathbf{G}\right].\mathbf{R}\right)\exp(ik_z z) + \sum_{\mathbf{G}'} \mathcal{R}_{\mathbf{G}',\mathbf{G}} \exp\left(i\left[\mathbf{K}+\mathbf{G}'\right].\mathbf{R}\right)\exp\left(\gamma_{\mathbf{G}'} z\right)$$

where $\mathcal{R}$ is the reflection matrix and $\gamma_{\mathbf{G}}$ is given by

$$\gamma_{\mathbf{G}'} = \left(\left|\mathbf{K}+\mathbf{G}'\right|^2 - 2E\right)^{\frac{1}{2}}$$

E being the energy of the incoming wave, namely $\frac{1}{2}\left(|\mathbf{K}+\mathbf{G}|^2 + k_z^2\right)$.

At the embedding plane (z=0), the Fourier components of Ψ are

$$\Psi_{\mathbf{G}'} = \delta_{\mathbf{G}',\mathbf{G}} + \mathcal{R}_{\mathbf{G}',\mathbf{G}}$$

Similarly those of $\frac{\partial\Psi}{\partial n_s}$ are

$$\left.\frac{\partial\Psi}{\partial n_s}\right|_{\mathbf{G}'} = \gamma_{\mathbf{G}'}(-\delta_{\mathbf{G}',\mathbf{G}} + \mathcal{R}_{\mathbf{G}',\mathbf{G}})$$

Now, the Fourier transform of equation 1.5 gives

$$\left.\frac{\partial\Psi}{\partial n_s}\right|_{\mathbf{G}'} = -2G^{\circ -1}_{\mathbf{G}',\mathbf{G}''}\Psi_{\mathbf{G}''}$$

So

$$\gamma_{G'}(-\delta_{G',G} + \mathcal{R}_{G',G}) = -2G^{o^{-1}}_{G',G''}(\delta_{G'',G} + \mathcal{R}_{G'',G})$$

In terms of matrices we obtain

$$G^{o^{-1}} = \frac{\gamma}{2}(1 - \mathcal{R})(1 + \mathcal{R})^{-1} \tag{1.18}$$

Hence the embedding potential is simply related to the reflection matrix of the crystal. To construct this matrix, the phase shift of the wavefunction for each atom is calculated, leading to the reflection and transmission matrices for a layer. The reflection matrix for multiple layers is then calculated using the layer doubling method, due to Pendry [5]. The energy at which the reflection matrix is calculated has a small imaginary component. This ensures rapid convergence of the reflection matrix elements as more layers of atoms are considered.

The type of potential used in the embedding potential calculation is of the simple 'muffin-tin' form. This consists of spheres centred on each nucleus, within which the potential is taken to be spherically symmetric, and a constant potential in the interstitial region. It is also possible to have spheres not containing a nucleus, should a constant interstitial potential be a poor approximation. The spheres must not overlap, but they can touch. A two dimensional representation of such a potential for a diatomic material is shown in the following diagram.

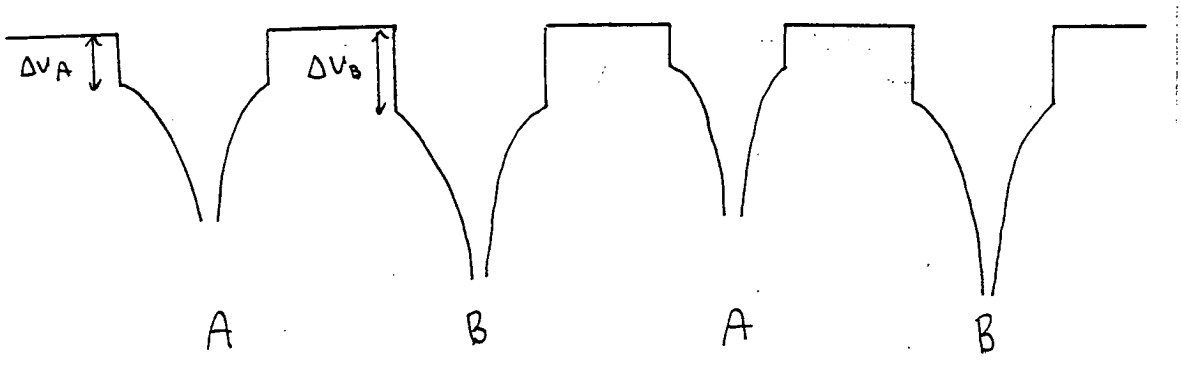

There are extensions to this simple muffin-tin form, but for constructing the embedding potential, the simple form is adequate, as it is a good approximation around the ion cores where most scattering occurs.

The discussion so far has been concerned with the embedding potential for the right substrate. We also require $G^{o^{-1}}$ for the left substrate. Conveniently, it turns out that the embedding potential for a given material appropriate to a substrate at the right can be used at the left with no changes. This is easy to see if one considers the point $\mathbf{K} = (K_x, K_y)$ at which $G^o_{\mathbf{K}}$ is evaluated, and the set of reciprocal lattice vectors $\{\mathbf{G} = (G_x, G_y)\}$ in which $G^o_{\mathbf{K}}$ is expanded. Let these be the parameters for $G^o_{\mathbf{K}}$ at the right side. For example, for two reciprocal lattice vectors $\mathbf{G}$ and $\mathbf{G}'$, looking at the right side gives

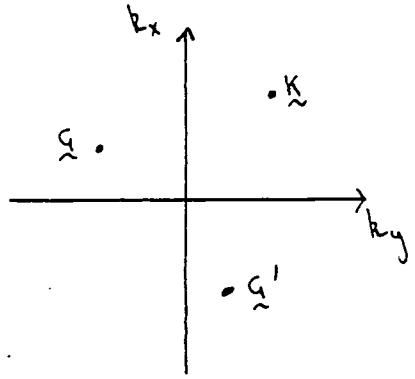

Looking at the left side, it is clear that we must evaluate $G^{o^{-1}}$ at $(K_x, -K_y)$, in terms of $\{(G_x, -G_y)\}$. i.e.

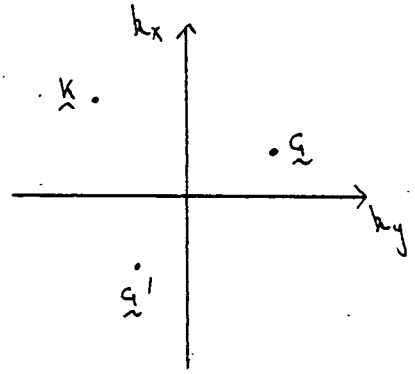

$G^{o^{-1}}$ for $(K_x, -K_y)$ expanded in $\{(G_x, -G_y)\}$ is clearly the same as $G^{o^{-1}}$ for (K_x, K_y) expanded in $\{(G_x, G_y)\}$, if there is a mirror plane perpendicular to $\langle 0, 1\rangle$. Thus we can use the embedding potentials generated by the existing program at either side, with no modification, as long as the lattice has the required symmetry plane.

1.4 Summary

The interface Hamiltonian has been derived in terms of the two substrate embedding potentials. The construction of the embedding potentials and their use has been described. Finally, one should take note of the method used to shift the embedding surfaces. This must be understood in order to make sense of later work dealing with the construction of the full potential in the interface.

Chapter 2

One Electron Theory

This chapter presents current methods of solving the many body problem in crystals, or in this case an interface, within a one electron framework. The development of one electron equations where each electron moves in the mean field of all the others is discussed. This leads on to density functional theory, and in its simplest form, the local density approximation. The limitations of this theory and the reason for its successes are dealt with, along with more recent work which attempts to explain its shortcomings. As the calculations in this thesis are of the self-consistent-field type, this chapter should be seen as explaining and justifying this approach.

2.1 The Many Body Problem in Crystals

It is important to consider how the many body problem of interacting electrons and nuclei can be reduced to one which can be readily solved. In practice we have of order 10^{23} electrons per mole of solid, which clearly makes any exact solution impossible to obtain. The solution is to use a mean field approach, where each electron moves in the average potential of all the others. This potential must include correlation effects between the electron in question and the rest of the electron gas. The result is a set of one electron equations.

The many body Hamiltonian for a crystal is written

$$H = -\frac{1}{2}\sum_a \frac{\nabla_a^2}{M_a} + \frac{e^2}{2}\sum_{a,b}{}' \frac{Z_a Z_b}{|\mathbf{R}_a - \mathbf{R}_b|}$$
$$-\frac{1}{2}\sum_i \nabla_i^2 + \frac{e^2}{2}\sum_{i,j}{}' \frac{1}{|\mathbf{r}_i - \mathbf{r}_j|} - e^2 \sum_{a,i} \frac{Z_a}{|\mathbf{R}_a - \mathbf{r}_i|} \tag{2.1}$$

Primes on summations exclude $i = j$ and $a = b$.

$\mathbf{r}$= electron positions

$\mathbf{R}$ = nuclei positions

M_a = nuclear masses

Atomic units are used, except that e^2 is explicitly included. In these units $\hbar = m_e = 1$.

The terms in equation 2.1 are, in order, nuclear kinetic energy, nuclear-nuclear potential energy, electronic kinetic energy, electron-electron potential energy, electron-nucleus potential energy.

In order to separate the electronic motion from that of the nuclei, we appeal to the 'adiabatic approximation'. The principle here is that the many electron wavefunction can be separated from the nuclear wavefunction.

$$\Psi(\mathbf{R}, \mathbf{r}) = \Phi_{\mathbf{R}}(\mathbf{r})\eta(\mathbf{R})$$

where $\Psi(\mathbf{R},\mathbf{r})$ is the total wavefunction, $\Phi_{\mathbf{R}}(\mathbf{r})$ is the many electron wavefunction for a fixed nuclear configuration $\{\mathbf{R}_a\}$, and $\eta(\mathbf{R})$ is the nuclear wavefunction. This is valid as the electrons move much faster than the nuclei, so that the electronic wavefunction can be considered as adjusting instantaneously to any change in the nuclear coordinates.

This gives the Hamiltonian, H_e, for the electronic motion, given some fixed nuclear configuration as (dropping the constant nuclear-nuclear potential)

$$H_e = -\frac{1}{2}\sum_i \nabla_i^2 + \frac{1}{2}\sum_{i,j}{}' \frac{e^2}{|\mathbf{r}_i - \mathbf{r}_j|} - \sum_{a,i} \frac{Z_a e^2}{|\mathbf{R}_a - \mathbf{r}_i|} \tag{2.2}$$

So the many electron eigenvalue equation is

$$H_e \Phi(\mathbf{r}_1, \mathbf{r}_2, \ldots, \mathbf{r}_n) = E\Phi(\mathbf{r}_1, \mathbf{r}_2, \ldots, \mathbf{r}_n) \tag{2.3}$$

where $\mathbf{r}$ denotes both the spatial and spin coordinates of an electron.

Before continuing, it is worth mentioning some recent work due to Car and Parinello [6]. They have tried to unify electronic structure and lattice dynamics. The general idea is to introduce a fictitious dynamics for the electronic wavefunction, nuclear coordinates, and any other system parameters. Using simulated annealing they obtain the equilibrium configuration of the system. It turns out that once the system is in equilibrium, the dynamics for the nuclear motion has the usual physical interpretation. Thus electronic states, atomic configurations, phonon frequencies, and information on electron-phonon interactions can be obtained in one simulation. This technique is likely to be of importance in future work on surface and interface reconstructions. However, as electronic structure work on such systems is still in its infancy, the Car-Parinello method will first find application in bulk crystal calculations.

Returning to the many electron hamiltonian, H_e, which we will now write as H, leaves us with the task of constructing a suitable form for the many electron wavefunction $\Phi(\mathbf{r}_1, \mathbf{r}_2, \ldots, \mathbf{r}_n)$. Hartree [7] wrote Φ as a simple product of one electron wavefunctions, ϕ. However, this completely ignores the fermion nature of electrons, which requires the total wavefunction to be antisymmetric under interchange of the electrons' coordinates or spins. Fock [8] and Slater [9] were the first to include this antisymmetry property by writing the total wavefunction as a determinant of one electron wavefunctions.

$$\Phi(\mathbf{r}_1, \mathbf{r}_2, \ldots, \mathbf{r}_n) = \frac{1}{\sqrt{n!}} \begin{vmatrix} \phi_1(\mathbf{r}_1) & \phi_1(\mathbf{r}_2) & \cdots & \phi_1(\mathbf{r}_n) \\ \phi_2(\mathbf{r}_2) & \phi_2(\mathbf{r}_2) & \cdots & \phi_2(\mathbf{r}_n) \\ \vdots & \vdots & & \vdots \\ \phi_n(\mathbf{r}_1) & \phi_n(\mathbf{r}_2) & \cdots & \phi_n(\mathbf{r}_n) \end{vmatrix} \tag{2.4}$$

Interchanging two rows or columns of 2.4 changes the sign of $\Phi(\mathbf{r}_1, \mathbf{r}_2, \ldots, \mathbf{r}_n)$, and is equivalent to changing the coordinates or spins of two electrons.

To derive the Hartree-Fock equations, 2.4 is inserted in 2.3, with H given by 2.2. The total energy is then minimised by varying E with respect to each ϕ_i, subject to the constraint that the $\{\phi_i\}$ are kept orthonormal. Lagrange multipliers are included to impose this constraint. The resulting equations are

$$\left[-\frac{1}{2}\nabla^2 - \sum_a \frac{Z_a e^2}{|\mathbf{R}_a - \mathbf{r}|} + \sum_j e^2 \int \frac{\phi_j^*(\mathbf{r}')\phi_j(\mathbf{r}')\, d^3r'}{|\mathbf{r} - \mathbf{r}'|}\right] \phi_i(\mathbf{r})$$
$$- \sum_j e^2 \phi_j(\mathbf{r}) \int \frac{\phi_j^*(\mathbf{r}')\phi_i(\mathbf{r}')\, d^3\tilde{r}'}{|\mathbf{r} - \mathbf{r}'|} = \epsilon_i \phi_i(\mathbf{r}) \qquad (2.5)$$

The last term on the left of 2.5 is the exchange term, and is non-local, making it difficult to evaluate.

The Hartree-Fock eigenvalues $\{\epsilon_i\}$ are a good approximation to the magnitudes of the energies required to remove a given electron from the system. i.e. $\epsilon_i = E_{HF}(n_i = 1) - E_{HF}(n_i = 0)$, where n_i is the occupancy of the i^{th} state. This is "Koopman's theorem". Note that the wavefunctions used for the $n_i = 0$ case are those which have been calculated for $n_i = 1$. i.e. they are not allowed to relax. This is therefore an approximation.

The summations in 2.5 now include j=i, leading to self-interaction terms. This poses no problem here, as the j=i term in the exchange sum exactly cancels the Coulomb self-interaction term.

Slater [10] has given a simple physical interpretation of the exchange term. Its effect is to exclude electrons of the same spin from the region of the electron in question. The charge removed equals one electronic charge, so that the total charge, excluding the electron in question is $(n-1)e$, as it should be. However, the Hartree-Fock equations do not include any Coulomb correlation effects. In the real system, electrons of opposite spin will also tend to remain apart due to Coulomb repulsion. Despite this, attempts were made, mainly by Slater [10], to produce a form of the Hartree-Fock equations which could be more easily solved.

First he rewrote the exchange term, V_{ex}, in the form of a normal potential

energy times the $\phi_i(\mathbf{r})$

$$V_{ex} = -e^2 \sum_j \int \frac{\phi_i^*(\mathbf{r})\phi_j^*(\mathbf{r}')\phi_j(\mathbf{r})\phi_i(\mathbf{r}')\, d^3r'}{\phi_i^*(\mathbf{r})\phi_i(\mathbf{r})|\mathbf{r}-\mathbf{r}'|}$$

Slater went on to calculate the average exchange potential for jellium, this being a uniform electron gas with a uniform distribution of positive charge, ensuring overall charge neutrality. The result is

$$\langle V_{ex} \rangle = -3e^2 \left(\frac{3}{8\pi}\rho\right)^{\frac{1}{3}}$$

This is then applied to the crystal charge density, using $\rho = \rho(\mathbf{r})$ at the point $\mathbf{r}$ in question. So ρ is now the local density of the inhomogeneous electron gas. Hence

$$V_{ex}(\mathbf{r}) = -3e^2 \left(\frac{3}{8\pi}\rho(\mathbf{r})\right)^{\frac{1}{3}} \tag{2.6}$$

This approximation is most likely to be valid in regions where ρ varies only slowly.

There is no formal justification for Slater's approach. However, the dependence of V_{ex} on ρ is clearly appealing as it greatly simplifies the calculation of the exchange potential. It is in fact possible to derive rigorous theorems relating the total energy to the charge density. This is the subject of the next section.

2.2 Density Functional Theory

This is based on two theorems proved by Hohenberg and Kohn [11]. These are, for the spinless case

1. The ground state energy of a system of identical spinless fermions is a unique functional of the particle density.

2. This functional attains its minimum value with respect to variation of the particle density, subject to the usual normalisation constraint, when the density has the correct value.

Including spin leads to similar results, except that the ground state is now a unique functional of the charge and spin densities.

Thus, if we know the charge density, we can calculate H, and hence all ground state properties of the system.

Kohn and Sham [12] went on to derive a set of single particle equations. Write the total energy as

$$E(\rho) = \int V_{ion}(\mathbf{r})\rho(\mathbf{r})\, d^3r + T(\rho) + \frac{e^2}{2}\int \frac{\rho(\mathbf{r})\rho(\mathbf{r}')\, d^3r'}{|\mathbf{r}-\mathbf{r}'|} + E_{xc}(\rho) \qquad (2.7)$$

$T(\rho)$ is the kinetic energy, and $E_{xc}(\rho)$ is the exchange-correlation energy.

Minimising E with respect to ρ, and keeping the total number of particles constant gives the Kohn-Sham equations

$$\left[-\frac{1}{2}\nabla^2 + V_{ion}(\mathbf{r}) + e^2\int \frac{\rho(\mathbf{r}')\, d^3r'}{|\mathbf{r}-\mathbf{r}'|} + V_{xc}(\mathbf{r})\right]\phi_i(\mathbf{r}) = \epsilon_i\phi_i(\mathbf{r}) \qquad (2.8)$$

$$V_{xc}(\mathbf{r}) = \frac{\partial E(\rho)}{\partial \rho(\mathbf{r})} \qquad (2.9)$$

$$\rho(\mathbf{r}) = \sum_{i \text{ occupied}} |\phi_i(\mathbf{r})|^2 \qquad (2.10)$$

$V_{xc}(\mathbf{r})$ may be non-local.

Note that we have now written an explicit form for $T(\rho)$, taking it to be the kinetic energy of a non-interacting electron gas.

As $\rho(\mathbf{r})$ is not known at the outset, equations 2.8 -2.10 must be solved self-consistently. i.e. We use an initial potential to calculate the wavefunctions $\phi_i(\mathbf{r})$ using 2.8. Then we use 2.10 to calculate $\rho(\mathbf{r})$, construct a new potential and repeat the cycle until the desired level of convergence is obtained. The form of V_{xc} is not specified by density functional theory (referred to as DFT in future). It is only an existence theorem. Note that in DFT, the $\{\epsilon_i\}$ no longer have any rigorous physical interpretation. In fact $\epsilon_i = \frac{\partial E}{\partial n_i}$, where the derivative is with respect to a set of continuous occupation numbers [13]. In practice the $\{\epsilon_i\}$ are taken to be the actual crystal eigenvalues. There are two pieces of evidence to support this stance.

1. The quasi-particle equation, which gives the true crystal eigenvalues, is

$$\left(-\nabla^2 + V_{ion}(\mathbf{r}) + e^2 \int \frac{\rho(\mathbf{r}')\, d^3r'}{|\mathbf{r} - \mathbf{r}'|} - \epsilon_i\right) \phi_i(\mathbf{r}) + \int \Sigma(\mathbf{r}, \mathbf{r}', E)\phi_i(\mathbf{r}')\, d^3r' = 0$$

where Σ is the self-energy operator.

This is of the same form as equation 2.8, but with V_{xc} replaced by Σ. Later we shall see that many of the approximations to V_{xc} in common use are very close to the actual self-energy for the ground state.

2. The energy of the highest occupied state can be shown to equal the ionisation energy of the relevant electron [16].

There have been numerous calculations bsed on DFT over the past twenty years. The results obtained have confirmed the validity of DFT for ground state properties. i.e. Total ground state energy, wavefunctions, energies of occupied states. In practice the problem is one of choosing a suitable E_{xc} from which we obtain V_{xc} from 2.9.

A generalisation of the Slater V_{ex} is to use the local density approximation (LDA), except that correlations can now be included. So within LDA

$$E_{xc} = \int \rho(\mathbf{r}) \epsilon_{xc}\left(\rho(\mathbf{r})\right)\, d^3r$$

where $\epsilon_{xc}\left(\rho(\mathbf{r})\right)$ is the exchange-correlation energy per unit volume of a homogeneous electron gas of density $\rho(\mathbf{r})$. Kohn and Sham [12] derive an expression for V_{ex} (neglecting correlation) of the form

$$V_{ex} = -2e^2 \left(\frac{3}{8\pi}\rho(\mathbf{r})\right)^{\frac{1}{3}} \tag{2.11}$$

Note that this differs from that given by Slater (equation 2.6) by a factor of $\frac{2}{3}$. This is because Kohn and Sham calculate V_{ex} for an electron at the Fermi energy, with wavevector $k = k_F$, rather than with average wavevector. Equation 2.11 is thus more realistic, since density adjustments occur by redistribution of the electrons near the Fermi level.

In practice, equations 2.6 and 2.11 led to the X_α method, with V_{xc} of the form

$$V_{xc}(\mathbf{r}) = -2\alpha e^2 \left(\frac{3}{8\pi}\rho(\mathbf{r})\right)^{\frac{1}{3}} \qquad \left(1 \leq \alpha \leq \frac{3}{2}\right) \tag{2.12}$$

The value of α to be used in a given situation was calculated using one of several approaches. The most common was to choose α such that the X_α total energies for isolated atoms agreed with the Hartree-Fock energies for the atom in question. This value of α was then used for the crystal calculations. If there was more than one element present, then typically an average value of α was used. Schwarz [14] gives suitable values of α for most elements.

Hedin-Lundqvist [15] produced an E_{xc} which included correlation effects. This gave rise to the exchange-correlation potential

$$V_{xc}(\mathbf{r}) = \beta(\mathbf{r}) V_{ex}(\mathbf{r}) \tag{2.13}$$

where

$$\beta(\mathbf{r}) = 1 + \left(\frac{4\pi^2}{9}\right)^{\frac{1}{3}} \ln\left(1 + \frac{r_s}{21}\right)$$

and

$$\frac{4}{3}\pi r_s^3 = \frac{1}{\rho}$$

V_{ex} in 2.13 is given by 2.11. r_s is the Wigner-Seitz radius.

β varies between about 1 for very high densities, and $\frac{3}{2}$ for very low densities. This therefore gives credibility to the X_α approach, which is still used to this day.

2.3 Problems with LDA

There are several known problems which appear when using the LDA [16]. The most important is the poor values which LDA gives for the excitation energies. That is, the energy of unoccupied states when the system is in its ground state. This leads to band gaps in insulators and semiconductors which are too small by a factor of 10% to 100%, and even negative in some cases.

There have been numerous attempts to resolve this problem, in particular to understand whether the errors are due to the use of the LDA or to a failure of density functional theory itself to cope with excited states, but only recently has any progress been made.

Of course, the cynic would say that DFT is only valid for the ground state, so cannot by definition be used to gain information about excited states. This is not strictly true, as the band gap can be expressed as the difference in total energies between the N-1, N, and N+1 electron states. The lowest conduction band energy is given as

$$\epsilon_c = E_{N+1} - E_N$$

where E_N is the total energy of the N electron insulating ground state. Similarly, the highest valence band energy is

$$\epsilon_v = E_N - E_{N-1}$$

So the fundamental band gap is

$$\begin{aligned} E_g &= \epsilon_c - \epsilon_v \\ &= E_{N+1} + E_{N-1} - 2E_N \end{aligned} \tag{2.14}$$

The problem is that the exchange-correlation potential has a discontinuity on going from the N particle insulating ground state to the N+1 particle system. If there was no discontinuity in V_{xc}, then use of the same V_{xc} for the terms in 2.14 would give the correct energy gap. This problem has been discussed in many recent papers [17,18,19,20,21,22]. Sham and Schlüter [17] show that $\epsilon_c = \epsilon_{N+1}(N+1)$, where this denotes the $(N+1)^{th}$ eigenvalue of the N+1 particle system, and $\epsilon_v = \epsilon_N(N)$ in the same notation. So the true bandgap is

$$E_g = \epsilon_{N+1}(N+1) - \epsilon_N(N) \tag{2.15}$$

The naive definition of the bandgap is

$$\epsilon_g = \epsilon_{N+1}(N) - \epsilon_N(N) \tag{2.16}$$

where $\epsilon_{N+1}(N)$ is the $(N+1)^{th}$ eigenvalue of the N particle system.
The difference $\triangle$ from 2.15 and 2.16 is

$$\triangle = \epsilon_{N+1}(N+1) - \epsilon_{N+1}(N)$$

Sham and Schlüter go on to show that

$$\Delta = V_{xc}^{+} - V_{xc}^{-}$$

where V_{xc}^{+} denotes the limit of particle number tending to N+1 from above, and V_{xc}^{-} denotes the limit tending to N-1 from below. For an insulator they show that $\Delta \neq 0$.

Godby et al. [21,22] have studied the relationship between the exact self-energy operator $\Sigma(\mathbf{r}, \mathbf{r}', E)$ and the exact DFT V_{xc}. It is easy to derive an expression linking V_{xc} and Σ.

$$\rho(\mathbf{r}) = \int_{-\infty}^{E_F} Im\, G_{DFT}(\mathbf{r}, \mathbf{r}, \omega)\, d\omega \tag{2.17}$$

Also

$$\rho(\mathbf{r}) = \int_{-\infty}^{E_F} Im\, G(\mathbf{r}, \mathbf{r}, \omega)\, d\omega$$

Now G and G_{DFT} obey the Dyson equation

$$G = G_{DFT} + G_{DFT}\,(\Sigma - V_{XC})\,G \tag{2.18}$$

Combining 2.17-2.18 gives

$$Im \int_{-\infty}^{E_F} d\omega\, (G_{DFT}\,(\Sigma - V_{XC})\,G) = 0$$

Σ is calculated using the 'GW' approximation. i.e. We write

$$\Sigma(\mathbf{r}, \mathbf{r}', \omega) = \frac{i}{2\pi} \int_{-\infty}^{\infty} W(\mathbf{r}, \mathbf{r}', \omega) G(\mathbf{r}, \mathbf{r}', \omega + \omega')\, d\omega' \tag{2.19}$$

W is the screened Coulomb inteaction, and is calculated using the random phase approximation (RPA) [21]. G_{DFT} is used for G in 2.19. Hence, the calculated Σ is itself an approximation. The result is that V_{xc} from Σ is very similar to V_{xc}^{LDA}. So for ground state properties, there is no point in going beyond LDA. However, for excitation spectra, the self energy approach must be explicitly used. In this work the LDA is used in the form of the Kohn-Sham equations. More accurate calculations of the energies of interface states would require extensions to DFT, though DFT is clearly adequate for the calculation of the potential shift across interfaces.

2.4 Summary

The many body problem has been reduced to that of a single electron, which can be more readily solved. The process is however computationally intensive due to the self-consistent procedure used. The justification for this approach, along with its limitations, has been given, so we can now proceed, confident that the foundations on which the work of this thesis rests are understood.

Chapter 3

Method of Solution

The method of solution in the interface is dealt with in this chapter. A suitable basis set for the interface wavefunction expansion is chosen, and the matrix elements of this basis are evaluated. The form of the potential used in the interface is described, and finally, the Green function is obtained from the Hamiltonian, which is then used to construct the density of states and the charge density. Most of the techniques in this chapter are based on standard methods of one electron band theory. Here they are applied to the particular geometry of the interface problem.

3.1 Interface Geometry and Symmetry

Before proceeding to consider the solution in the interface region, it is first necessary to describe the geometry involved, and also include the use of symmetry.

The various planes are as shown in the following diagram.

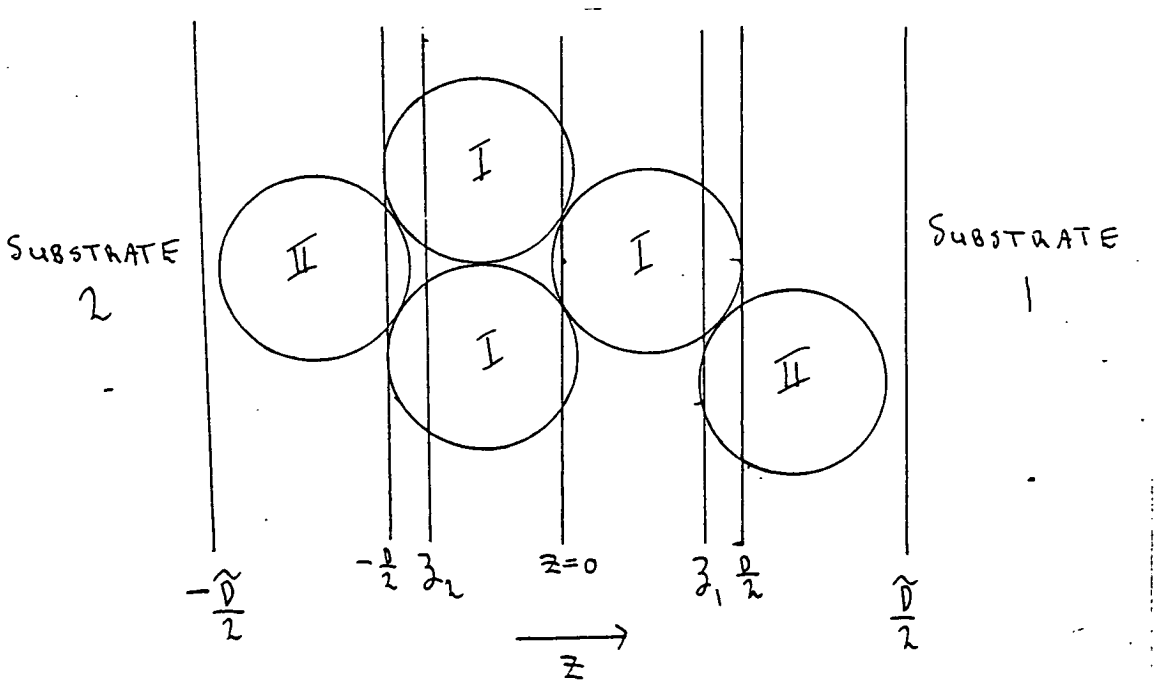

The interface is of width D. ζ_1 and ζ_2 are the embedding planes. The basis to be used in the wavefunction expansion is defined over $-\tilde{D}/2$ to $\tilde{D}/2$. The reason for this will become apparent later (section 3.4).

Region I is the muffin-tins. Region II is the substrate mufffin-tins which intersect ζ_1 or ζ_2. The z-axis points to the right, with the x-y axes parallel to the embedding planes.

The two dimensional real space lattice basis, $\mathbf{a}_1$, $\mathbf{a}_2$ are written with respect to the x-y axes. $\mathbf{b}_1$,$\mathbf{b}_2$ is the two dimensional reciprocal lattice basis, related to $\mathbf{a}_1$,$\mathbf{a}_2$ in the usual manner.

For simplicity, only fourteen 2-D point group symmetry operations are used. These are

Number	Symmetry Operation
1	Identity
2	Rotate by π
3	Rotate by $\frac{\pi}{2}$
4	Rotate by $-\frac{\pi}{2}$
5	Rotate by $\frac{2\pi}{3}$
6	Rotate by $-\frac{2\pi}{3}$
7	Reflection in mirror plane $\perp$ to $\langle 0,1\rangle$
8	Reflection in mirror plane $\perp$ to $\langle 1,0\rangle$
9	Reflection in mirror plane $\perp$ to $\langle \bar{1},1\rangle$
10	Reflection in mirror plane $\perp$ to $\langle 1,1\rangle$
11	Reflection in mirror planr $\perp$ to $\langle \overline{\sqrt{3}},1\rangle$
12	Reflection in mirror plane $\perp$ to $\langle \sqrt{3},1\rangle$
13	Reflection in mirror plane $\perp$ to $\langle 1,\sqrt{3}\rangle$
14	Reflection in mirror plane $\perp$ to $\langle 1,\overline{\sqrt{3}}\rangle$

Six-fold rotations are not included.

The symmetry of the two dimensional lattice is used to greatly reduce the amount of computation done, as all the data for symmetry related atoms and wavevectors can be generated if we know the result for any one of them.

Let S_i denote a 2×2 matrix representing one of the symmetry operations, α denote an atom, and $\mathbf{K}$ a two dimensional wavevector. Consider the construction of the crystal charge density as an example, written as

$$\rho(\mathbf{r}) = \sum_{l,m\geq 0} \left[\rho_{l,m}(\mathbf{r}) \cos m\phi + \rho_{l,-m}(\mathbf{r}) \sin m\phi\right] P_{l,m}(\theta) \tag{3.1}$$

Now

$$\rho_{S_i(\alpha);S_i(\mathbf{K})}\left(S_i(\mathbf{r})\right) = \rho_{\alpha;\mathbf{K}}(\mathbf{r})$$

$\rho_{\alpha;\mathbf{K}}(\mathbf{r})$ being the charge density at $\mathbf{r}$, on atom α, associated with wavevector $\mathbf{K}$.

So, the sum over symmetry related **K** points gives

$$\begin{pmatrix} \rho_{l,m;\alpha;\sum \mathbf{K}} \\ \rho_{l,-m;\alpha;\sum \mathbf{K}} \end{pmatrix} = \sum_i \left(S_i^{-1}\right) \begin{pmatrix} \rho_{l,m;S_i(\alpha);\mathbf{K}} \\ \rho_{l,-m;S_i(\alpha);\mathbf{K}} \end{pmatrix} \tag{3.2}$$

So given $\rho_{l,\pm m;\alpha;\mathbf{K}}$, we evaluate $\rho_{l,\pm m;S_i(\alpha);\mathbf{K}}$ for each atom in the star, multiply by S_i^{-1}, and add to obtain $\rho_{l,\pm m;\alpha;\sum \mathbf{K}}$.

The relevant matrices for rotations by χ are

$$R^{-1} = \begin{pmatrix} \cos m\chi & \sin m\chi \\ -\sin m\chi & \cos m\chi \end{pmatrix}$$

and for reflections through a mirror plane rotated by η are

$$M^{-1} = \begin{pmatrix} \cos 2m\eta & \sin 2m\eta \\ \sin 2m\eta & -\cos 2m\eta \end{pmatrix}$$

Atoms or wavevectors related by symmetry form 'stars'. The stars of atoms, 2-D and 3-D wavevectors are evaluated. Incomplete stars of wavevectors are not used.

3.2 The LAPW Method of Solution

The technique used to expand the wavefunction in the interface region is the Linear Augmented Plane Wave (LAPW) method. This is a development of the older Augmented Plane Wave (APW) method [23,24]. Each APW basis state of wavevector **k** consists of the solution to the radial Schrödinger (or Dirac) equation within the muffin-tins joined onto a plane wave of wavevector **k** in the interstitial region. This is a good basis to use as it is rapidly varying near the nucleus, and smooth far from the nucleus, as in the real crystal. There are however three main problems with the APW method

1. The basis is not continuous in gradient at the muffin-tin radius. This makes extensions to the simple muffin-tin form of the potential harder to incorporate.

2. The solution of the radial equation involves the evaluation of the logarithmic derivatives of the wavefunction at the muffin-tin radius. If the wavefunction has a node here, then the solution has an asymptote at this point, making the computation harder to control.

3. The radial Schrödinger equation must be solved at the actual crystal eigenvalue energy. As this is what we wish to find, repeated calculation of the Hamiltonian matrix elements over a wide range of energies is necessary. The zeros in the determinant of the secular equation are then searched for. This is very time consuming.

There have been several attempts to improve the APW method. The main effort was concentrated on removing the energy dependence of the APW matrix elements. Schlosser and Marcus [25] removed this problem by using a variational expression suitable for trial functions discontinuous in both value and gradient at the sphere radii. The reason this works is that the wavefunction expansion outside the sphere, which minimises the energy, will not in general be continuous with the radial solution, unless it is evaluated at the relevant crystal eigenvalue. In this case, a series of trial energies are used for the evaluation of the radial wavefunction.

The other approach due to Andersen [26], and first used by Koelling and Arbman [27], is the LAPW method. Here the basis is taken to be a linear combination of the radial solution and its energy derivative within the spheres. This is then matched in value and gradient to the plane wave in the interstitial region. The result is to eliminate the three main problems associated with the APW approach. The basic features of the LAPW method are given here, but for full details, and the relationship between the LAPW method and pseudopotential theory, see Andersen's paper [26].

The radial solutions for an energy parameter E_l (different for each angular momentum.quantum number l) are solutions of the equation (non-relativistic here, but generalised to the relativistic case later)

$$h_l u_l - E_l u_l = 0$$

u_l is the radial wavefunction, and h_l is the radial hamiltonian, defined in this case as

$$h_l = -\frac{1}{r}\frac{d^2}{dr^2}r + \frac{l(l+1)}{r^2} + V(r)$$

The normalisation condition is

$$\int_0^R r^2 u_l^2 \, dr = 1 \tag{3.3}$$

where R is the radius of the muffin-tin sphere in question. From 3.3

$$\int_0^R r^2 u_l \dot{u}_l \, dr = 0$$

So u_l and $\dot{u}_l$ are orthogonal, $\dot{u}_l$ being the energy derivative of u_l. The equation for $\dot{u}_l$ is obviously

$$h_l \dot{u}_l - E_l \dot{u}_l = E u_l$$

In the interstitial region the LAPWs are plane waves

$$\phi(\mathbf{k}_n, \mathbf{r}) = \Omega^{-\frac{1}{2}} \exp(i\mathbf{k}_n.\mathbf{r}) \tag{3.4}$$

where

$$\mathbf{k}_n = \mathbf{k} + \mathbf{K}_n$$

Ω is the unit cell volume. $\{\mathbf{K}_n\}$ are the reciprocal lattice vectors.

Inside the spheres, the LAPW is a linear combination of u_l and $\dot{u}_l$

$$\phi(\mathbf{k}_n, \mathbf{r}) = \sum_{l,m} \left[A_{l,m}(\mathbf{k}_n) u_l(r, E_l) + B_{l,m}(\mathbf{k}_n) \dot{u}_l(r, E_l)\right] Y_{l,m}(\hat{\mathbf{r}}) \tag{3.5}$$

3.5 is now matched in value and gradient to 3.4 for each $\{\mathbf{k}_n\}$, giving a set of coefficients $\{A_{l,m}(\mathbf{k}_n), B_{l,m}(\mathbf{k}_n)\}$.

3.3 The Radial Dirac Equation

Before going on to consider the use of the LAPW technique in the interface calculation, it is first necessary to derive a suitable form for the Dirac equation which can be readily solved in the muffin-tins. To do this we consult Rose [28]. A form is required which includes relativistic effects, but excludes the spin-orbit

interaction, which we do not consider in our calculations except for the core states. Justification for this approach is discussed later.

The Dirac equation in a usual notation is

$$i\hbar\frac{\partial\psi}{\partial t} = \left[c\underline{\alpha}.\mathbf{p} + \beta mc^2\right]\psi$$

$$\alpha = \begin{pmatrix} 0 & \underline{\sigma} \\ \underline{\sigma} & 0 \end{pmatrix} \; ; \; \beta = \begin{pmatrix} I_2 & 0 \\ 0 & -I_2 \end{pmatrix}$$

$$\sigma_x = \begin{pmatrix} 0 & 1 \\ 1 & 0 \end{pmatrix} \; ; \; \sigma_y = \begin{pmatrix} 0 & -i \\ i & 0 \end{pmatrix} \; ; \; \sigma_z = \begin{pmatrix} 1 & 0 \\ 0 & -1 \end{pmatrix}$$

The radial Dirac equation is

$$H\psi = \left[i\gamma_5\sigma_r\left(\frac{\partial}{\partial r} + \frac{1}{r} - \frac{\beta}{r}K\right) + V + \beta\right]$$

$$\gamma_5 = i\gamma_1\gamma_2\gamma_3\gamma_4 \quad \gamma_i = -i\beta\alpha_i \;\; (i = 1,2,3) \quad \gamma_4 = \beta \quad K = \beta(\underline{\sigma}.\underline{l} + 1)$$

Writing

$$\psi_{\kappa,\mu} = \begin{pmatrix} g(r)\chi^{\mu}_{\kappa} \\ if(r)\sigma_r\chi^{\mu}_{\kappa} \end{pmatrix}$$

gives two coupled differential equations for f and g

$$\frac{\partial f_\kappa}{\partial r} = \frac{1}{c}(V - E)g_\kappa + \left(\frac{\kappa - 1}{r}\right)f_\kappa \tag{3.6}$$

$$\frac{\partial g_\kappa}{\partial r} = -\left(\frac{\kappa + 1}{r}\right)g_\kappa + 2Mcf_\kappa \tag{3.7}$$

E is the energy with the rest mass subtracted.

$$M = m + \frac{1}{2c^2}(E - V)$$

$$\kappa = \begin{cases} -(l+1) & j = l + \frac{1}{2} \\ l & j = l - \frac{1}{2} \end{cases}$$

We solve for the large component g_κ only, as the lower component is smaller by a factor of $E_K/(E + mc^2)$ [29] for the outer electrons. For core electrons, both components must be considered [29].

Loucks [24], Koelling and Harmon [29] give the method of solving 3.6 and 3.7, which is straightforward. The results are

$$-\frac{1}{2M}\left(\frac{\partial^2 g}{\partial r^2}+\frac{2}{r}\frac{\partial g}{\partial r}-\frac{l(l+1)}{r^2}g\right)+Vg-\frac{V'}{4M^2c^2}-\frac{\kappa+1}{r}\frac{V'}{4M^2c^2}g=Eg \quad (3.8)$$

The terms are, in order, non-relativistic equation but including mass-velocity effects via M, Darwin term, and spin-orbit. We do not consider the spin-orbit term for the valence bands as for most elements its effect is only a first order change in the energy of the states. If detailed excitation spectra for heavy elements were required, then the spin-orbit term would have to be included. So, dropping the spin-orbit term from 3.8 leads to another two coupled equations

$$\begin{aligned}\phi_l &= \frac{1}{2Mc}\frac{\partial g_l}{\partial r}\\ \frac{\partial \phi_l}{\partial r} &= \frac{-2\phi_l}{r}\left[\frac{l(l+1)}{2Mcr^2}+\frac{V-E}{c}\right]g_l\end{aligned}$$

Putting

$$P=rg \qquad Q=rc\phi$$

gives

$$\frac{\partial P}{\partial r} = \frac{P}{r}+2M\phi \quad (3.9)$$

$$\frac{\partial Q}{\partial r} = -\frac{Q}{r}+\left[\frac{l(l+1)}{2Mr^2}+V-E\right]P \quad (3.10)$$

Changing to a logarithmic grid which becomes more coarse as r increases

$$x=\ln r$$

leads to

$$\frac{\partial P}{\partial x} = P+2M\exp(x)Q \quad (3.11)$$

$$\frac{\partial Q}{\partial x} = -Q+\left[\frac{l(l+1)}{2M}\exp(-x)+(V-E)\exp(x)\right]P \quad (3.12)$$

Now as $r\to 0$, $V(r)\to -\frac{Z}{r}$ and $M\to \frac{Z}{2c^2 r}$, Z being the atomic nunber. So starting values for the numerical solution of 3.11 and 3.12 are (from 3.9 and 3.10)

$$q=\left(\frac{\alpha-1}{Z}\right)c^2$$

where

$$P = r^{\alpha} \qquad Q = qr^{\alpha}$$

The normalisation condition is

$$\begin{aligned} \int_0^{r_{MT}} r^2 g^2 \, dr &= 1 \\ \Rightarrow \int_0^{r_{MT}} P^2 \, dr &= 1 \end{aligned}$$

or on the logarithmic scale

$$\int_0^{\ln(r_{MT})} \exp(x) P^2 \, dx = 1$$

The energy derivative of g is obtained from

$$\frac{\partial \dot{P}}{\partial x} = \dot{P} + 2M \exp(x) \dot{Q} + \frac{\exp(x) Q}{c^2} \tag{3.13}$$

and

$$\begin{aligned} \frac{\partial \dot{Q}}{\partial x} &= -\dot{Q} + \left[\frac{l(l+1)}{2M} \exp(-x) + (V - E) \exp(x) \right] \dot{P} \\ &- \left[\frac{l(l+1)}{4M^2 c^2} \exp(-x) + \exp(x) \right] \dot{P} \end{aligned} \tag{3.14}$$

The starting values for 3.13 and 3.14 are $\dot{P} = \dot{Q} = 0$.

3.11, 3.12, 3.13, 3.14 are solved using Milne's predictor-corrector method [30]. The foremention starting values are used to generate the first six values using the Runge-Kutta algorithm [30], which are then used to initiate the Milne algorithm.

The integration in 3.3 uses Simpson's rule on a grid of points. The contribution up to the first grid point, r_1, is explicitly added, but only for the $l = 0$ component. The value of $g(r)$ for $r < r_1$ and $l \neq 0$ is insignificant. For $r < r_1$ and $l = 0$, $g \approx$ constant. Hence

$$\int_0^{r_1} dr \, r^2 g = \frac{r_1 P_1^2}{3}$$

Hence, g and $\frac{\partial g}{\partial E}$ are calculated, as required for the construction of the LAPW basis. Note that the energies at which the radial equation is solved can

be different for each l. The exact choice of $\{E_l\}$ is not critical in the LAPW method. Koelling and Arbman [29] suggest using the E_l at the centre of the band for that l character. They also find that the $\{E_l\}$ can differ from the true eigenvalues by up to 0.5Ryd. for non-d-states, and 0.1Ryd. for d-states, while still maintaining good accuracy.

3.4 Construction of the LAPW Basis in the Interface

The LAPWs in the interstitial region are defined to be

$$\phi_{m,n}(\mathbf{K},\mathbf{r}) = \sqrt{\frac{2}{\Omega}}\exp(i\mathbf{K}_m.\mathbf{R}) \begin{cases} \cos k_n z & n \text{ even} \\ \sin k_n z & n \text{ odd} \end{cases} \tag{3.15}$$

where

$$\begin{aligned} \mathbf{K}_m &= \mathbf{K} + \mathbf{G}_m \\ \mathbf{G}_m &= h\mathbf{b}_1 + k\mathbf{b}_2 \qquad h,k \in \mathcal{Z} \\ \mathbf{r} &= \mathbf{R} + z\hat{\mathbf{k}} \\ k_n &= \frac{n\pi}{\tilde{D}} \\ \Omega &= AD \end{aligned}$$

A is the area of the 2-D unit cell, and D is the slab thickness. k_n is defined over $\tilde{D}$, not D, in order to give sufficient variational freedom to the basis when matching the logarithmic derivatives of the wavefunction over the embedding planes.

The LAPWs are put in the order even first, then odd, with each section being ordered in terms of increasing $|\mathbf{K}_m|^2 + k_n^2$.

Inside the muffin-tins the LAPW is the large component of the solution of the radial Dirac equation with no spin-orbit coupling, as derived in section 3.3. We write in muffin-tin α

$$\phi_{m,n,\alpha}(\mathbf{r}) = \sum_{l,m}\left[A_{l,m,\alpha}(\mathbf{K})u_{l,\alpha}(r) + B_{l,m,\alpha}(\mathbf{K})\dot{u}_{l,\alpha}(r)\right]Y_{l,m}(\hat{\mathbf{r}}) \begin{cases} i^l \\ i^{l-1} \end{cases} \tag{3.16}$$

where the upper term is for n even, and the lower for n odd. This convention will be implied in future equations. Also

$$\mathbf{k} = \mathbf{K} + k_n \hat{\mathbf{z}}$$

For r on the surface of muffin-tin α write $\mathbf{r} = \mathbf{r}_\alpha + \underset{\sim}{\rho}_\alpha$.

i.e.

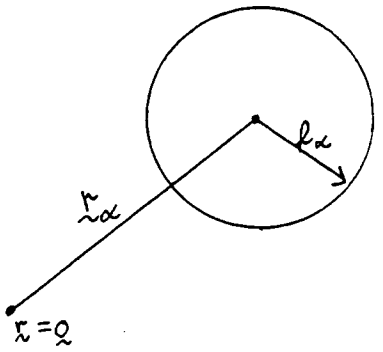

Write 3.15 in the form

$$\phi_{m,n} = \sqrt{\frac{2}{\Omega}} \exp(i\mathbf{K}_m.\mathbf{r}_\alpha) \begin{cases} \frac{1}{2} \\ \frac{1}{2i} \end{cases} \times \left[\exp\left(i\left(\mathbf{K}_m.\underset{\sim}{\rho}_\alpha + k_n\rho_{\alpha,z}\right)\right)\exp(ik_nz_\alpha)\right.$$
$$\left. \pm \exp\left(i\left(\mathbf{K}_m.\underset{\sim}{\rho}_\alpha - k_n\rho_{\alpha,z}\right)\right)\exp(-ik_nz_\alpha)\right]$$

Defining

$$\mathbf{K}^{\pm}_{m,n} = \mathbf{K}_m \pm k_n\hat{\mathbf{z}}$$

and using the Rayleigh expansion of a plane wave

$$\exp(i\mathbf{K}.\underset{\sim}{\rho}_\alpha) = 4\pi \sum_{l,m} i^l \mathcal{J}_l(K\rho_\alpha) Y^*_{l,m}(\hat{\mathbf{K}}) Y_{l,m}(\hat{\underset{\sim}{\rho}}_\alpha) \tag{3.17}$$

where $\mathcal{J}_l$ is the Bessel function of order l, gives $\phi_{m,n}$ in the interstitial region as

$$\begin{aligned} \phi_{m,n} &= \sqrt{\frac{2}{\Omega}} 2\pi \begin{cases} 1 \\ i \end{cases} \exp\left(i\mathbf{K}_m.\mathbf{r}_\alpha\right) \sum_{l,m} i^l \left[\exp\left(ik_nz_\alpha\right) Y^*_{l,m}(\hat{\mathbf{K}}^+_{m,n})\right. \\ &\pm \left.\exp\left(-ik_nz_\alpha\right) Y^*_{l,m}(\hat{\mathbf{K}}^-_{m,n})\right] \mathcal{J}_l(K_m\rho_\alpha) Y_{l,m}(\hat{\underset{\sim}{\rho}}_\alpha) \end{aligned} \tag{3.18}$$

Use 3.16, 3.18, and their first derivative with respect to ρ, to solve for $A_{l,m,\alpha}$, $B_{l,m,\alpha}$. This produces

$$A_{l,m,\alpha} = \frac{4\pi}{\sqrt{\Omega}} \exp\left(i\mathbf{K}_m.\mathbf{R}_\alpha\right) Y^{\pm}_{l,m,\alpha}(m,n) \frac{\mathcal{J}_l \dot{u}'_{l,\alpha} - \mathcal{J}'_l u_{l,\alpha}}{u_{l,\alpha}\dot{u}'_{l,\alpha} - u'_{l,\alpha}\dot{u}_{l,\alpha}}$$

$$B_{l,m,\alpha} = \frac{4\pi}{\sqrt{\Omega}} \exp\left(i\mathbf{K}_m.\mathbf{R}_\alpha\right) Y^{\pm}_{l,m,\alpha}(m,n) \frac{\mathcal{J}_l u'_{l,\alpha} - \mathcal{J}'_l u_{l,\alpha}}{u'_{l,\alpha}\dot{u}_{l,\alpha} - u_{l,\alpha}\dot{u}_{l,\alpha}}$$

where

$$Y^{\pm}_{l,m,\alpha}(m,n) = \frac{1}{\sqrt{2}}\left[\exp\left(ik_n z_\alpha\right) Y^{*}_{l,m}(\hat{\mathbf{K}}^{+}_{m,n}) \pm \exp\left(-ik_n z_\alpha\right) Y^{*}_{l,m}(\hat{\mathbf{K}}^{-}_{m,n})\right] \quad (3.19)$$

$u_{l,\alpha}$, $\dot{u}_{l,\alpha}$, $u'_{l,\alpha}$, $\dot{u}'_{l,\alpha}$ are evaluated at $\mathbf{r} = \underline{\rho}_\alpha$.

Define

$$W = \rho_\alpha^2(u_{l,\alpha}\dot{u}'_{l,\alpha} - u'_{l,\alpha}\dot{u}_{l,\alpha})$$

to give

$$A_{l,m,\alpha} = \frac{4\pi\rho_\alpha^2}{\sqrt{\Omega}} \exp\left(i\mathbf{K}_m.\mathbf{R}_\alpha\right) a_{l,\alpha}(m,n) Y^{\pm}_{l,m,\alpha}(m,n) \quad (3.20)$$

$$B_{l,m,\alpha} = \frac{4\pi\rho_\alpha^2}{\sqrt{\Omega}} \exp\left(i\mathbf{K}_m.\mathbf{R}_\alpha\right) b_{l,\alpha}(m,n) Y^{\pm}_{l,m,\alpha}(m,n) \quad (3.21)$$

where

$$a_{l,\alpha}(m,n) = \frac{1}{W}\left[\mathcal{J}_l(K_{m,n}\rho_\alpha)\dot{u}'_{l,\alpha} - \frac{\partial}{\partial\rho}\left(\mathcal{J}_l(K_{m,n}\rho_\alpha)\right)\dot{u}_{l,\alpha}\right]$$

$$b_{l,\alpha}(m,n) = \frac{1}{W}\left[\frac{\partial}{\partial\rho}\left(\mathcal{J}_l(K_{m,n}\rho_\alpha)\right)u_{l,\alpha} - \mathcal{J}_l(K_{m,n}\rho_\alpha)u'_{l,\alpha}\right]$$

We now have the LAPW basis.

3.5 Form of Potential used in the Interface

The simple muffin-tin type of potential was described in section 1.3. In the interface region we do not restrict the potential to have this form, but include non-spherical components within the spheres, and a Fourier expansion in the interstitial region. Within the spheres we write

$$V(\mathbf{r}) = \sum_{l,m\geq 0} \left[V_{l,m}(r)\cos m\phi + V_{l,-m}\sin m\phi\right] P_{l,m}(\theta) \quad (3.22)$$

The $P_{l,m}$ are the Legendre polynomials, and θ, ϕ are the usual spherical polar angles.

In the interstitial region we have the 'warping potential'

$$V(\mathbf{r}) = \sum_{m,n} V_{m,n} \exp(i\mathbf{G}_m.\mathbf{R}) \begin{cases} \cos k_n z \\ \sin k_n z \end{cases} + V_1 z + V_2 z^2$$
$$+ \sum_{m}{}' (V_{m,+} \exp(G_m z) + V_{m,-} \exp(-G_m z)) \exp(i\mathbf{G}_m.\mathbf{R}) \quad (3.23)$$

3.6 LAPW Matrix Elements

The overlap and Hamiltonian matrix elements must be evaluated. The matrix elements of the warping potential are also required.

Overlap Inside the Muffin-Tins

Consider first the even-even and odd-odd contributions. The following results are required

$$\sum_m Y^*_{l,m}(\hat{\mathbf{K}}^+_{m,n}) Y_{l,m}(\hat{\mathbf{K}}^+_{m',n'}) = \frac{2l+1}{4\pi} P_l(\mathbf{K}^+_{m,n}.\mathbf{K}^-_{m,n}) \quad (3.24)$$

$$\Rightarrow \frac{1}{2} \sum_m \left(\exp(-ik'_n z_\alpha) Y_{l,m}(\hat{\mathbf{K}}^+_{m',n'}) \pm \exp(ik'_n z_\alpha) Y_{l,m}(\hat{\mathbf{K}}^-_{m',n'}) \right)$$
$$\times \left(\exp(ik_n z_\alpha) Y^*_{l,m}(\hat{\mathbf{K}}^+_{m,n}) \pm \exp(-ik_n z_\alpha) Y^*_{l,m}(\hat{\mathbf{K}}^-_{m,n}) \right)$$
$$= \frac{2l+1}{4\pi} \left\{ [\cos(k_n - k_{n'}) z_\alpha] P_l(\mathbf{K}^+_{m,n}.\mathbf{K}^+_{m',n'}) \right.$$
$$\left. \pm [\cos(k_n + k_{n'}) z_\alpha] P_l(\mathbf{K}^+_{m,n}.\mathbf{K}^-_{m',n'}) \right\} \quad (3.25)$$

So, putting 3.20, and 3.21 in 3.16 and using 3.19 and 3.25 gives for the even-even and odd-odd overlap (summing over the muffin tins α)

$$\left\langle \phi^\pm_{m',n'} \mid \phi^\pm_{m,n} \right\rangle = \frac{4\pi}{\Omega} \sum_\alpha \rho^4_\alpha \exp(i(\mathbf{K}_m - \mathbf{K}_{m'}).\mathbf{R}_\alpha$$
$$\times \sum_l (2l+1) (a_{l,\alpha}(m',n') a_{l,\alpha}(m,n) + b_{l,\alpha}(m',n') b_{l,\alpha}(m,n) N_{l,\alpha})$$
$$\times \left\{ [\cos(k_n - k'_n) z_\alpha] P_l(\mathbf{K}^+_{m,n}.\mathbf{K}^+_{m',n'}) \pm [\cos(k_n + k'_n) z_\alpha] P_l(\mathbf{K}^+_{m,n}.\mathbf{K}^-_{m',n'}) \right\}$$

where

$$N_{l,\alpha} = \int_0^{\rho_\alpha} r^2 u^2_{l,\alpha} \, dr$$

A similar derivation gives the even-odd term as

$$\left\langle \phi^{+}_{m',n'} \mid \phi^{-}_{m,n} \right\rangle = \frac{4\pi}{\Omega} \sum_{\alpha} \rho_{\alpha}^{4} \exp(i(\mathbf{K}_m - \mathbf{K}_{m'}).\mathbf{R}_{\alpha}$$
$$\times \sum_{l} (2l+1) \left(a_{l,\alpha}(m',n') a_{l,\alpha}(m,n) + b_{l,\alpha}(m',n') b_{l,\alpha}(m,n) N_{l,\alpha} \right)$$
$$\times \left\{ [\sin(k_n - k_{n'}) z_{\alpha}] \, P_l(\mathbf{K}^{+}_{m,n}.\mathbf{K}^{+}_{m',n'}) + [\sin(k_n + k_{n'}) z_{\alpha}] \, P_l(\mathbf{K}^{+}_{m,n}.\mathbf{K}^{-}_{m',n'}) \right\}$$

Hamiltonian Inside the Muffin-Tins

The even-even/odd-odd terms, after some manipulation are

$$\left\langle \phi^{\pm}_{m',n'} \middle| \phi^{\pm}_{m,n} \right\rangle = \frac{4\pi}{\Omega} \sum_{\alpha} \rho_{\alpha}^{4} \exp(i(\mathbf{K}_m - \mathbf{K}_{m'}).\mathbf{R}_{\alpha}$$
$$\times \sum_{l} (2l+1) \left(a_{l,\alpha}(m',n') a_{l,\alpha}(m,n) E_l + b_{l,\alpha}(m',n') b_{l,\alpha}(m,n) \left\langle \dot{u}_{l,\alpha} \middle| H \middle| \dot{u}_{l,\alpha} \right\rangle \right.$$
$$\left. + a_{l,\alpha}(m',n') b_{l,\alpha}(m,n) \left\langle u_{l,\alpha} \middle| H \middle| \dot{u}_{l,\alpha} \right\rangle \right)$$
$$\times \left\{ [\cos(k_n - k_{n'}) z_{\alpha}] \, P_l(\mathbf{K}^{+}_{m,n}.\mathbf{K}^{+}_{m',n'}) \pm [\cos(k_n + k_{n'}) z_{\alpha}] \, P_l(\mathbf{K}^{+}_{m,n}.\mathbf{K}^{-}_{m',n'}) \right\}$$

The even-odd term is

$$\left\langle \phi^{+}_{m',n'} \middle| \phi^{-}_{m,n} \right\rangle = \frac{4\pi}{\Omega} \sum_{\alpha} \rho_{\alpha}^{4} \exp(i(\mathbf{K}_m - \mathbf{K}_{m'}).\mathbf{R}_{\alpha}$$
$$\times \sum_{l} (2l+1) \left(a_{l,\alpha}(m',n') a_{l,\alpha}(m,n) E_l + b_{l,\alpha}(m',n') b_{l,\alpha}(m,n) \left\langle \dot{u}_{l,\alpha} \middle| H \middle| \dot{u}_{l,\alpha} \right\rangle \right.$$
$$+ a_{l,\alpha}(m',n') a_{l,\alpha}(m,n) E_l + b_{l,\alpha}(m',n') b_{l,\alpha}(m,n) \left\langle \dot{u}_{l,\alpha} \middle| H \middle| \dot{u}_{l,\alpha} \right\rangle$$
$$\left. + a_{l,\alpha}(m',n') b_{l,\alpha}(m,n) \left\langle u_{l,\alpha} \middle| H \middle| \dot{u}_{l,\alpha} \right\rangle \right)$$
$$\times \left([\sin(k_n - k_{n'}) z_{\alpha}] \, P_l(\mathbf{K}^{+}_{m,n}.\mathbf{K}^{+}_{m',n'}) + [\sin(k_n + k_{n'}) z_{\alpha}] \, P_l(\mathbf{K}^{+}_{m,n}.\mathbf{K}^{-}_{m',n'}) \right)$$

Overlap in the Interstitial Region

The even-even/odd-odd terms are

$$\begin{aligned} \left\langle \phi^{\pm}_{m',n'} \middle| \phi^{\pm}_{m,n} \right\rangle &= \int_{\zeta_2}^{\zeta_1} dz \int_{\text{2D unit cell}} \tilde{\phi}^{\pm *}_{m',n'} \tilde{\phi}^{\pm}_{m,n} \, d^2\mathbf{R} \\ &- \sum_{\alpha} \int_{\mathbf{r} \text{ in MT } \alpha} \tilde{\phi}^{\pm *}_{m',n'} \tilde{\phi}^{\pm}_{m,n} \, d^3r \end{aligned} \tag{3.26}$$

Note that ζ_2 is negative.

$\tilde{\phi}_{m,n} = \phi_{m,n}$ in the interstitial region and its continuation into the muffin-tins.

The first term in 3.26 is (using 3.15)

$$\frac{2\delta_{m',m}}{D}\int_{\zeta_2}^{\zeta_1} dz \begin{cases} \cos k_{n'}z \\ \sin k_{n'}z \end{cases} \begin{cases} \cos k_n z \\ \sin k_n z \end{cases} \tag{3.27}$$

After integration this is

$$\frac{\delta_{m',m}}{D}\left[\frac{-\sin(k_{n'}-k_n)\zeta_2}{k_{n'}-k_n} \mp \frac{\sin(k_{n'}+k_n)\zeta_2}{k_{n'}+k_n} + \frac{\sin(k_{n'}-k_n)\zeta_1}{k_{n'}-k_n} \pm \frac{\sin(k_{n'}+k_n)\zeta_1}{k_{n'}+k_n}\right] \tag{3.28}$$

The choice of signs is determined by the integrand in 3.27.

If $k_{n'} = k_n$, we have

$$\frac{\delta_{m',m}}{D}\int_{\zeta_2}^{\zeta_1} dz\,(1 \pm \cos 2k_n z) = \frac{\delta_{m',m}}{D}\left[\zeta_1 - \zeta_2 \mp \frac{\sin 2k_n\zeta_2}{2k_n} \pm \frac{\sin 2k_n\zeta_1}{2k_n}\right]$$

Now the second term in 3.26 is

$$\begin{aligned}\frac{2}{\Omega}\int_{\mathbf{r}\text{ in MT }\alpha} d^3r\,\exp\left(i(\mathbf{K}_m - \mathbf{K}_{n'}).\mathbf{R}\right) &\begin{cases} \cos k_{n'}z \\ \sin k_{n'}z \end{cases} \begin{cases} \cos k_n z \\ \sin k_n z \end{cases} \\ = \frac{4\pi}{\Omega}\rho_\alpha^2 \exp(i(\mathbf{K}_m - \mathbf{K}_{m'}).\mathbf{R}_\alpha &\left\{[\cos(k_n - k_{n'})z_\alpha]\, J_\alpha\left(\mathbf{K}^+_{m',n'}, \mathbf{K}^+_{m,n}\right)\right. \\ &\left. \pm\,[\cos(k_n + k_{n'})z_\alpha]\, J_\alpha\left(\mathbf{K}^+_{m',n'}, \mathbf{K}^-_{m,n}\right)\right\} \end{aligned} \tag{3.29}$$

using

$$\int_0^{\rho_\alpha} d\underline{\rho}\,\exp(i\mathbf{K}.\underline{\rho}) = \frac{4\pi\rho_\alpha^2}{K}\mathcal{J}_1(K\rho_\alpha) \tag{3.30}$$

and defining

$$J_\alpha(\mathbf{K}_1, \mathbf{K}_2) = \frac{\mathcal{J}_1(|\mathbf{K}_1 - \mathbf{K}_2|\rho_\alpha)}{|\mathbf{K}_1 - \mathbf{K}_2|}$$

If $\mathbf{K}_{m,n} - \mathbf{K}_{m',n'} = \mathbf{0}$, then $J_\alpha = \frac{\rho_\alpha}{3}$

Grouping 3.28 and 3.29 together gives

$$\left\langle \phi^{\pm}_{m',n'} \middle| \phi^{\pm}_{m,n} \right\rangle = \frac{\delta_{m,m'}}{D} \left\{ \frac{-\sin(k_{n'}-k_n)\zeta_2}{k_{n'}-k_n} \mp \frac{\sin(k_{n'}+k_n)\zeta_2}{k_{n'}+k_n} \right.$$
$$+\frac{\sin(k_{n'}-k_n)\zeta_1}{k_{n'}-k_n} \pm \frac{\sin(k_{n'}+k_n)\zeta_1}{k_{n'}+k_n}$$
$$-\frac{4\pi}{\Omega}\sum_{\alpha}\rho_{\alpha}^2 \exp(i(\mathbf{K}_m-\mathbf{K}_{m'}).\mathbf{R}_{\alpha}\left([\cos(k_{n'}-k_n)z_{\alpha}]J_{\alpha}\left(\mathbf{K}^{+}_{m',n'},\mathbf{K}^{+}_{m,n}\right)\right.$$
$$\left.\left. \pm [\cos(k_{n'}+k_n)z_{\alpha}]J_{\alpha}\left(\mathbf{K}^{+}_{m',n'},\mathbf{K}^{-}_{m,n}\right)\right)\right\}$$

The even-odd overlap is likewise derived, giving

$$\left\langle \phi^{+}_{m',n'} \middle| \phi^{-}_{m,n} \right\rangle = \frac{\delta_{m,m'}}{D} \left\{ \frac{-\cos(k_{n'}+k_n)\zeta_1}{k_{n'}+k_n} + \frac{\cos(k_{n'}+k_n)\zeta_2}{k_{n'}+k_n} \right.$$
$$\left. + \frac{\cos(k_{n'}-k_n)\zeta_1}{k_{n'}-k_n} - \frac{\cos(k_{n'}-k_n)\zeta_2}{k_{n'}-k_n} \right\}$$
$$-\frac{4\pi}{\Omega}\sum_{\alpha}\rho_{\alpha}^2 \exp(i(\mathbf{K}_m-\mathbf{K}_{m'}).\mathbf{R}_{\alpha}\left\{-\sin[(k_{n'}-k_n)z_{\alpha}]J_{\alpha}\left(\mathbf{K}^{+}_{m',n'},\mathbf{K}^{+}_{m,n}\right)\right.$$
$$\left. + \sin[(k_{n'}+k_n)z_{\alpha}]J_{\alpha}\left(\mathbf{K}^{+}_{m',n'},\mathbf{K}^{-}_{m,n}\right)\right\}$$

Hamiltonian in the Interstitial Region

This is

$$\langle \phi_{m',n'} | H | \phi_{m,n} \rangle = \frac{|\mathbf{K}_m|^2 + k_n^2}{2} \langle \phi_{m',n'} | \phi_{m,n} \rangle$$

This assumes zero potential in the interstitial region, and does not include the warping potential. As there is a potential shift across the interface, the potential used in shifting the embedding planes is not zero at both sides. The integral of the constant substrate potentials across the muffin-tin caps which intersect the embedding planes must therefore be added/subtracted. The following diagram shows the signs to be used when adding the volume

integrals over the caps.

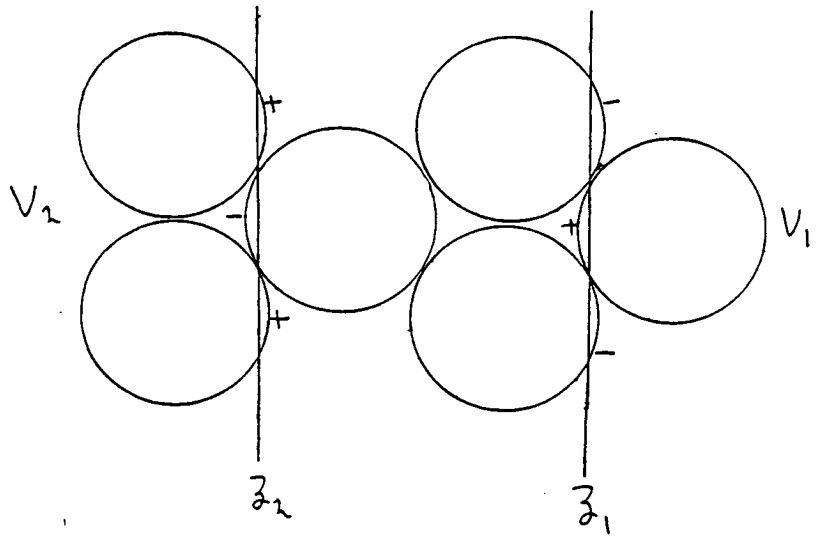

In practice, the addition of these terms is done in the program along with the evaluation of the warping potential, but this is purely for convenience. Before considering the evaluation of the warping potential matrix elements, the surface integrals in the Hamiltonian 1.16 will be dealt with.

On ζ_1, i.e. S_2, we have

$$\frac{1}{2}\int_{\zeta_1} d^2r_{S_2}\,\phi^*_{m',n'}\frac{\partial\phi_{m,n}}{\partial z}$$

$$= \frac{k_n}{\Omega}\int_{\text{2D cell}} d^2R\,\exp\left(i(\mathbf{K}_m-\mathbf{K}_{n'}).\mathbf{R}\right)\begin{cases}\cos k_{n'}\zeta_1\\ \sin k_{n'}\zeta_1\end{cases}\begin{cases}-\sin k_n\zeta_1\\ \cos k_n\zeta_1\end{cases}$$

$$= \delta_{m,m'}\frac{k_n}{D}\begin{cases}\cos k_{n'}\zeta_1\\ \sin k_{n'}\zeta_1\end{cases}\begin{cases}-\sin k_n\zeta_1\\ \cos k_n\zeta_1\end{cases}$$

On ζ_2, i.e. S_3, we have a similar contribution

$$\frac{1}{2}\int_{\zeta_2} d^2r_{S_3}\,\phi^*_{m',n'}\frac{\partial\phi_{m,n}}{\partial z} = \delta_{m',m}\frac{k_n}{D}\begin{cases}\cos k_{n'}\zeta_2\\ \sin k_{n'}\zeta_2\end{cases}\begin{cases}-\sin k_n\zeta_2\\ \cos k_n\zeta_2\end{cases}$$

Now consider the matrix elements of the warping potential. The potential is defined in equations 3.22 and 3.23. Consider first the warping potential in the muffin-tins. Write 3.22 in the form

$$V(\mathbf{r}) = \frac{1}{2} \sum_{l,m \geq 0} \Big[V_{l,m}(r) \left\{ Y_{l,m}(\theta,\phi) + Y^*_{l,m}(\theta,\phi) \right\} \\ -iV_{l,-m}(r) \left\{ Y_{l,m}(\theta,\phi) - Y^*_{l,m}(\theta,\phi) \right\} \Big] \tag{3.31}$$

The matrix element between $\phi_{m,n}$ and $\phi_{m',n'}$ of a typical term in 3.31 is

$$\sum_{l,l',m,m'} \int_{\mathbf{r} \text{ in MT } \alpha} d^3r \left(A^*_{l',m',\alpha}(m',n') u_{l',\alpha} + B_{l',m',\alpha}(m',n') \dot{u}_{l',\alpha} \right) V_{l'',m''}(r) \\ \times \left(A_{l,m,\alpha}(m,n) u_{l,\alpha} + B_{l,m,\alpha}(m,n) \dot{u}_{l,\alpha} \right) Y^*_{l',m'} Y_{l'',m''} Y_{l,m} \\ \times \begin{cases} -i^{l'} \\ -i^{l'-1} \end{cases} \begin{cases} i^{l} \\ i^{l-1} \end{cases}$$

$$= \sum_{l,l',m,m'} \int_{\mathbf{r} \text{ in MT } \alpha} d^3r \, Y^*_{l',m'} Y_{l'',m''} Y_{l,m} \\ \times \Big\{ A^*_{l',m',\alpha}(m',n') A_{l,m,\alpha}(m,n) \int_\alpha r^2 u_{l',\alpha} V_{l'',m''} u_{l,\alpha} \, dr \\ + B_{l',m',\alpha}(m',n') B_{l,m,\alpha}(m,n) \int_\alpha r^2 \dot{u}_{l',\alpha} V_{l'',m''} \dot{u}_{l,\alpha} \, dr \\ + A^*_{l',m',\alpha}(m',n') B_{l,m,\alpha}(m,n) \int_\alpha r^2 u_{l',\alpha} V_{l'',m''} \dot{u}_{l,\alpha} \, dr \\ + B_{l',m',\alpha}(m',n') A_{l,m,\alpha}(m,n) \int_\alpha r^2 \dot{u}_{l',\alpha} V_{l'',m''} u_{l,\alpha} \, dr \Big\} \\ \times \begin{cases} -i^{l'} \\ -i^{l'-1} \end{cases} \begin{cases} i^{l} \\ i^{l-1} \end{cases} \tag{3.32}$$

To evaluate 3.32 the following procedure is used

1. Determine the $\{A_{l,m,\alpha}, B_{l,m,\alpha}\}$
2. Evaluate the radial integrals in 3.32
3. Evaluate the part of 3.32 independent of (m,n) and (m',n')

The radial integrals for different atoms in the same star are easily determined from those for one atom, by operating on the $V_{l'',m''}$ and $V_{l'',-m''}$ integrals with the symmetry matrices.

The matrix elements of the warping potential in the interstitial region are somewhat more complicated to evaluate. They must be evaluated between the **true** embedding planes, with no warping potential between these and the flat embedding planes.

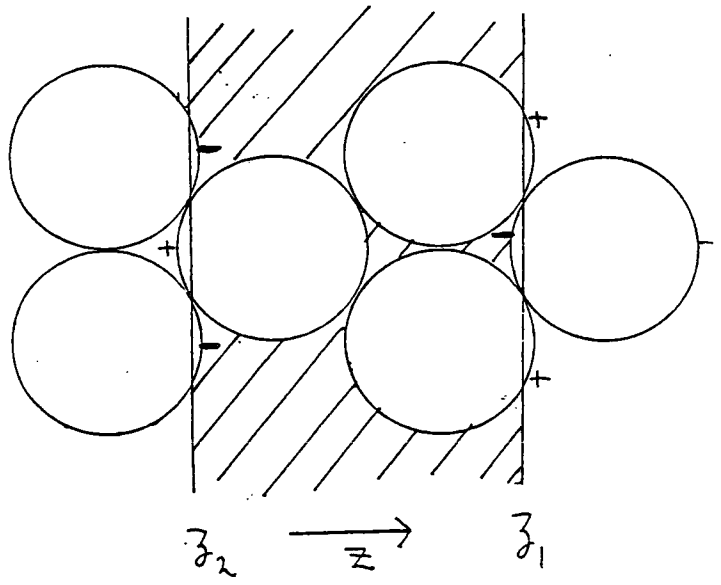

We only evaluate the matrix elements of the warping potential in the shaded region. In practice this is done by evaluating the matrix elements between ζ_2 and ζ_1, and subtracting the volume integrals of V_{warp} over the muffin-tin caps which intersect ζ_1 and ζ_2. It is also at this stage where the cap integrals of the constant substrate potentials referred to earlier are incorporated.

The general form of the matrix elements of the warping potential is as follows.

$$\begin{aligned}\langle \phi_{m',n'} | V_{warp} | \phi_{m,n} \rangle &= \int_{\zeta_2}^{\zeta_1} dz \int_{\text{2D cell}} \phi^*_{m',n'} V_{warp} \phi_{m,n} \, d^2R \\ &- \sum_{\alpha} \int_{\text{r in MT-}\alpha} d^3r \, \phi^*_{m',n'} V_{warp} \phi_{m,n} \\ &\pm \sum_{\beta} \int_{\text{r in cap } \beta} d^3r \, \phi^*_{m',n'} V_{warp} \phi_{m,n} \qquad (3.33)\end{aligned}$$

The sign in the last integral of 3.33 over the caps is as shown in the previous diagram.

Consider first the plane wave contribution from the first term in 3.23 to the first term in 3.33. This is

$$\frac{2}{\Omega}V_{m'',n''}\int_{\zeta_2}^{\zeta_1}dz\int_{\text{2D unit cell}}d^2R\,\exp\left(i(\mathbf{K}_m+\mathbf{G}_{m''}-\mathbf{K}_{m'}).\mathbf{R}\right)$$
$$\times\begin{Bmatrix}\cos k_{n'}z\\ \sin k_{n'}z\end{Bmatrix}\begin{Bmatrix}\cos k_{n''}z\\ \sin k_{n''}z\end{Bmatrix}\begin{Bmatrix}\cos k_nz\\ \sin k_nz\end{Bmatrix} \tag{3.34}$$

$$=\frac{2V_{m'',n''}}{D}\delta_{m'',m'-m}\int_{\zeta_2}^{\zeta_1}dz\begin{Bmatrix}\cos k_{n'}z\\ \sin k_{n'}z\end{Bmatrix}\begin{Bmatrix}\cos k_{n''}z\\ \sin k_{n''}z\end{Bmatrix}\begin{Bmatrix}\cos k_nz\\ \sin k_nz\end{Bmatrix} \tag{3.35}$$

The trigonometric triple products can be expanded as

$$\begin{Bmatrix}\cos k_{n'}z\\ \sin k_{n'}z\end{Bmatrix}\begin{Bmatrix}\cos k_{n''}z\\ \sin k_{n''}z\end{Bmatrix}\begin{Bmatrix}\cos k_nz\\ \sin k_nz\end{Bmatrix}=\frac{1}{4}\sum_{i=1}^{4}\begin{Bmatrix}a_i\cos\kappa_iz\\ b_i\sin\kappa_iz\end{Bmatrix} \tag{3.36}$$

where

$$\kappa_1=k_{n'}+k_{n''}-k_n \qquad \kappa_2=k_{n'}-k_{n''}+k_n$$
$$\kappa_3=-k_{n'}+k_{n''}+k_n \qquad \kappa_4=k_{n'}+k_{n''}+k_n$$

The $\{a_i,b_i\}$ in 3.36 are given by the following table.

ccc	$a_i=1,1,1,1$
ccs	$b_i=-1,1,1,1$
csc	$b_i=1,-1,1,1$
css	$a_i=1,1,-1,-1$
scc	$b_i=1,1,-1,1$
scs	$a_i=1,-1,1,-1$
ssc	$a_i=-1,1,1,-1$
sss	$b_i=1,1,1,-1$

Note that 's'=sin and 'c'=cos. Where not explicitly stated, the relevant coefficients are zero.

Hence 3.35 becomes

$$\frac{V_{m'',n''}}{2D}\delta_{m'',m'-m}\sum_{i=1}^{4}\frac{1}{\kappa_i}\begin{Bmatrix}a_i\left(\sin\kappa_i\zeta_1-\sin\kappa_i\zeta_2\right)\\ b_i\left(-\cos\kappa_i\zeta_1+\cos\kappa_i\zeta_2\right)\end{Bmatrix}$$

The plane wave contribution to the second term in 3.33 is

$$\frac{V_{m'',n''}}{2\Omega}\sum_{i=1}^{4}\left\{\begin{array}{l}a_i\\ b_i\end{array}\right.\int_{\mathbf{r}\text{ in MT }\alpha} d^3r\,\exp\left(i(\mathbf{G}_m+\mathbf{G}_{m''}-\mathbf{G}_{m'}).\mathbf{R}\right)\left\{\begin{array}{l}\cos\kappa_i z\\ \sin\kappa_i z\end{array}\right. \tag{3.37}$$

Now, putting

$$\mathbf{G}(m,m'',m')=\mathbf{G}_m+\mathbf{G}_{m''}-\mathbf{G}_{m'} \tag{3.38}$$

and

$$\mathbf{r}=\mathbf{R}_\alpha+z_\alpha\hat{\mathbf{z}}+\underline{\rho}_\alpha$$

gives

$$\int d^3r\,\exp\left(i(\mathbf{G}_m+\mathbf{G}_{m''}-\mathbf{G}_{m'}).\mathbf{R}\right)\left\{\begin{array}{l}\cos\kappa_i z\\ \sin\kappa_i z\end{array}\right.$$

$$=\frac{4\pi\rho_\alpha^2}{|\mathbf{G}+\kappa_i\hat{\mathbf{z}}|}\exp\left(i\mathbf{G}.\mathbf{R}_\alpha\right)\left\{\begin{array}{l}\cos\kappa_i z_\alpha\\ \sin\kappa_i z_\alpha\end{array}\right.\mathcal{J}_1(|\mathbf{G}+\kappa_i\hat{\mathbf{z}}|\rho_\alpha)$$

where equation 3.30 has been used.

So 3.37 becomes

$$2\pi\rho_\alpha^2 V_{m'',n''}\sum_{i=1}^{4}\left\{\begin{array}{l}a_i\\ b_i\end{array}\right.\exp\left(i\mathbf{G}.\mathbf{R}_\alpha\right)\left\{\begin{array}{l}\cos\kappa_i z_\alpha\\ \sin\kappa_i z_\alpha\end{array}\right.\frac{\mathcal{J}_1(|\mathbf{G}+\kappa_i\hat{\mathbf{z}}|\rho_\alpha)}{|\mathbf{G}+\kappa_i\hat{\mathbf{z}}|}$$

Hence

$$\begin{aligned}\langle\phi_{m',n'}|V_{warp}|\phi_{m,n}\rangle_{pw}=&\sum_{m'',n''}\frac{V_{m'',n''}}{2}\sum_{i=1}^{4}\left\{\begin{array}{l}a_i\\ b_i\end{array}\right.\left[\frac{\delta_{m'',m'-m}}{D}\frac{1}{\kappa_i}\left\{\begin{array}{l}\sin\kappa_i\zeta_1-\sin\kappa_i\zeta_2\\ -\cos\kappa_i\zeta_1+\cos\kappa_i\zeta_2\end{array}\right.\right.\\ &\left.-\sum_\alpha\frac{4\pi}{\Omega}\rho_\alpha^2\exp\left(i\mathbf{G}.\mathbf{R}_\alpha\right)\left\{\begin{array}{l}\cos\kappa_i z_\alpha\\ \sin\kappa_i z_\alpha\end{array}\right.\frac{\mathcal{J}_1(|\mathbf{G}+\kappa_i\hat{\mathbf{z}}|\rho_\alpha)}{|\mathbf{G}+\kappa_i\hat{\mathbf{z}}|}\right]\\ &+\text{ corrections from the caps}\end{aligned}$$

The cap corrections will be dealt with later. The next stage is to consider the other terms in the warping potential (3.23), with regard to the first two terms in 3.33. So we require the matrix elements of the linear, quadratic, and exponential terms in 3.23.

Linear Term

The integral between ζ_2 and ζ_1 is

$$\frac{2V_I}{\Omega}\int_{\zeta_2}^{\zeta_1} dz \int_{\text{2D unit cell}} d^2R \exp\left(i(\mathbf{K}_m - \mathbf{K}_{n'}).\mathbf{R}\right) z \begin{Bmatrix} \cos k_{n'}z \\ \sin k_{n'}z \end{Bmatrix} \begin{Bmatrix} \cos k_n z \\ \sin k_n z \end{Bmatrix} \tag{3.39}$$

Writing

$$\begin{Bmatrix} \cos k_{n'}z \\ \sin k_{n'}z \end{Bmatrix} \begin{Bmatrix} \cos k_n z \\ \sin k_n z \end{Bmatrix} = \frac{1}{2}\sum_{i=1}^{2} \begin{Bmatrix} a_i \cos \kappa_i z \\ b_i \sin \kappa_i z \end{Bmatrix}$$

where

$$\kappa_1 = k_{n'} - k_n \qquad \kappa_2 = k_{n'} + k_n$$

and the $\{a_i, b_i\}$ are

$$\begin{aligned} \text{cc} \quad & a_i = 1, 1 \\ \text{cs} \quad & b_i = -1, 1 \\ \text{ss} \quad & a_i = 1, -1 \end{aligned}$$

gives 3.39, after some integration, as

$$\frac{V_I}{D}\delta_{m',m}\sum_{i=1}^{2}\frac{1}{\kappa_i^2}\begin{Bmatrix} a_i(\cos\kappa_i\zeta_1 - \cos\kappa_i\zeta_2 + \kappa_i\zeta_1 \sin\kappa_i\zeta_1 - \kappa_i\zeta_2 \sin\kappa_i\zeta_2) \\ b_i(\sin\kappa_i\zeta_1 - \sin\kappa_i\zeta_2 - \kappa_i\zeta_1 \cos\kappa_i\zeta_1 + \kappa_i\zeta_2 \cos\kappa_i\zeta_2) \end{Bmatrix} \tag{3.40}$$

When $\kappa_i = 0$

$$\int_{\zeta_2}^{\zeta_1} z\, dz = \frac{1}{2}(\zeta_1^2 - \zeta_2^2)$$

The muffin-tin contribution is

$$\frac{V_I}{\Omega}\sum_{i=1}^{2}\begin{Bmatrix} a_i \\ b_i \end{Bmatrix} \int_{\mathbf{r} \text{ in MT } \alpha} d^3r \exp\left(i(\mathbf{K}_m - \mathbf{K}_{n'}).\mathbf{R}\right) z \begin{Bmatrix} \cos\kappa_i z \\ \sin\kappa_i z \end{Bmatrix} \tag{3.41}$$

We require the result

$$\begin{aligned} &\int_{\mathbf{r} \text{ in MT } \alpha} d^3r\, z \exp\left(i(\mathbf{K}_m - \mathbf{K}_{n'}).\mathbf{R}\right) \exp(i\kappa_i z) \\ &\quad = \exp(i(\mathbf{K}_m - \mathbf{K}_{m'}).\mathbf{R}_\alpha \exp(i\kappa_i z_\alpha) \\ &\quad \times \left[z_\alpha \frac{4\pi\rho_\alpha^2}{\kappa^+}\mathcal{J}_1(\kappa^+\rho_\alpha) + \frac{4\pi i\rho_\alpha^3\kappa_i}{(\kappa^+)^2}\mathcal{J}_2(\kappa^+\rho_\alpha)\right] \end{aligned} \tag{3.42}$$

where

$$\kappa^+ = |\mathbf{K}_m - \mathbf{K}_{m'} + \kappa_i \hat{\mathbf{z}}|$$

As $\kappa_i \to 0$, 3.42 becomes

$$\frac{4\pi}{3}\rho_\alpha^3 z_\alpha$$

Taking real and imaginary parts of 3.42 gives the $\cos \kappa_i z$ and $\sin \kappa_i z$ integrals in 3.41 respectively, giving the final result (using 3.40) as

$$\langle \phi_{m',n'} | V_{warp} | \phi_{m,n} \rangle \text{ linear term} = V_1 \sum_{i=1}^{2} \left\{ \begin{array}{l} a_i \\ b_i \end{array} \right. \left[\frac{\delta_{m',m}}{D\kappa_i^2} \right.$$

$$\times \left\{ \begin{array}{l} \cos\kappa_i\zeta_1 - \cos\kappa_i\zeta_2 + \kappa_i\zeta_1 \sin\kappa_i\zeta_1 - \kappa_i\zeta_2 \sin\kappa_i\zeta_2 \\ \sin\kappa_i\zeta_1 - \sin\kappa_i\zeta_2 - \kappa_i\zeta_1 \cos\kappa_i\zeta_1 + \kappa_i\zeta_2 \cos\kappa_i\zeta_2 \end{array} \right.$$

$$- \sum_\alpha \frac{4\pi}{\Omega}\rho_\alpha^3 \exp(i(\mathbf{K}_m - \mathbf{K}_{m'}).\mathbf{R}_\alpha \left(z_\alpha \frac{\mathcal{J}_1(\kappa^+\rho_\alpha)}{\kappa^+\rho_\alpha} \left\{ \begin{array}{l} \cos\kappa_i z_\alpha \\ \sin\kappa_i z_\alpha \end{array} \right. \right.$$

$$\left. \left. + \frac{\kappa_i}{(\kappa^+)^2}\mathcal{J}_2(\kappa^+\rho_\alpha) \left\{ \begin{array}{l} -\sin\kappa_i z_\alpha \\ \cos\kappa_i z_\alpha \end{array} \right. \right) \right]$$

+ corrections from the caps

Quadratic Term

The derivation is similar to that for the linear term, but more cumbersome. The following result is required.

$$\int_{\mathbf{r} \text{ in MT } \alpha} d^3r \, \exp\left(i\left(\underline{\kappa}^+.\mathbf{r}\right)\right) z^2 = 4\pi\rho_\alpha^3 \exp(i(\mathbf{K}_m - \mathbf{K}_{m'}).\mathbf{R}_\alpha \exp(i\kappa_i z_\alpha)$$

$$\times \left\{ z_\alpha^2 \frac{\mathcal{J}_1(\kappa^+\rho_\alpha)}{\kappa^+\rho_\alpha} + \frac{2iz_\alpha\kappa_i}{(\kappa^+)^2}\mathcal{J}_2(\kappa^+\rho_\alpha) + \frac{(\kappa^+)^2 - 3\kappa_i^2}{3(\kappa^+)^3}\rho_\alpha\mathcal{J}_3(\kappa^+\rho_\alpha) \right.$$

$$\left. + \frac{1}{3(\kappa^+)^5\rho_\alpha^3}\left[(3(\kappa^+)^2\rho_\alpha^2 - 6)\sin\kappa^+\rho_\alpha - ((\kappa^+)^3\rho_\alpha^3 - \kappa^+\rho_\alpha)\cos\kappa^+\rho_\alpha\right]. \right\} \quad (3.43)$$

Taking real and imaginary parts of 3.43, and including the matrix element of z^2 over ζ_2 to ζ_1 gives

$$\begin{aligned}
&\langle\phi_{m',n'}|V_{warp}|\phi_{m,n}\rangle_{\text{quadratic term}} \\
&= V_2 \sum_{i=1}^{2} \left\{ \begin{array}{c} a_i \\ b_i \end{array} \right. \left[\frac{\delta_{m',m}}{D\kappa_i^3} \left\{ \begin{array}{l} 2\kappa_i\zeta_1 \cos\kappa_i\zeta_1 - 2\kappa_i\zeta_2 \cos\kappa_i\zeta_2 + \kappa_i^2\zeta_1^2 \sin\kappa_i\zeta_1 \\ 2\kappa_i\zeta_1 \sin\kappa_i\zeta_1 - 2\kappa_i\zeta_2 \sin\kappa_i\zeta_2 - \kappa_i^2\zeta_1^2 \cos\kappa_i\zeta_1 \end{array} \right. \right. \\
&\qquad\qquad -\kappa_i^2\zeta_2^2 \sin\kappa_i\zeta_2 - 2\sin\kappa_i\zeta_1 + 2\sin\kappa_i\zeta_2 \\
&\qquad\qquad +\kappa_i^2\zeta_2^2 \cos\kappa_i\zeta_2 + 2\cos\kappa_i\zeta_1 - 2\cos\kappa_i\zeta_2 \\
&- \sum_\alpha \frac{4\pi}{\Omega}\rho_\alpha^3 \exp(i(\mathbf{K}_m - \mathbf{K}_{m'}).\mathbf{R}_\alpha \left(z_\alpha^2 \frac{\mathcal{J}_1(\kappa^+\rho_\alpha)}{\kappa^+\rho_\alpha} \left\{ \begin{array}{c} \cos\kappa_i z_\alpha \\ \sin\kappa_i z_\alpha \end{array} \right. \right. \\
&+ \frac{2z\kappa_i}{(\kappa^+)^2}\mathcal{J}_2(\kappa^+\rho_\alpha) \left\{ \begin{array}{c} -\sin\kappa_i z_\alpha \\ \cos\kappa_i z_\alpha \end{array} \right. + \frac{(\kappa^+)^2 - 3\kappa_i^2}{3(\kappa^+)^3}\rho_\alpha \mathcal{J}_3(\kappa^+\rho_\alpha) \left\{ \begin{array}{c} \cos\kappa_i z_\alpha \\ \sin\kappa_i z_\alpha \end{array} \right. \\
&+ \left. \left. \frac{(3(\kappa^+)^2\rho_\alpha^2 - 6)\sin\kappa^+\rho_\alpha - ((\kappa^+)^3\rho_\alpha^3 - 6\kappa^+\rho_\alpha)\cos\kappa^+\rho_\alpha}{3(\kappa^+)^5\rho_\alpha^3} \left\{ \begin{array}{c} \sin\kappa_i z_\alpha \\ \cos\kappa_i z_\alpha \end{array} \right. \right) \right] \\
&+ \text{corrections from the caps} \qquad (3.44)
\end{aligned}$$

As $\kappa_i \to 0$, 3.44 becomes

$$\begin{aligned}
&\langle\phi_{m',0}|V_{warp}|\phi_{m,0}\rangle_{\text{quadratic term}} \\
&= \frac{2V_2\delta_{m',m}}{3}\left[\frac{(\zeta_1^3 - \zeta_2^3)}{D} - \sum_\alpha \frac{4\pi}{\Omega}\rho_\alpha^3\left(z_\alpha^2 + \frac{\rho_\alpha^2}{5}\right)\right]
\end{aligned}$$

Exponential Terms

The integral between ζ_2 and ζ_1 of $\exp(G_{m''}z)$ is

$$\begin{aligned}
&\frac{2V_{m'',+}}{\Omega}\int_{\zeta_2}^{\zeta_1} dz \int d^2R \exp\left(i(\mathbf{K}_m + \mathbf{G}_{m''} - \mathbf{K}_{m'}).\mathbf{R}\right) \\
&\qquad \times \left\{ \begin{array}{c} \cos k_{n'}z \\ \sin k_{n'}z \end{array} \right. \exp(G_{m''}z) \left\{ \begin{array}{c} \cos k_n z \\ \sin k_n z \end{array} \right. \qquad (3.45) \\
&= \frac{V_{m'',+}}{D}\delta_{m'',m'-m}\sum_{i=1}^{2} \left\{ \begin{array}{c} a_i \\ b_i \end{array} \right. \int_{\zeta_2}^{\zeta_1} dz \left\{ \begin{array}{c} \cos\kappa_i z \\ \sin\kappa_i z \end{array} \right. \exp(G_{m''}z) \qquad (3.46)
\end{aligned}$$

After integrating, 3.46 becomes

$$\frac{V_{m'',+}}{D}\delta_{m'',m'-m}\sum_{i=1}^{2}\left\{\begin{array}{ll} a_i & \frac{1}{|\mathbf{G}_{m''}|^2+\kappa_i^2} \\ b_i & \end{array}\right.$$
$$\times\left\{\begin{array}{l} (G_{m''}\cos\kappa_i\zeta_1+\kappa_i\sin\kappa_i\zeta_1)\exp(G_{m''}\zeta_1) \\ (G_{m''}\sin\kappa_i\zeta_1-\kappa_i\cos\kappa_i\zeta_1)\exp(G_{m''}\zeta_1) \end{array}\right.$$
$$+(-G_{m''}\cos\kappa_i\zeta_2-\kappa_i\sin\kappa_i\zeta_2)\exp(G_{m''}\zeta_2)$$
$$+(-G_{m''}\sin\kappa_i\zeta_2+\kappa_i\cos\kappa_i\zeta_2)\exp(G_{m''}\zeta_2) \qquad (3.47)$$

The muffin-tin terms are

$$\frac{V_{m'',+}}{\Omega}\sum_{i=1}^{2}\left\{\begin{array}{ll} a_i & \int_{\mathbf{r}\text{ in MT }\alpha} d^3r\,\exp\left(i(\mathbf{K}_m+\mathbf{G}_{m''}-\mathbf{K}_{m'}).\mathbf{R}\right) \\ b_i & \end{array}\right.$$
$$\times\exp(G_{m''}z)\left\{\begin{array}{l}\cos\kappa_i z \\ \sin\kappa_i z\end{array}\right. \qquad (3.48)$$

Now

$$\int_{\mathbf{r}\text{ in MT }\alpha} d^3r\,\exp\left(i(\mathbf{K}_m+\mathbf{G}_{m''}-\mathbf{K}_{m'}).\mathbf{R}\right)\exp(G_{m''}z)\exp(i\kappa_i z)$$
$$=\exp(G_{m''}z_\alpha)\exp(i(\mathbf{G}_m+\mathbf{G}_{m''}-\mathbf{G}_{m'}).\mathbf{R}_\alpha)\exp(i\kappa_i z_\alpha)$$
$$\times\int_0^{\rho_\alpha} d^3\rho\,\exp(i(\mathbf{G}_m+\mathbf{G}_{m''}-\mathbf{G}_{m'}).\mathbf{R}')\exp(G_{m''}z')\exp(i\kappa_i z') \qquad (3.49)$$

where $(\mathbf{R}', z')$ are now understood to be referred to the centre of muffin-tin alpha. In future the prime on these coordinates will be dropped, but has been included explicitly here, to avoid confusion. Write

$$\exp\left(i(\mathbf{G}_m+\mathbf{G}_{m''}-\mathbf{G}_{m'}).\mathbf{R}\right)\exp(G_{m''}z)\exp(i\kappa_i z)=\exp(iKr)$$

where

$$K=x-iy$$

and

$$x = +\frac{1}{2}\left\{|\mathbf{G}|^2+\kappa_i^2-G_{m''}^2+\sqrt{(|\mathbf{G}|^2+\kappa_i^2-G_{m''}^2)+4\kappa_i^2G_{m''}^2}\right\}^{\frac{1}{2}}$$
$$y = \pm\frac{1}{2}\left\{-|\mathbf{G}|^2-\kappa_i^2+G_{m''}^2+\sqrt{(|\mathbf{G}|^2+\kappa_i^2-G_{m''}^2)+4\kappa_i^2G_{m''}^2}\right\}^{\frac{1}{2}}$$

Note that $\mathbf{G}$ is defined as in 3.38. y has the same sign as $\kappa_i G_{m''}$.

Now $\exp(iKr)$ can be expanded using the Rayleigh expansion as in 3.17. On integrating 3.17 through the muffin-tin, only the $l = 0$ term is non-zero. This term is given as $\mathcal{J}_0(Kr)$. So

$$\begin{aligned}
&\int_0^{\rho_\alpha} d^3\rho \, \exp(i\mathbf{G}.\mathbf{R}) \exp(G_{m''} z) \exp(i\kappa_i z) \\
&= \int_o^{\rho_\alpha} d^3\rho \, \mathcal{J}_0([x - iy]\rho_\alpha) \\
&= 4\pi\rho_\alpha^2 \frac{\mathcal{J}_1([x - iy]\rho_\alpha)}{[x - iy]}
\end{aligned}$$

So 3.49 becomes

$$4\pi\rho_\alpha^2 \exp(G_{m''} z_\alpha) \exp(i\mathbf{G}.\mathbf{R}_\alpha) \exp(i\kappa_i z_\alpha) \frac{\mathcal{J}_1([x - iy]\rho_\alpha)}{[x - iy]} \tag{3.50}$$

If $\mathbf{G}_m = \mathbf{G}_{m'}$, $\kappa_i = 0$, then

$$\begin{aligned}
&\int_{\mathbf{r} \text{ in MT } \alpha} d^3 r \, \exp(i\mathbf{G}_{m''}.\mathbf{R}) \exp(\pm G_{m''} z) \\
&\quad = \frac{4\pi}{3}\rho_\alpha^3 \exp(i\mathbf{G}_{m''}.\mathbf{R}_\alpha) \exp(\pm G_{m''} z_\alpha)
\end{aligned}$$

Putting 3.50 in 3.48, taking the real and imaginary parts, and adding 3.47, gives for the $V_{m'',+}$ and $V_{m'',-}$ terms

$$
\begin{aligned}
&\langle \phi_{m',n'} | V_{warp} | \phi_{m,n} \rangle_{\text{exponential terms}} \\
&= \sum_{m''}{}' V_{m'',+} \sum_{i=1}^{2} \left\{ \begin{array}{l} a_i \\ b_i \end{array} \right. \left(\frac{\delta_{m'',m'-m}}{D(G_{m''}^2 + \kappa_i^2)} \right) \\
&\times \left\{ \begin{array}{l} (G_{m''} \cos \kappa_i \zeta_1 + \kappa_i \sin \kappa_i \zeta_1) \exp(G_{m''} \zeta_1) \\ (G_{m''} \sin \kappa_i \zeta_1 - \kappa_i \cos \kappa_i \zeta_1) \exp(G_{m''} \zeta_1) \end{array} \right. \\
&\quad + (-G_{m''} \cos \kappa_i \zeta_2 - \kappa_i \sin \kappa_i \zeta_2) \exp(G_{m''} \zeta_2) \\
&\quad + (-G_{m''} \sin \kappa_i \zeta_2 + \kappa_i \cos \kappa_i \zeta_2) \exp(G_{m''} \zeta_2) \\
&- \sum_{\alpha} \frac{4\pi}{\Omega} \rho_\alpha^2 \exp(i(\mathbf{G}_m + \mathbf{G}_{m''} - \mathbf{G}_{m'}).\mathbf{R}_\alpha) \exp(G_{m''} z_\alpha) \\
&\quad \times \left\{ \begin{array}{l} \text{Re} \\ \text{Im} \end{array} \right. \left(\exp(i\kappa_i z_\alpha) \frac{\mathcal{J}_1([x - iy]\rho_\alpha)}{[x - iy]} \right) \\
&+ \sum_{m''}{}' V_{m'',-} \sum_{i=1}^{2} \left\{ \begin{array}{l} a_i \\ b_i \end{array} \right. \left(\frac{\delta_{m'',m'-m}}{D(G_{m''}^2 + \kappa_i^2)} \right) \\
&\quad \times \left\{ \begin{array}{l} (-G_{m''} \cos \kappa_i \zeta_1 + \kappa_i \sin \kappa_i \zeta_1) \exp(-G_{m''} \zeta_1) \\ (-G_{m''} \sin \kappa_i \zeta_1 - \kappa_i \cos \kappa_i \zeta_1) \exp(-G_{m''} \zeta_1) \end{array} \right. \\
&\quad\quad + (G_{m''} \cos \kappa_i \zeta_2 + \kappa_i \sin \kappa_i \zeta_2) \exp(-G_{m''} \zeta_2) \\
&\quad\quad + (G_{m''} \sin \kappa_i \zeta_2 + \kappa_i \cos \kappa_i \zeta_2) \exp(-G_{m''} \zeta_2) \\
&- \sum_{\alpha} \frac{4\pi}{\Omega} \rho_\alpha^2 \exp(i(\mathbf{G}_m + \mathbf{G}_{m''} - \mathbf{G}_{m'}).\mathbf{R}_\alpha) \exp(-G_{m''} z_\alpha) \\
&\quad \times \left\{ \begin{array}{l} \text{Re} \\ \text{Im} \end{array} \right. \left(\exp(i\kappa_i z_\alpha) \frac{\mathcal{J}_1([x + iy]\rho_\alpha)}{[x + iy]} \right) \\
&+ \text{ corrections from the caps}
\end{aligned}
$$

The integrals over the muffin-tin caps (third term in 3.33) are now required. Consider the problem for the right embedding plane (ζ_1). The left embedding

plane (ζ_2) is treated similarly. The geometry for the caps to the right of ζ_1 is

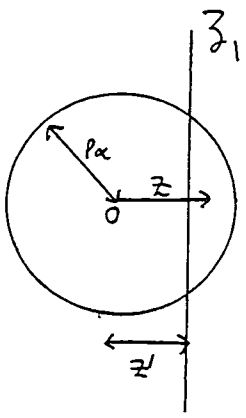

We wish to integrate some function of z, $f(z)$ over the caps. The matrix element has the form

$$\int_{z'}^{\rho_\alpha} dz\, f(z) \int_0^{\sqrt{\rho_\alpha^2 - z^2}} R\, dR \int_0^{2\pi} d\theta\, \exp(iGR\cos\theta) \tag{3.51}$$

Now

$$\int_0^{2\pi} d\theta\, \exp(iGR\cos\theta) = 2\pi \mathcal{J}_0(GR)$$

and

$$\int_0^x x' \mathcal{J}_0(x')\, dx' = x\ \mathcal{J}_1(x)$$

So 3.51 becomes

$$\frac{2\pi}{G} \int_{z'}^{\rho_\alpha} dz\, f(z) \sqrt{\rho_\alpha^2 - z^2}\ \mathcal{J}_1\left(G\sqrt{\rho_\alpha^2 - z^2}\right) \tag{3.52}$$

For the caps to the left of ζ_1 we have the geometry

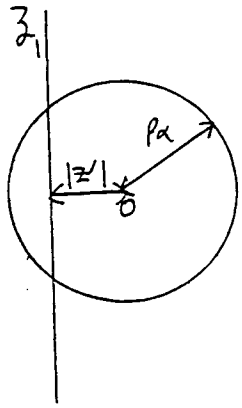

The cap integral is now

$$\frac{2\pi}{G}\int_{-\rho_\alpha}^{-|z'|} dz\, f(z)\sqrt{\rho_\alpha^2 - z^2}\; \mathcal{J}_1\left(G\sqrt{\rho_\alpha^2 - z^2}\right) \qquad (3.53)$$

Now consider the left embedding plane (ζ_2). Caps to the left of ζ_2 are treated using 3.53, and caps to the right of ζ_2 using 3.52. The integrations in 3.52 and 3.53 are done by a Gauss-Chebyshev method [30].

Finally, the energy dependent matrix elements of the embedding potential are required over both embedding planes. Over ζ_1, these are

$$\left\langle \phi_{m',n'} | G_2^{o^{-1}} | \phi_{m,n} \right\rangle_{\zeta_1}$$
$$= \frac{1}{A}\sum_{m'',m'''} G^{o^{-1}}_{2,m'',m'''} \int_{\zeta_1} d^2R \int_{\zeta_1} d^2R\, \phi_{m',n'} \exp(i(\mathbf{K}_{m''}.\mathbf{R} - \mathbf{K}_{m'''}.\mathbf{R}'))\phi_{m,n} \quad (3.54)$$

where the embedding potential has been expanded in two dimensional plane waves

$$G^{o^{-1}}_{2,\mathbf{K}}(\mathbf{R},\mathbf{R}') = \frac{1}{A}\sum_{m'',m'''} G^{o^{-1}}_{2,m'',m'''} \exp(i(\mathbf{K}_{m''}.\mathbf{R} - \mathbf{K}_{m'''}.\mathbf{R}'))$$

Hence, 3.54 reduces to

$$\frac{2}{D} G^{o^{-1}}_{2,m',m} \begin{Bmatrix} \cos k_{n'}\zeta_1 \\ \sin k_{n'}\zeta_1 \end{Bmatrix} \begin{Bmatrix} \cos k_n\zeta_1 \\ \sin k_n\zeta_1 \end{Bmatrix} \qquad (3.55)$$

The matrix element of $G_3^{o^{-1}}$ over ζ_2 is identical to 3.55 except ζ_1 is replaced by ζ_2.

The matrix $H - ES$ can now be evaluated. It is inverted to give G as in equation 1.14. i.e.

$$G_{\mathbf{K}}(\mathbf{r},\mathbf{r}') = \sum_{m,n,m',n'} \phi_{m',n'}(\mathbf{r}) G_{m',n',m,n} \phi^{\star}_{m,n}(\mathbf{r}') \tag{3.56}$$

3.7 Construction of the Density of States and Charge Density

The local density of states with wavevector $\mathbf{K}$ is related to the Green function via

$$\sigma_{\mathbf{K}}(\mathbf{r},E) = \frac{1}{\pi} Im\, G_{\mathbf{K}}(\mathbf{r},\mathbf{r},E+i\epsilon) \tag{3.57}$$

The $i\epsilon$ shifts the energy off the real axis where G has a branch cut. Using 3.56 gives 3.57 as

$$\sigma_{\mathbf{K}}(\mathbf{r},E) = \frac{1}{\pi} Im \sum_{m,n,m',n'} \phi_{m',n'}(\mathbf{r}') G_{m',n',m,n} \phi^{\star}_{m,n}(\mathbf{r}') \tag{3.58}$$

To evaluate the density of states in a particular region, 3.58 is integrated over the volume of interest. In practice the density of states in the muffin-tins of each star, and the density of states in the embedded region (between S_2 and S_3) are evaluated. Also, the total density of states, summed over wavevector $\mathbf{K}$ is evaluated.

The charge density is found by integrating the Green function over the energy range of interest. In practice this energy will encompass the valence bands of both substrates, allowing for the potential shift across the interface. So

$$\rho_{\mathbf{K}}(\mathbf{r}) = \int_{E_I}^{E_F} dE\, \sigma_{\mathbf{K}}(\mathbf{r},E) \tag{3.59}$$

$$= \int_{E_I}^{E_F} Im \sum_{m,n,m',n'} \phi_{m',n'}(\mathbf{r}) G_{m',n',m,n}(E+i\epsilon) \phi^{\star}_{m,n}\, dE \tag{3.60}$$

E_I and E_F are the initial and final energies respectively. In the case of a metallic interface, E_F is the Fermi energy. Write 3.60 as

$$\rho_{\mathbf{K}}(\mathbf{r}) = \sum_{m,n,m',n'} \phi_{m',n'}(\mathbf{r}) \hat{G}_{m',n',m,n} \phi^*_{m,n}(\mathbf{r}) \tag{3.61}$$

where

$$\hat{G}_{m',n',m,n} = \frac{1}{\pi} \int_{E_I}^{E_F} Im\, G_{m',n',m,n}(E + i\epsilon)\, dE \tag{3.62}$$

Equation 3.62 is evaluated on the contour which is a semi-circle in the upper half plane, of radius $(E_F - E_I)/2$. Rearranging this integral into a more suitable form yields

$$\hat{G}_{m',n',m,n} = \frac{(E_F - E_I)}{2\pi} \int_0^{\pi} d\phi \, [\sin\phi \, Im\, G_{m',n',m,n} - \cos\phi \, Re\, G_{m',n',m,n}]$$

The charge density inside the muffin-tins is expanded in the form (equation 3.1)

$$\rho_{\mathbf{K}}(\mathbf{r}) = \sum_{l'',m'' \geq 0} (\rho_{l'',m'',\mathbf{K}}(\mathbf{r}) \cos m''\phi + \rho_{l'',-m'',\mathbf{K}}(\mathbf{r}) \sin m''\phi) P_{l'',m''}(\theta)$$

where the $\{\rho_{l'',m'',\mathbf{K}}, \rho_{l'',-m'',\mathbf{K}}\}$ are real.

If we initially write

$$\rho_{\mathbf{K}}(\mathbf{r}) = \sum_{l'',m''} \rho'_{l'',m'',\alpha,\mathbf{K}}(\mathbf{r}) Y_{l'',m''}(\theta,\phi) \tag{3.63}$$

then the real coefficients are related to the complex coefficients in 3.63 by

$$\left.\begin{aligned} \rho_{l'',m'',\alpha,\mathbf{K}} &= 2\, Re\, \rho'_{l'',m'',\alpha,\mathbf{K}} \\ \rho_{l'',-m'',\alpha,\mathbf{K}} &= -2\, Im\, \rho'_{l'',m'',\alpha,\mathbf{K}} \end{aligned}\right\} \tag{3.64}$$

If $m'' = 0$, then $\rho_{l'',0,\mathbf{K}} = Re\, \rho_{l'',0,\mathbf{K}}$.

The $\rho_{l'',m'',\alpha,\mathbf{K}}$ of 3.63, using 3.16, 3.61, 3.63 are

$$\rho_{l'',m'',\alpha,\mathbf{K}} = \sum_{m,n,m','} \hat{G}_{m',n',m,n} \sum_{l,m,l',m'} \left(A_{l',m',\alpha}(m',n')u_{l',\alpha} + B_{l',m',\alpha}(m',n')\dot{u}_{l',\alpha}\right)$$
$$\times \left(A^{\star}_{l,m,\alpha}(m,n)u_{l,\alpha} + B^{\star}_{l,m,\alpha}(m,n)\dot{u}_{l,\alpha}\right)$$
$$\times \begin{cases} i^{l'} \\ i^{l'-1} \end{cases} \begin{cases} -i^{l} \\ -i^{l-1} \end{cases} \int_{\mathbf{r} \text{ in MT } \alpha} Y_{l',m'} Y^{\star}_{l'',m''} Y^{\star}_{l,m}\, d\Omega$$

So

$$\rho_{l'',m'',\alpha,\mathbf{K}} = \sum_{l,m,l',m'} \Big(u_{l',\alpha}(\mathbf{r})u_{l,\alpha}(\mathbf{r})C^{1}_{l',m',l,m} + \dot{u}_{l',\alpha}(\mathbf{r})\dot{u}_{l,\alpha}(\mathbf{r})C^{2}_{l',m',l,m}$$
$$+u_{l',\alpha}(\mathbf{r})\dot{u}_{l,\alpha}(\mathbf{r})C^{3}_{l',m',l,m} + \dot{u}_{l',\alpha}(\mathbf{r})u_{l,\alpha}(\mathbf{r})C^{4}_{l',m',l,m}\Big)$$
$$\times \int_{\mathbf{r} \text{ in MT } \alpha} Y_{l',m'} Y^{\star}_{l,m} Y^{\star}_{l'',m''}\, d\Omega$$

where

$$C^{1}_{l',m',l,m} = \sum_{m,n \geq m',n';m',n'} f\hat{G}_{m',n',m,n}$$
$$\times \left[\tilde{A}_{l',m',\alpha}(m',n')\tilde{A}^{\star}_{l,m,\alpha}(m,n) + \tilde{A}_{l',m',\alpha}(m,n)\tilde{A}^{\star}_{l,m,\alpha}(m',n')\right]$$

$$C^{2}_{l',m',l,m} = \sum_{m,n \geq m',n';m',n'} f\hat{G}_{m',n',m,n}$$
$$\times \left[\tilde{B}_{l',m',\alpha}(m',n')\tilde{B}^{\star}_{l,m,\alpha}(m,n) + \tilde{B}_{l',m',\alpha}(m,n)\tilde{B}^{\star}_{l,m,\alpha}(m',n')\right]$$

$$C^{3}_{l',m',l,m} = \sum_{m,n \geq m',n';m',n'} f\hat{G}_{m',n',m,n}$$
$$\times \left[\tilde{A}_{l',m',\alpha}(m',n')\tilde{B}^{\star}_{l,m,\alpha}(m,n) + \tilde{A}_{l',m',\alpha}(m,n)\tilde{B}^{\star}_{l,m,\alpha}(m',n')\right]$$

$$C^{4}_{l',m',l,m} = \sum_{m,n \geq m',n';m',n'} f\hat{G}_{m',n',m,n}$$
$$\times \left[\tilde{B}_{l',m',\alpha}(m',n')\tilde{A}^{\star}_{l,m,\alpha}(m,n) + \tilde{B}_{l',m',\alpha}(m,n)\tilde{B}^{\star}_{l,m,\alpha}(m',n')\right]$$

where

$$f = \begin{cases} 1 & \text{if } m',n' \neq m,n \\ \frac{1}{2} & \text{if } m',n' = m,n \end{cases}$$

and

$$\bar{A}_{l,m,\alpha}(m,n) = \begin{cases} i^l \\ i^{l-1} \end{cases} A_{l,m,\alpha}(m,n)$$

$$\bar{B}_{l,m,\alpha}(m,n) = \begin{cases} i^l \\ i^{l-1} \end{cases} B_{l,m,\alpha}(m,n)$$

The sum over symmetry related **K** points is obtained by using the symmetry operations as described in section 3.1, and given in equation 3.2.

In the interstitial region, the charge density is expanded as

$$\rho_{\mathbf{K}}(\mathbf{r}) = \sum_{m'',n''} \rho_{\mathbf{K},m'',n''} \exp\left(i\mathbf{G}_{m''}.\mathbf{R}\right) \begin{cases} \cos k_n z \\ \sin k_n z \end{cases} \tag{3.65}$$

Using 3.15 and 3.61, gives $\rho_{\mathbf{K}}(\mathbf{r})$ as

$$\rho_{\mathbf{K}}(\mathbf{r}) = \frac{2}{\Omega} \sum_{m',n',m,n} \hat{G}_{m',n',m,n} \exp\left(i(\mathbf{K}_{m'} - \mathbf{K}_m).\mathbf{R}\right) \begin{cases} \cos k_{n'} z \\ \sin k_{n'} z \end{cases} \begin{cases} \cos k_n z \\ \sin k_n z \end{cases} \tag{3.66}$$

Writing the trigonometric products in the form of a trigonometric sum, gives for the coefficients in 3.65

n'' even

$$\rightarrow \rho_{m'',n''} = \frac{1}{\Omega} \sum_{m',n',m,n} \hat{G}_{m',n',m,n} \delta_{m'',m'-m} (\delta_{n'',|n'-n|} \pm \delta_{n'',n'+n})$$

where

$$+ \rightarrow \cos k_{n'} z \cos k_n z$$

$$- \rightarrow \sin k_{n'} z \sin k_n z$$

in 3.66.

n'' odd

$$\rightarrow \rho_{m'',n''} = \frac{1}{\Omega} \sum_{m',n',m,n} \hat{G}_{m',n',m,n} \delta_{m'',m'-m} (\delta_{n'',n'+n} \pm \delta_{n'',|n'-n|}) \tag{3.67}$$

In 3.67 we use the + sign if $k_{even} < k_{odd}$, and the - sign if $k_{even} > k_{odd}$.

The total charge density is found by summing over 'special **K** points'. These will be described in the next chapter.

3.8 Summary

Much of the work presented in this chapter is somewhat laborious to work through in detail. However, this is mainly an artefact of the geometry invloved, and the reader need only understand the principles involved in order to gain insight into the method of solution. The key points to note are the use of symmetry, the LAPW basis set, and the form of the potential used. If the calculations were non-self-consistent, then the work would end here, as we now have the density of states and the charge density, given some form for the potential. Since in this work the self-consistent field procedure is used, we must now go on to construct the new potential from the charge density calculated above.

Chapter 4

Construction of the New Potential

The second part of the self-consistent process, namely obtaining the new potential, is developed here. In chapter 3, the valence charge density was evaluated. The core charge density must now be calculated and added to this valence density. Fortunately, this part of the calculation is identical to the surface case, so this section of the surface program is unchanged. A description of the method of obtaining the core charge density is given.

As we are interested in calculating the total charge density, we require a method of integrating the charge density, evaluated at different wavevectors, across the Brillouin zone. The 'special **K** points' scheme is described, this being an efficient and computationally feasible method to perform this integration.

In order to compute the Fourier coefficients of the potential, the charge density must first be Fourier transformed. Due to the rapid variations in the charge density near the nuclei, this is not an easy task. The problem is overcome by forming a pseudo charge density inside the muffin-tins, which gives rise to the same interstitial potential as the real muffin-tin charge density. The construction of this pseudo charge density is described, as an understanding of this is required in order to make sense of the parameters chosen in the calculations presented later.

Finally, the construction of the potential from this pseudo charge density

is dealt with. Having obtained the interstitial potential, the boundary value problem for the muffin-tin spheres is solved. The exchange-correlation potential is then added to give a potential which is mixed with the potential of the previous iteration, to give the new potential.

4.1 The Core Charge Density

For the core states, a fully relativistic treatment is used, but only the spherically symmetric part of the muffin-tin potential is used. So we require both the lower and upper parts of the wavefunction given by 3.6 and 3.7.
Now, putting

$$P = rg \qquad\qquad Q = rf$$

and using a logarithmic grid, $x = \ln r$, changes 3.6 and 3.7 to

$$\frac{\partial Q}{\partial x} = \exp(x)\left(\frac{V-E}{c}\right)P + \kappa Q \tag{4.1}$$

$$\frac{\partial P}{\partial x} = -\kappa P + \exp(x)2McQ \tag{4.2}$$

where

$$2Mc = \frac{2mc^2 + (E-V)}{c}$$

The starting values are obtained from the limit of small and large r, giving as $r \to 0$

$$q \to \frac{z}{c(\kappa - \alpha)}$$

where

$$P = r^\alpha \qquad\qquad Q = qr^\alpha$$

As $r \to \infty$

$$Q \to -\sqrt{\frac{|E|}{2mc^2 + E}}\exp(-\gamma r)$$

where

$$\gamma = \frac{\sqrt{|E|(2mc^2 + E)}}{c}$$

The method of solution closely resembles that described by Liberman et al. [31], except that the self-consistency part of his paper does not arise here.

Liberman performs calculations on free atoms and ions, for as we are only interested in the solution for the core electrons here. The total charge density is calculated from the sum of the core and valence charge densities.

Briefly, the equations 4.1 and 4.2 are first integrated outwards from $r = 0$ to the classical turning point (r_1) at some initial trial energy. The number of nodes of the wavefunction is evaluated, and if this is not equal to the correct number, $(n - l - 1)$, then the energy is successively refined until this is true. The equations are then integrated inwards from an 'effective infinity' (r_2), determined from the condition that

$$\prod_{r_1 \to r_2} \exp - \{2(V(r) - E)\}^{\frac{1}{2}} \, dr \leq 10^{-3}$$

From the discontinuity in the upper and lower components of the wavefunction at r_1, a correction to the energy can be found [31]. This procedure is continued until $\delta E/E \leq 10^{-6}$. Thus the core charge density can now be calculated using

$$\rho(r) = \frac{\sum_j \left[f_j^2(r) + g_j^2(r)\right]}{r^2}$$

4.2 Special K Points

Section 3.7 dealt with the construction of the valence charge density at fixed wavevector, $\rho_{\mathbf{K}}(\mathbf{r})$. The total valence charge density $\rho(\mathbf{r})$ is required. The obvious approach is to sum the $\{\rho_{\mathbf{K}_i}(\mathbf{r})\}$ over a fine mesh of points $\{\mathbf{K}_i\}$ in the irreducible part of the Brillouin zone. However, this would be very time consuming. Another, and a more practical approach, is to use the so called 'special' or 'representative' $\mathbf{K}$ points. These are chosen so that the sum of a weighted charge density at these points is a good approximation to the total charge density. This approach was initiated by Baldereschi [32], who suggested using a single mean value point. This is the optimal $\mathbf{K}$ point for approximating the mean value of a periodic function across the Brillouin zone. The technique has been generalised to the case of more $\mathbf{K}$ points in papers by Chadi and Cohen [33,34], and Monkhorst and Pack [35]. The method is most suitable for insulators and semiconductors, where the valence bands are full.

Since the interface Brillouin zone is two dimensional, we require the 2-D special **K** points. Cunningham [36] has derived suitable points for each of the five 2-D lattices. The periodic function $f(\mathbf{K})$ is expanded as

$$f(\mathbf{K}) = f_o + \sum_{m=1}^{\infty} f_m A_m(\mathbf{K}) \tag{4.3}$$

where

$$A_m(\mathbf{K}) = \sum_{|\mathbf{R}|=C_m} \exp(i\mathbf{K}.\mathbf{R}) \qquad (m \in \mathcal{N})$$

K, **R** are the two dimensional wavevectors and lattice vectors respectively. The C_m correspond to the rings of 2-D lattice vectors. As m increases, $|\mathbf{R}|$ also increases.

Now we require the integral of $f(\mathbf{K})$ over the two dimensional Brillouin zone. The mean value of $f(\mathbf{K})$ is

$$\bar{f} = \frac{A}{(2\pi)^2} \int_{BZ} f(\mathbf{K})\, d^2K$$

Also

$$\bar{f} = f_o$$

The following conditions are imposed on the $\{\mathbf{K}_i\}$ and weights $\{\alpha_i\}$

$$\begin{aligned} \sum_i \alpha_i A_m(\mathbf{K}_i) &= 0 \qquad (m = 1 \rightarrow N) \\ \sum_i \alpha_i &= 1 \end{aligned}$$

So 4.3 becomes

$$f_o = \sum_i \alpha_i f(\mathbf{K}_i) - \sum_{m>N}^{\infty} f_m \sum_i \alpha_i A_m(\mathbf{K}_i) \tag{4.4}$$

As m increases, $|f_m|$ decreases, since the valence charge density is in general well behaved and smooth. Thus the second term in 4.4 can be made as small as one chooses, by choosing N large enough. The method used to obtain the $\{\mathbf{K}_i\}$ is given in Cunningham [36].

This method can also be used for metals although the discontinuity in the charge density at the Fermi energy means that a larger set of $\{\mathbf{K}_i\}$ may be required. Metal surface calculations performed by my co-workers at Daresbury have shown that three **K** points in the irreducible part of the Brillouin zone are often adequate, and even only one **K** point is sufficient for the first few iterations in the self-consistent process.

4.3 Construction of the Pseudo Charge Density

The charge density has already been determined, and the problem is now to solve Poisson's equation to obtain the potential. This is done by Fourier transforming the charge density, and then calculating the Fourier components of the potential via Poisson's equation. However, due to the rapid variation of the charge density near the nuclei, any Fourier expansion will be slowly convergent. To overcome this, a recently developed method of solution due to Weinert [37] is used, which uses the concept of multipole moments of the charge density inside the muffin-tins. A description of multipole moments can be found in Jackson [38], but briefly, given a charge distribution $\rho(\mathbf{x}')$, the potential at $\mathbf{x}$ is

$$\Phi(\mathbf{x}) = \int \frac{\rho(\mathbf{x}')}{|\mathbf{x}-\mathbf{x}'|}\, d^3x' \tag{4.5}$$

Now, $\frac{1}{|\mathbf{x}-\mathbf{x}'|}$ can be expanded as [38]

$$\frac{1}{|\mathbf{x}-\mathbf{x}'|} = 4\pi \sum_{l=0}^{\infty} \sum_{m=-l}^{l} \frac{1}{2l+1} \frac{r_<^l}{r_>^{l+1}} Y^*_{l,m}(\hat{\mathbf{x}}') Y_{l,m}(\hat{\mathbf{x}}) \tag{4.6}$$

$r_<$ ($r_>$) is the smaller (larger) of $|\mathbf{x}|$ and $|\mathbf{x}'|$.

Consider a sphere, outside of which $\rho(\mathbf{x}') = 0$. Write the potential outside the sphere as

$$\Phi(\mathbf{x}) = \sum_{l=0}^{\infty} \sum_{m=-l}^{l} \frac{4\pi}{2l+1} q_{l,m} \frac{Y_{l,m}(\hat{\mathbf{x}})}{r^{l+1}} \tag{4.7}$$

Now use 4.6 in 4.5 to obtain another expression for $\Phi(\mathbf{x})$

$$\Phi(\mathbf{x}) = 4\pi \sum_{l,m} \frac{1}{2l+1} \left[\int Y^*_{l,m}(\hat{\mathbf{x}}') r'^l \rho(\mathbf{x}')\, d^3x' \right] \frac{Y_{l,m}(\hat{\mathbf{x}})}{r^{l+1}}$$

where $r' = r_<$, and $r = r_>$.

So the $\{q_{l,m}\}$ are

$$q_{l,m} = \int Y^*_{l,m}(\hat{\mathbf{x}}') r'^l \rho(\mathbf{x}')\, d^3x' \tag{4.8}$$

These are the multipole moments.

Weinert [37] derives a pseudo charge density which is the same as the actual charge density in the interstitial region, and has the same multipole moments as the real charge density inside the muffin tins. It therefore gives rise to the correct interstitial potential via 4.7. Knowing this potential, the boundary value problem for the potential inside the muffin-tins is then solved, finally giving the potential throughout the interface. Weinert's analysis assumes three dimensional periodicity, but this can be readily generalised to the two dimensional case, as exists in the interface.

As in equation 3.65, the charge density in the interstitial region is expanded as

$$\rho(\mathbf{r}) = \sum_{m,n} \rho_{m,n} \exp(i\mathbf{G}_m.\mathbf{R}) \begin{cases} \cos k_n z \\ \sin k_n z \end{cases} \tag{4.9}$$

Inside the muffin-tins ρ is expanded as

$$\rho(\mathbf{r}) = \sum_{l,m\geq 0} \left(\rho_{l,m}(r) \cos m\phi + \rho_{l,-m} \sin m\phi\right) P_{l,m}(\theta)$$

The total charge density in the interface is now written in the form

$$\rho(\mathbf{r}) = \rho_{\text{int}}(\mathbf{r}) + \sum_{\text{mt } \alpha} \left[\rho_{\text{mt-}\alpha}(\mathbf{r} - \mathbf{r}_\alpha) - \rho_{\text{int}}(\mathbf{r})\right] \Theta(\mathbf{r} \text{ in } \alpha) \tag{4.10}$$

Θ is the unit step function. $\rho_{\text{int}}(\mathbf{r})$ has been extended over the entire interface, including inside the muffin-tins.

As real spherical harmonics are used for the charge density expansion inside the muffin-tins, real multipole moments of the charge density inside muffin-tin α are defined as

$$\begin{aligned} q_{l,m,\alpha} &= \int_0^{\rho_\alpha} r^{l+2} \rho_{l,m,\alpha}(r)\, dr \\ q_{l,-m,\alpha} &= \int_0^{\rho_\alpha} r^{l+2} \rho_{l,-m,\alpha}(r)\, dr \end{aligned} \tag{4.11}$$

ρ_α is the radius of muffin-tin α.

The real $q_{l,\pm m}$ in 4.11 are related to the complex $q'_{l,m}$ in 4.8 via

$$\sum_m q'_{l,m,\alpha} Y_{l,m}(\hat{\mathbf{k}}) = \sum_{m \geq 0} \left(q_{l,m,\alpha} \cos m\phi + q_{l,-m,\alpha} \sin m\phi \right) P_{l,m}(\theta) \tag{4.12}$$

The real multipole moments (q_{mt}) of the muffin-tin charge density can therefore be easily calculated via the integrals in 4.11.

To find the multipole moments of the interstitial charge density in muffin-tin α, first write this charge density (4.9) relative to the sphere centres. So

$$\rho^{\alpha}_{\mathrm{int}}(\mathbf{r}) = \sum_{m,n} \rho_{m,n,\alpha} \exp(i\mathbf{G}_m.\mathbf{r}_\alpha) \exp(i\mathbf{G}_m.\rho) \quad \begin{cases} \cos k_n z_\alpha \cos k_n \rho_z \\ \sin k_n z_\alpha \sin k_n \rho_z \\ - \sin k_n z_\alpha \sin k_n \rho_z \\ + \cos k_n z_\alpha \sin k_n \rho_z \end{cases} \tag{4.13}$$

where $\mathbf{r} = \mathbf{r}_\alpha + \underline{\rho}$, $\mathbf{r}_\alpha$ being the centre of muffin-tin α, z_α being the z component. Hence, the multipole moments of

$$\cos k_n \rho_z \exp(i\mathbf{G}_m.\underline{\rho})$$

$$\sin k_n \rho_z \exp(i\mathbf{G}_m.\underline{\rho})$$

are required in muffin-tin α.

Using the definition of the ordinary multipole moments (4.8), and following Weinert [37], gives the multipole moments of $\cos k_n \rho_z \exp(i\mathbf{G}_{m'}.\underline{\rho})$ as

$$q_{l,m} = \begin{cases} 4\pi i^l \rho_\alpha^{l+3} \frac{\mathcal{J}_{l+1}(g_{m',n}\rho_\alpha)}{g_{m',n}\rho_\alpha} Y^*_{l,m}(\hat{\mathbf{g}}_{m',n}) & (l+m) \text{ even} \\ 0 & (l+m) \text{ odd} \end{cases} \tag{4.14}$$

and those of $\sin k_n\rho_z \exp(i\mathbf{G}_{m'}.\rho)$ as

$$q_{l,m} = \begin{cases} 4\pi i^{l-1}\rho_\alpha^{l+3}\frac{\mathcal{J}_{l+1}(g_{m',n}\rho_\alpha)}{g_{m',n}\rho_\alpha}Y^*_{l,m}(\hat{\mathbf{g}}_{m',n}) & (l+m)\text{ odd} \\ 0 & (l+m)\text{ even} \end{cases} \tag{4.15}$$

where

$$\mathbf{g}_{m',n} = \mathbf{G}_{m'} + k_n\hat{\mathbf{z}} \qquad\qquad g_{m',n} = |\mathbf{g}_{m',n}|$$

The $g_{m',n} = 0$ terms are

$$q_{l,0} = \begin{cases} \frac{\sqrt{4\pi}}{3}\rho_\alpha^3 & l = 0 \\ 0 & l \neq 0 \end{cases} \tag{4.16}$$

Equations 4.14, 4.15, and 4.16, substituted into 4.13, give the multipole moments of $\rho_{\text{int}}(\mathbf{r})$ inside muffin-tin α. The real and imaginary parts of these complex multipole moments are taken to give the real multipole moments (q_{int}). Hence, the second term in 4.10 gives rise to multipole moments (including the nuclear charge)

$$\begin{aligned} &q_{\text{mt}} - q_{\text{int}} && l \neq 0 \\ &q_{\text{mt}} - q_{\text{int}} - \tfrac{Z}{\sqrt{4\pi}} && l = 0 \end{aligned} \tag{4.17}$$

The problem now is to find a pseudo charge density inside the muffin-tins which has the multipole moments 4.17, but which can be easily Fourier transformed. Weinert writes in muffin-tin α

$$\tilde{\rho}_\alpha(\mathbf{r}) = \sum_{l,m} Q_{l,m}Y_{l,m}(\hat{\mathbf{r}})\sum_\eta a_\eta r_\alpha^{\nu_\eta}$$

where a_η, ν_η are parameters for the power series, and the $\{Q_{l,m}\}$ are chosen such that the pseudo charge density, $\hat{\rho}$, has the correct multipole moments. These are (using 4.8)

$$\tilde{q}_{l,m} = \frac{Q_{l,m}\sum_\eta a_\eta\rho_\alpha^{\nu_\eta+l+3}}{\nu_\eta + l + 3} \tag{4.18}$$

Again, following Weinert, we choose

$$\nu_\eta = l + 2\eta \qquad (\eta \in \mathcal{Z}^+)$$

and determine the Fourier transform of $\tilde{\rho}$ in muffin-tin α as

$$\int_{\mathrm{MT}\ \alpha} d^3r\ \tilde{\rho}_\alpha(\mathbf{r}) \exp(-i\mathbf{k}.\mathbf{r}) = \sum_{l,m} 4\pi Q_{l,m}(-i)^l Y_{l,m}(\hat{\mathbf{k}}) \rho_\alpha^{l+3}$$
$$\times \sum_{\nu=0}^{n} (-2)^\nu \frac{\mathcal{J}_{l+\nu+1}(k\rho_\alpha)}{(k\rho_\alpha)^{\nu+1}} \sum_{\eta=\nu}^{n} a_\eta \frac{\eta!}{(\eta-\nu)!} \rho_\alpha^{2\eta} \tag{4.19}$$

where for the present, $\mathbf{k}$ is a three dimensional wavevector.

Weinert imposes the condition

$$\sum_{\eta=\nu}^{n} a_\eta \frac{\eta!}{(\eta-\nu)!} \rho_\alpha^{2\eta} = 0 \qquad (\nu = 0, 1, 2, \ldots, n-1) \tag{4.20}$$

This set of equations has the solution

$$a_\eta = (-1)^{n-\eta} \frac{n!}{(n-\eta)!\eta!} \rho_\alpha^{2(n-\eta)} a_n \tag{4.21}$$

At this stage it is very easy to lose track of the Physics involved, so the meaning of equation 4.20 will be considered. Weinert proves that imposing condition 4.20 is equivalent to setting the first $(n-1)$ derivatives, $\frac{\partial^k \tilde{\rho}}{\partial r^k}$, equal to zero at the muffin-tin surface. Thus n measures the smoothness of the pseudo charge density. With hindsight, the conditions imposed by Weinert are chosen to give this result. Using 4.20 and 4.21 in 4.19 gives

$$\int_{\mathrm{MT}\ \alpha} d^3r\ \tilde{\rho}_\alpha(\mathbf{r}) \exp(-i\mathbf{k}.\mathbf{r}) = \sum_{l,m} 4\pi Q_{l,m}(-i)^l Y_{l,m}(\hat{\mathbf{k}})$$
$$\times \rho_\alpha^{l+2n+3} (-2)^n \frac{\mathcal{J}_{l+n+1}(k\rho_\alpha)}{(k\rho_\alpha)^{n+1}} a_n n! \tag{4.22}$$

Now $Q_{l,m}$ is defined by 4.18, with $\nu_\eta = 2\eta + l$ as before, and using a_η defined in 4.21 gives

$$Q_{l,m} = \frac{\tilde{q}_{l,m}}{a_n(-1)^n \rho_\alpha^{2l+2n+3} \sum_{\eta=0}^{n} (-1)^\eta \frac{n!}{(n-\eta)!\eta!(2l+2\eta+3)}} \tag{4.23}$$

The following result, proved by Weinert is required

$$\sum_{\eta=0}^{n}(-1)^{\eta}\frac{n!}{(n-\eta)!\eta!(2l+2\eta+3)} = \frac{2^n n!(2l+1)!!}{(2l+2n+3)!!} \tag{4.24}$$

Using 4.24 in 4.23 and rearranging gives

$$Q_{l,m} = \frac{(-1)^n \tilde{q}_{l,m}}{a_n 2^n n! \rho_\alpha^{2l+2n+3}} \times \frac{(2l+2n+3)!!}{(2l+1)!!} \tag{4.25}$$

Put 4.25 into 4.22 to obtain

$$\begin{aligned}\int_{\mathrm{MT}\ \alpha} d^3r\, \tilde{\rho}_\alpha(\mathbf{r})\exp(-i\mathbf{k}.\mathbf{r}) &= 4\pi \sum_{l,m} \frac{\tilde{q}_{l,m}}{\rho_\alpha^{2l+2n+3}} \times \frac{(2l+2n+3)!!}{(2l+1)!!} \\ &\times\ (-i)^l Y_{l,m}(\hat{\mathbf{k}})\rho_\alpha^{l+2n+3}\frac{\mathcal{J}_{l+n+1}(k\rho_\alpha)}{(k\rho_\alpha)^{n+1}} \end{aligned} \tag{4.26}$$

We now wish to find the Fourier coefficients of the pseudo charge density, having two dimensional periodicity. The total $\tilde{\rho}$ is written in a form analagous to the real ρ. This is

$$\tilde{\rho}(\mathbf{r}) = \sum_{m,n} \tilde{\rho}_{m,n}\exp(i\mathbf{G}_m.\mathbf{R}) \begin{cases} \cos k_n z \\ \sin k_n z \end{cases}$$

So

$$\tilde{\rho}_{m,n} = \int_{\text{2D unit cell}} \tilde{\rho}(\mathbf{r})\exp(-i\mathbf{G}_m.\mathbf{R}) \begin{cases} \cos k_n z \\ \sin k_n z \end{cases} \qquad (\times\frac{1}{2} \text{ if } n=0)$$

Again, writing $\mathbf{r} = \mathbf{r}_\alpha + \underline{\rho}$, using 4.26, and the relationship between real and complex multipole moments (4.12) gives after some manipulation, in muffin-tin α

$$\tilde{\rho}^\alpha_{m,n} = \exp(-i\mathbf{G}_m.\mathbf{r}_\alpha) \begin{cases} \cos k_n z_\alpha\, C^\alpha_{m,n} - \sin k_n z_\alpha\, S^\alpha_{m,n} \\ \sin k_n z_\alpha\, C^\alpha_{m,n} + \cos k_n z_\alpha\, S^\alpha_{m,n} \end{cases} \tag{4.27}$$

where the $\{C^{\alpha}_{m,n}, S^{\alpha}_{m,n}\}$ are

$$C^{\alpha}_{m,n} = \frac{8\pi}{A\tilde{D}}(\times\frac{1}{2} \text{ if } n=0) \sum_{l,m\geq 0;(l+m) \text{ even}} (-i)^l \frac{(2l+2n+3)!!}{(2l+1)!!} \times \frac{\mathcal{J}_{l+n+1}(k\rho_\alpha)}{k^{n+1}\rho_\alpha^{l+n+1}} \times (\tilde{q}_{l,m}\cos m\phi + \tilde{q}_{l,-m}\sin m\phi)\, P_{l,m}(\theta)$$

and

$$S^{\alpha}_{m,n} = \frac{8\pi}{A\tilde{D}} \sum_{l,m\geq 0;(l+m) \text{ odd}} (-i)^{l-1} \frac{(2l+2n+3)!!}{(2l+1)!!} \times \frac{\mathcal{J}_{l+n+1}(k\rho_\alpha)}{k^{n+1}\rho_\alpha^{l+n+1}} \times (\tilde{q}_{l,m}\cos m\phi + \tilde{q}_{l,-m}\sin m\phi)\, P_{l,m}(\theta)$$

where $\mathbf{k} = \mathbf{G}_m + k_n\hat{\mathbf{z}}$, and (θ, ϕ) are the spherical polar angles defining $\hat{\mathbf{k}}$. For $k = 0$

$$\frac{\mathcal{J}_{l+n+1}(k\rho_\alpha)}{k^{n+1}\rho_\alpha^{l+n+1}} = \begin{cases} \frac{1}{(2n+3)!!} & l=0 \\ 0 & l\neq 0 \end{cases}$$

So, from4.27, we now have the pseudo charge density coefficients. Note that the maximum value of $\eta(=n)$ can be different for each l (See equation 4.19). Weinert suggests using n such that the first zero of $\mathcal{J}_{l+n+1}(z)$ occurs at about $z = k_{max}\rho_\alpha$, where ρ_α is the radius of muffin-tin α, and k_{max} is the magnitude of the largest wavevector in the plane wave expansion of ρ. k_{max} is given by

$$\left(\frac{6\pi^2 N}{V}\right)^{\frac{1}{3}}$$

V being the unit cell volume, and N the number of plane waves. The table of n values for different values of l and $(k_{max}\rho_\alpha)$ is reproduced from Weinert's paper in figure 4.1.

= 0)	15 20.54	14 19.45	13 18.35	12 17.25	11 16.14	10 15.03	9 13.92	8 12.79	7 11.66	6 10.51	5 9.36	4 8.18	3 6.99	2 5.76	1 4.49
	14	13	12	11	10	9	8	7	6	5	4	3	2	1	0
	13	12	11	10	9	8	7	6	5	4	3	2	1	0	
	12	11	10	9	8	7	6	5	4	3	2	1	0		
	11	10	9	8	7	6	5	4	3	2	1	0			
	10	9	8	7	6	5	4	3	2	1	0				
	9	8	7	6	5	4	3	2	1	0					
	8	7	6	5	4	3	2	1	0						
	7	6	5	4	3	2	1	0							
	6	5	4	3	2	1	0								

Figure 4.1: n values for different l and $(k_{max}\rho_\alpha)$. From Weinert [37].

4.4 Construction of the Electrostatic Potential

The charge density is now in the required form. The next step involves the solution of Poisson's equation. Initially we solve for the interstitial potential, using the potential shift across the interface as boundary conditions. Knowledge of the position of the Fermi level (E_F) in each bulk material, and the fact that E_F is constant across the interface, allows this shift to be calculated at the outset. In metals, E_F is known, so the shift can be easily calculated. In a semiconductor system we do not know E_F, so either the experimentally measured value is used, or one places E_F at the centre of the band gap, as a first approximation. The muffin-tin potential is now a boundary value problem, the boundary conditions being determined by the expansion of the interstitial potential over the muffin-tin surfaces.

Interstitial Potential

In the interstitial region the charge density is written as

$$\rho_{int}(\mathbf{r}) + \tilde{\rho}(\mathbf{r}) \tag{4.28}$$

$\rho_{int}(\mathbf{r})$ being the charge density as defined by equation 3.65, and $\tilde{\rho}(\mathbf{r})$ is the pseudo charge density.

4.28 is expanded as

$$\sum_{m,n} \hat{\rho}_{m,n} \exp\left(i\mathbf{G}_m.\mathbf{R}\right) \begin{cases} \cos k_n z \\ \sin k_n z \end{cases}$$

where

$$\hat{\rho}_{m,n} = \rho_{m,n} + \tilde{\rho}_{m,n}$$

First consider the $\mathbf{G}_m = \mathbf{0}$ component of the charge density. The $\hat{\rho}_{0,0}$ term is given by

$$-\frac{\partial^2 V_{0,0}}{\partial z^2} = 4\pi\hat{\rho}_{0,0}$$

with solution

$$V = V_{0,0} + V_1 z - 2\pi\hat{\rho}_{0,0} z^2$$

$V_{0,0}$, V_1 being constants.

The full $\mathbf{G}_m = \mathbf{0}$ component is

$$V(z) = V_{0,0} + V_1 z - 2\pi\hat{\rho}_{0,0} z^2 + {\sum_n}' \frac{4\pi}{k_n^2}\hat{\rho}_{0,n} \begin{cases} \cos k_n z \\ \sin k_n z \end{cases} \qquad (4.29)$$

4.29 must match onto the $\mathbf{G}_m = \mathbf{0}$ component of the substrate potential over the two true embedding surfaces. At present, the potential is specified at $\pm\frac{D}{2}$, with corrections being included later. Letting the $\mathbf{G}_m = \mathbf{0}$ component of the potential at $\pm\frac{D}{2}$ be $V_0\left(\pm\frac{D}{2}\right)$, and solving for $V_{0,0}$ and V_1 gives

$$V_{0,0} = \left[\pi\hat{\rho}_{0,0}\frac{D^2}{2} - {\sum_n}' \frac{4\pi}{k_n^2}\hat{\rho}_{0,n} \begin{cases} \cos k_n \frac{D}{2} \\ 0 \end{cases} + \phi_0\right]$$

where

$$\phi_0 = V_0\left(-\frac{D}{2}\right) + V_0\left(+\frac{D}{2}\right)$$

$$V_1 = -\frac{1}{D}\left[2{\sum_n}' \frac{4\pi}{k_n^2}\hat{\rho}_{0,n} \begin{cases} 0 \\ \sin k_n \frac{D}{2} \end{cases} + \phi_1\right]$$

where

$$\phi_1 = V_0\left(+\frac{D}{2}\right) - V_0\left(-\frac{D}{2}\right)$$

The general solution of Poisson's equation (finite $\mathbf{G}_m$), given by

$$-\frac{\partial^2 V_m}{\partial z^2} + \mathbf{G}_m^2 V_m = 4\pi \sum_n \hat{\rho}_{m,n} \begin{cases} \cos k_n z \\ \sin k_n z \end{cases}$$

where

$$V = \sum_m V_m \exp(i\mathbf{G}_m.\mathbf{R})$$

is given by

$$V_m(z) = V_{m,+}\exp(G_m z) + V_{m,-}\exp(-G_{mm} z) + \sum_n \frac{4\pi}{k_n^2 + G_m^2}\hat{\rho}_{m,n} \begin{cases} \cos k_n z \\ \sin k_n z \end{cases} \tag{4.30}$$

Matching 4.30 onto the m^{th} component of the substrate potentials at $\pm\frac{D}{2}$ gives

$$V_{m,+} = -\frac{1}{\sinh G_m D}\left[\sum_n \frac{4\pi}{k_n^2 + G_m^2}\hat{\rho}_{m,n} \begin{cases} \cos k_n \frac{D}{2} \sinh G_m \frac{D}{2} \\ \sin k_n \frac{D}{2} \cosh G_m \frac{D}{2} \end{cases} - \phi_{2,m}\right]$$

where

$$\phi_{2,m} = V_m\left(\frac{D}{2}\right)\exp\left(G_m\frac{D}{2}\right) - V_m\left(-\frac{D}{2}\right)\exp\left(-G_m\frac{D}{2}\right)$$

and

$$V_{m,-} \doteq -\frac{1}{\sinh G_m D}\left[\sum_n \frac{4\pi}{k_n^2 + G_m^2}\hat{\rho}_{m,n} \begin{cases} \cos k_n \frac{D}{2} \sinh G_m \frac{D}{2} \\ -\sin k_n \frac{D}{2} \cosh G_m \frac{D}{2} \end{cases} - \phi_{3,m}\right]$$

where

$$\phi_{3,m} = V_m\left(-\frac{D}{2}\right)\exp\left(G_m\frac{D}{2}\right) - V_m\left(\frac{D}{2}\right)\exp\left(-G_m\frac{D}{2}\right)$$

The potential is now in the form

$$V(\mathbf{r}) = \sum_{m,n} V_{m,n} \exp(i\mathbf{G}_m.\mathbf{R}) \begin{cases} \cos k_n z \\ \sin k_n z \end{cases} + V_1 z + V_2 z^2$$

$$+ \sum_{m}{}' (V_{m,+} \exp(G_m z) + V_{m,-} \exp(-G_m z)) \exp(i\mathbf{G}_m.\mathbf{R}) \quad (4.31)$$

We specify the bulk potential ($V_{bulk}(\mathbf{r})$) at random points $\{\mathbf{r}_i\}$ across the interface, and must adjust all the potential coefficients so as to make $\{V(\mathbf{r}_i)\}$ as calculated by 4.31, the best fit to $\{V_{bulk}(\mathbf{r}_i)\}$. This is done using a least squares fit. The procedure is

1. Set $\{\phi_{i,m}\} = 0 \quad \forall i, m$, then calculate $\{V(\mathbf{r}_i)\}$.
2. Subtract $V_{xc}(\mathbf{r}_i)$ from $V_{bulk}(\mathbf{r}_i)$ to give the electrostatic potential, $V_{elec}(\mathbf{r}_i)$.
3. Form $\delta V(\mathbf{r}_i) = V_{elec}(\mathbf{r}_i) - V(\mathbf{r}_i)$

Also

$$\delta V(\mathbf{r}_i) = \delta V_{0,0} + \delta V_1 z$$

$$+ \sum_{\text{2D stars } p} \delta V_{p,+} \sum_{\text{2D waves in star } p} \exp(G_m z_i) \cos \mathbf{G}_m.\mathbf{r}_i$$

$$+ \sum_{\text{2D stars } p} \delta V_{p,-} \sum_{\text{2D waves in star } p} \exp(-G_m z_i) \cos \mathbf{G}_m.\mathbf{r}_i$$

Note that in practice the sum over 2D waves is taken as a sum over the 2D stars, with a coefficient $V_{p,\pm}$ for each star.

Let N1 and N2 be the number of random points on ζ_1 and ζ_2 respectively, and NVSTR be the number of 2D stars. We set up a (N1 + N2) by (2*NVSTR + 2) matrix, A, containing in each row

$$1 \quad z_i \quad \sum \exp(G_m z_i) \cos \mathbf{G}_m.\mathbf{r}_i \ldots \quad \sum \exp(-G_m z_i) \cos \mathbf{G}_m.\mathbf{r}_i \ldots$$

Also, a column matrix P with (N1 + N2) entries $\delta V(\mathbf{r}_i)$ is set up. So

$$Ax = P$$

The least squares fit gives the 2*NVSTR+2 coefficient corrections in x.

Muffin-Tin Potential

The muffin tin potential can now be determined from the charge density inside the muffin tin spheres and using the boundary conditions set by the previously evaluated interstitial potential. First, this interstitial potential must be expanded over the surface of each muffin-tin α, to give the components of the potential for each value of l and m.

Plane Wave Term

$$\exp(i\mathbf{G}_m.\mathbf{R}) \begin{cases} \cos k_n z \\ \sin k_n z \end{cases} = \exp(i\mathbf{G}_m.\mathbf{r}_\alpha) \begin{cases} \frac{1}{2} \\ \frac{1}{2i} \end{cases} \Big[\exp(i\mathbf{K}^+_{m,n}.\underline{\rho}_\alpha)\exp(ik_n z_\alpha) \pm \exp(i\mathbf{K}^-_{m,n}.\underline{\rho}_\alpha)\exp(-ik_n z_\alpha)\Big]$$

where

$$\mathbf{K}^\pm_{m,n} = \mathbf{G}_m \pm k_n\hat{\mathbf{z}}$$

and

$$\mathbf{r}_\alpha + \underline{\rho}_\alpha = \mathbf{R} + z\hat{\mathbf{z}}$$

The coefficient of $Y_{l,m}(\hat{\underline{\rho}}_\alpha)$ in the expansion of $\exp(i\mathbf{K}^+_{m,n}.\underline{\rho}_\alpha)$ is

$$4\pi\mathcal{J}_l(K_{m,n}\rho_\alpha)Y^*_{l,m}(\theta,\phi)$$

where $K_{m,n} = |\mathbf{K}^\pm_{m,n}|$, and (θ,ϕ) are the spherical polar angles defining $\mathbf{K}^+_{m,n}$. Also, the coefficient of $\exp(i\mathbf{K}^-_{m,n}.\underline{\rho}_\alpha)$ is

$$\begin{aligned} &4\pi i^l\mathcal{J}_l(K_{m,n}\rho_\alpha)Y^*_{l,m}(\pi-\theta,\phi) \\ &\quad = (-1)^{l+m}4\pi i^l\mathcal{J}_l(K_{m,n}\rho_\alpha)Y^*_{l,m}(\theta,\phi) \end{aligned}$$

After some manipulation

$$\exp(i\mathbf{G}_m.\mathbf{R})\cos k_n z|_{l,m,\alpha} = \exp(i\mathbf{G}_m.\mathbf{r}_\alpha)4\pi i^l \mathcal{J}_l(K_{m,n}\rho_\alpha)Y^*_{l,m}(\theta,\phi) \times \begin{cases} \cos k_n z_\alpha & (l+m) \text{ even} \\ i\sin k_n z_\alpha & (l+m) \text{ odd} \end{cases}$$

and

$$\exp(i\mathbf{G}_m.\mathbf{R})\cos k_n z|_{l,m,\alpha} = \exp(i\mathbf{G}_m.\mathbf{r}_\alpha)4\pi i^{l-1} \mathcal{J}_l(K_{m,n}\rho_\alpha)Y^*_{l,m}(\theta,\phi) \times \begin{cases} i\sin k_n z_\alpha & (l+m) \text{ even} \\ \cos k_n z_\alpha & (l+m) \text{ odd} \end{cases}$$

z Term

$$\begin{aligned} z_{l,m} &= \int_{\text{surface of MT }\alpha} Y^*_{l,m}(\Omega) z \, d\Omega \\ &= \int_{\text{surface of MT }\alpha} Y^*_{l,m}(\Omega)(z_\alpha + \rho_\alpha \cos\theta)\, d\Omega \\ &= \sqrt{4\pi} z_\alpha \delta_{l,0;m,o} + \sqrt{\frac{4\pi}{3}} \rho_\alpha \delta_{l,1;m,o} \end{aligned}$$

z^2 Term

$$\begin{aligned} z^2|_{l,m,\alpha} &= \int_{\text{surface of MT }\alpha} Y^*_{l,m}(\Omega)(z_\alpha^2 + 2z_\alpha\rho_\alpha\cos\theta + \rho_\alpha^2\cos^2\theta)\, d\Omega \\ &= \int_{\text{surface of MT }\alpha} Y^*_{l,m}(\Omega) \left(z_\alpha^2 + 2z_\alpha\rho_\alpha\sqrt{\frac{4\pi}{3}}Y_{1,0}(\Omega) \right. \\ &+ \left. \rho_\alpha^2 \left\{ \sqrt{\frac{16\pi}{45}}Y_{2,0}(\Omega) + \frac{1}{3} \right\} \right) \\ &= \sqrt{4\pi}\left(z_\alpha^2 + \frac{\rho_\alpha^2}{3} \right)\delta_{1,0;m,0} + \sqrt{\frac{4\pi}{3}} 2 z_\alpha \rho_\alpha \delta_{l,1;m,0} \\ &+ \sqrt{\frac{16\pi}{45}}\rho_\alpha^2 \delta_{l,2;m,0} \end{aligned}$$

$\exp(i\mathbf{G}_m.\mathbf{R} \pm G_m z)$ Terms

$$\exp(i\mathbf{G}_m.\mathbf{R} \pm G_m z) = \exp(i\mathbf{G}_m.\mathbf{r}_\alpha \pm G_m z_\alpha)\exp(i\mathbf{G}_m.\boldsymbol{\rho}_\alpha \pm G_m \rho_z)$$

Now

$$\exp(i\mathbf{G}_m.\boldsymbol{\rho}_\alpha \pm G_m\rho_z) = \exp(G_m\rho_\alpha(i\sin\theta\cos\phi \pm \cos\theta)) \tag{4.32}$$

where θ is the usual spherical polar angle of ρ_α, and ϕ is the angle between $\boldsymbol{\rho}_\alpha$ and $\mathbf{G}_m$. 4.32 is expanded as

$$\sum_l \frac{(G_m\rho_\alpha)^l}{l!}(\pm 1)^l(\cos\theta \pm i\sin\theta\cos\phi)^l$$

But from Hobson [39]

$$\begin{aligned}
(\cos\theta \pm i\sin\theta\cos\phi)^l &= P_l(\cos\theta) + 2\sum_{m=1}^{l}(\mp 1)^m \exp\left(-im\frac{\pi}{2}\right) \\
&\times \frac{l!}{(l+m)!}P_l^{|m|}(\cos\theta)\cos m\phi \\
&= \left(\frac{4\pi}{2l+1}\right)^{\frac{1}{2}}\left\{Y_{1,0}(\theta,\phi) + 2\sum_{m=1}^{l}(\pm 1)^m \exp\left(im\frac{\pi}{2}\right)\frac{l!}{((l+m)!(l-m)!)^{\frac{1}{2}}}\right. \\
&\times \left. Y_{l,m}(\theta)\cos m\phi\right\} \\
&= \left(\frac{4\pi}{2l+1}\right)^{\frac{1}{2}}\left\{Y_{1,0}(\theta,\phi) + \sum_{m=1}^{l}(\pm 1)^m \frac{l!}{((l+m)!(l-m)!)^{\frac{1}{2}}}\right. \\
&\times \left.\left[\exp\left(im\frac{\pi}{2}\right)Y_{l,-m}(\theta,\phi) + \exp\left(-im\frac{\pi}{2}\right)Y_{l,m}(\theta,\phi)\right]\right\} \\
&= \sum_{m=-l}^{l}\left[\frac{4\pi}{(2l+1)(l+m)!(l-m)!}\right]^{\frac{1}{2}}(\pm 1)^m(-i)^m l!Y_{l,m}(\theta,\phi)
\end{aligned}$$

Hence

$$\begin{aligned}
\exp(i\mathbf{G}_m.\boldsymbol{\rho}_\alpha \pm G_m\rho_z)|_{l,m,\alpha} &= (\pm 1)^{l+m}(-i)^m\left[\frac{4\pi}{(2l+1)(l+m)!(l-m)!}\right]^{\frac{1}{2}} \\
&\times (G_m\rho_\alpha)^l Y_{l,m}(\theta,\phi)
\end{aligned} \tag{4.33}$$

Now ϕ in 4.33 is given by $\phi_{\rho_\alpha} - \phi_{\mathbf{G}_m}$ these being the usual spherical polar angles of ρ_α and $\mathbf{G}_m$ respectively. So

$$\exp(i\mathbf{G}_m.\mathbf{R} \pm G_m z)|_{l,m,\alpha} = \exp(i\mathbf{G}_m.\mathbf{r}_\alpha \pm G_m z_\alpha)(\pm 1)^{l+m}(-i)^m \times \left[\frac{4\pi}{(2l+1)(l+m)!(l-m)!}\right]^{\frac{1}{2}} (G_m\rho_\alpha)^l \exp(-im\phi_{\mathbf{G}})$$

The coefficients of the real spherical harmonics are determined as in the construction of the charge density (3.64).

Now that we have derived the $(l,m)^{th}$ components of the interstitial potential on the muffin tin surfaces, we can integrate Poisson's equation, using these as the boundary conditions, to find $V_{l,m}(r)$. In spherical coordinates, Poisson's equation is

$$\frac{\partial}{\partial r}\left(r^2\frac{\partial V_{l,m}}{\partial r}\right) + 4\pi^2 r^2 \rho_{l,m}(r) - l(l+1)V_{l,m} = 0$$

A similar procedure to that used for solving the Dirac equation is implemented here. Change variables to

$$r = \exp(x)$$

$$\Rightarrow \frac{\partial}{\partial r} = \exp(-x)\frac{\partial}{\partial x}$$

Also, put $W = \exp(\frac{x}{2})V_{l,m}$. So

$$\exp(-x)\frac{\partial}{\partial x}\left(\exp(x)\frac{\partial}{\partial x}\left(\exp(-\frac{x}{2})W\right)\right) + 4\pi\exp(2x)\rho_{l,m} - l(l+1)\exp(-\frac{x}{2})W = 0$$

$$\Rightarrow W'' = (l+\frac{1}{2})^2 W - 4\pi\exp(\frac{5x}{2})\rho_{l,m} \qquad (4.34)$$

r and x are discretised as before.

$$r_n = r_0\exp(\delta(n-1)) \qquad x_n = \ln r_0 + \delta(n-1)$$

To solve $W'' = f(W)$, first find a predictor

$$W_+^P = 2W_0 - W_- + \delta^2 f_0$$

where

$$f_0 = f(W_0)$$

The corrected value for W_+ is

$$W_+^C = W_+^P + \frac{\delta^2}{12}(f_+^P + f_- - 2f_0)$$

Finally, take

$$W_+ = W_+^C + \frac{\delta^2}{30}(f_+^C - f_+^P)$$

This is the Baylis-Peel version of the Numerov algorithm [40].

The first two values of W are required. Neglecting the inhomogeneous term in 4.34 gives

$$W'' = (l + \frac{1}{2})^2 W$$

So, take $W = \exp((l + \frac{1}{2})x)$ for the first two values of x.

Now integrate Poisson's equation to obtain a solution $\tilde{V}_{l,m}(r)$. Add $-\sqrt{4\pi}Z\delta_{l,0}/r$ (nuclear potential) to this, and a solution to Laplace's equation such that the total potential equals $V_{l,m}(\rho_\alpha)$ as given by the interstitial expansion. So

$$V_{l,m}(r) = \tilde{V}_{l,m}(r) - \frac{\sqrt{4\pi}Z\delta_{l,0}}{r} + \left(\frac{r}{\rho_\alpha}\right)^l \left\{ V_{l,m}(\rho_\alpha) - \tilde{V}_{l,m}(\rho_\alpha) + \frac{\sqrt{4\pi}Z\delta_{l,0}}{r} \right\}$$

The average pseudo charge density and potential in a plane at given z are evaluated. These are given by

$$\bar{\rho} = \sum_{0,n} \hat{\rho}_{0,n} \begin{cases} \cos k_n z \\ \sin k_n z \end{cases}$$

and

$$\bar{V} = V_{0,0} z + V_1 z^2 + \sum_{0,n} V_{0,n} \begin{cases} \cos k_n z \\ \sin k_n z \end{cases}$$

4.5 Exchange-Correlation Potential

The exchange-correlation potential must now be added to the electrostatic potential determined in section 4.4. In the interstitial region, $V_{xc}(\mathbf{r})$ is expanded as

$$V_{xc}(\mathbf{r}) = \sum_{\text{stars } j} V_{xc,j} \sum_{m,n \text{ in } j} \exp(i\mathbf{G}_m.\mathbf{R}) \begin{cases} \cos k_n z \\ \sin k_n z \end{cases}$$

Random points $\{\mathbf{r}_i\}$ are chosen in the interstitial region and $\{V_{xc}(\mathbf{r}_i)\}$ is calculated, the coefficients $\{V_{xc,j}\}$ then being determined via a least squares fit at these points. The calculations in this thesis use the Kohn-Sham local density approximation to V_{xc}, as given by equation 2.11.

Inside the muffin-tins, a Taylor expansion for V_{xc} is used. Write

$$\rho(\mathbf{r}) = \frac{1}{\sqrt{4\pi}}\rho_{0,0}(r) + \sum_{l,m}{}' \rho_{l,m}(r)Y_{l,m}(\Omega)$$

Hence, to first order

$$V_{xc}(\mathbf{r}) = V_{xc}\left(\frac{1}{\sqrt{4\pi}}\rho_{0,0}(r)\right) + \sum_{l,m}{}' \frac{\partial V_{xc}}{\partial \rho}\left(\frac{1}{\sqrt{4\pi}}\rho_{0,0}(r)\right)\rho_{l,m}(r)Y_{l,m}(\Omega)$$

Having added the exchange-correlation potential to the previously calculated electrostatic potential, the new potential is mixed with that from the previous iteration. Let f be the mixing factor. Then

$$V_{n+1}^{\text{in}} = fV_n^{\text{out}} + (1-f)V_n^{\text{in}}$$

Once partial convergence has been achieved using a constant mixing factor, the alternating factor scheme of Dederichs and Zeller [41] has been found to greatly increase the rate of convergence.

4.6 Summary

The self-consistent cycle has now be completed, with the construction of the new potential. The mixing is necessary in order to prevent instabilities in the

potential from building up at the next iteration. The analytic and implementation details are now finished, and the next stage involves program tests and applications.

Chapter 5

Program Tests and Metallic Systems

In this chapter the method and program are applied to several metallic systems, and the problems encountered are discussed. An obvious first test is to consider the junction between two identical materials, by treating a slab of that material embedded between the same material in both substrates, which should recover the bulk electronic structure. This test is done for the nearly free electron metal, Al, and the transition metal, Ni, and the results compared with the known electronic structure of bulk Al and Ni respectively. Finally, an aluminium-nickel (001) junction is used as an example of a simple metallic interface. Calculations have been done using different numbers of LAPWs, charge density plane waves, and different positions of the embedding planes. It is observed that instabilities in the charge density or density of states can arise with certain sizes of basis set, although consistent results can be obtained by avoiding these particular bases. The Al-Ni (001) calculation shows the existence of states other than those due to the bulk, and the nature of these states is discussed.

The calculations were performed on the FPS-164 vector processor attached to the 'NAS' mainframe at Daresbury Laboratory.

5.1 Bulk Aluminium System

The ⟨001⟩ direction is considered, by including two layers of Al in the interface slab, with an Al embedding potential on either side. Fig. 5.1 shows the geometry, parameters used, and illustrates the two dimensional direct lattice basis. The embedding planes are placed half way between the layers of Al atoms. The starting potential is of the simple muffin tin form, and is taken from the output of a self consistent LMTO bulk Al calculation. The Fermi energy for this potential is known, and is used as the upper energy limit for the charge density construction, with the lower energy limit lying below the bottom of the valence bands, but above the core states.

The basis set parameters used are as in Table 5.1. NAPW refers to the number of LAPWs, NSM to the number of rings of two dimensional wavevectors in the LAPW basis set, and NCPW to the number of charge density plane waves. Initially the volume of reciprocal space filled by the LAPWs

NAPW	100
NSM	4
NCPW	1500

Table 5.1: Basis set parameters for bulk Al

was spherical, as is usually the case in band structure calculations. However, for this work, this has often been found to produce instabilities in the charge density. Typically, these cause large non-physical fluctuations in the charge density, with virtually no charge in large volumes of the unit cell, and very high concentrations elsewhere. This problem is also characterised by the loss of overall charge neutrality when evaluating the total charge in the embedded region. Increasing the number of wavevector components perpendicular to the embedding plane, (k_z), by restricting the number of (k_x, k_y) vectors has reduced, but not eliminated this problem. Essentially this is equivalent to filling an ellipsoidal volume of reciprocal space, with the major axis of the ellipse

perpendicular to the embedding planes. The effect of this is to allow greater variation of the wavefunction along the z-axis. One conclusion may be that the improvement could be obtained by simply increasing the LAPW basis set size, while keeping it spherical. There are two problems associated with this. Firstly, using 200 LAPWs with no ring restriction did not eliminate the problem. Secondly, attempts to use more than 200 LAPWs would involve using a prohibitively large amount of computer time. The value of NSM in Table 5.1 above refers to the number of rings used for this restriction. Note that the 'n' values for the pseudo charge density expansion, as described in section 4.3, are given in Fig. 5.1. The program reads in nine values for $l = 0$ to 8, but in this case only the first four are used, as using larger l has not been found to be necessary. The values are taken from Table 4.1.

Before continuing this discussion it is worth noting the parameters used for constructing the embedding potentials. There are four parameters of interest. These are

1. Number of rings of real space lattice vectors to be used in the real space contribution to the structure constants.

2. As **1** but for reciprocal space.

3. Maximum number of reciprocal lattice vectors to be used for expanding the embedding potentials.

4. Number of energy points at which the embedding potentials are evaluated.

The values 6,6,8,16 have been found to be suitable in most cases. Smaller values more often give rise to unstable charge densities. This is because there must be sufficient plane waves in the embedding potential expansion to match the two dimensional components of each LAPW in the interface slab. Increasing **3** or **4** above uses considerably more computer time. The values chosen reflect a suitable compromise, having been arrived at via trial and error. Of course, for density of states calculations, many more energy points are used, typically 100. In this case **3** above is reduced from 8 to 6.

Initially only one cycle is done, with the charge density and density of states shown in Figs. 5.2 to 5.5. The core region is omitted from the charge density plots for clarity. The density of states is calculated at the symmetry points $\bar{\Gamma}$, $\bar{X}$, $\bar{M}$ of the two dimensional Brillouin zone, which is related to the $k_z = 0$ plane of the usual face centred cubic Brillouin zone as shown in Fig. 5.6. The bandstructure of Al has been calculated at the symmetry points $\bar{\Gamma}$, $\bar{X}$, $\bar{M}$ (Figs. 5.7-5.9), to facilitate comparison with the density of states. The program to construct the embedding potentials has an option to produce the bands, which is used here. Since the density of states is inversely proportional to $\nabla_k E$, there will be a peak wherever the bands are flat. Comparison of Figs. 5.3 to 5.5 with Figs. 5.7 to 5.9 shows remarkably good agreement. The peaks in the density of states are broadened due to the energy points being shifted off the real axis by including a small imaginary part in the energy, in this case taken to be 0.002 Hartrees.

As the starting potential is a good approximation to the real Al potential, we should expect self-consistency to be rapidly attained. This is indeed the case, with the maximum error in the output potential being 0.004 Hartrees after 15 iterations. This error refers to the difference in potential at the muffin tin grid points for the output potential, relative to the input potential. Three representative **K** points are used. The first five iterations use a mixing factor of 0.05, and the last ten use alternating mixing factors of 0.05 and 0.25. The charge density, potential, and density of states are in Figs. 5.10 to 5.14. These compare well with the non-self-consistent results, showing no major changes, which would be indicative of a program problem in the self-consistent loop.

Finally we examine the effect of moving the embedding planes. For self consistency these must be half way between atomic planes in order to preserve charge neutrality. Hence, moving the planes to some other position will not allow self consistency to be attempted. A calculation using the LMTO potential as before, but for ζ_1 and ζ_2 at $\pm$D/2, has been performed and agrees well with the previous results (See Figs. 5.15 to 5.18). The number of LAPWs in this case is 150, but 4 rings are still used. It has been found that charge

density instabilities are less of a problem with the embedding planes at $\pm D/2$ than half way between the atomic planes. The main difference in this case is that the embedding planes no longer intersect the muffin tin spheres in the interface slab, although it is not apparent why this should improve matters.

This completes the program tests for Al, an example of a nearly free electron metal. Next we consider the case of a transition metal, namely nickel.

5.2 Bulk Nickel System

The lattice is still face centered cubic as for Al, with parameters as in Table 5.2. The list of figures relevant to bulk Ni is given in Table 5.3.

a	=	4.699 au
ζ_1	=	3.322695 au
ζ_2	=	-3.322695au
Ni muffin tin radius	=	2.34957 au
D	=	8.021835 au
$\bar{D}$	=	9 au
E	=	-0.08 $\rightarrow$ 0.215 Hartrees, 16 energy points.
'n' for pseudo ρ expansion	=	11,10,9,8

Table 5.2: Parameters for bulk Ni

5.19 $\rightarrow$ 5.22	Non self consistent, NAPW=100, NSM=4, NCPW=1500.
5.23 $\rightarrow$ 5.25	Bands at $\bar{\Gamma}$, $\bar{X}$, $\bar{M}$.
5.26 $\rightarrow$ 5.30	Self consistent, maximum error=0.01,
	10 iterations required. Constant mixing factor of 0.02 used.
5.31 $\rightarrow$ 5.34	Embedding planes at $z = \pm D/2$, NAPW=150.

Table 5.3: List of Figures for bulk Ni

In Figs. 5.23-5.25, the interpolation between the discrete points in the calculated band structure was aided by using existing energy band diagrams [42]. As for Al, the calculated density of states correlates very well with the band structure. Also, good agreement between the non-self consistent, self consistent, and shifted embedding plane densities of states is obtained. Slight differences in the appearance of some plots can be attributed to small movements of peaks, which because of the relatively flat Ni d-bands, are very sharp. The only anomaly is a peak in the density of states at $\bar{M}$ $(\frac{1}{2}, \frac{1}{2})$ of energy 0.16

Hartrees, for the embedding planes at $\pm D/2$ (Fig. 5.34), which does not appear in the other Ni densities of states at $\bar{M}$, nor in the Ni bands at $\bar{M}$. As is to be expected, the Ni densities of states are dominated by the effect of the relatively flat d-bands.

5.3 Aluminium-Nickel Junction

The Al-Ni (001) interface is considered in this section, as an example of an s-p bonded metal on a transition metal. Experimental data using electron induced x-ray emission spectroscopy [43] indicates that there is little $3d$-sp interaction, and that the interface is steep, with little AlNi compound being formed. The geometry and parameters are as shown in Figs. 5.35. Only one layer each of Al and Ni are explicitly considered, due to the short screening length in metals. Thirty iterations using 150 LAPWs were required for maximum errors in the Al and Ni muffin tin potentials of 0.004 Hartrees. Alternating mixing factors of 0.05 and 0.200, and three representative **K** points were used.

Account had to be taken of the potential shift across the interface. This is easily evaluated as the Fermi energy (E_F) in each material is known, and when in equilibrium, E_F is constant across the interface. The relevant shifts for Al-Ni are shown below, and the zero of energy in the interface is taken as the average of the interstitial potential in each of the two substrates.

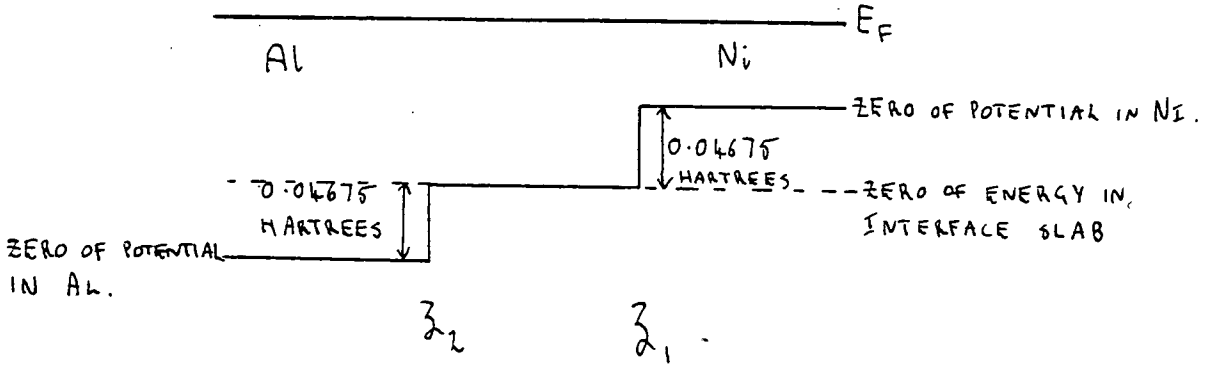

The shift at each side is used as the boundary conditions when solving Poisson's equation, as described in section 4.4.

The charge density, potential, and density of states are in Figs. 5.36 to 5.48. The charge density and potential plots are for each plane of atoms, that is, through the Al and Ni planes respectively, and containing the z-axis. Where the potential is negative, dashed lines are used, and solid lines are used where positive (Figs. 5.38-5.39). The density of states plots are at the symmetry points $\bar{\Gamma}$, $\bar{X}$, $\bar{M}$, and are plotted for each atomic star, as well as for the whole embedded region. Atomic star 1 is Al, and star 2 is Ni. Note that 120 LAPWs are used for the density of states, but 150 for the charge density. 150 LAPWs produced no problems with the charge density, but led to spurious peaks in the density of states, which disappeared when using either 80, 100, 120, or 200 LAPWs. Finally note that when comparing the Al-Ni results with the bulk case, one should remember to take account of the shift in zero of energy across the interface. The potential shift (0.04675 Hartrees) must be subtracted on the Al side, and added on the Ni side, in order to obtain the energy in the interface calculation.

Referring first to the density of states at $\bar{\Gamma}$ in the Al muffin tin (Fig. 5.40), shows an initial broad peak due to the Al s-p band, then a flat section from the overlap of the Ni s-p band inside the Al muffin tin. Most interesting is the peak at 0.192 Hartrees, which lies in the nearly free electron gap of the bulk Al as in Fig. 5.12. This peak is also seen in the Ni muffin tin (Fig. 5.41), but it is not so evident, due to the proximity of the Ni d-bands. To examine this further, the charge density for this state has been plotted (Figs. 5.49-5.51). This shows the localised state to be due to the d_{z^2} orbitals on the Ni, meaning that it is of Δ_1 symmetry. To facilitate comparison with the bulk electronic structure, the band structures have been calculated for the same lattice constant as used in the interface (Figs. 5.58-5.63). The Ni bands at $\bar{\Gamma}$ (Fig. 5.61) show the states of Δ_1 symmetry in bulk Ni, and it is easily seen that the localised state lies at about the middle of the Δ_1 band gap, proving that it is not a bulk Ni state. It is a true interface state in the sense of decaying exponentially into both materials, but the fact that most of its charge density is localised on the Ni suggests that it is akin to a Ni surface state. The electronic structure of

the Ni (001) surface shows d_{z^2} surface states at $\bar{\Gamma}$ near the top and bottom of the Δ_1 gap [44], and these presumably become the interface state of this calculation. The Al is behaving almost like the vacuum as far as the Ni states are concerned, for energies in the Al band gap.

Turning now to the density of states at $\bar{X}$ in the Al and Ni muffin tins (Figs. 5.43 and 5.44) reveals a localised state at energy 0.12 Hartrees. This state lies in the Al free electron gap at $\bar{X}$ as shown in Fig. 5.59. The charge density of this state (Figs. 5.52-5.54) shows it to be due to either d_{zx} or d_{zy} orbitals on the Ni. Since the program symmetrises the charge density, we cannot say which. The localised state is similar to the one at $\bar{\Gamma}$, as it is mainly associated with the Ni, but decays exponentially into both materials.

Finally, the density of states at $\bar{M}$ (Figs. 5.46-5.48) shows a sharp peak at energy 0.216 Hartrees, which is not present in either the bulk Al (Fig. 5.14) or bulk Ni (Fig. 5.30) densities of states. The charge density for this state (Figs. 5.55-5.57) reveals that it is a d_{z^2} state on the Ni, thus implying Z_1 symmetry. Examination of the Ni bands at $\bar{M}$ (Fig. 5.63) reveals that this state lies in the Z_1 gap, near the bottom of the upper Z_1 band. This time the state does not decay into a direct band gap of the Al (Fig. 5.60), but it lies just below the Al Z_1 band, and cannot interact with the Al Z_3 band which is of different symmetry, so essentially the situation is as before, with the state decaying exponentially into the Al.

Apart from the features noted above, the Al and Ni densities of states are very similar to the bulk calculations, indicating little interaction between the two materials, in agreement with the experimental data of Fargues *et al* [43]. To conclude this section, the planar averaged pseudo charge density and electrostatic potential are given in Fig. 5.64.

5.4 Summary

The bulk aluminium and nickel results have verified the correct operation of the program. Good agreement between results, and with the known band

structures is obtained. Problems with instabilities when using certain sizes of basis set have been noted. The exact reason for these problems remains unknown, but with care they can be reduced or even eliminated. The Al-Ni results show the existence of localised states at the Ni surface which decay into the Al band gap. These states are easily distinguished from the continuum of bulk states.

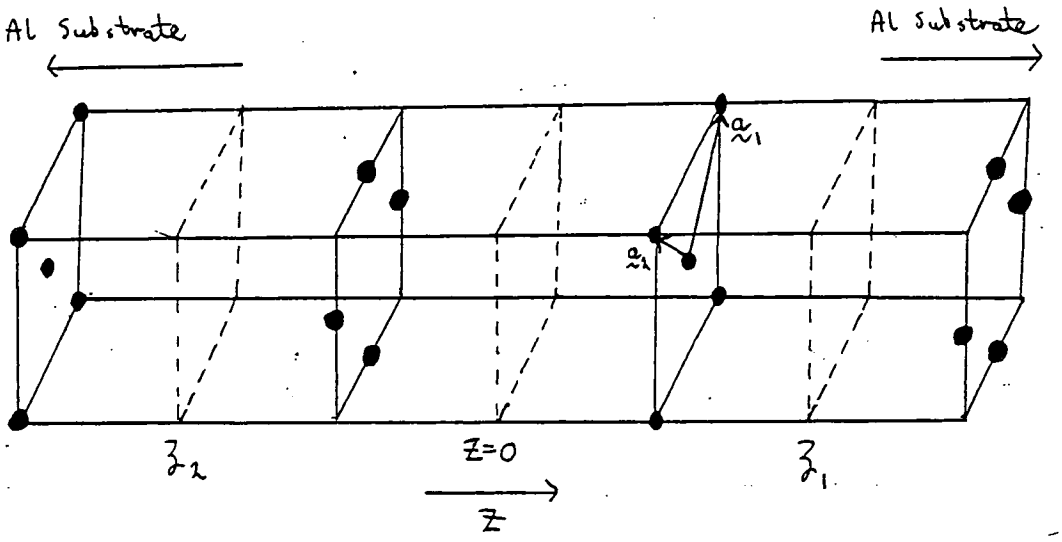

$\|a_1\| = \|a_2\|$	=	5.374au
Al muffin tin radius	=	2.687 au
D	=	9.173992 au
$\tilde{D}$	=	10.0 au
ζ_1	=	3.799992 au
ζ_2	=	-3.799992 au
E	=	-0.12 $\rightarrow$ 0.3085 Hartrees
		16 energy points
n for pseudo ρ expansion	=	12 11 10 9

Fig. 5.1: Bulk Aluminium geometry and parameters.

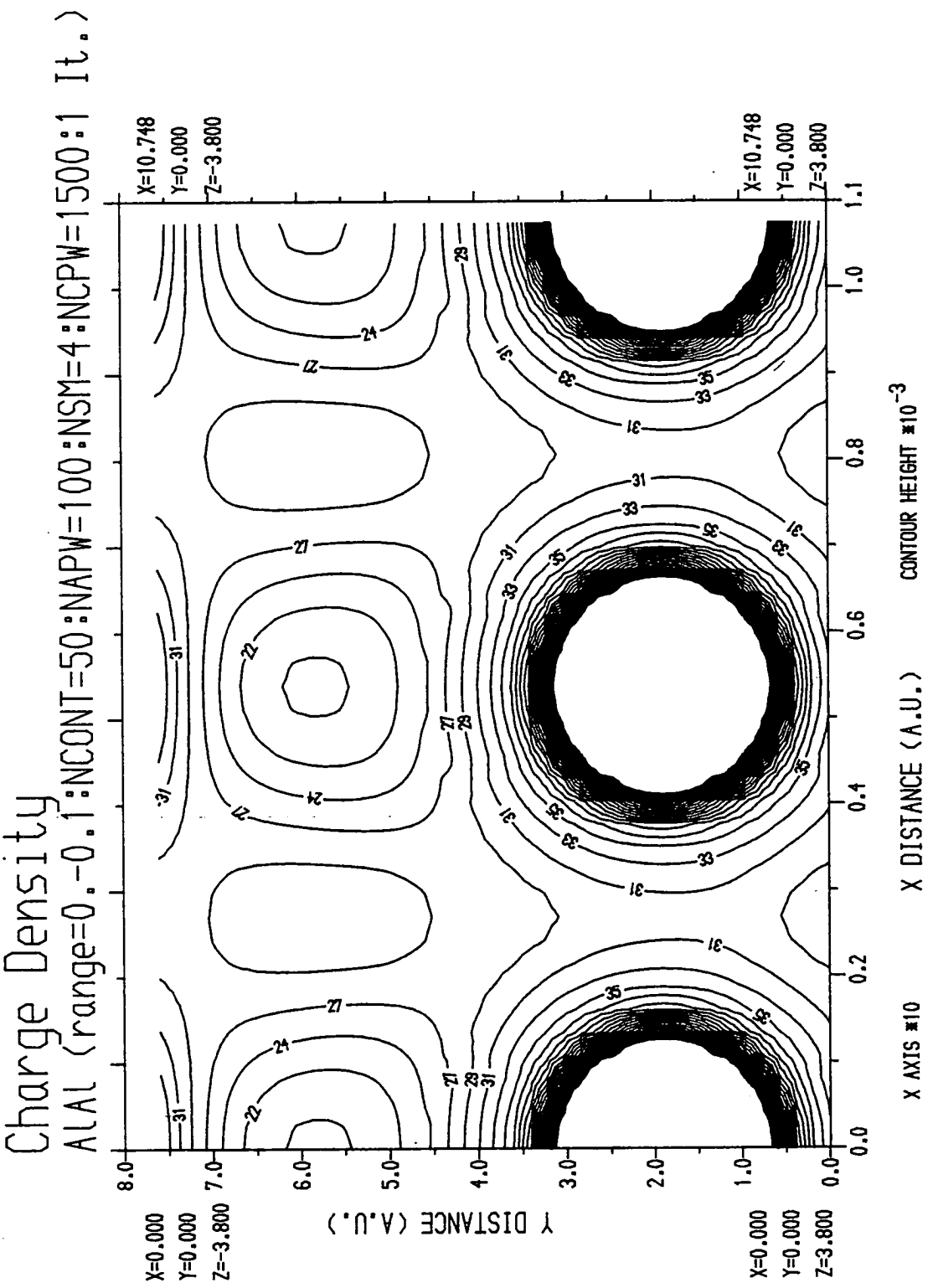

Fig.5.2: Bulk Aluminium charge density after one cycle

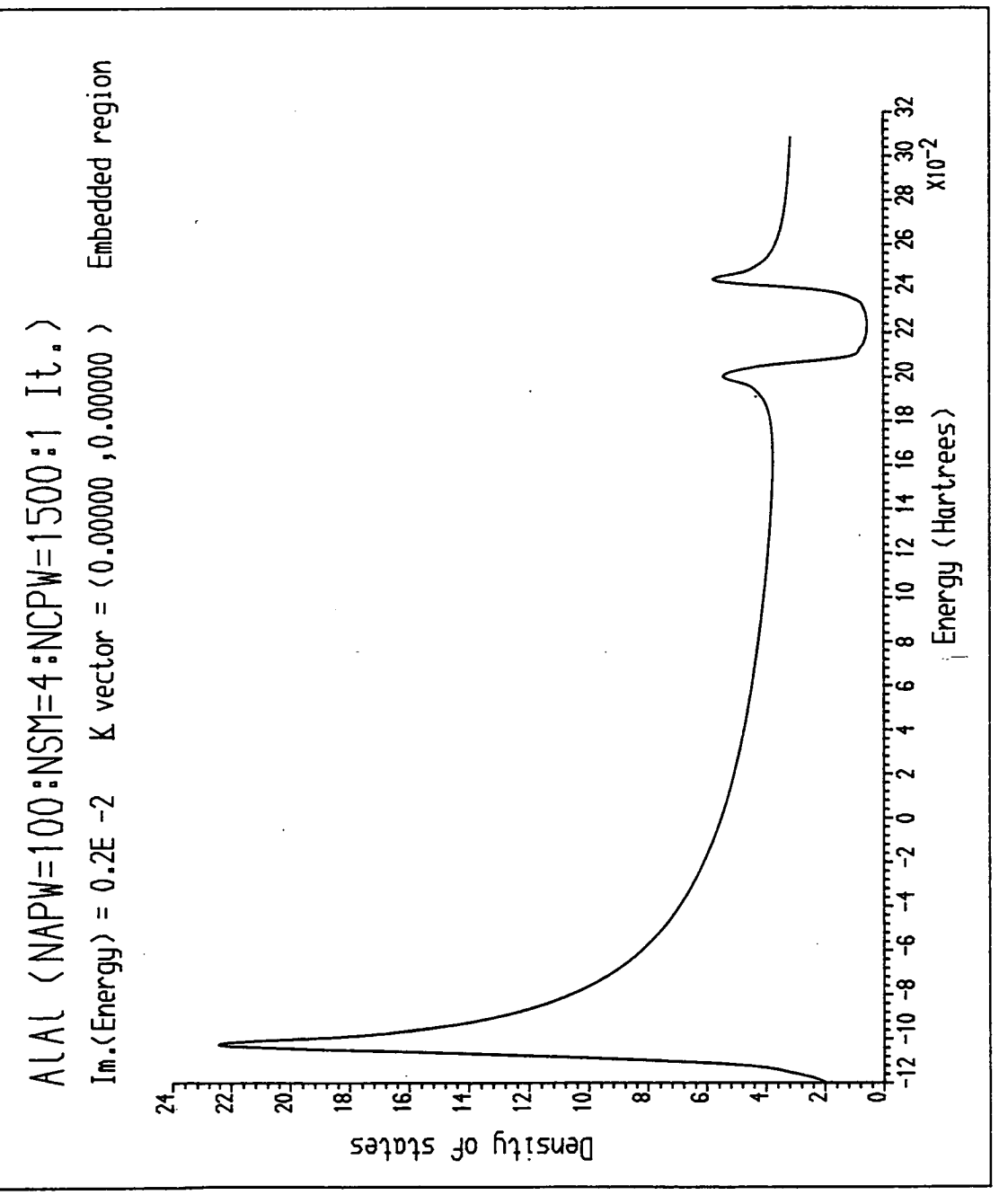

Fig.5.3: Density of states at $\bar{\Gamma}$ for bulk Al after one cycle

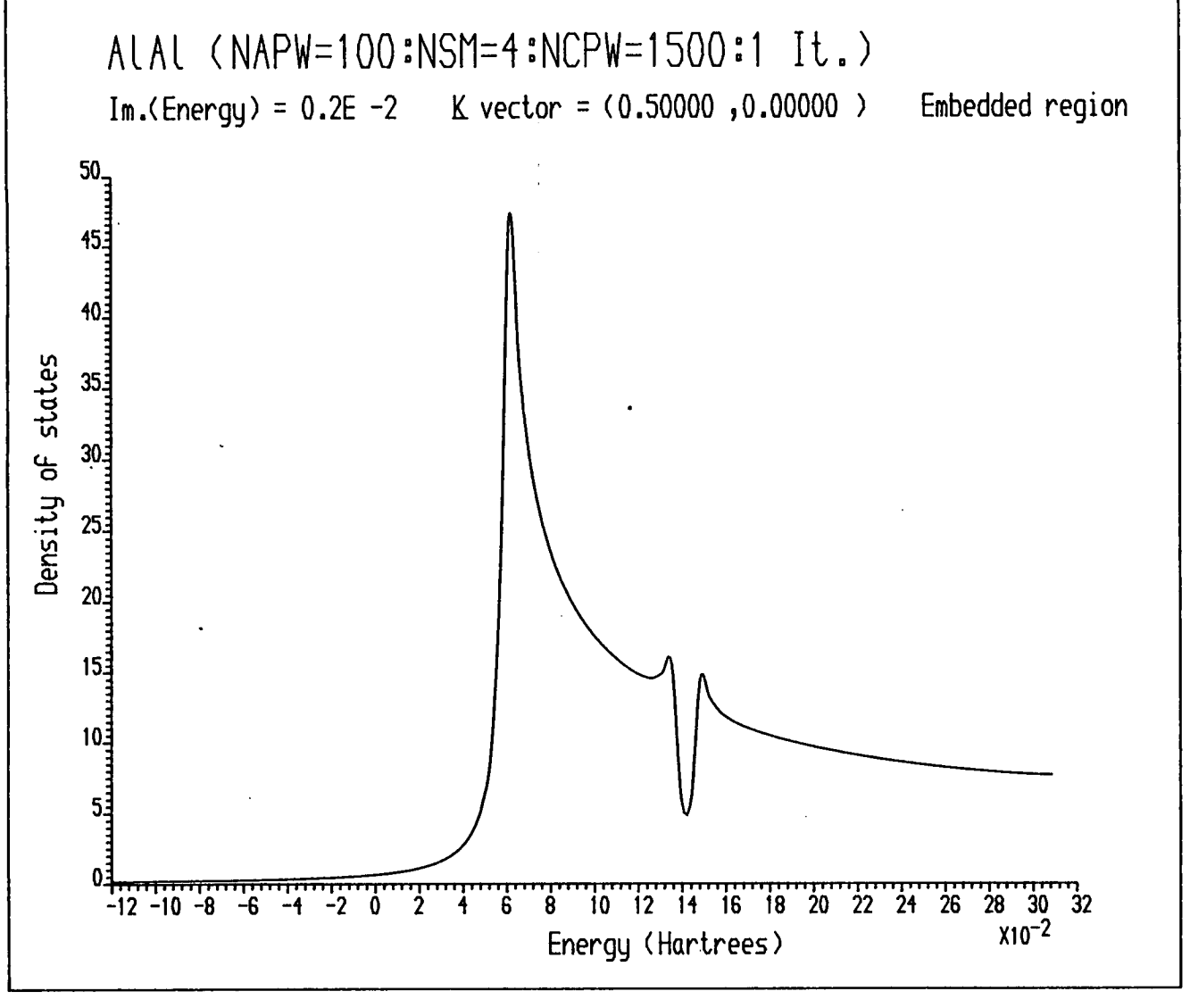

Fig.5.4: Density of states at $\overline{X}$ for bulk Al after one cycle

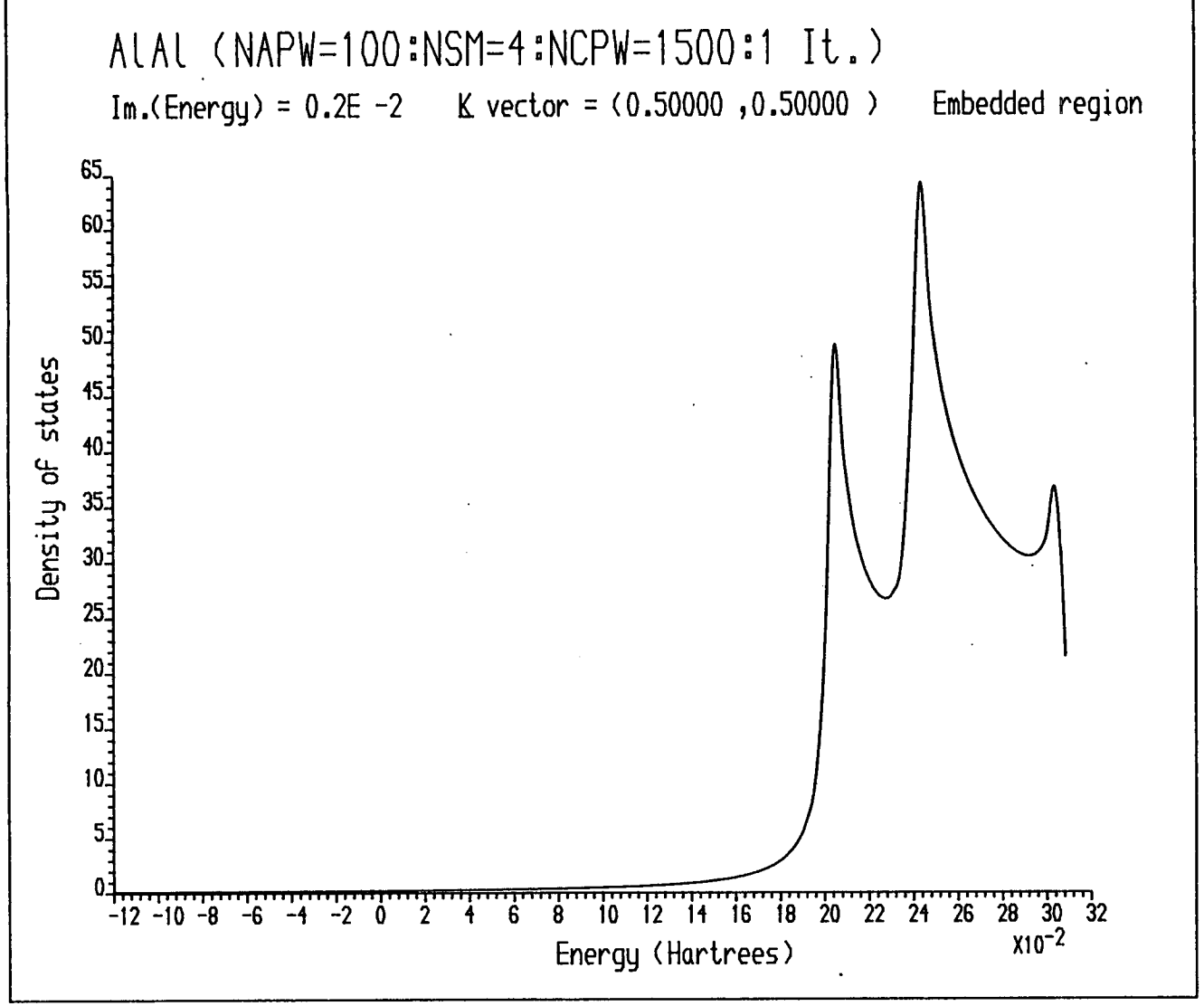

Fig.5.5: Density of states at $\bar{M}$ for bulk Al after one cycle

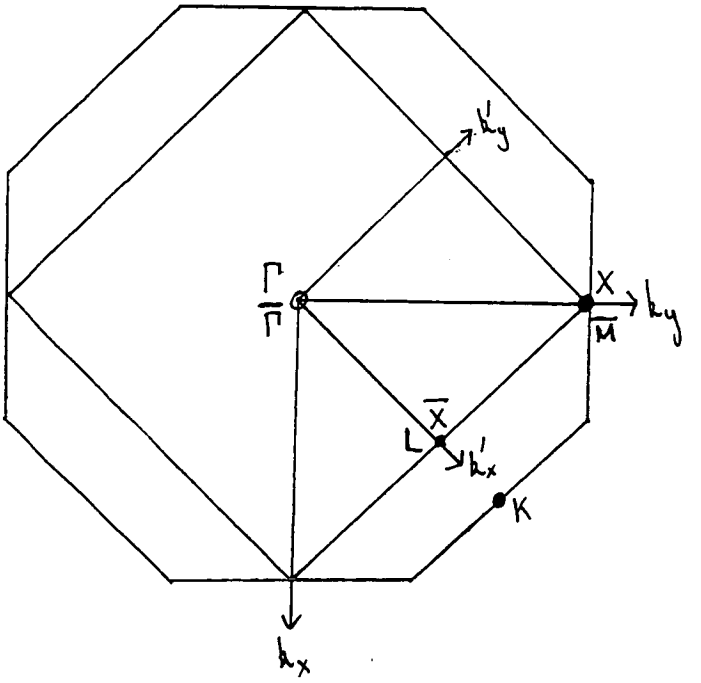

$\bar{\Gamma} = (0,0)$ $\quad \bar{X} = (\frac{1}{2}, 0)$ $\quad \bar{M} = (\frac{1}{2}, \frac{1}{2})$

k_x, k_y : FCC axes $\qquad$ k'_x, k'_y : 2-D axes

Fig.5.6 : Relationship between $k_z = 0$ plane of FCC Brillouin zone and 2-D Brillouin zone

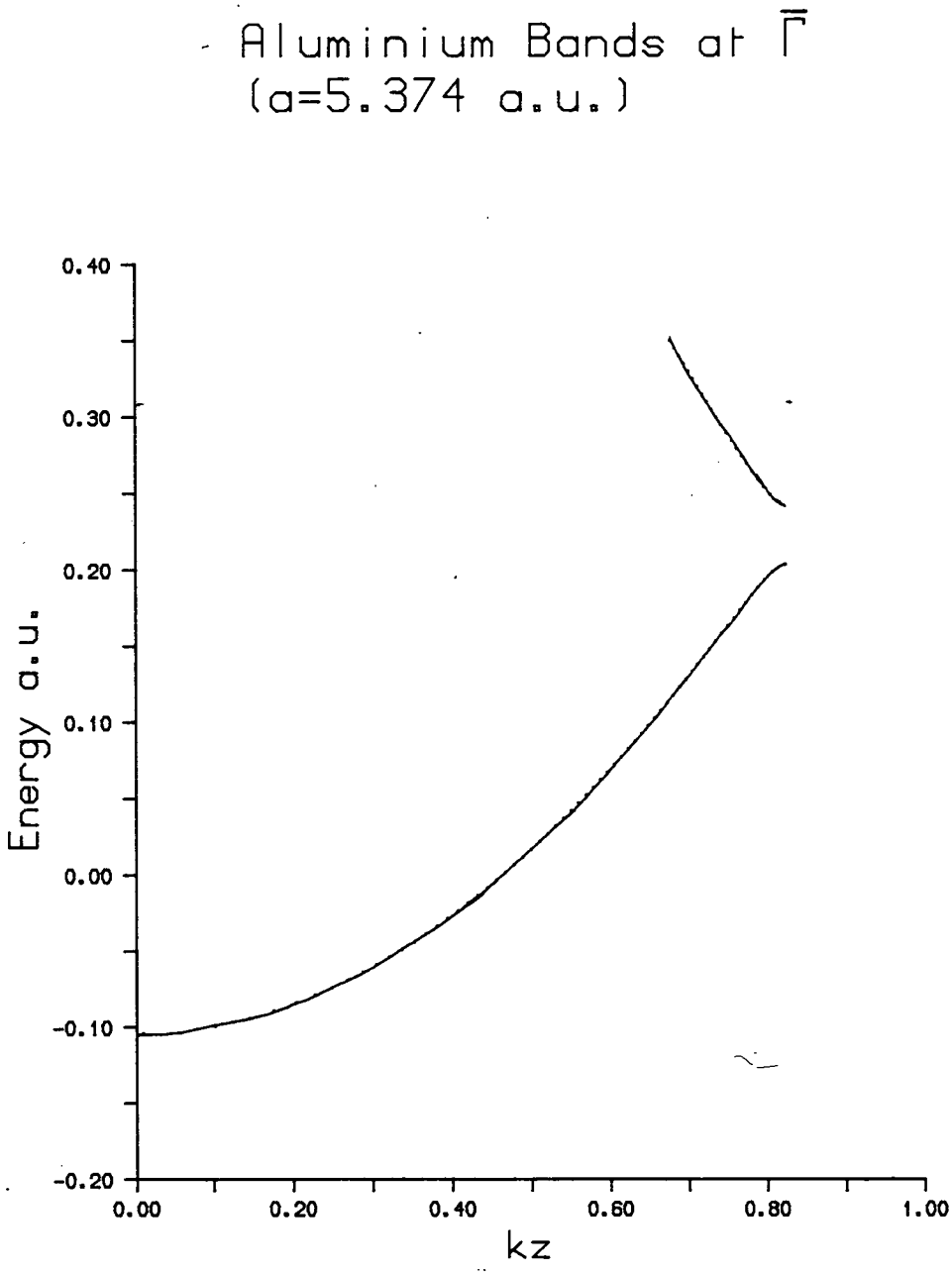

Fig.5.7: Bulk Al bands at $\bar{\Gamma}$

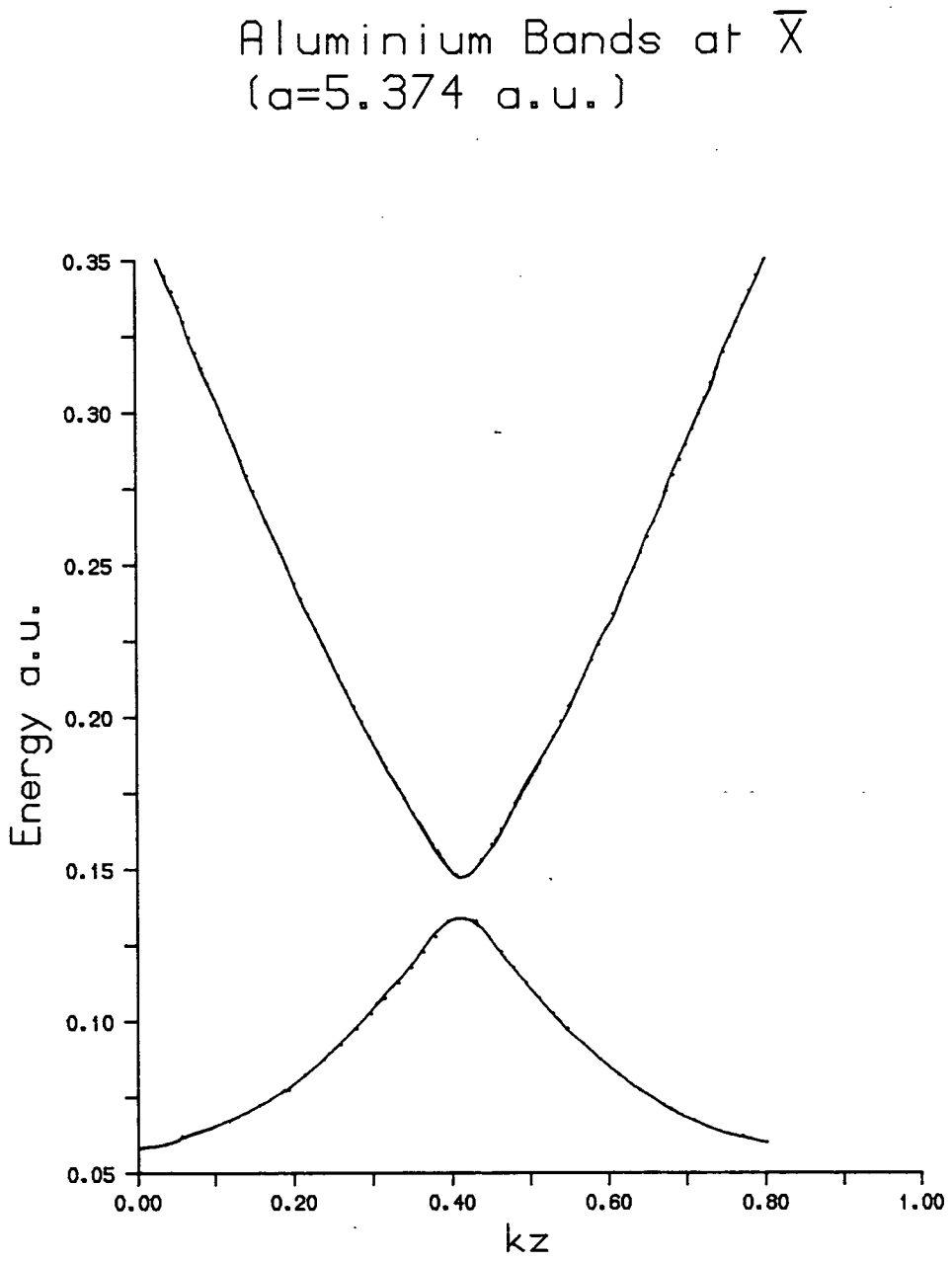

Fig.5.8: Bulk Al bands at $\overline{X}$

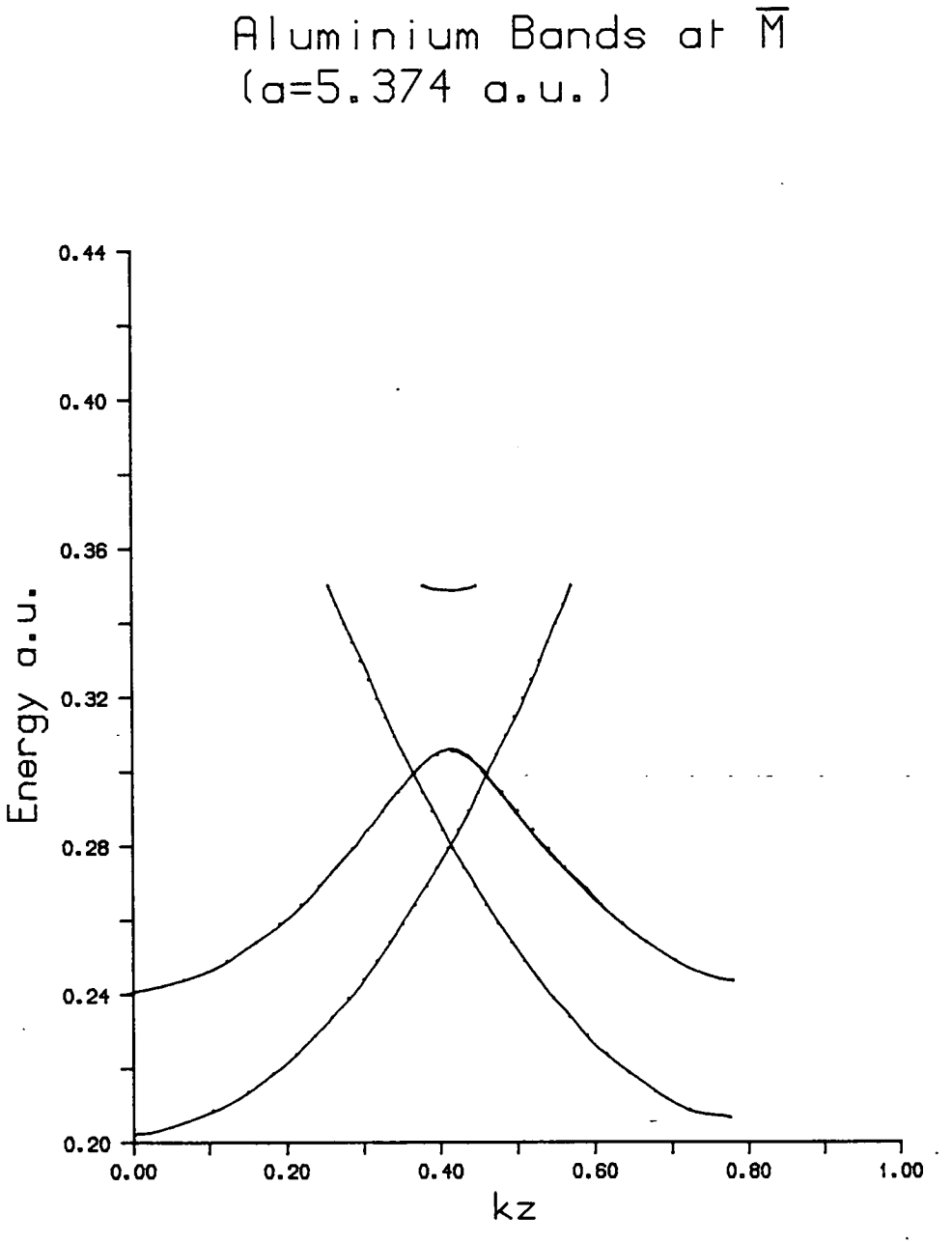

Fig.5.9: Bulk Al bands at $\overline{M}$

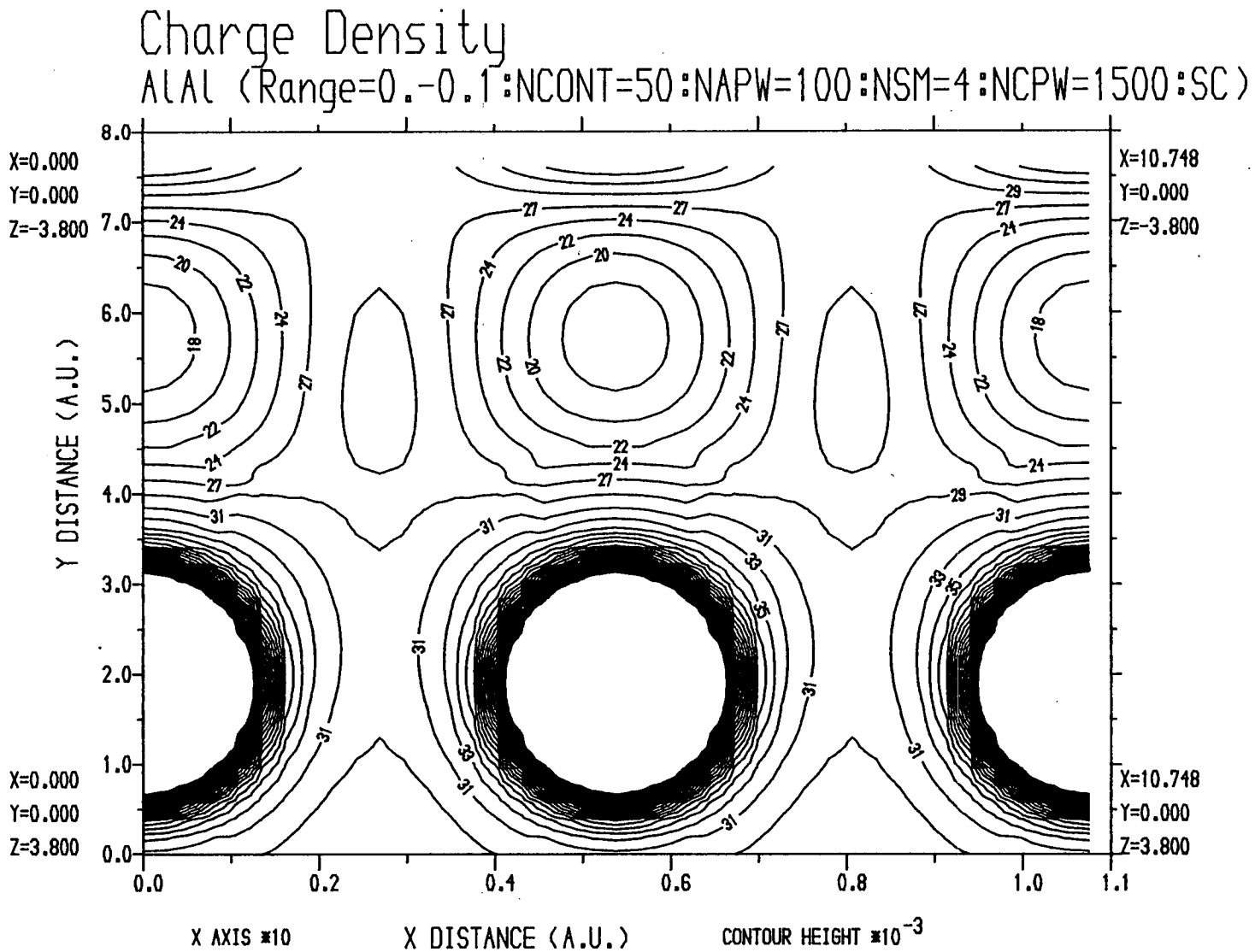

Fig.5.10: Self consistent bulk Al charge density

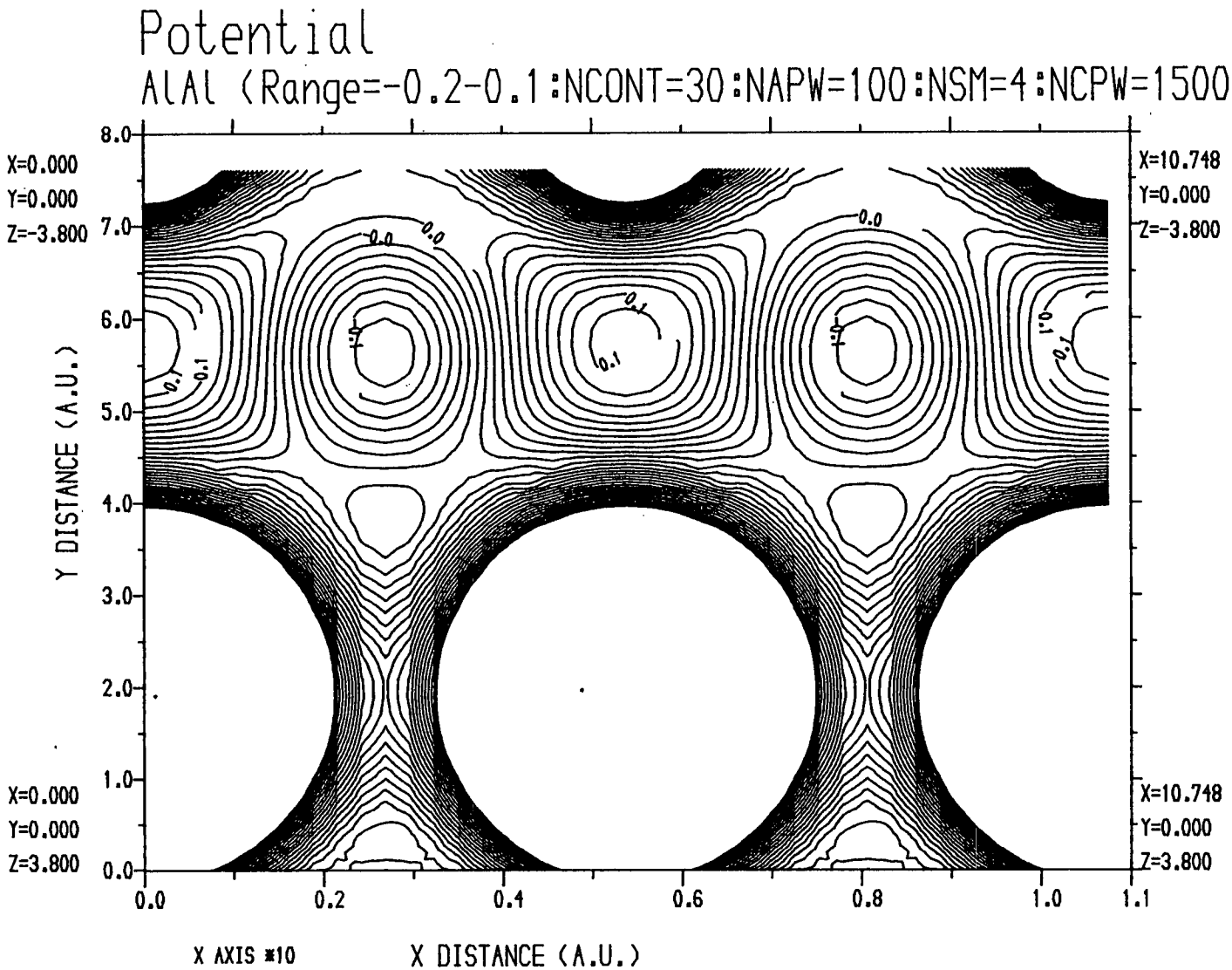

Fig.5.11: Self consistent bulk Al potential

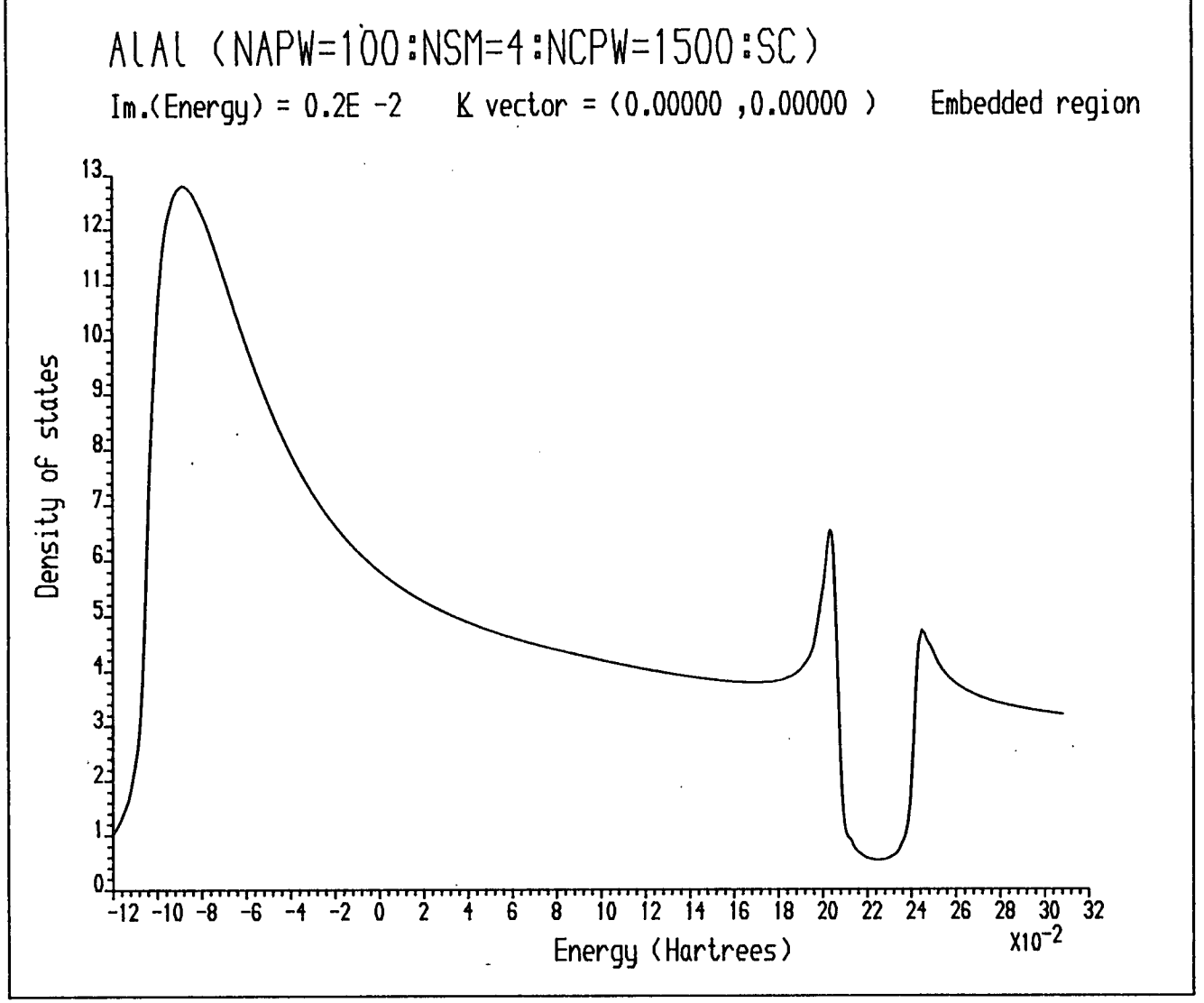

Fig.5.12: Self consistent bulk Al density of states at Γ

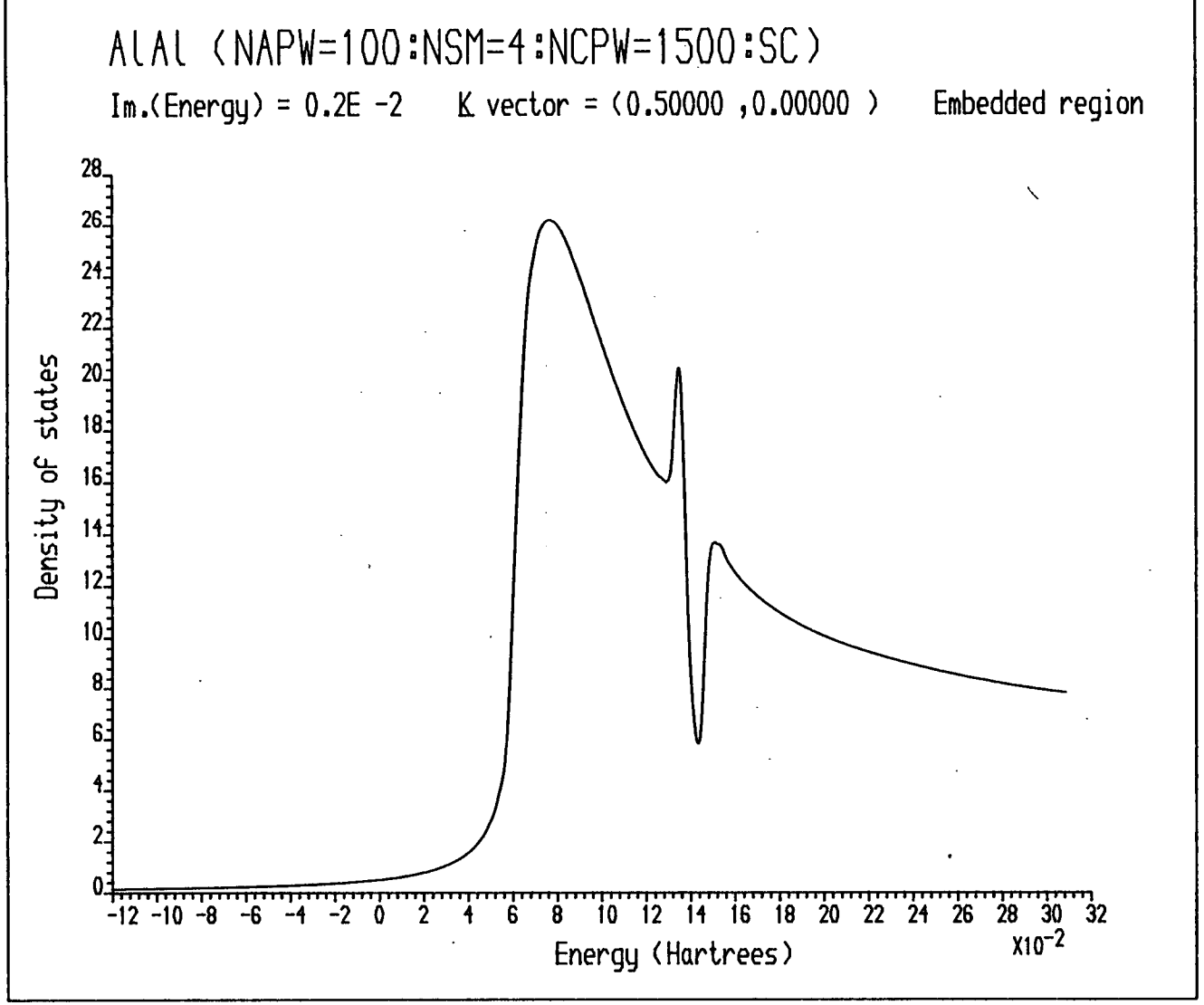

Fig.5.13: Self consistent bulk Al density of states at $\bar{X}$

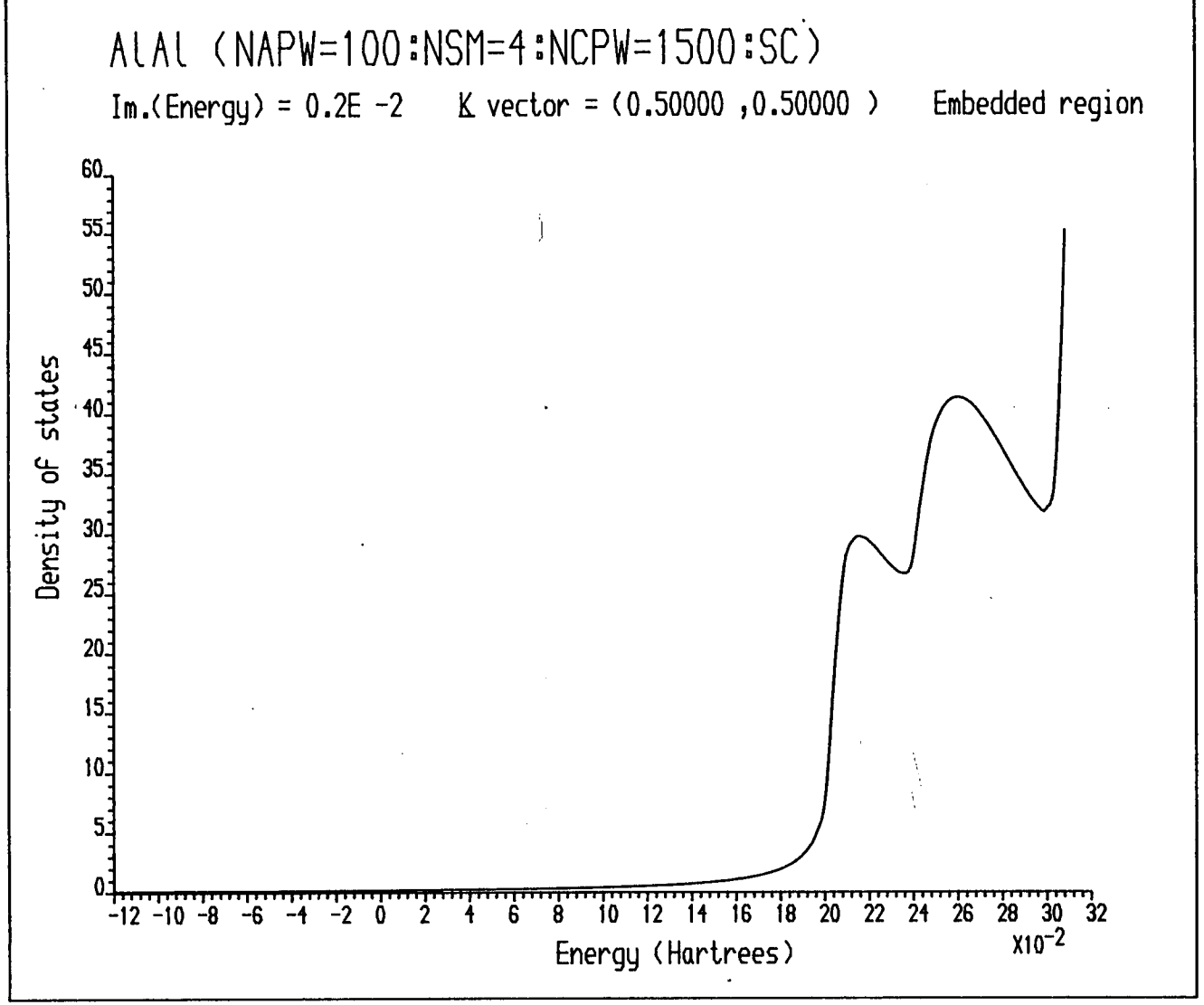

Fig.5.14: Self consistent bulk Al density of states at $\bar{M}$

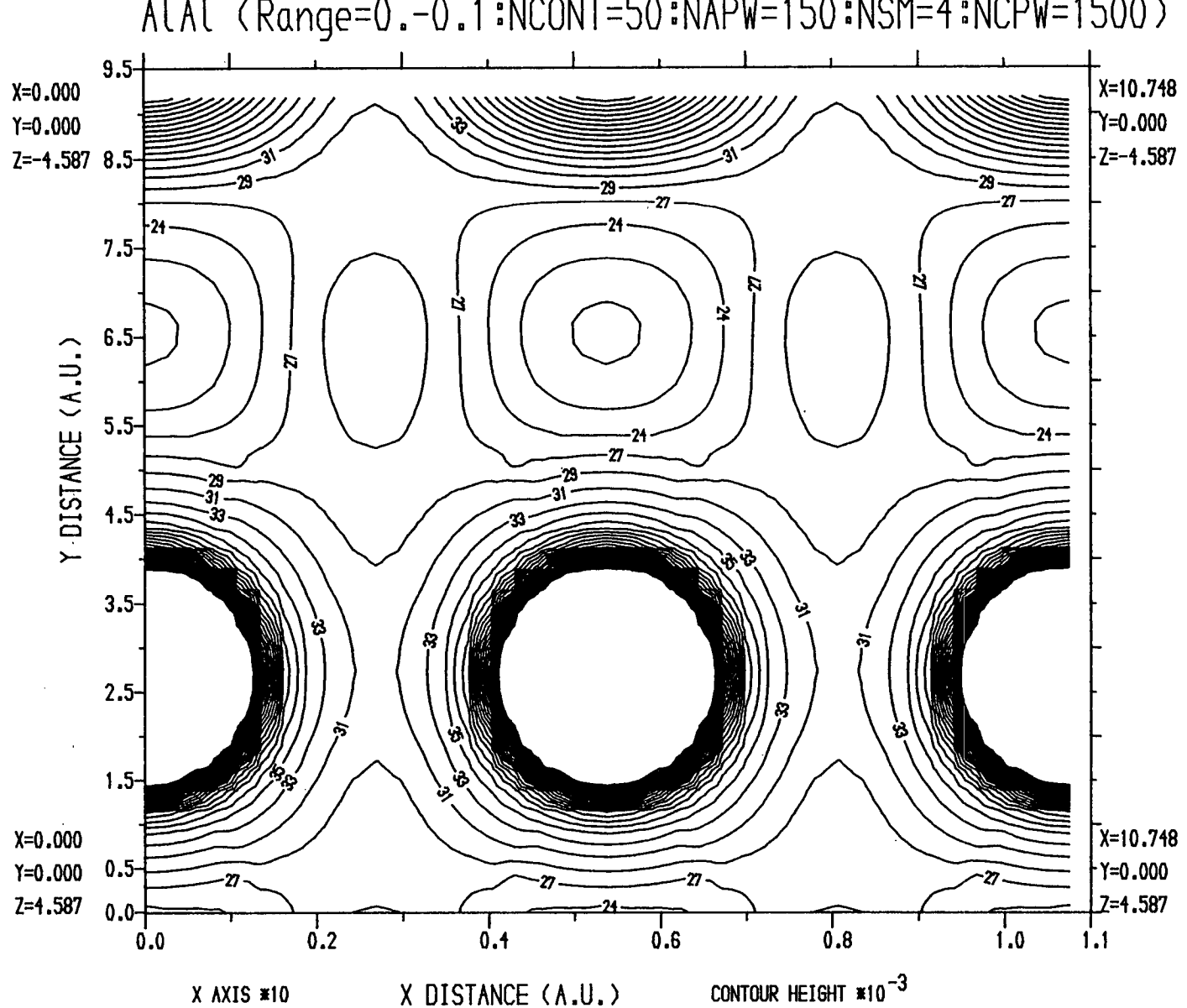

Fig.5.15: Bulk Al charge density for embedding planes at ±D/2

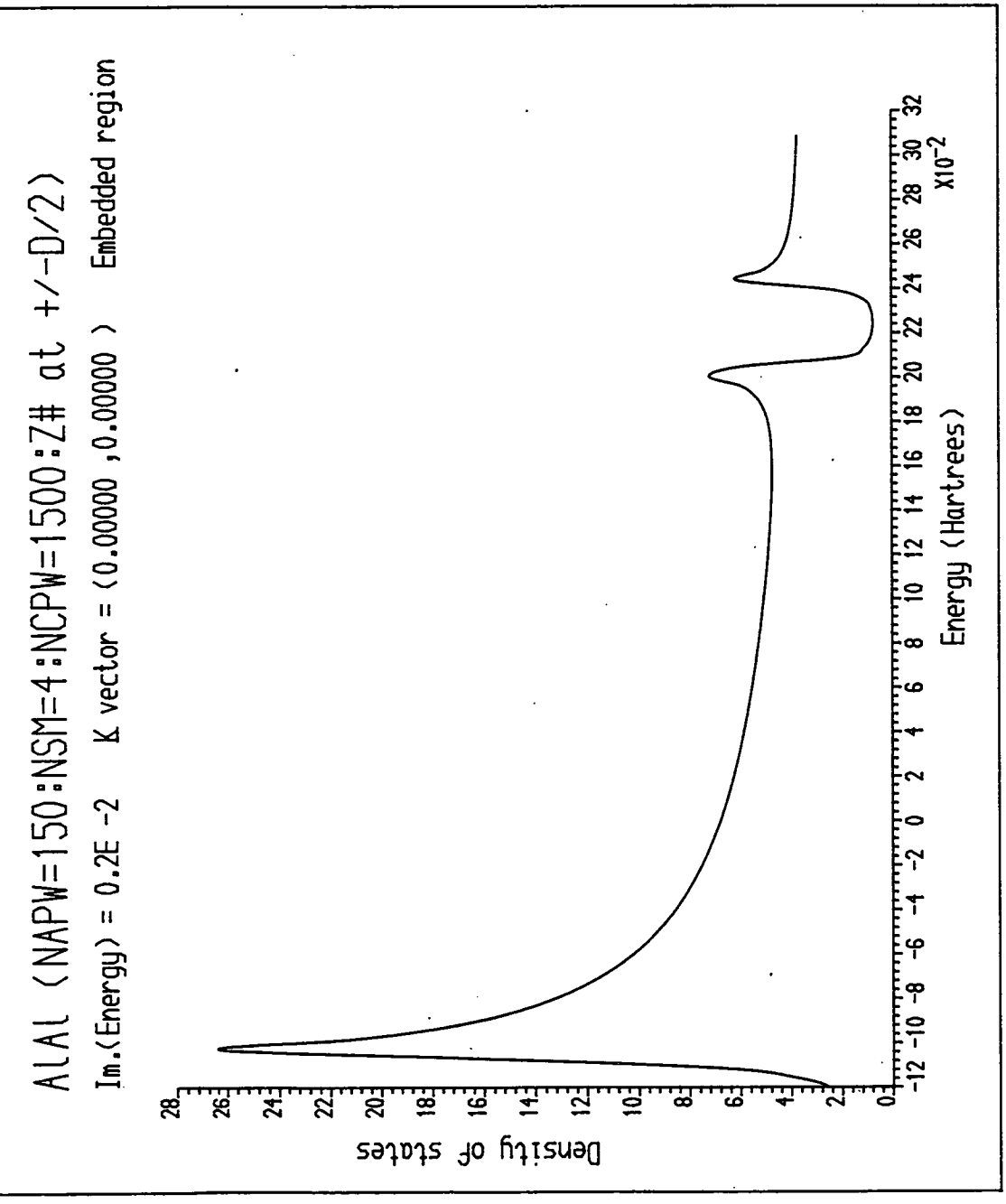

Fig.5.16: Bulk Al density of states for embedding planes at ±D/2, at $\bar{\Gamma}$

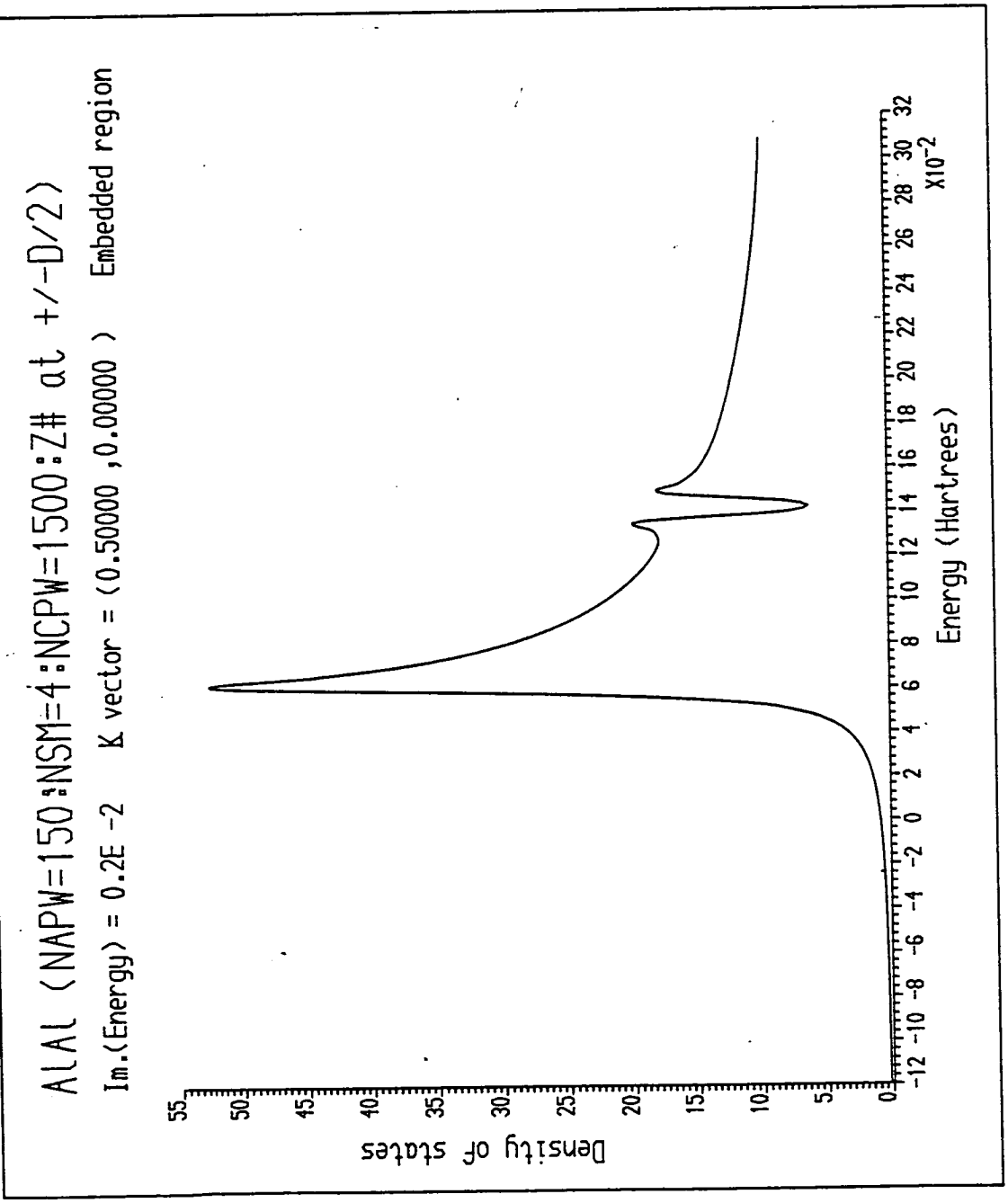

Fig. 5.17: Bulk Al density of states for embedding planes at ±D/2, at $\bar{X}$

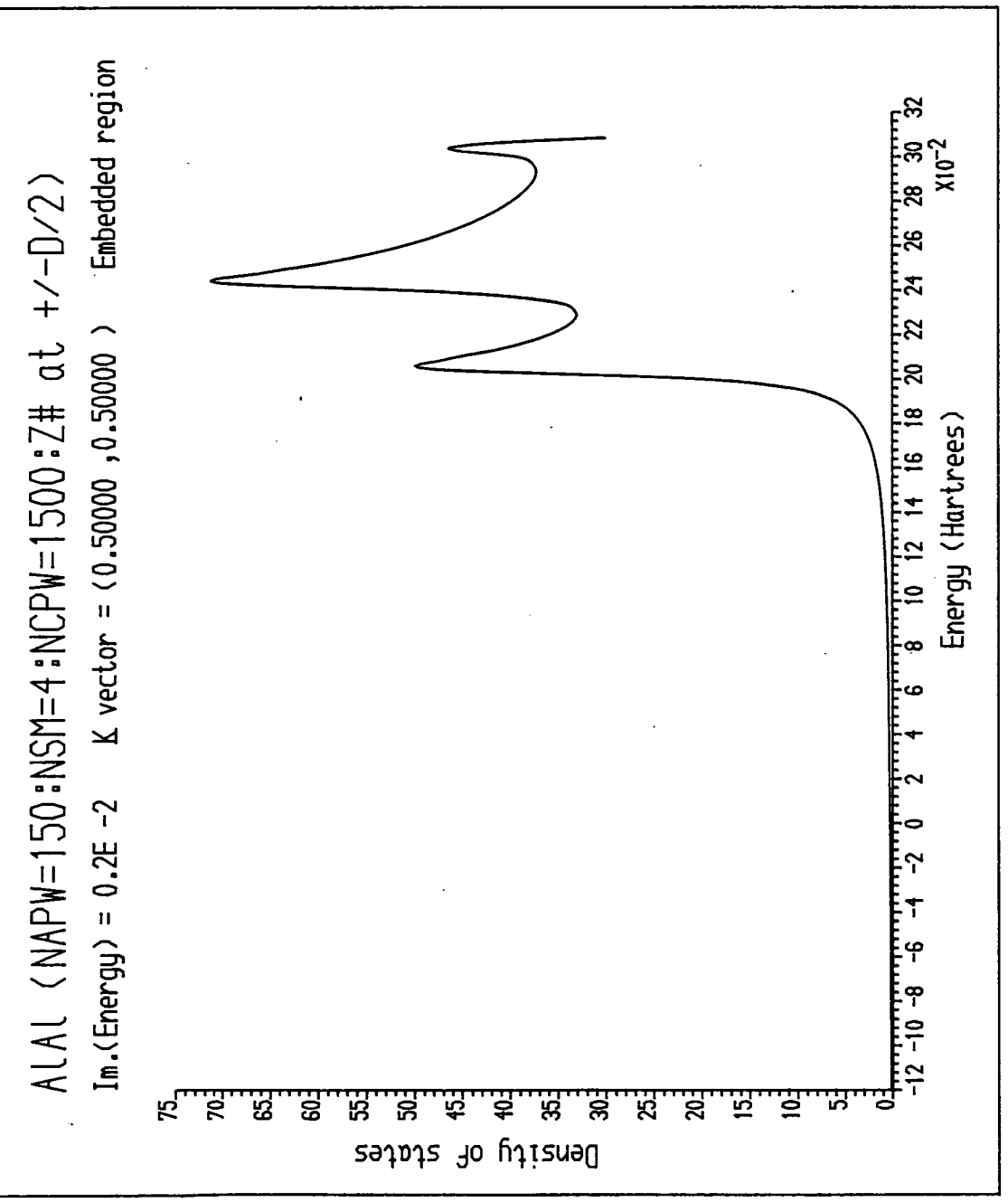

Fig.5.18: Bulk Al density of states for embedding planes at ±D/2, at $\overline{M}$

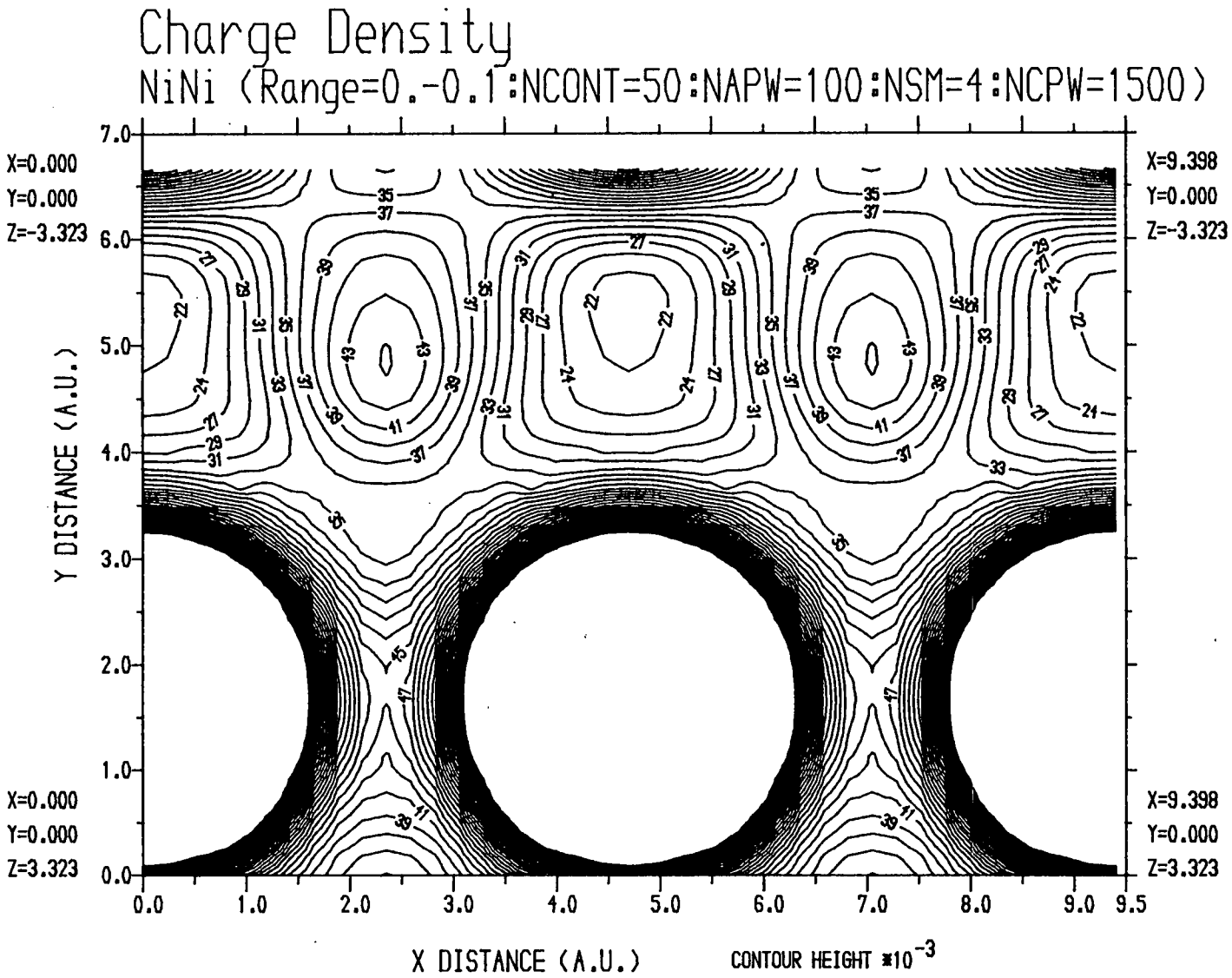

Fig.5.19: Bulk Ni charge density after one cycle

Fig.5.20: Bulk Ni density of states at $\overline{\Gamma}$ after one cycle

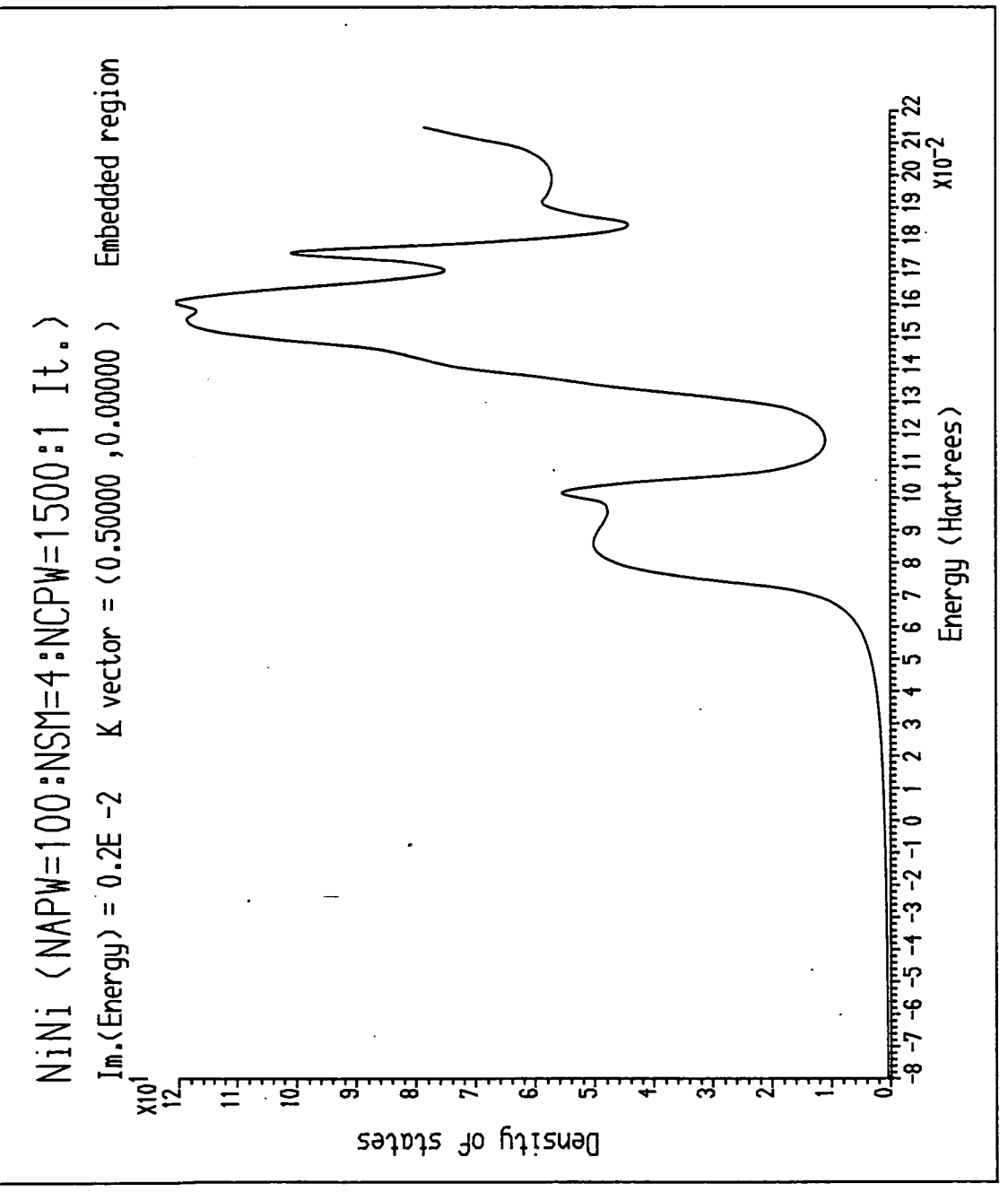

Fig.5.21: Bulk Ni density of states at $\overline{X}$ after one cycle

Fig.5.22: Bulk Ni density of states at $\bar{M}$ after one cycle

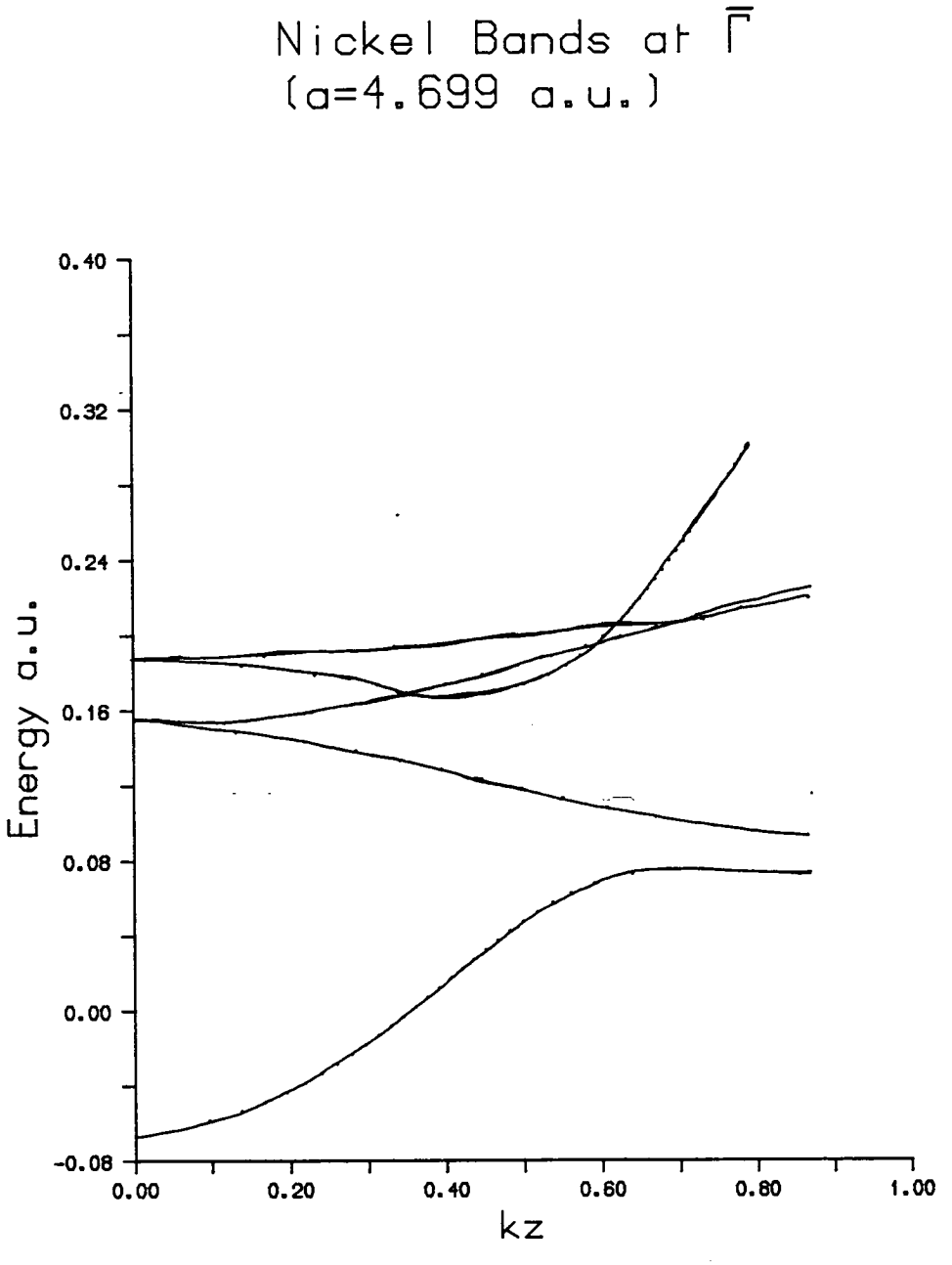

Fig.5.23: Bulk Ni bands at $\overline{\Gamma}$

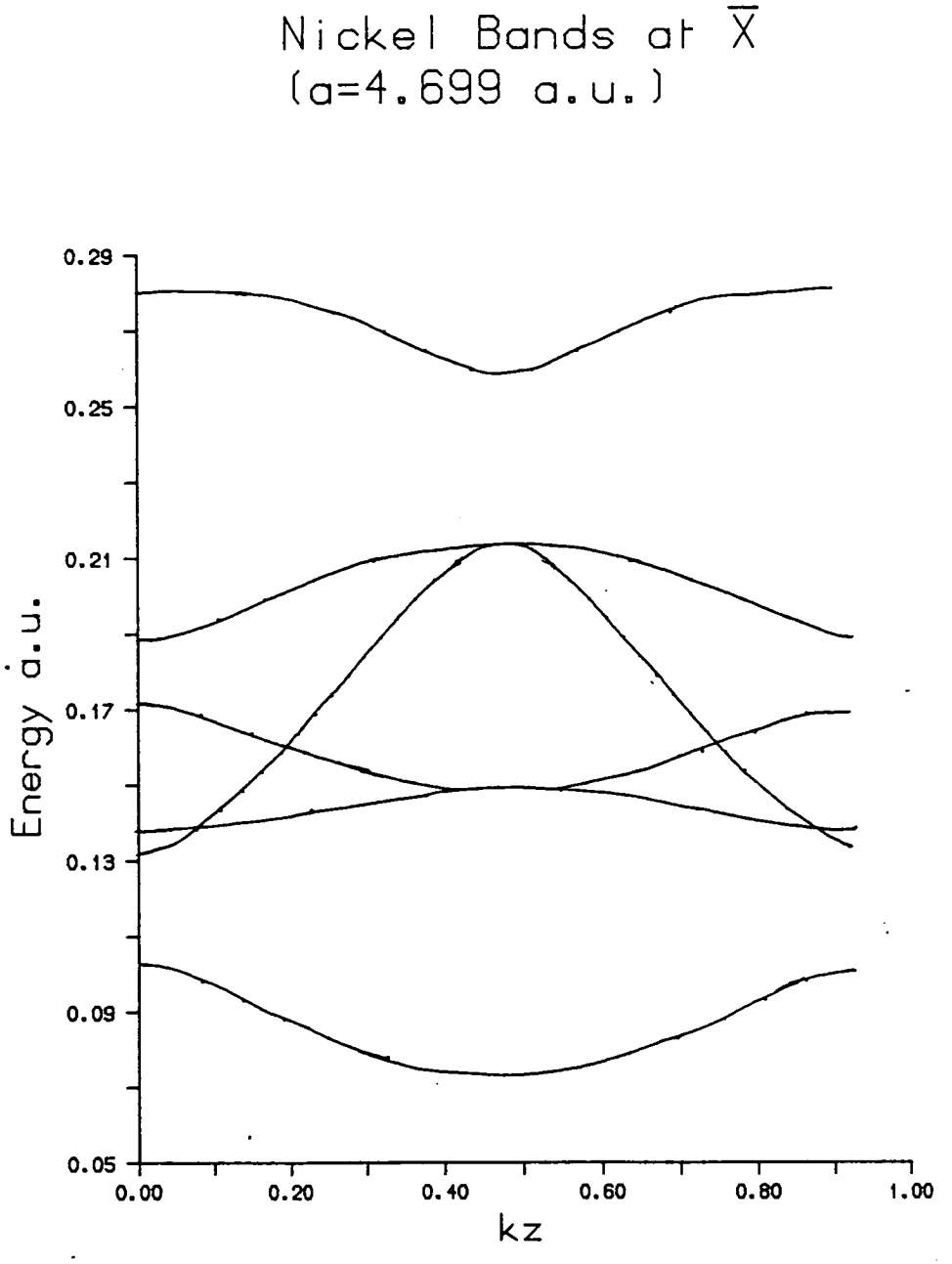

Fig.5.24: Bulk Ni bands at $\overline{X}$

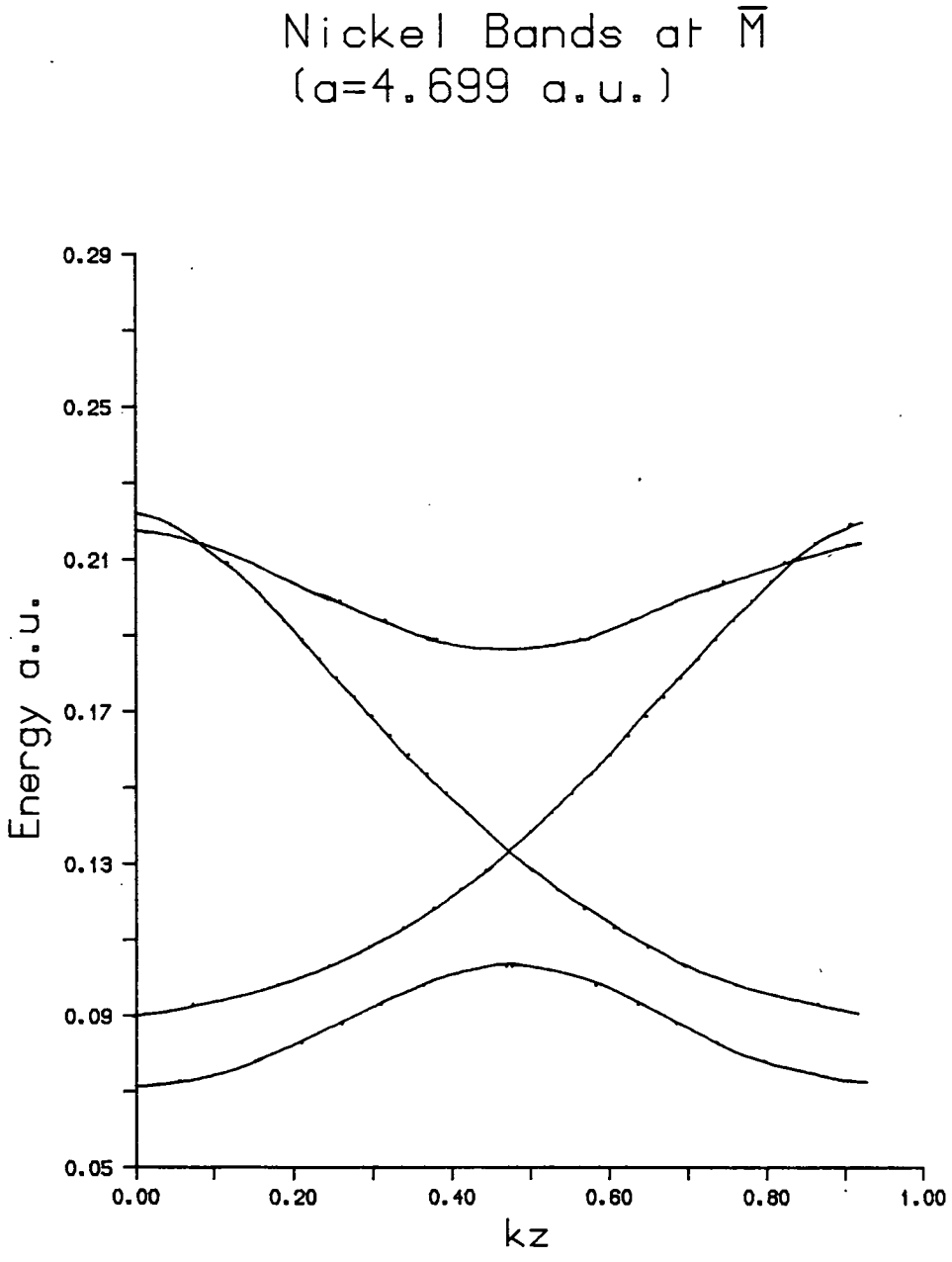

Fig.5.25: Bulk Ni bands at $\overline{M}$

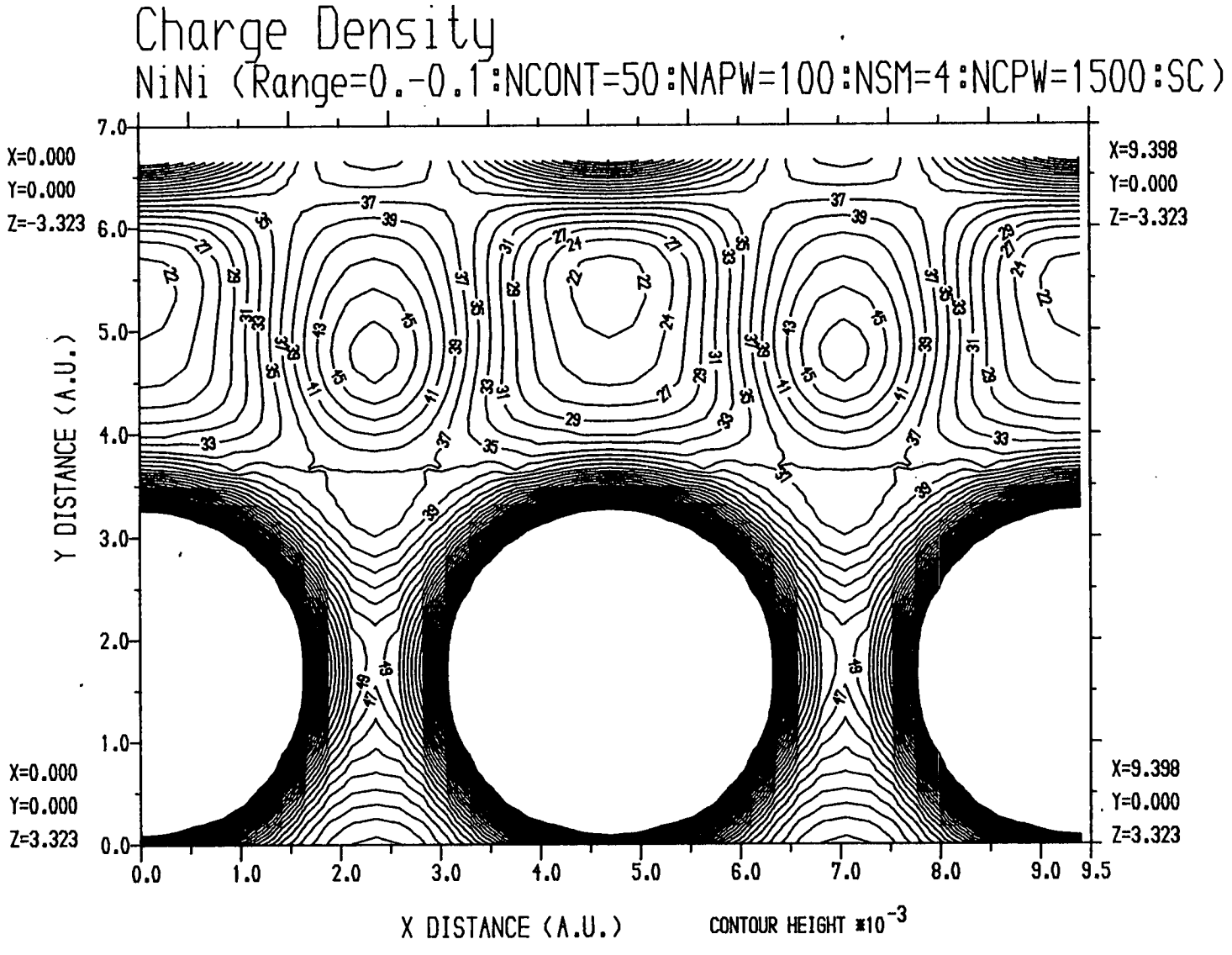

Fig.5.26: Self consistent bulk Ni charge density

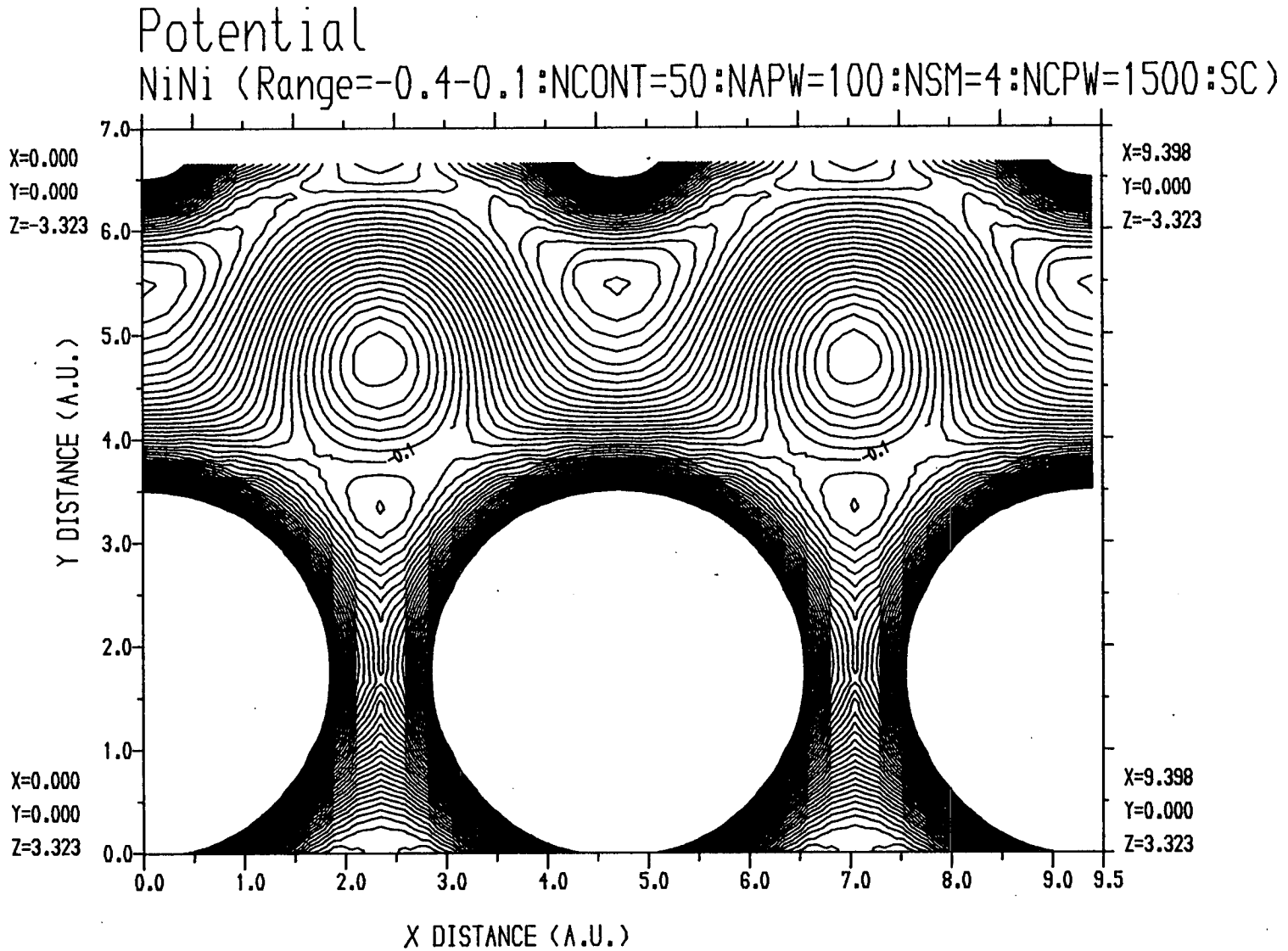

Fig.5.27: Self consistent bulk Ni potential

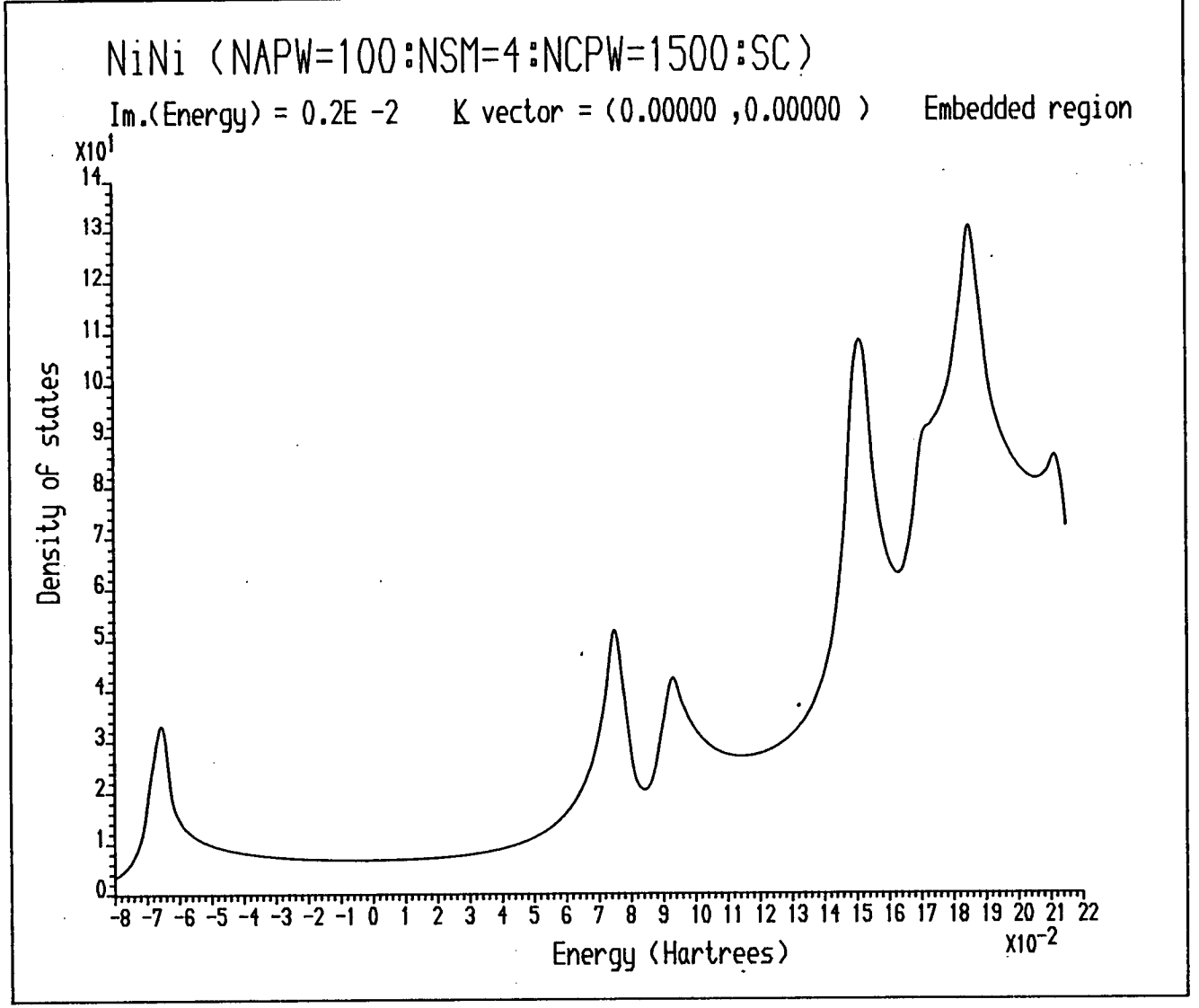

Fig.5.28: Self consistent bulk Ni density of states at Γ

Fig.5.29: Self consistent bulk Ni density of states at $\bar{X}$

Fig.5.30: Self consistent bulk Ni density of states at M

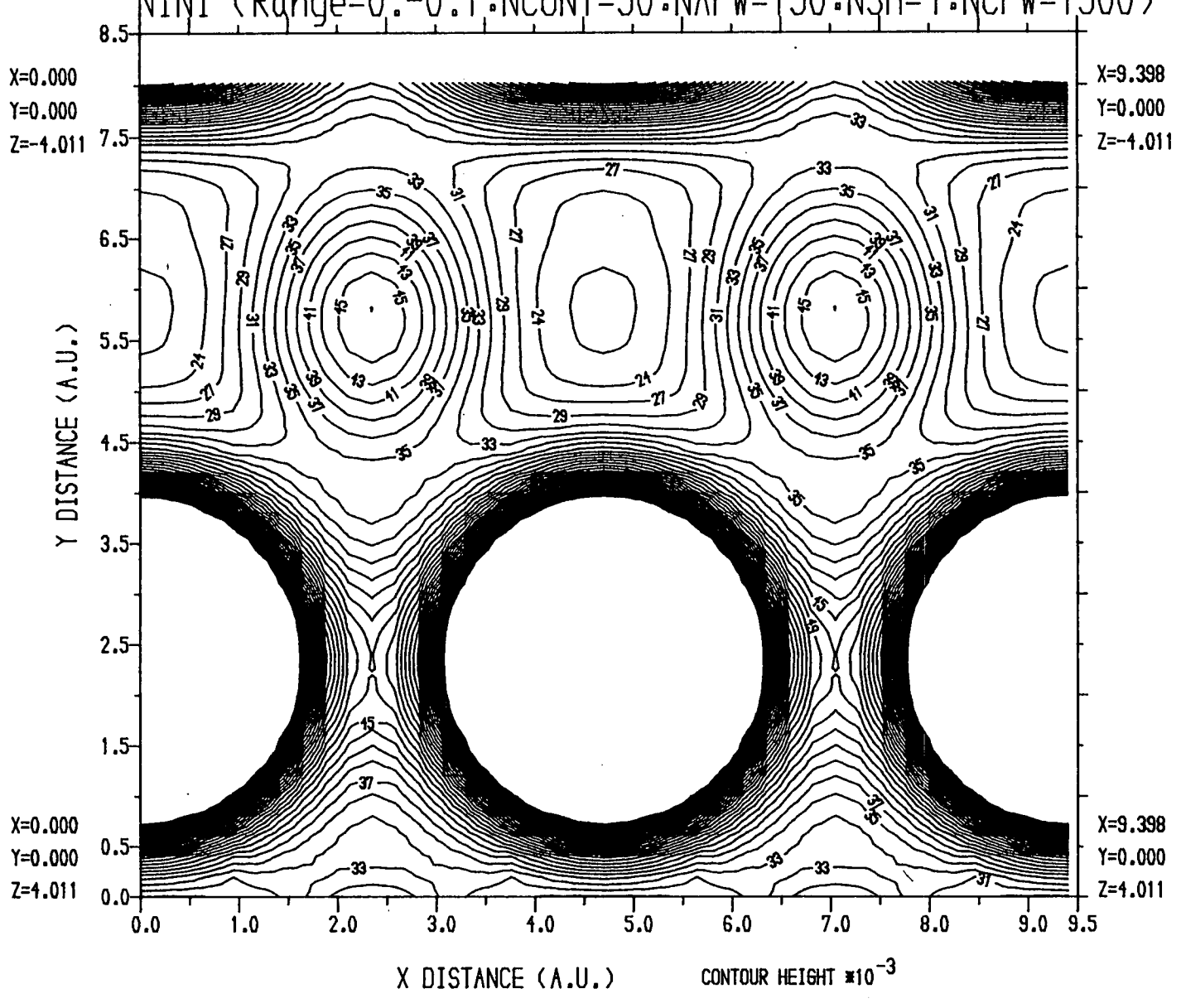

Fig.5.31: Bulk Ni charge density for embedding planes at ±D/2

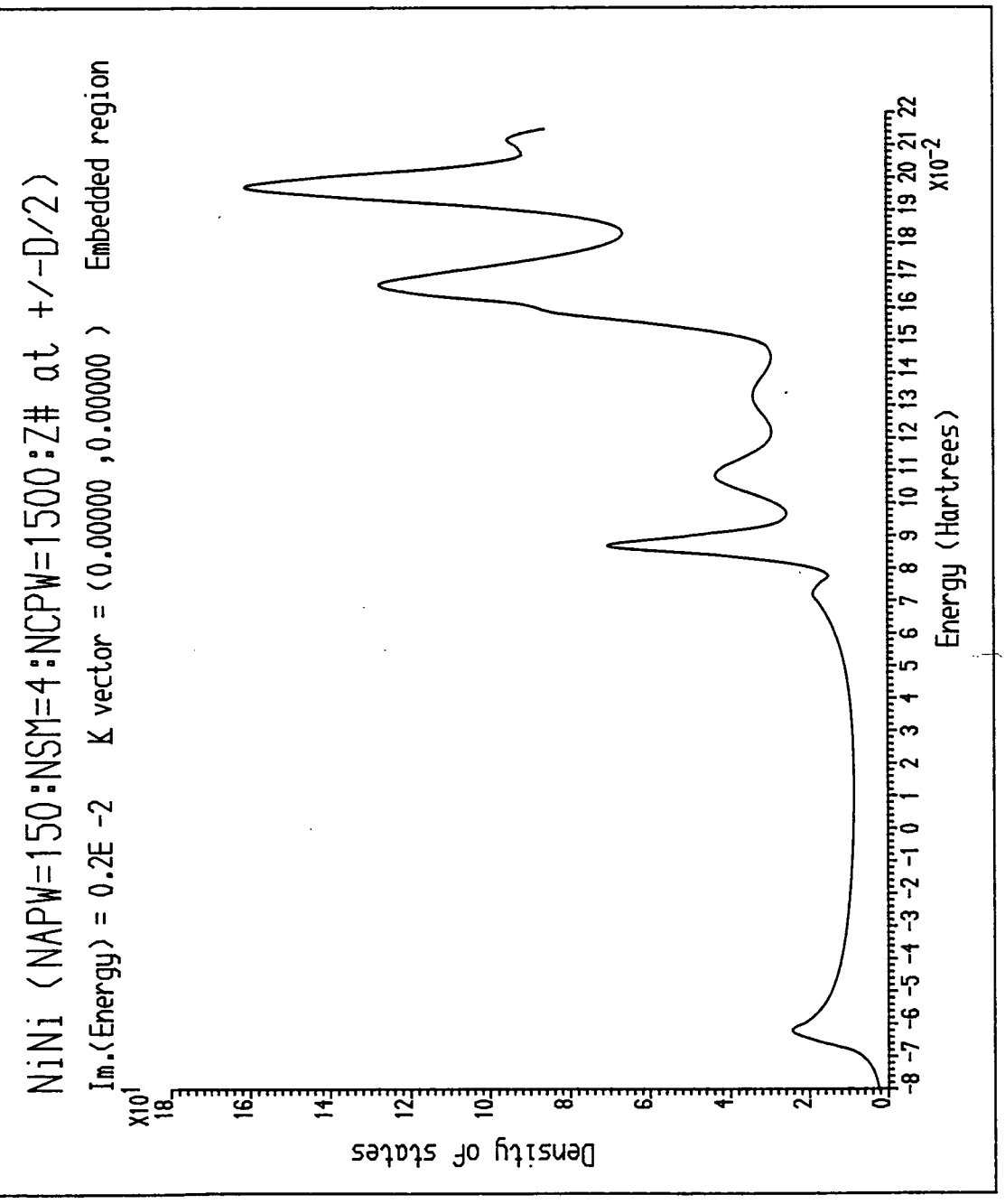

Fig.5.32: Bulk Ni density of states for embedding planes at $\pm D/2$, at Γ

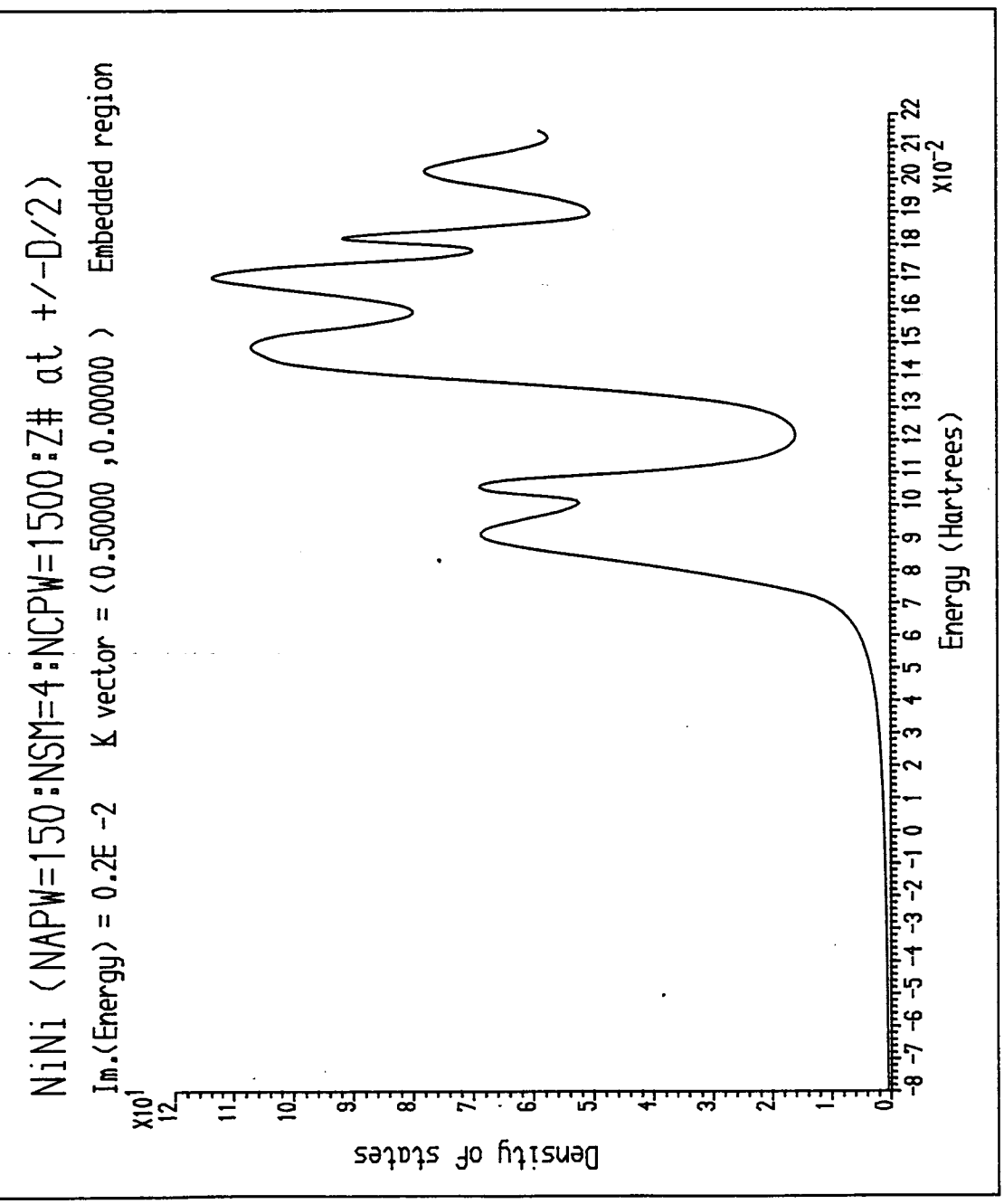

Fig.5.33: Bulk Ni density of states for embedding planes at $\pm D/2$, at $\overline{X}$

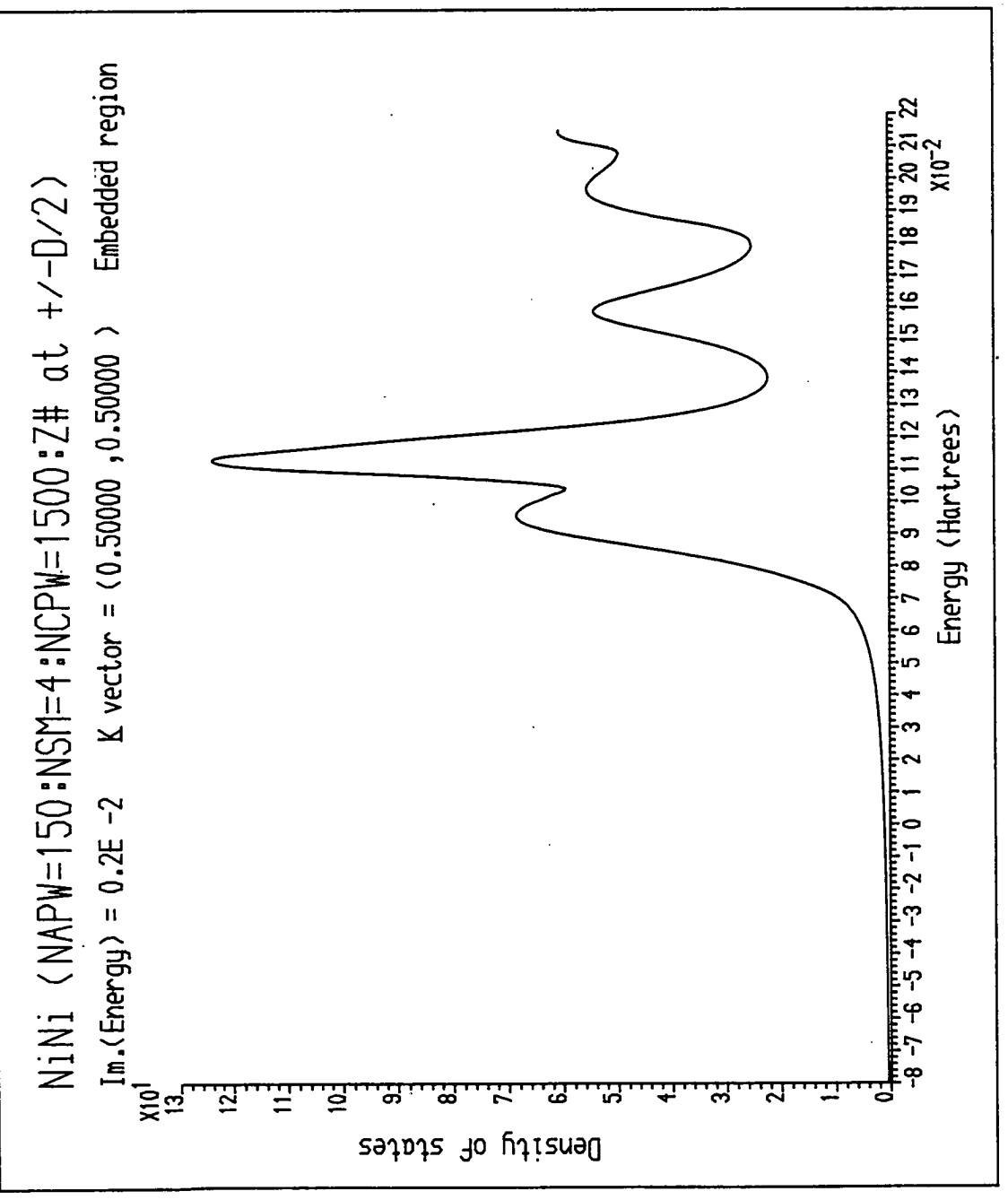

Fig.5.34: Bulk Ni density of states for embedding planes at ±D/2, at $\overline{M}$

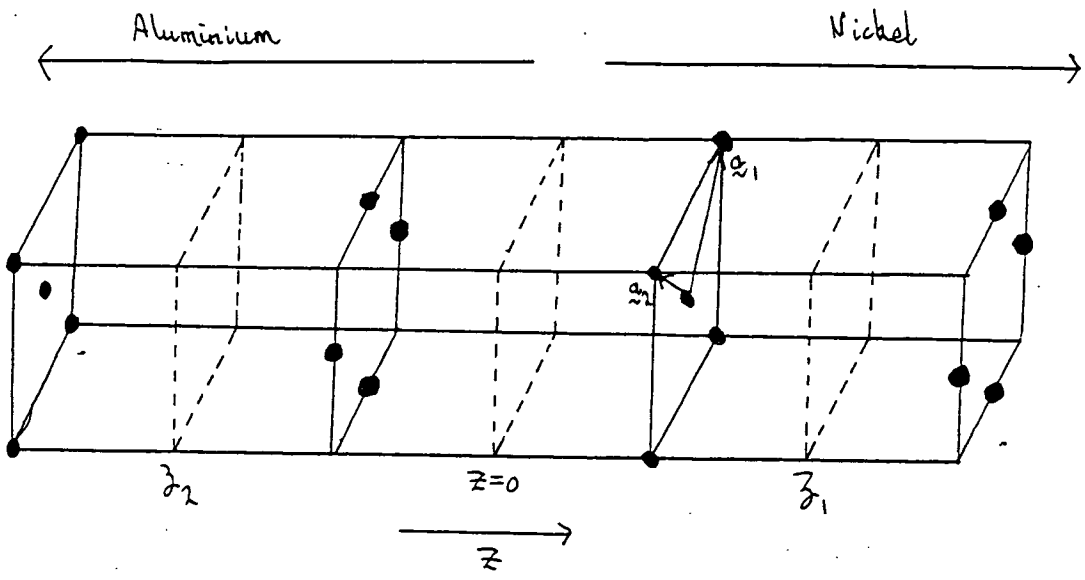

a	=	5.00 au
Al muffin tin radius	=	2.4557 au
Ni muffin tin radius	=	2.3496 au
D	=	8.3408 au
$\bar{D}$	=	9.00 au
ζ_1	=	3.588584 au
ζ_2	=	-3.492484 au
E	=	$\begin{cases} -0.1200 \rightarrow 0.3085 & \text{in Al} \\ -0.2135 \rightarrow 0.2150 & \text{in Ni} \end{cases}$
		16 energy points
n for pseudo ρ expansion	=	Al: 11 10 9 8 Ni: 10 9 8 7

Fig. 5.35: Al-Ni geometry and parameters.

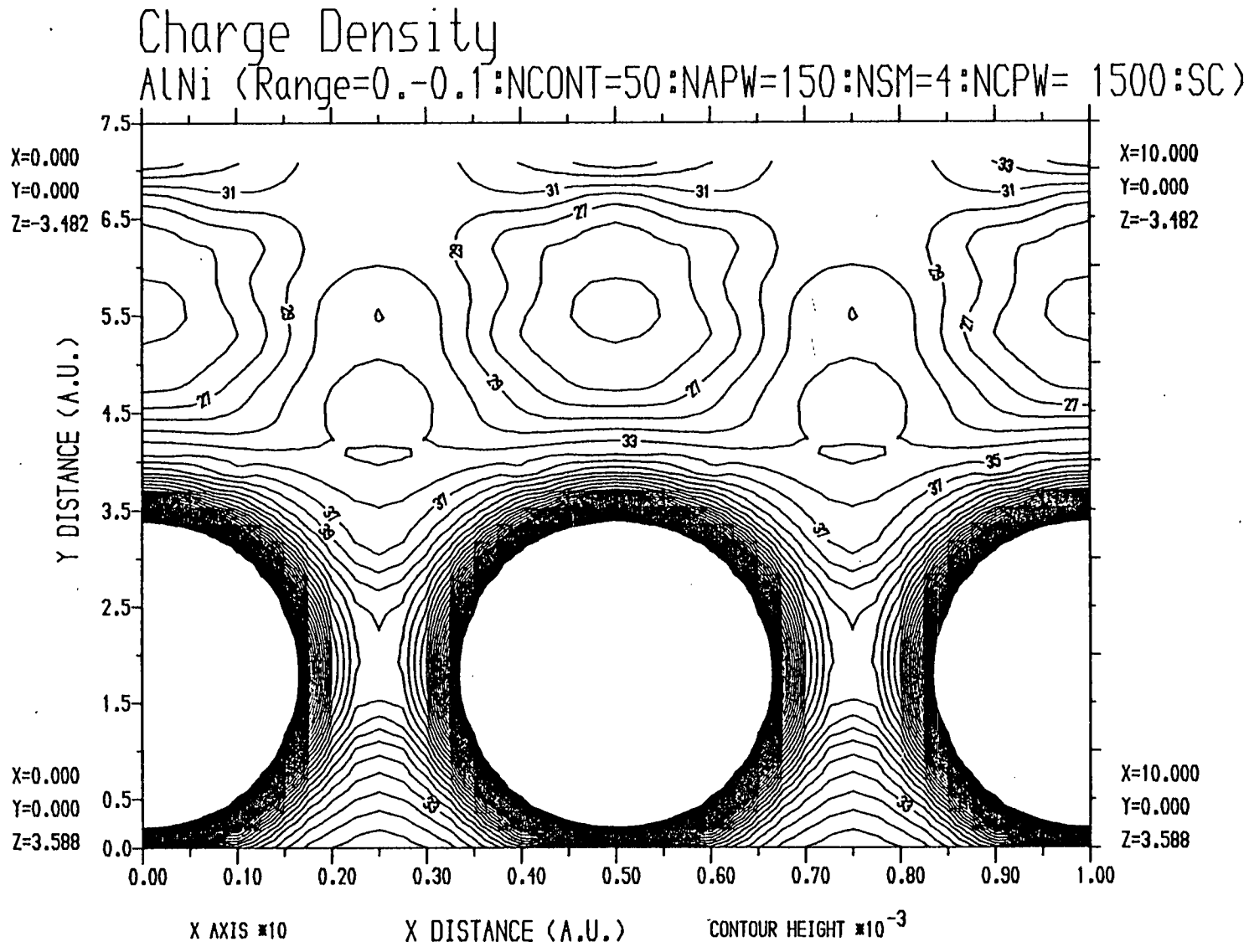

Fig.5.36: Self consistent AlNi charge density, in plane of Ni atoms

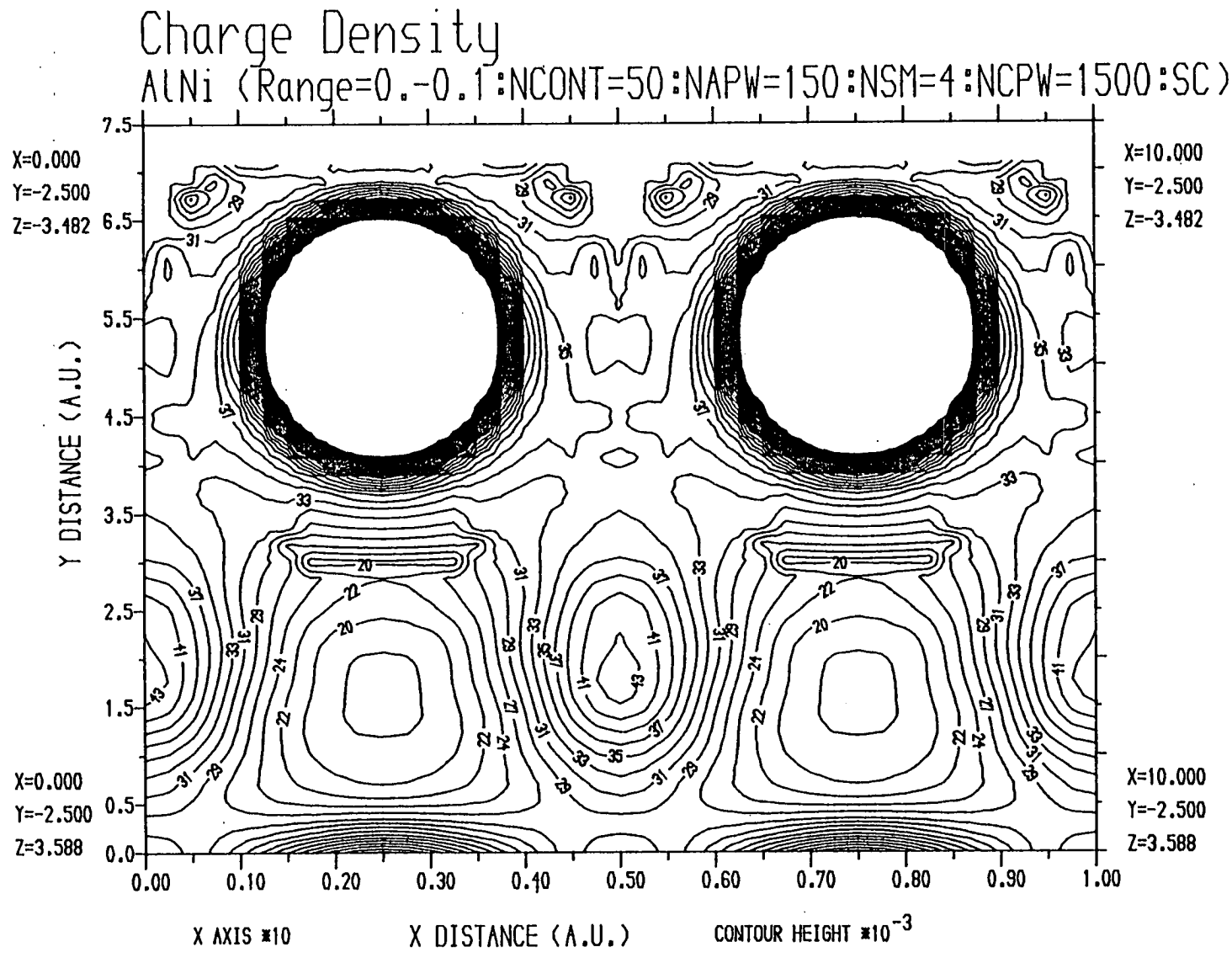

Fig.5.37: Self consistent AlNi charge density, in plane of Al atoms

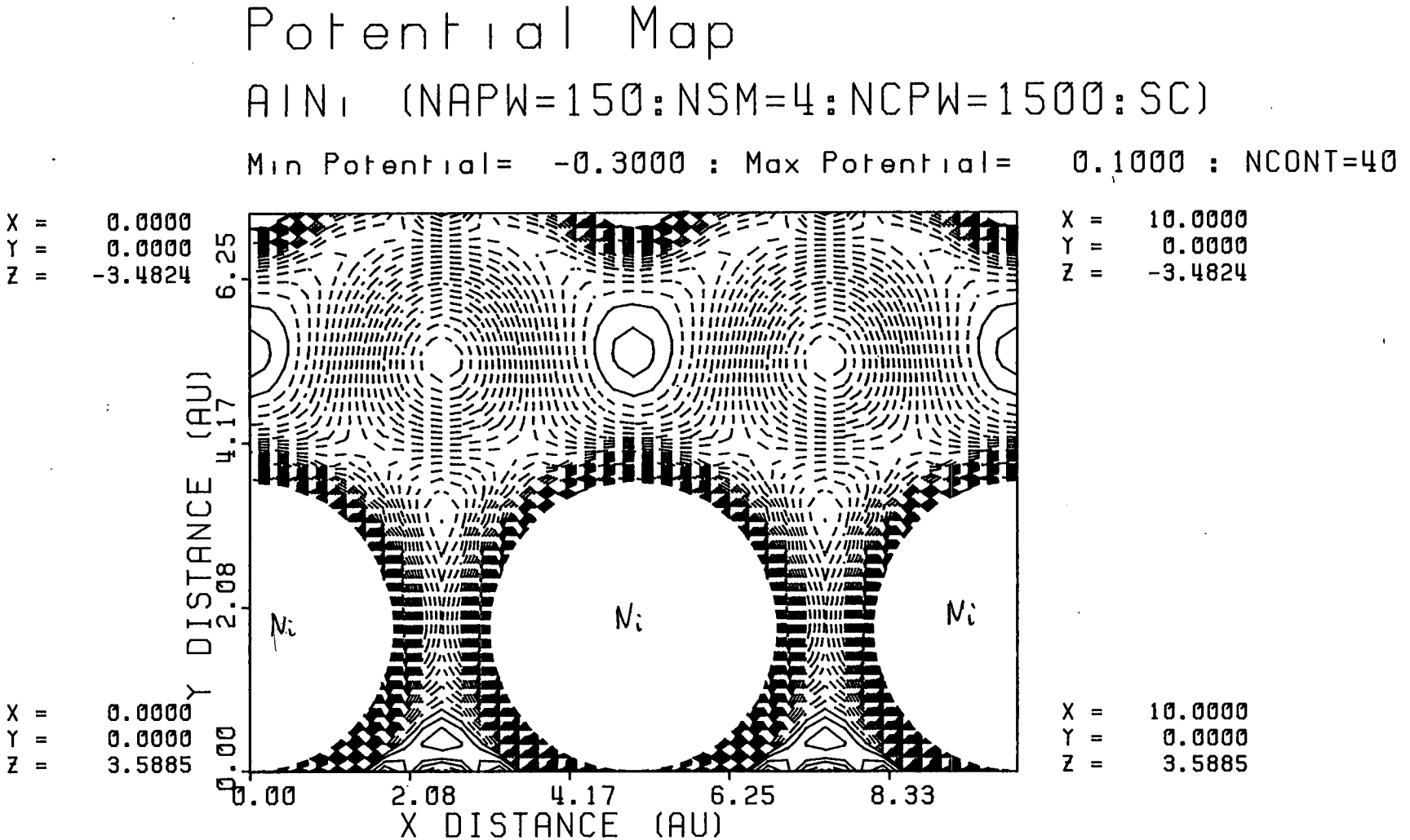

Fig.5.38: Self consistent AlNi potential, in plane of Ni atoms

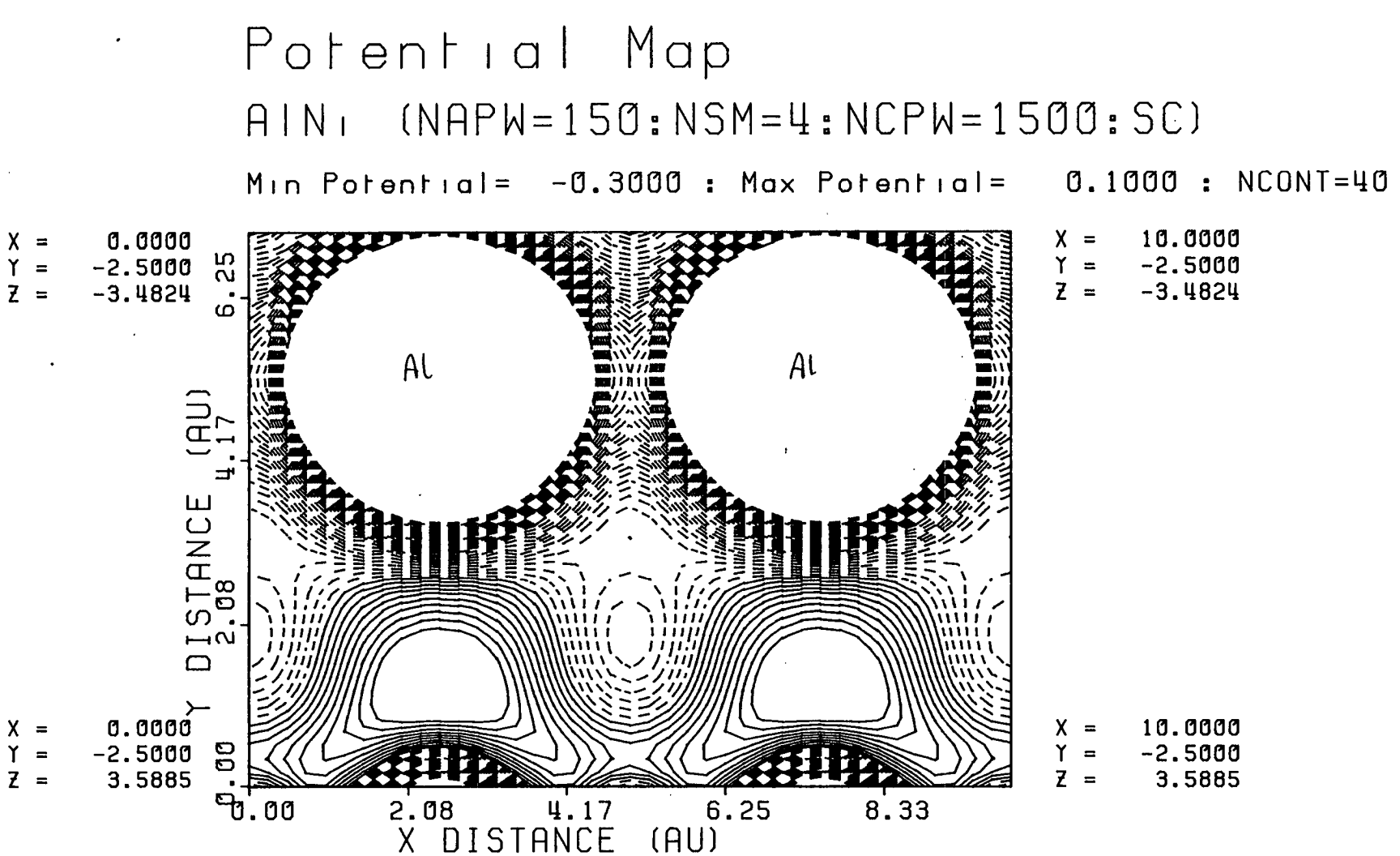

Fig.5.39: Self consistent AlNi potential,in plane of Al atoms

Fig.5.40: Self consistent AlNi density of states, in Al spheres, at Γ

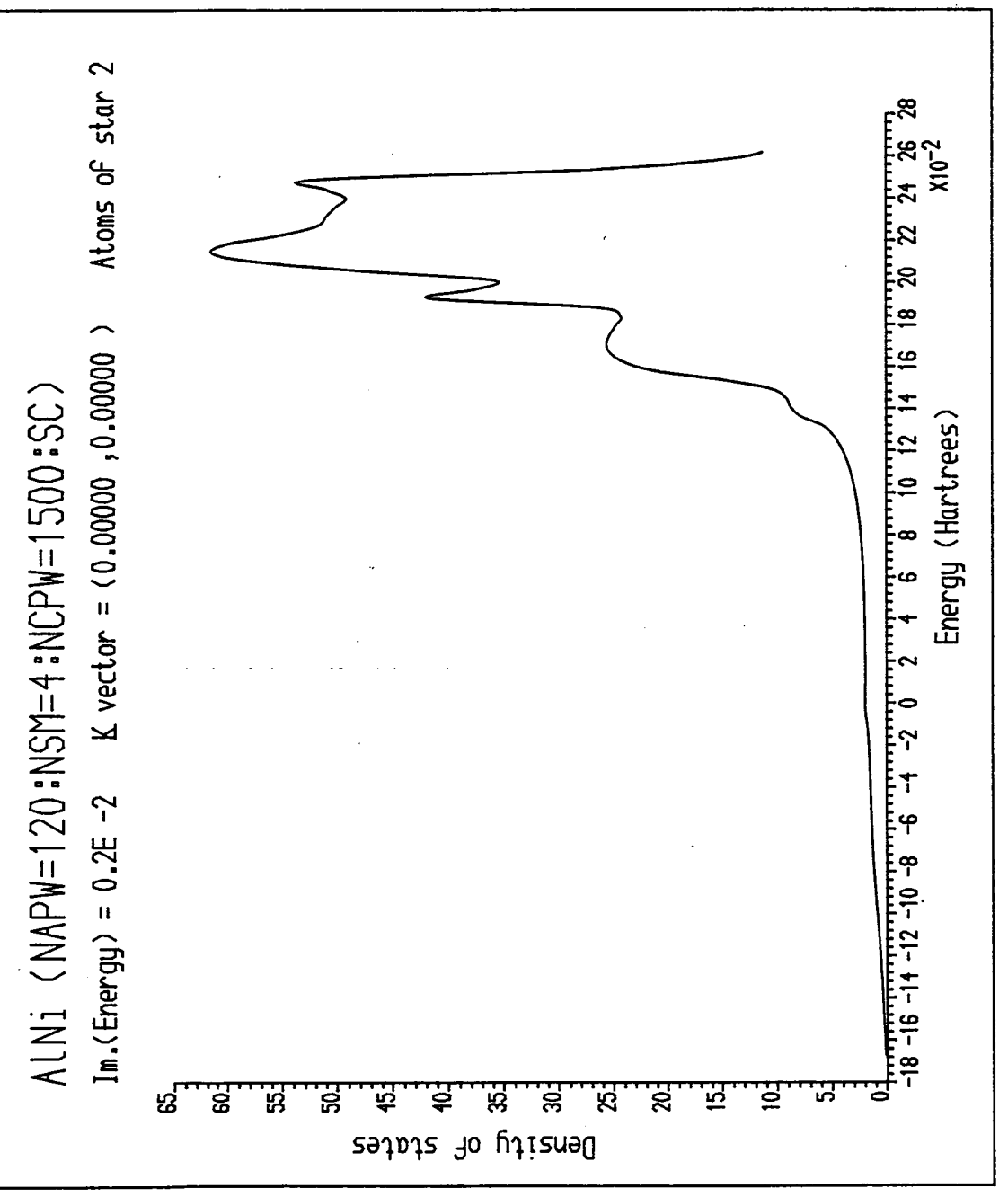

Fig.5.41: Self consistent AlNi density of states, in Ni spheres, at Γ_1

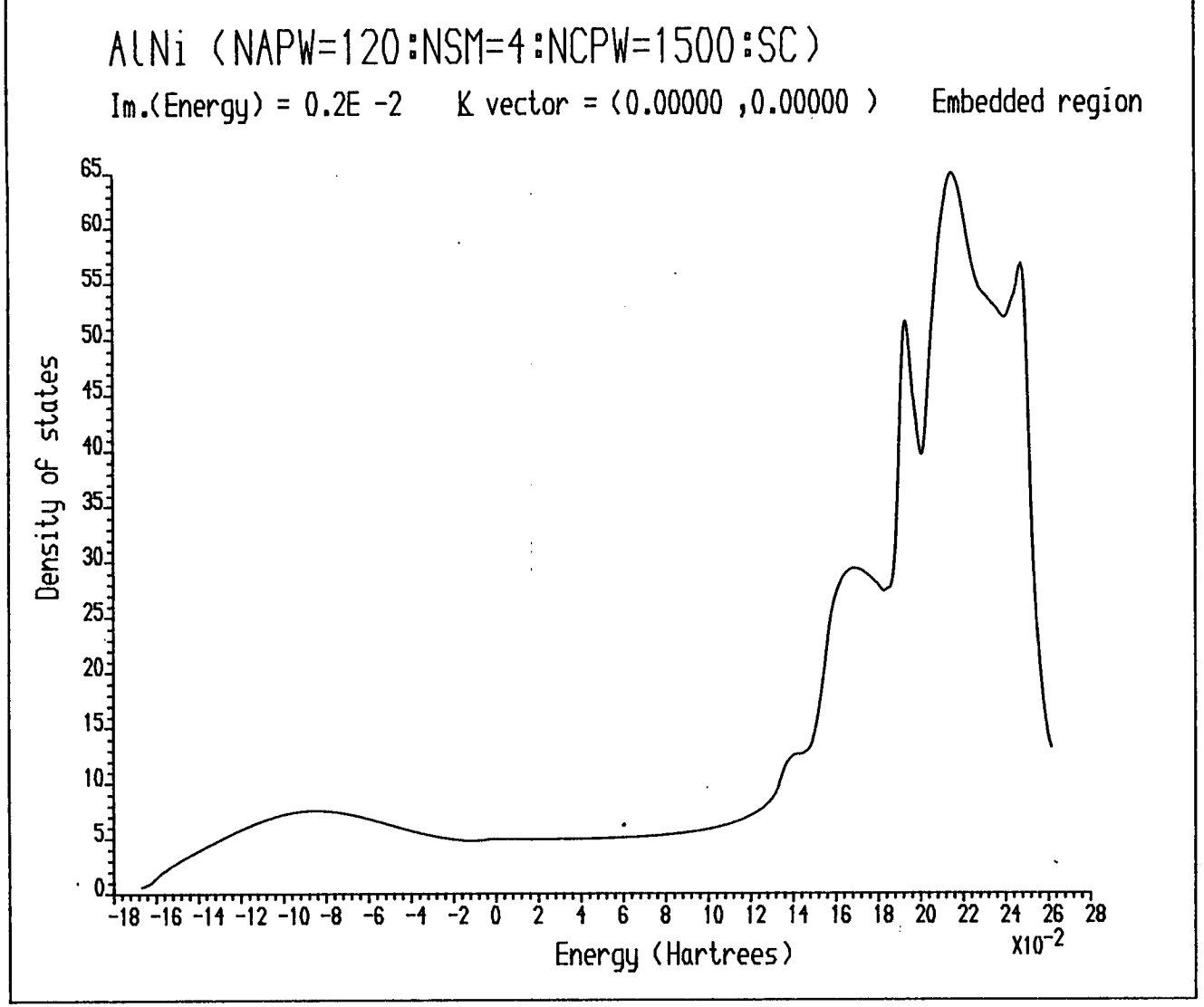

Fig.5.42: Self consistent AlNi density of states, in embedded region, at Γ

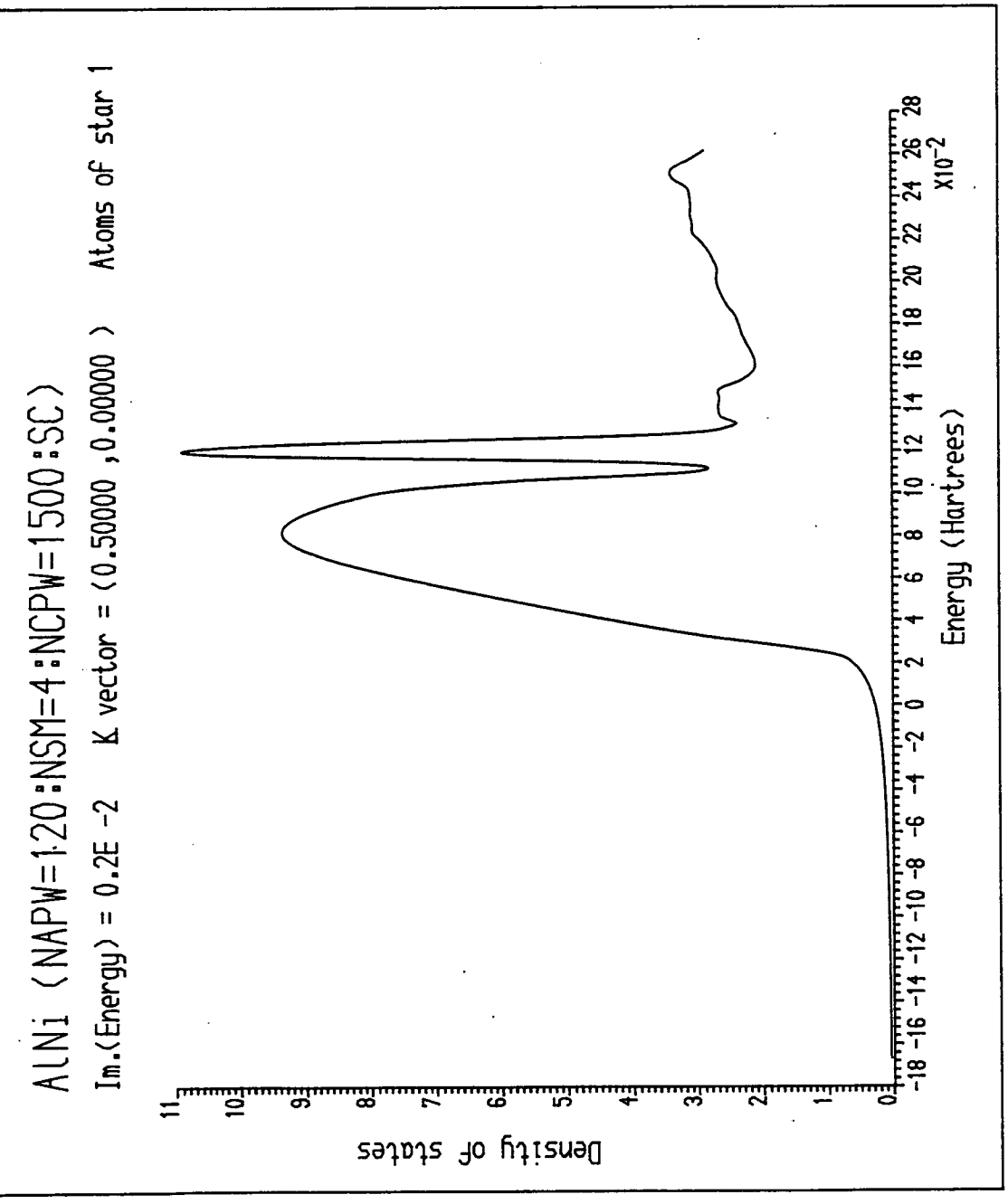

Fig.5.43: Self consistent AlNi density of states, in Al spheres, at $\overline{X}$

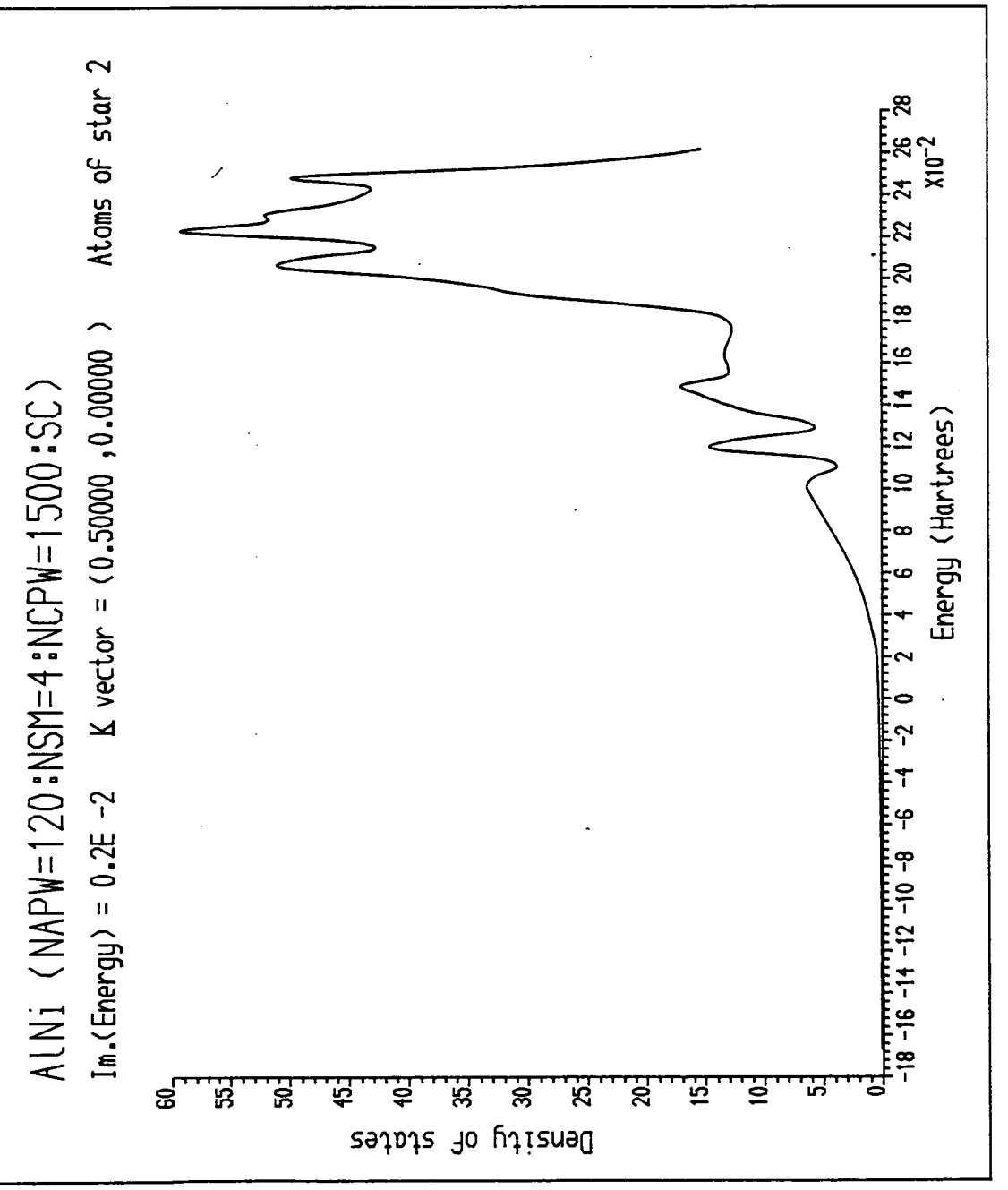

Fig.5.44: Self consistent AlNi density of states, in Ni spheres, at $\bar{X}$

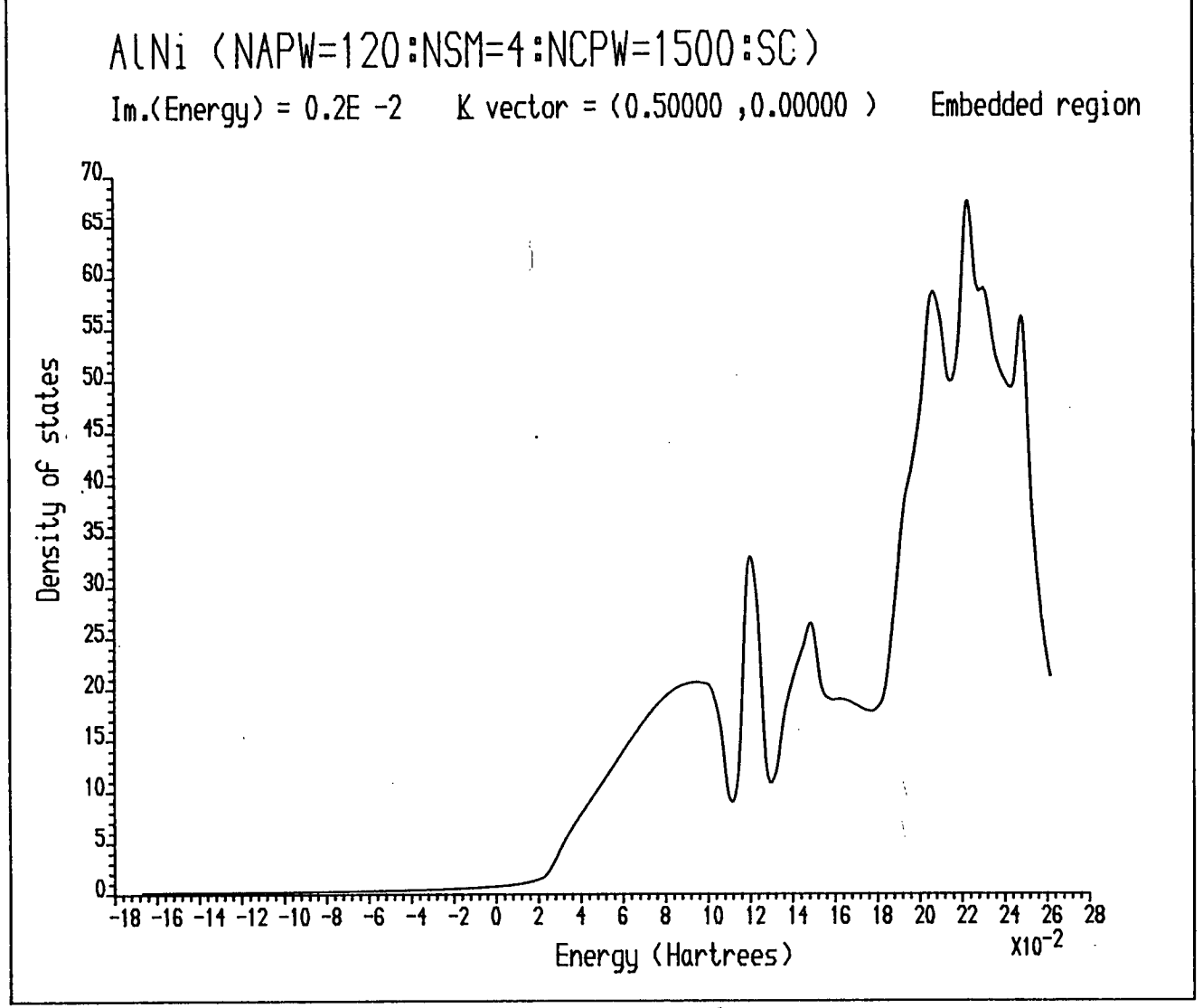

Fig.5.45: Self consistent AlNi density of states, in embedded region, at $\bar{X}$

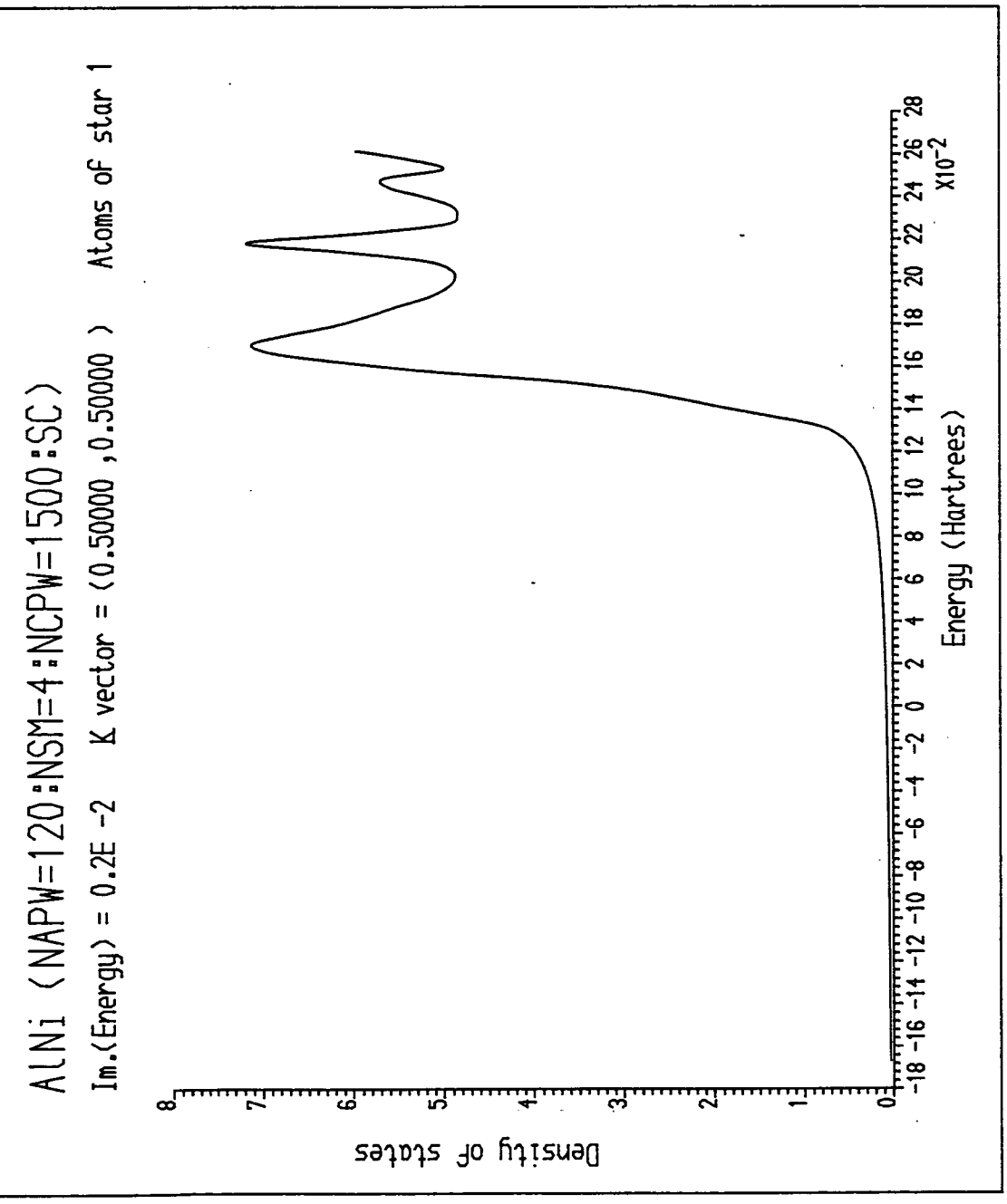

Fig.5.46: Self consistent AlNi density of states, in Al spheres, at $\overline{M}$

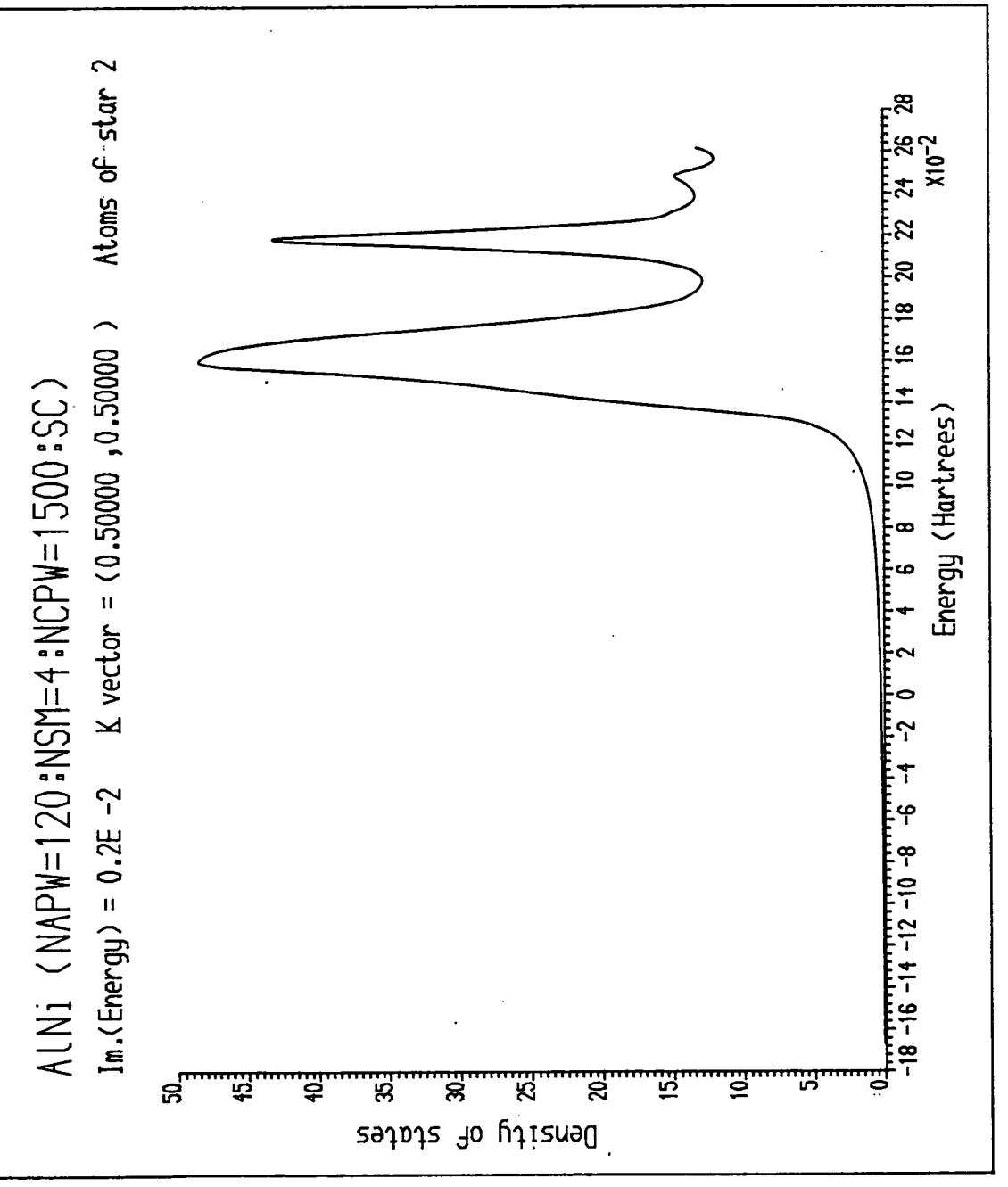

Fig.5.47: Self consistent AlNi density of states, in Ni spheres, at $\overline{M}$

Fig.5.48: Self consistent AlNi density of states, in embedded region, at $\overline{M}$

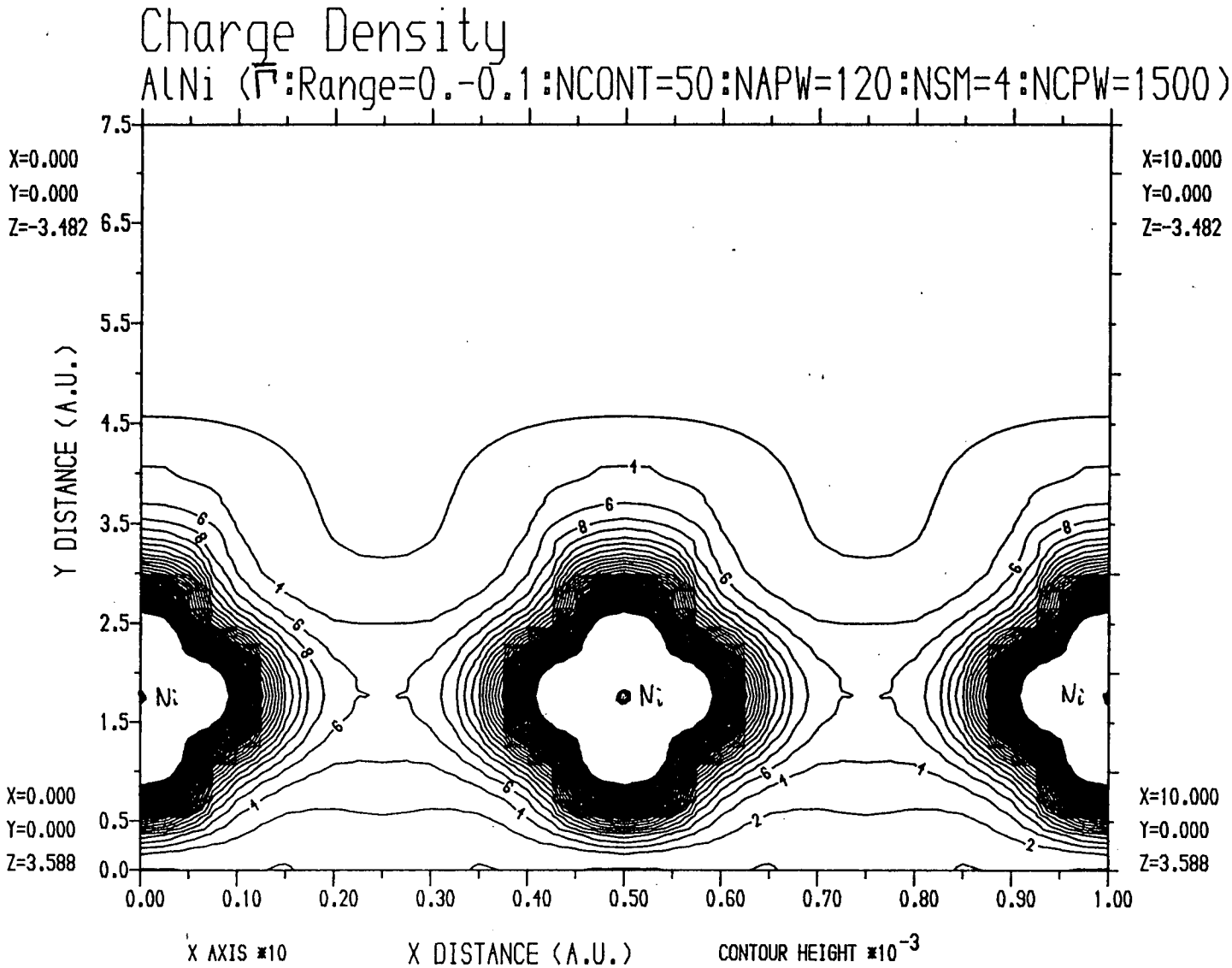

Fig.5.49: Charge density for interface state at $\bar{\Gamma}$, in plane of Ni atoms

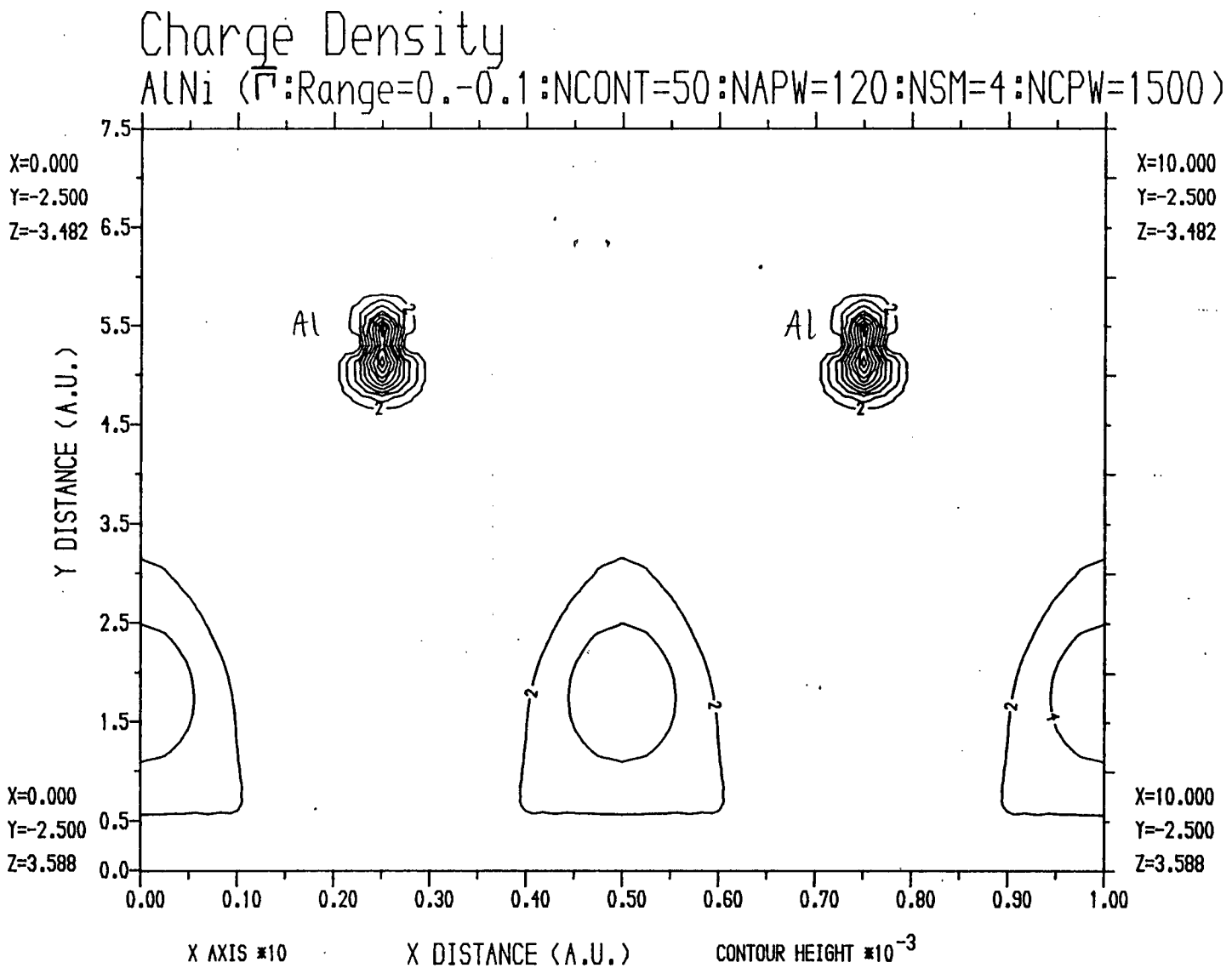

Fig.5.50: Charge density for interface state at $\bar{\Gamma}$, in plane of Al atoms

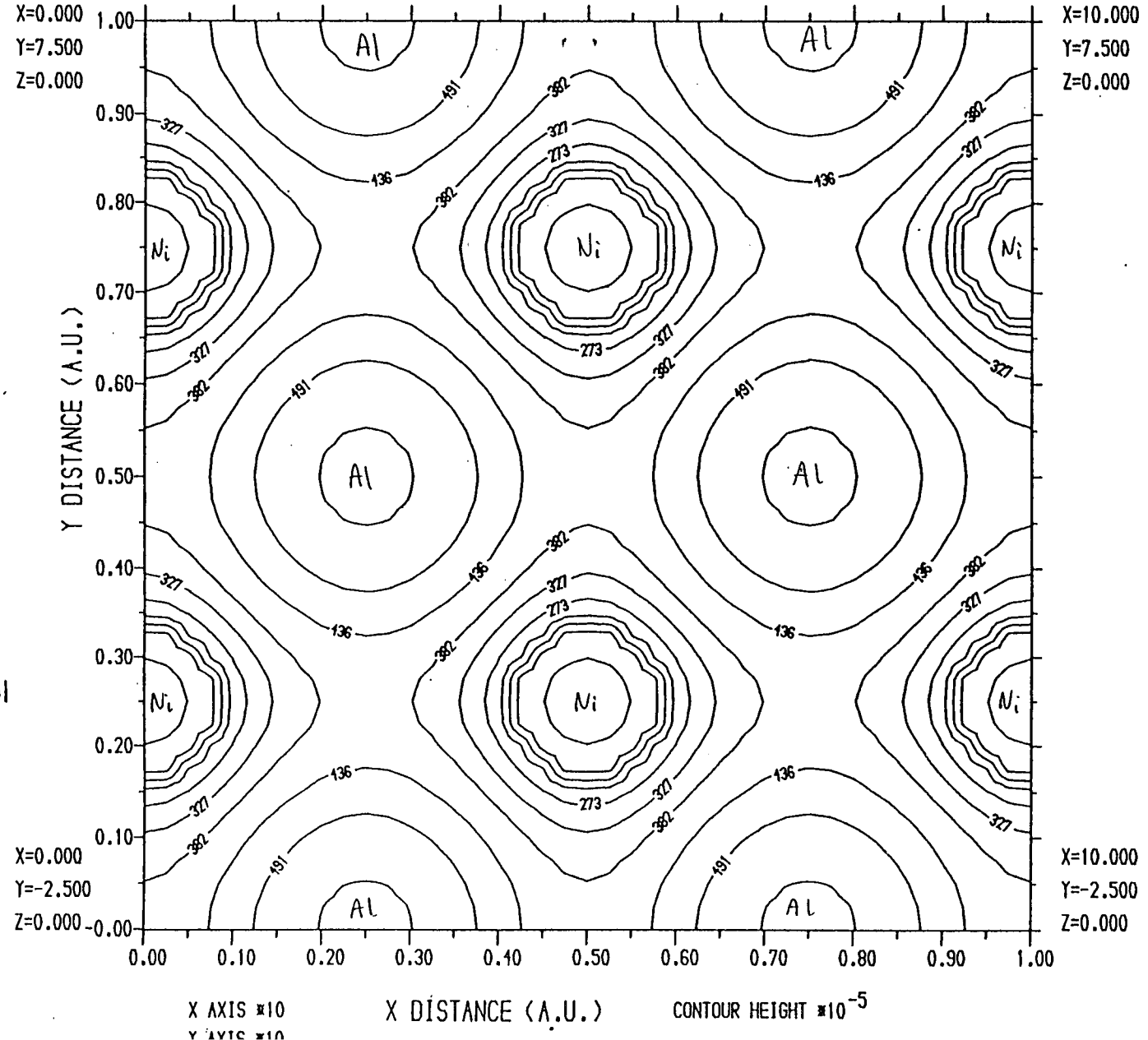

Fig.5.51: Charge density for interface state at $\bar{\Gamma}$, in z=0 plane

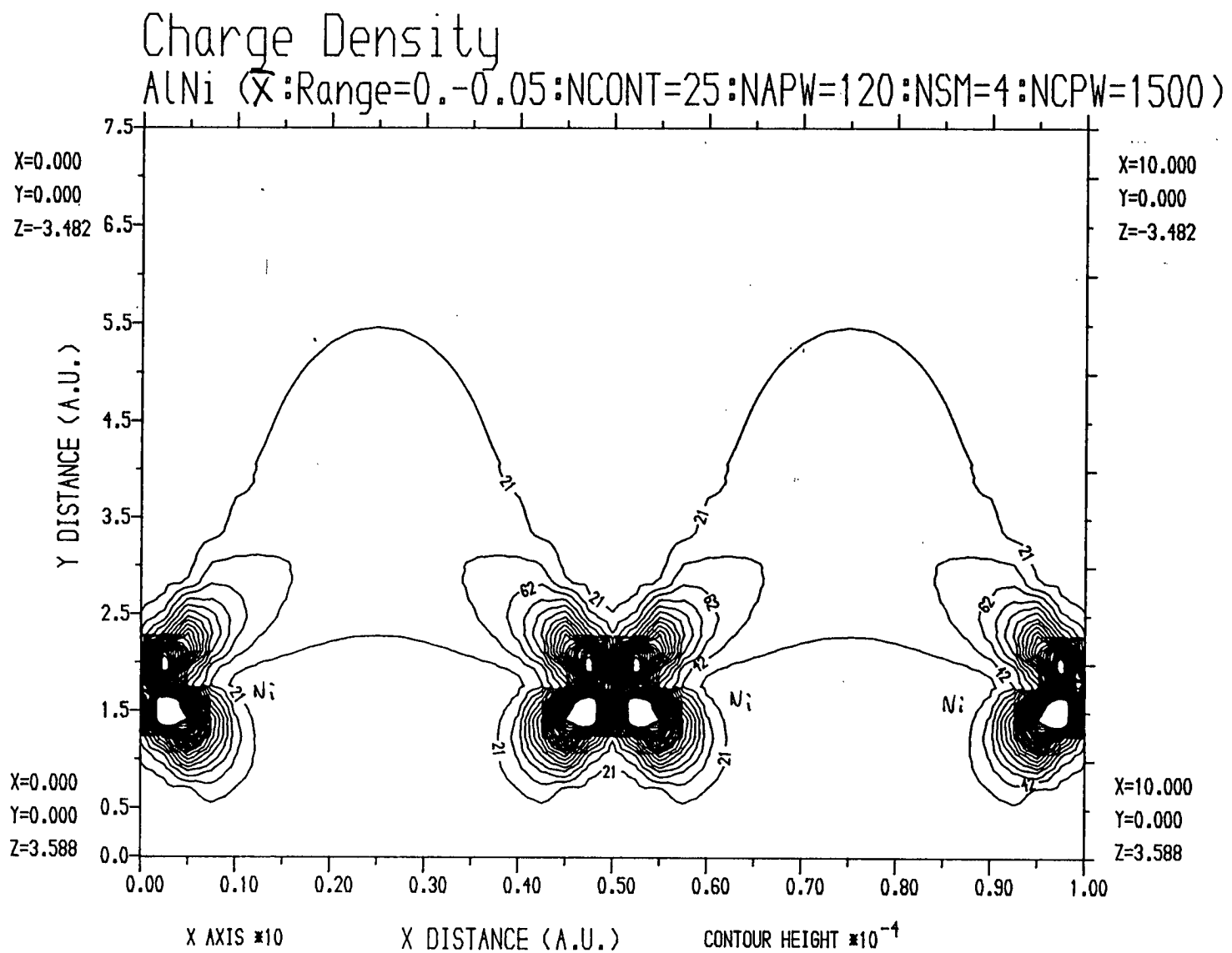

Fig.5.52: Charge density for interface state at $\bar{X}$, in plane of Ni atoms

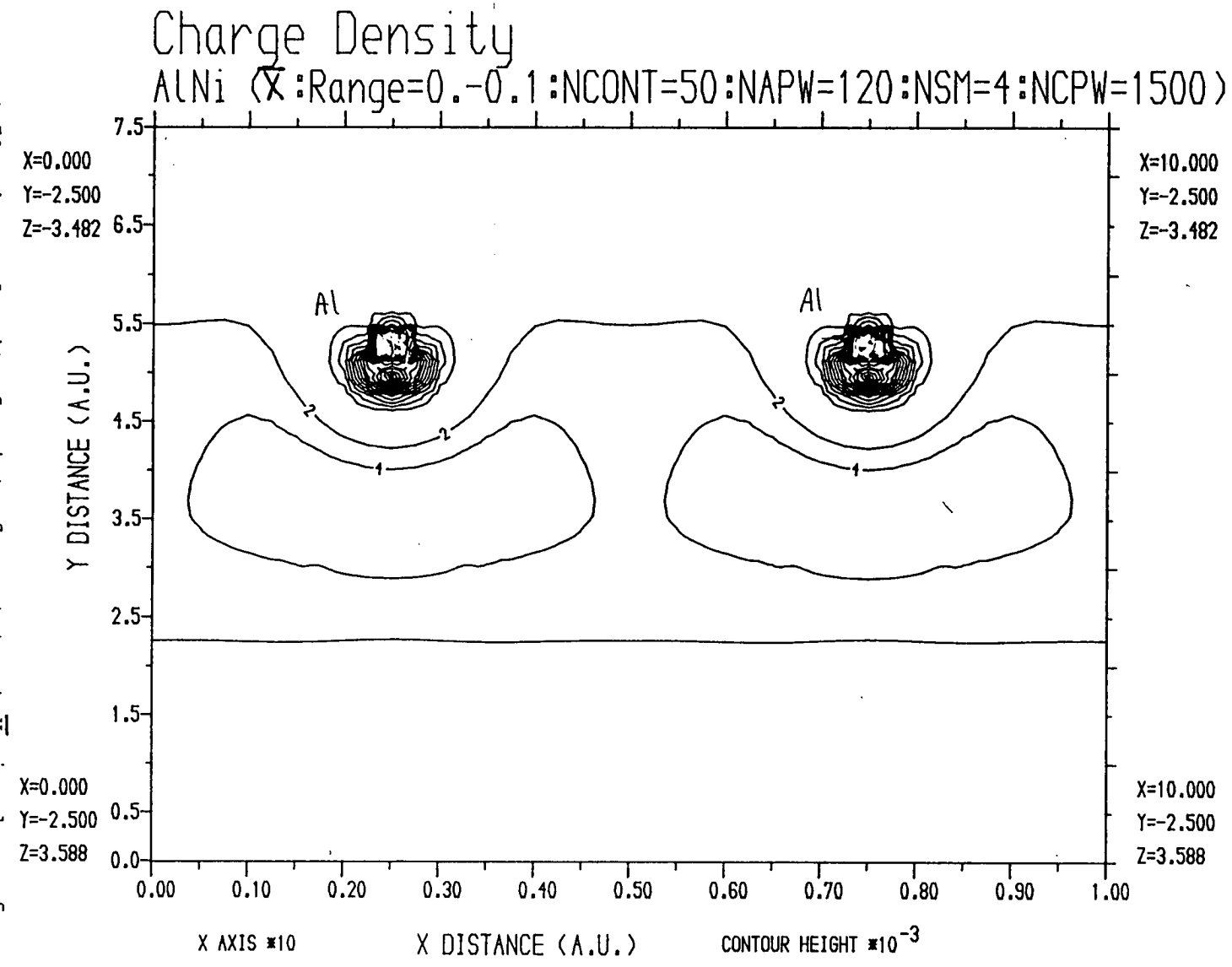

Fig.5.53: Charge density for interface state at $\bar{X}$, in plane of Al atoms

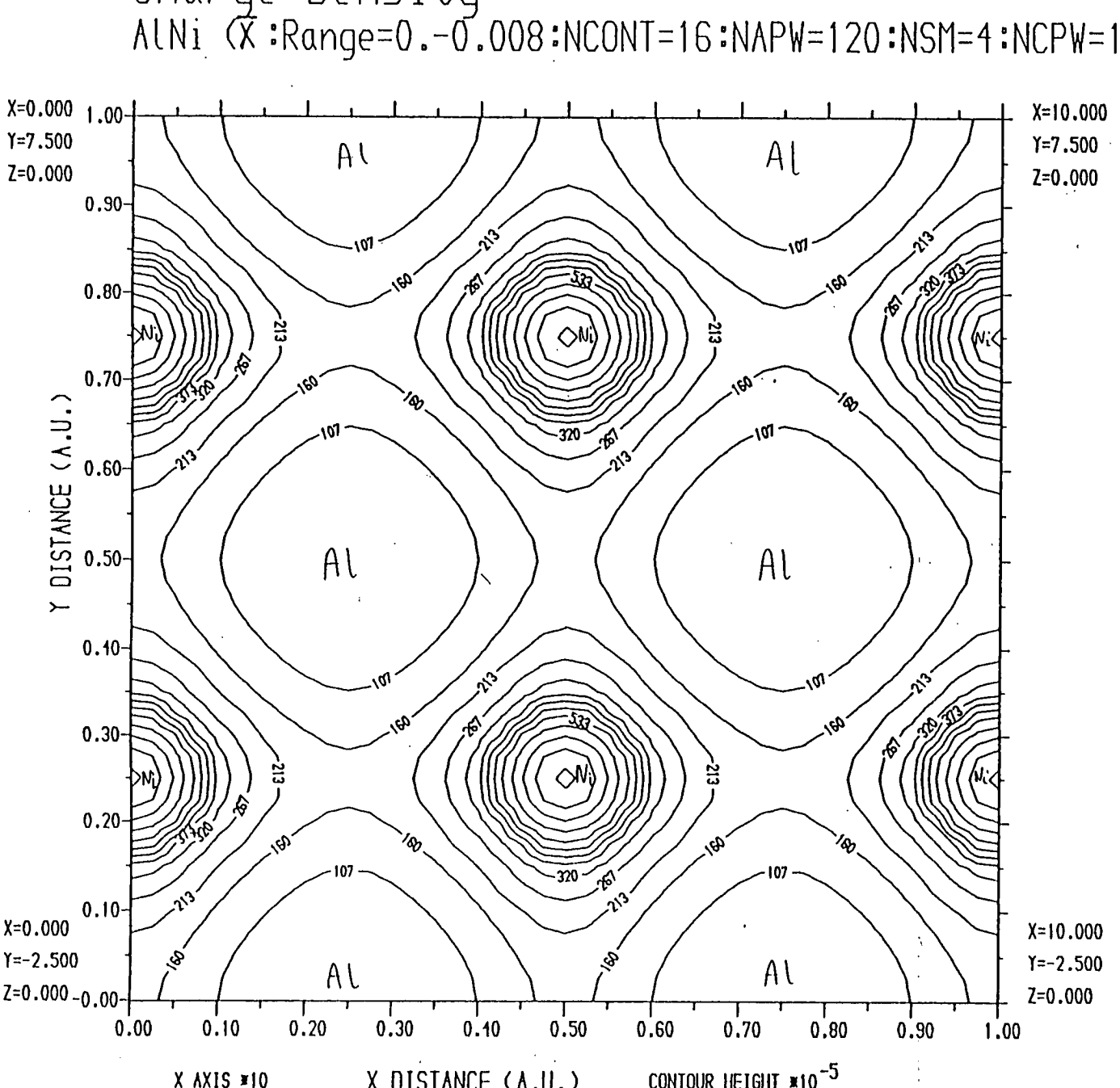

Fig.5.54: Charge density for interface state at $\bar{X}$, in z=0 plane

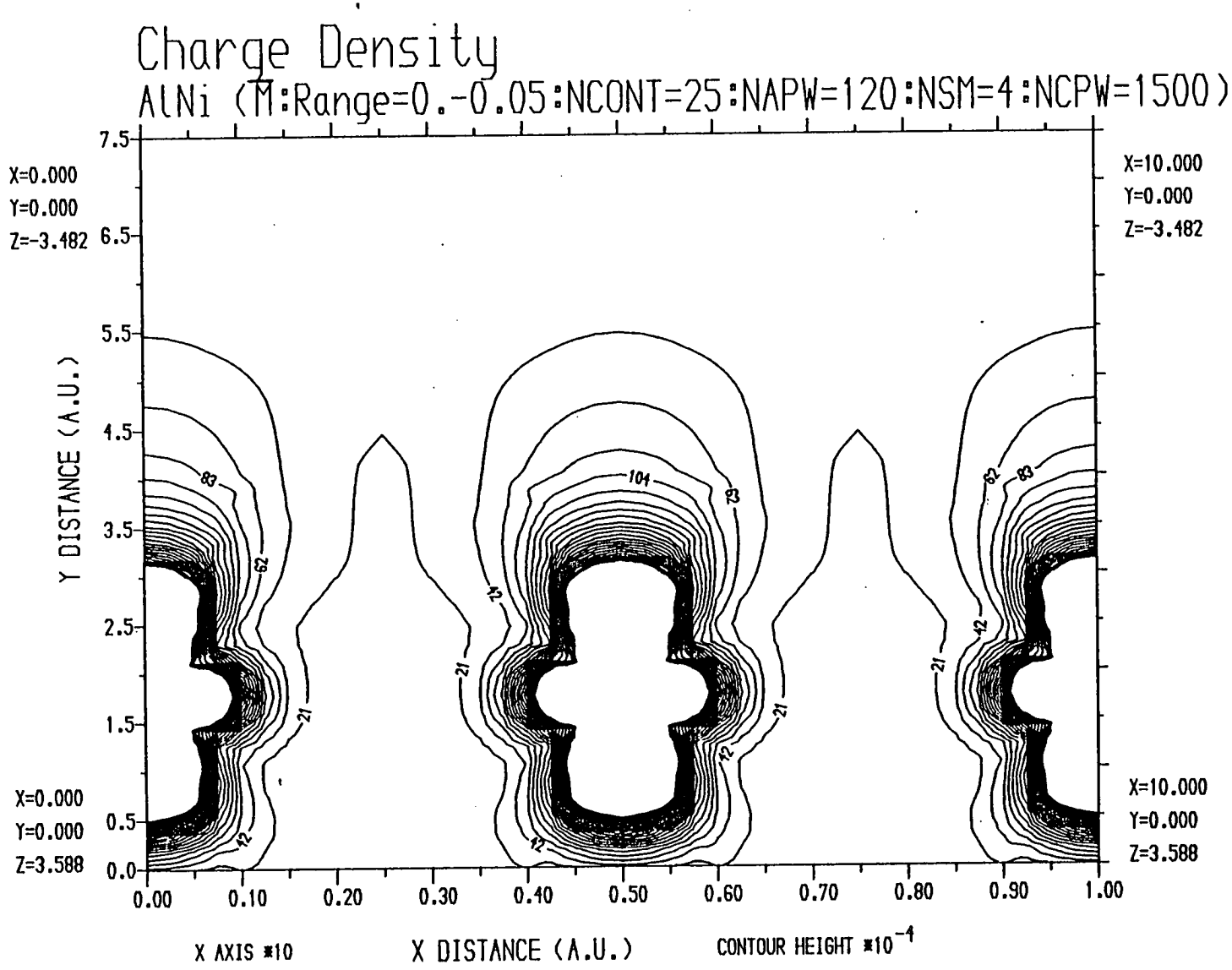

Fig.5.55: Charge density for interface state at $\overline{M}$, in plane of Ni atoms

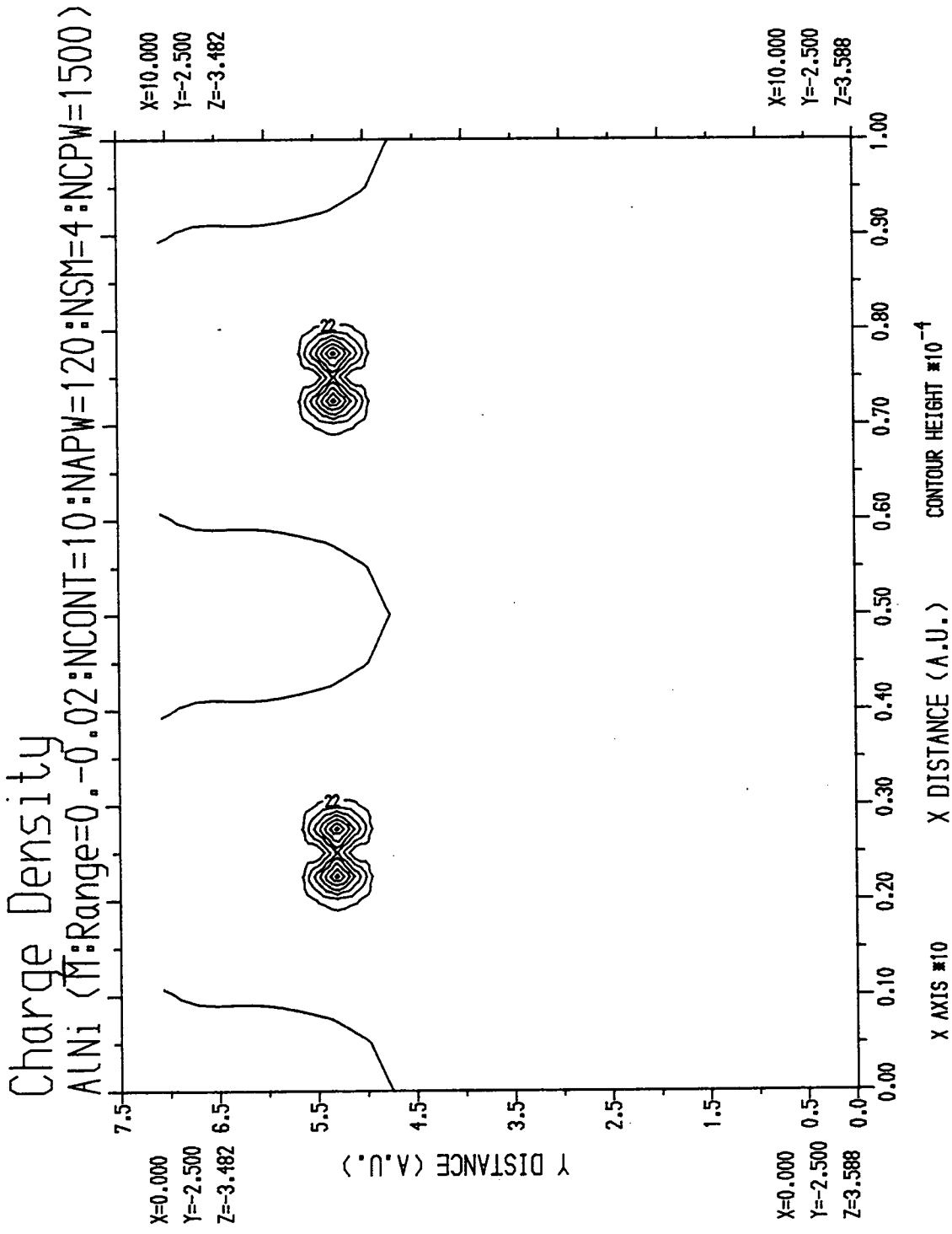

Fig.5.56: Charge density for interface state at $\overline{M}$, in plane of Al atoms

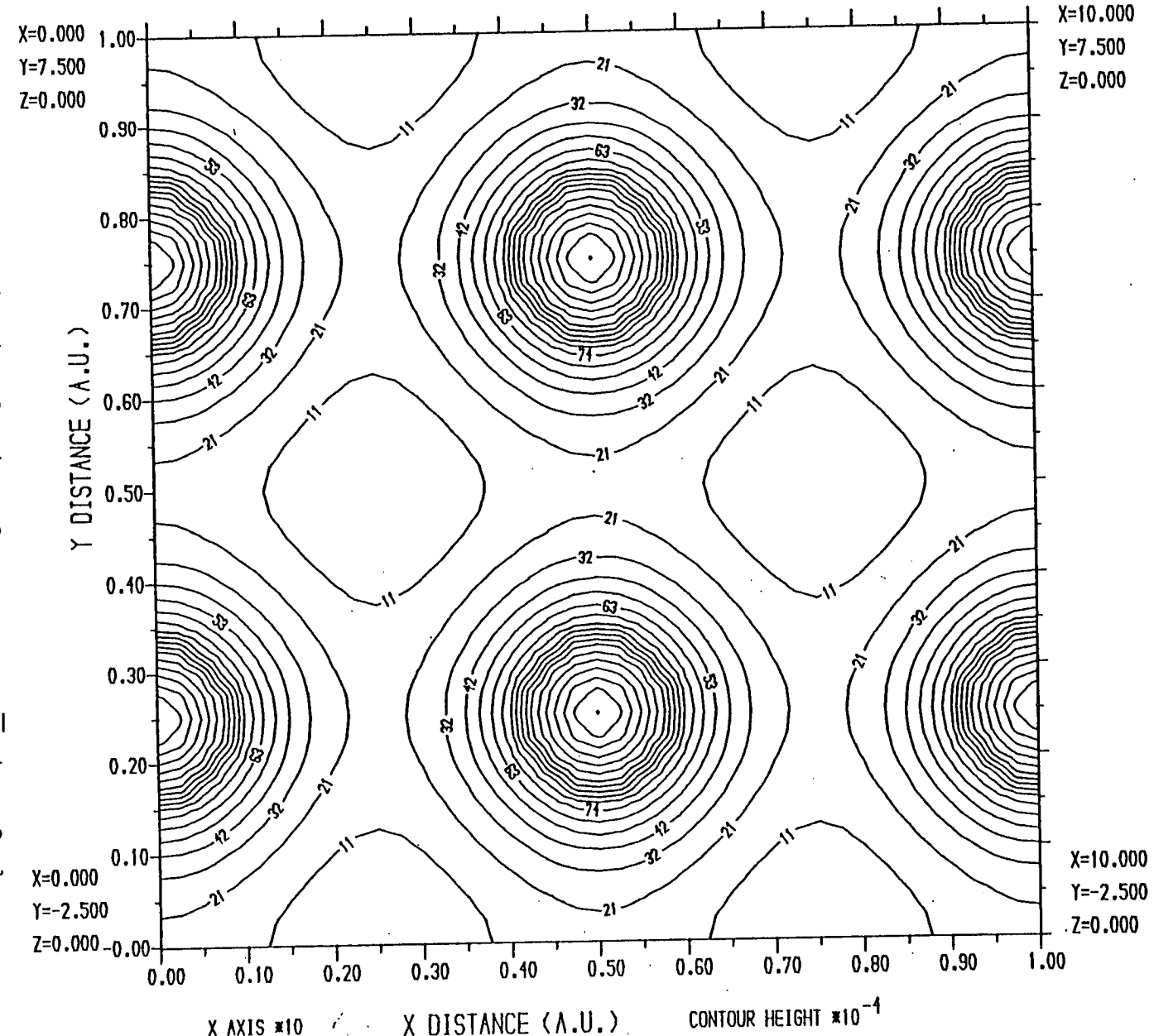

Fig.5.57: Charge density for interface state at $\overline{M}$, in z=0 plane

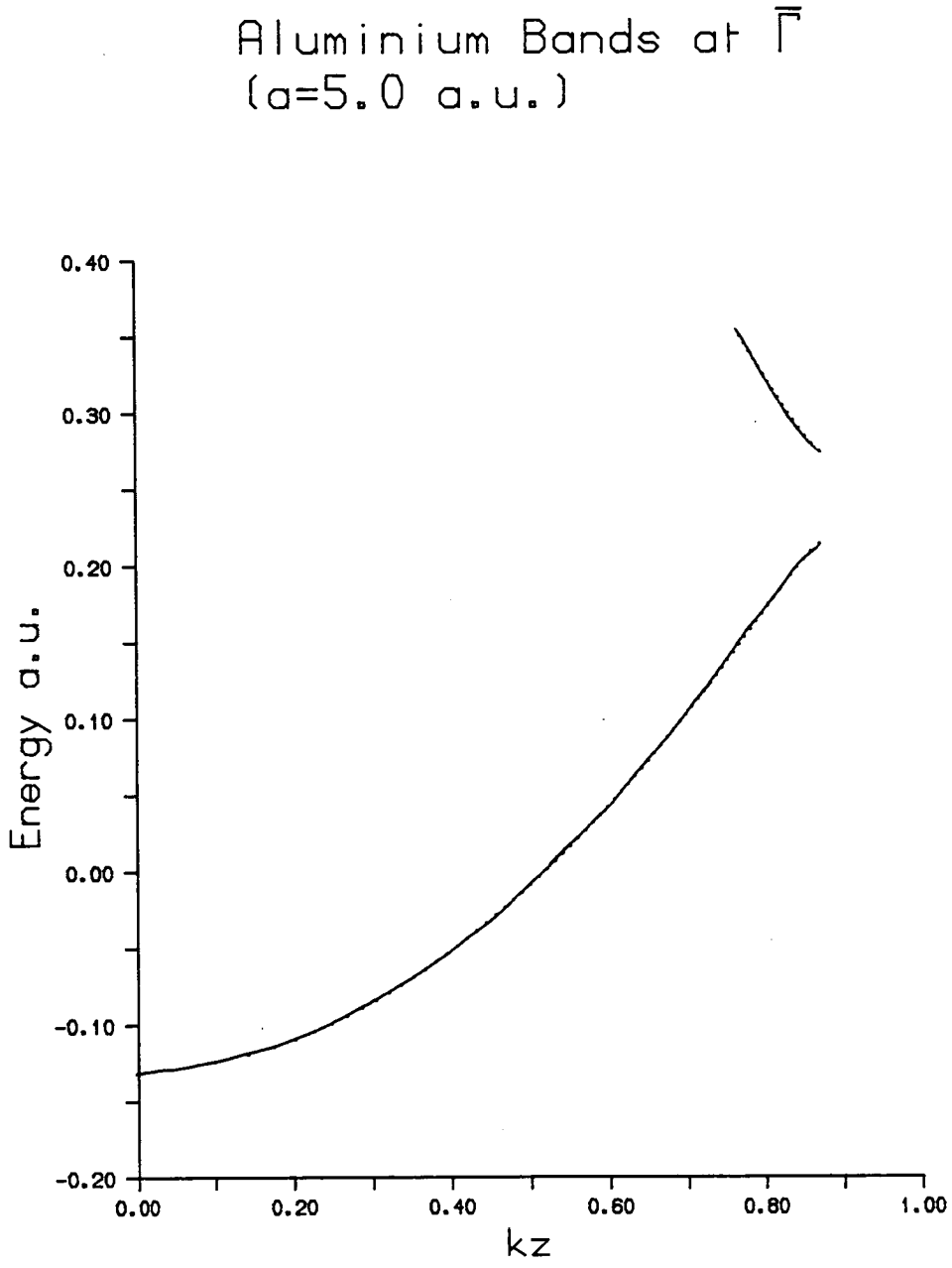

Fig.5.58: Bulk Al bands at $\bar{\Gamma}$, with 5.0au lattice constant

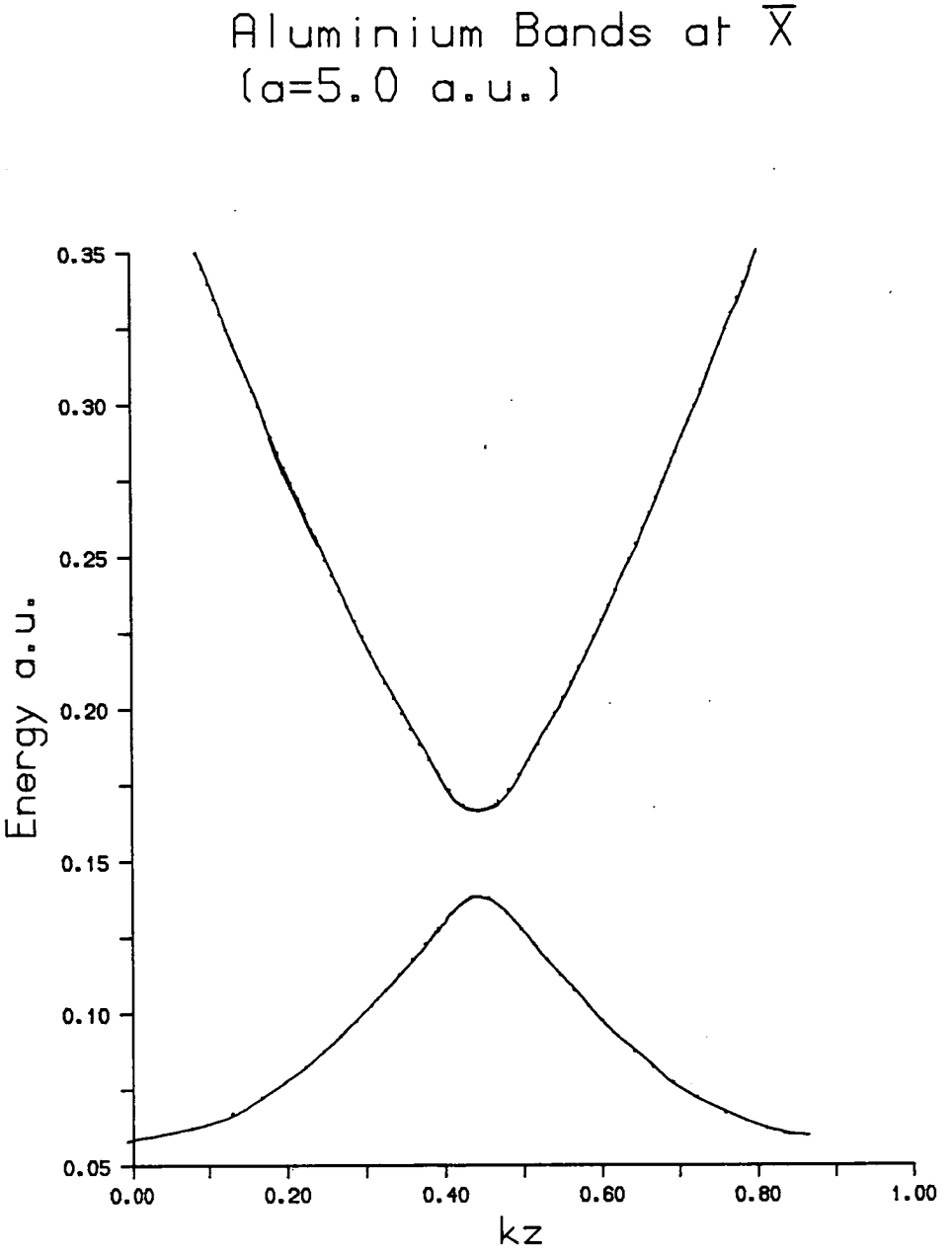

Fig.5.59: Bulk Al bands at $\bar{X}$, with 5.0au lattice constant

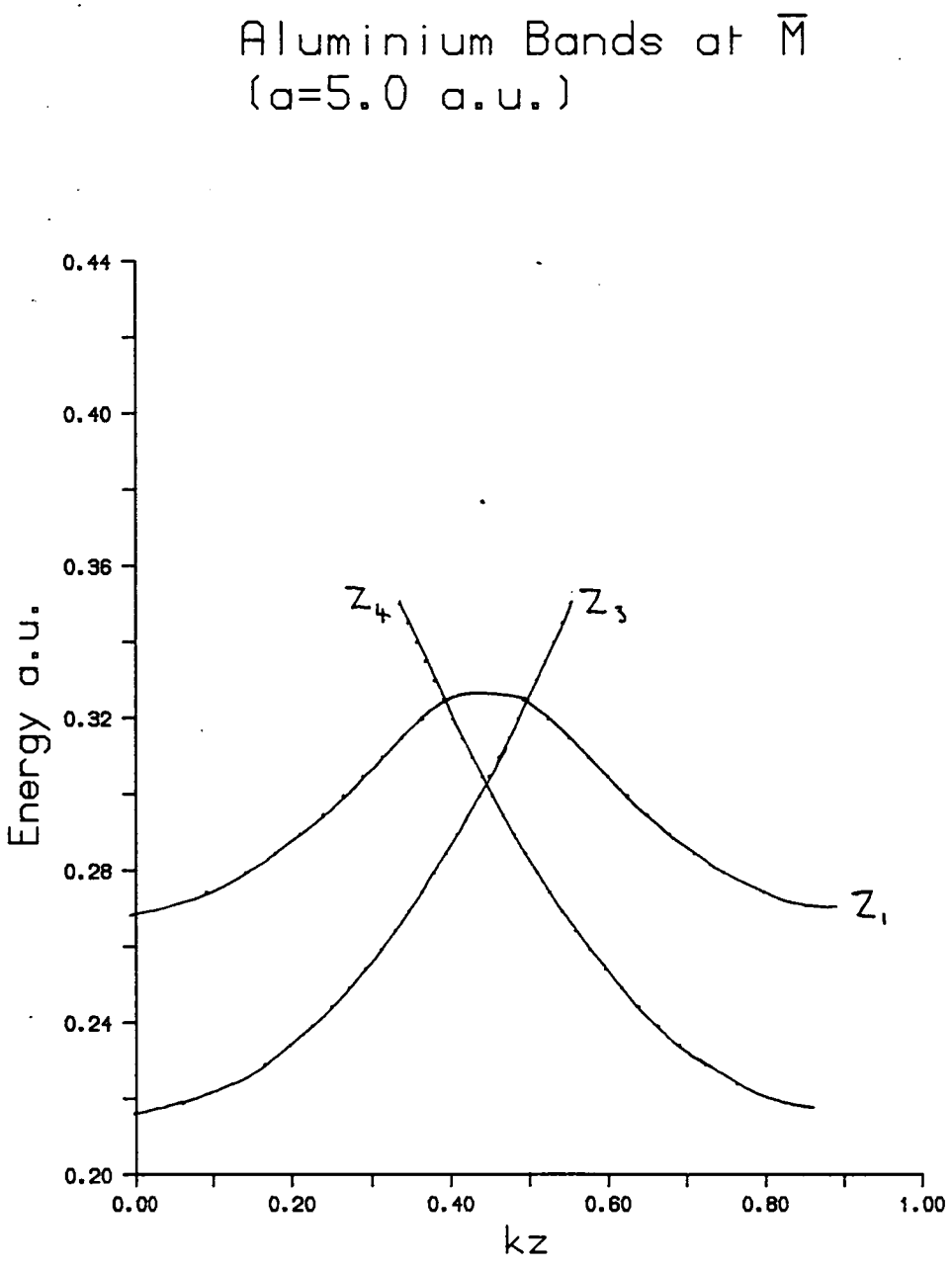

Fig.5.60: Bulk Al bands at $\overline{M}$, with 5.0au lattice constant

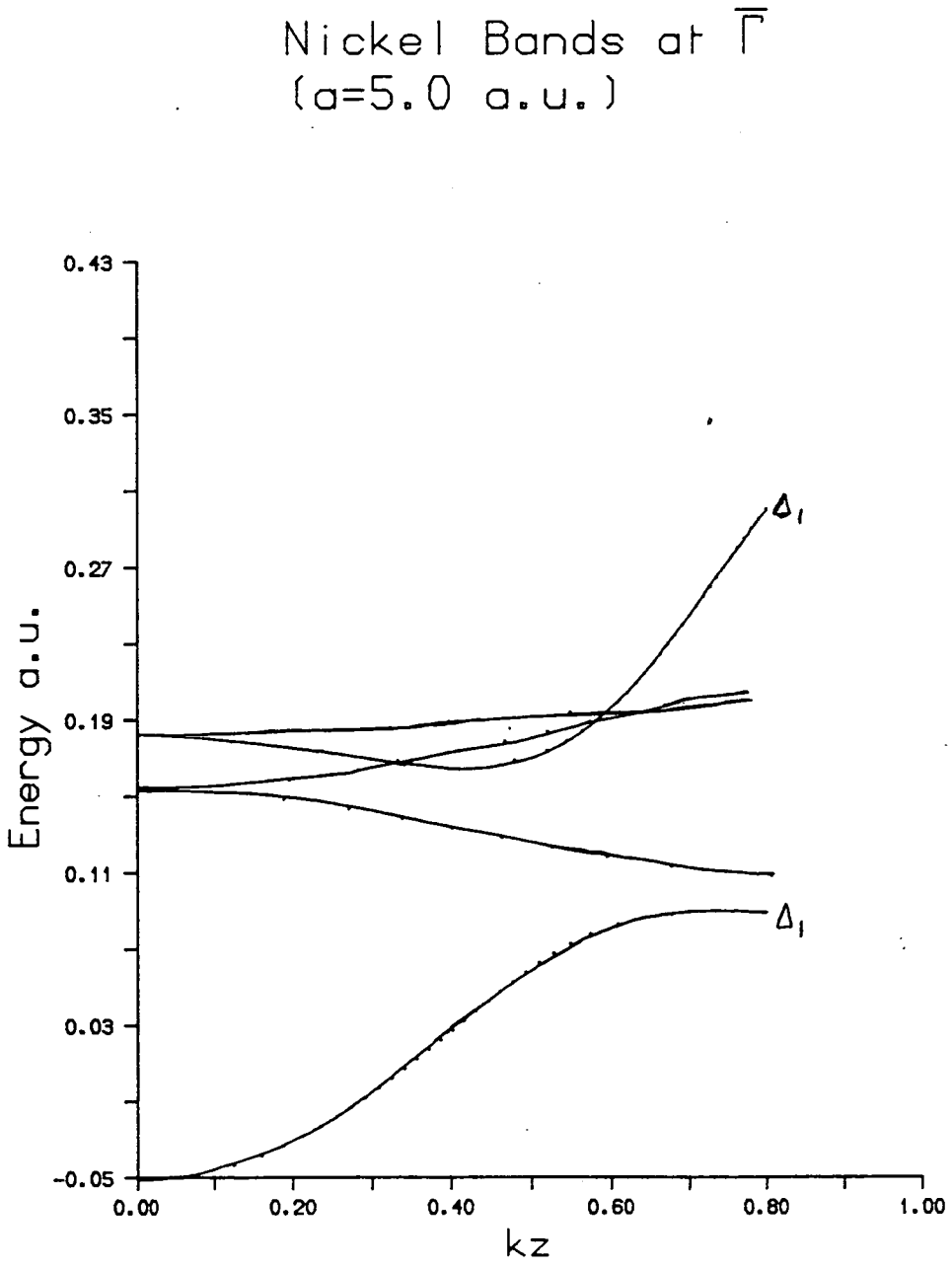

Fig.5.61: Bulk Ni bands at $\bar{\Gamma}$, with 5.0 au lattice constant

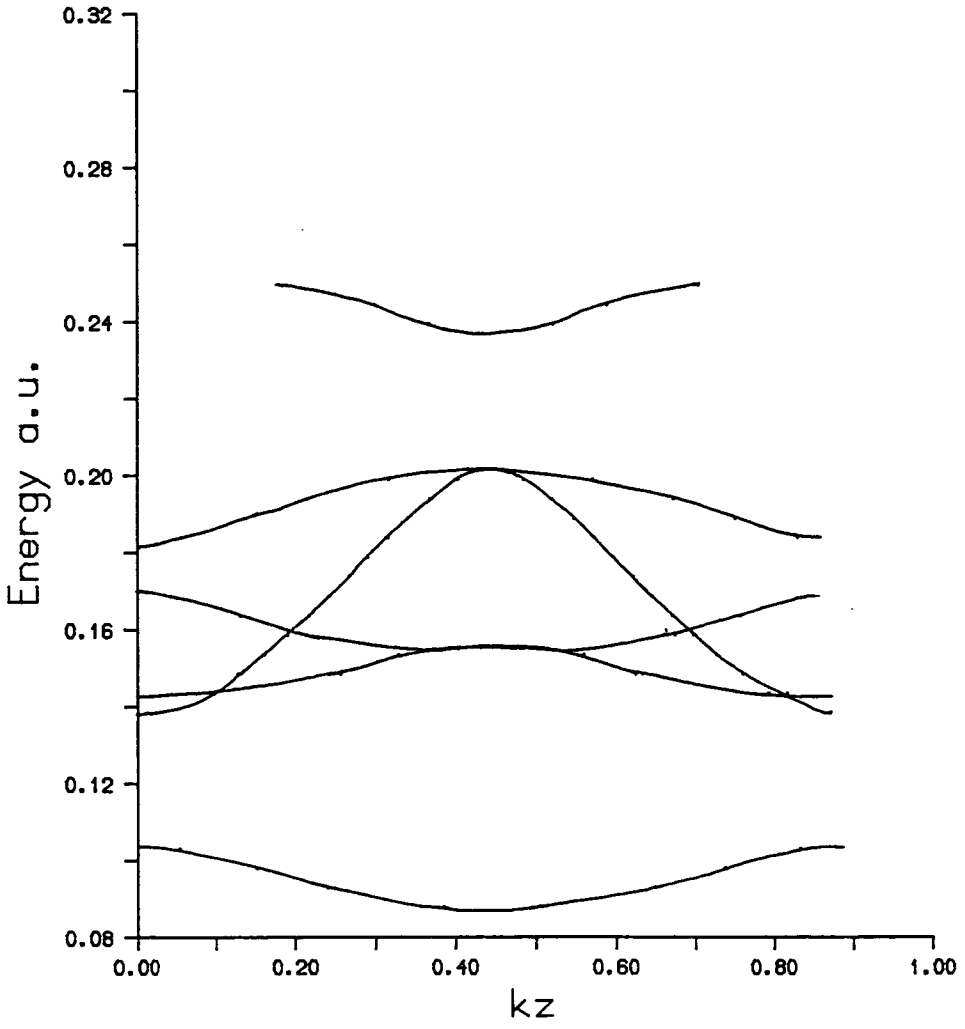

Fig.5.62: Bulk Ni bands at $\overline{X}$, with 5.0au lattice constant

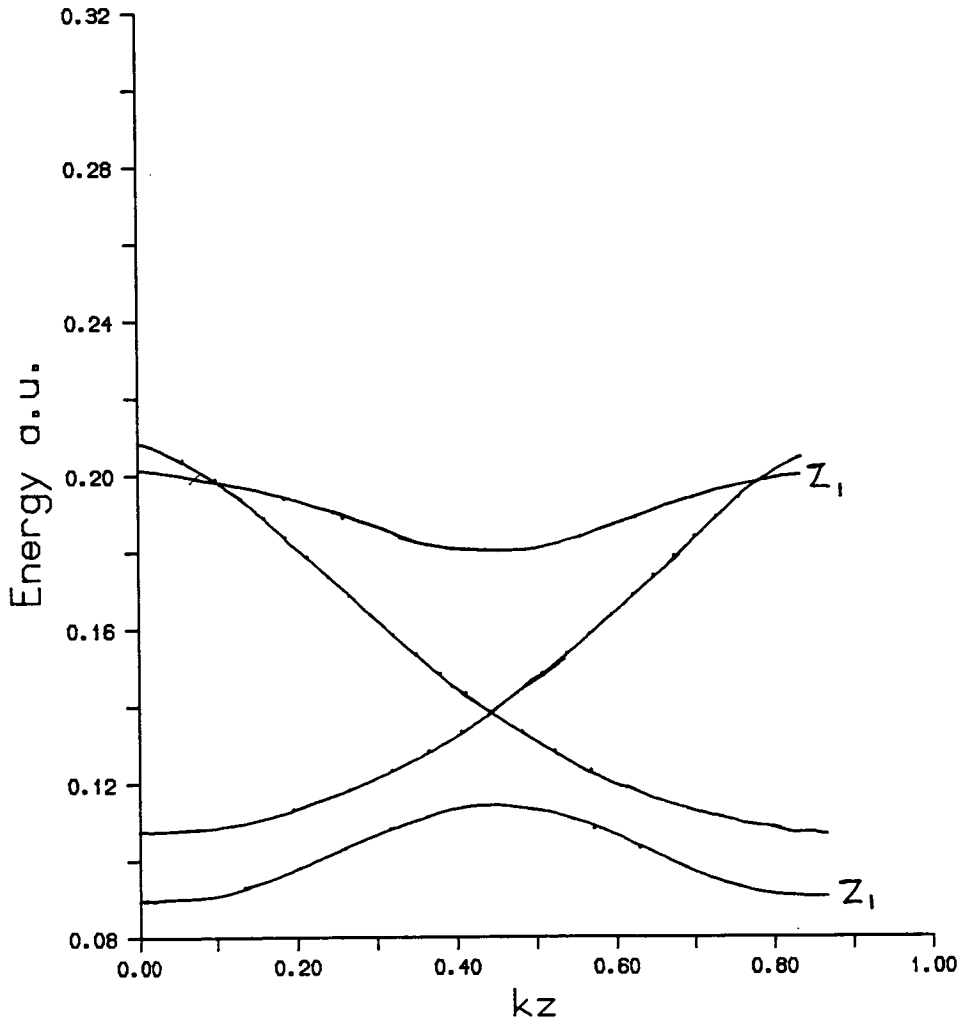

Fig.5.63: Bulk Ni bands at $\overline{M}$, with 5.0au lattice constant

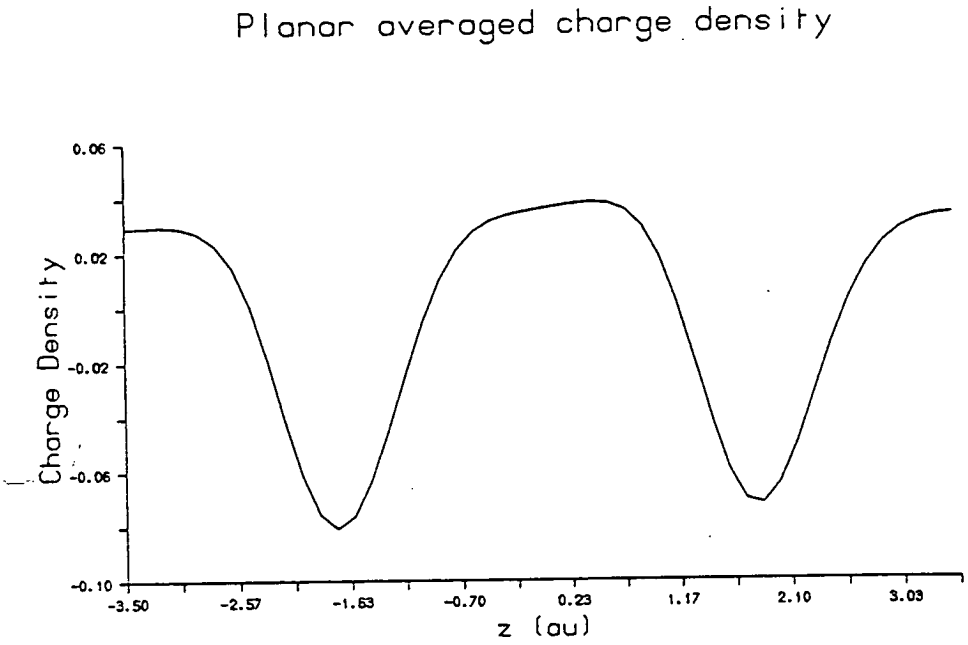

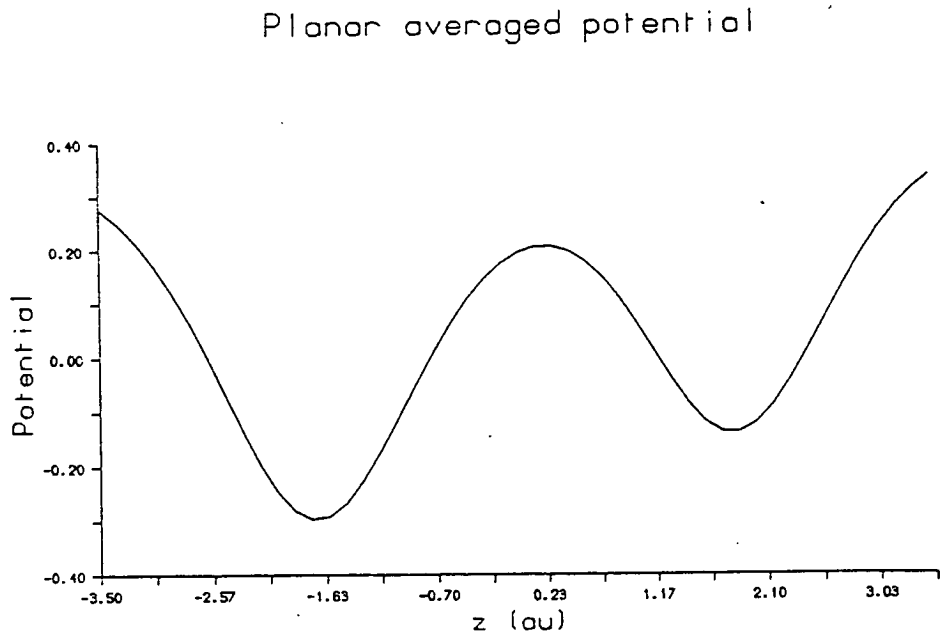

Fig.5.64: Planar averaged charge density and potential across AlNi interface (Al at left).

Chapter 6

Aluminium-Silicon Junction

In this chapter an Al-Si (001) junction is considered as an example of a metal-semiconductor system. Such interfaces are important for the operation of many electronic devices, in particular the Schottky barrier diode. As might be expected, the Si band gaps are predominately filled with bulk states from the Al which decay into the Si side of the interface. However, true interface states are also observed in regions of reciprocal space where both materials have a band gap.

The Si lattice is face centred cubic of side 10.22au, with a basis at (0,0,0) and $(\frac{1}{4},\frac{1}{4},\frac{1}{4})$, which can be represented by the repeat sequence of two dimensional unit cells in Fig. 6.1, of side 7.227au. The Al lattice constant is also taken to be 7.227au, which is close to the true value of 7.600au. One layer of each material is explicitly considered, with the interface separation being the mean of that between the layers in each substrate (Fig. 6.2). The final geometry chosen is somewhat *ad hoc*, but constitutes a plausable guess at the likely atomic arrangement, assuming no diffusion. In reality, it is likely that diffusion occurs at the interface, mainly of the Al into the relatively open Si lattice, as this has been found to be the case in the Si-Ni (001) interface [45]. As the Si structure is relatively open, extra spheres are inserted in the Si substrate, which is a better representation to the true potential, rather than the usual constant potential in the interstitial region. This is not necessary in the interface region, where the full 'warping' potential is used. The Fermi level in

Si is taken to lie at the middle of the optical gap at $\bar{\Gamma}$, and consideration of the Fermi level in the Al leads to the potential shifts shown below.

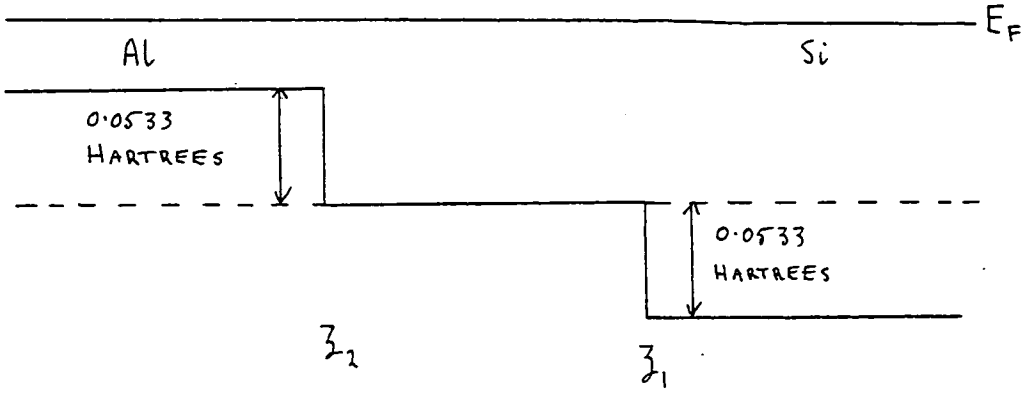

42 iterations, using 200 LAPWs and 8 rings in the interface and embedding potential expansions, were required to obtain maximum errors in the Al and Si potentials of 0.002 and 0.02 Hartrees respectively. Good overall charge neutrality was obtained in the interface slab, with there being 9.8 valence electrons in the interface after convergence, compared with the expected value of 10 electrons. This suggests that the potential shifts used are close to the true values, and also that consideration of more than one layer of each material would not greatly alter the results, even though the screening length in semiconductors is larger than in metals. The charge density (Figs. 6.3-6.4) looks fairly smooth, and does not exhibit any of the instabilities noted in Chapter 5. The potential (Figs. 6.5-6.6) is found to be a good fit at each boundary, and over the muffin tin surfaces. Initially, problems were encountered with 'extra' non-physical spheres appearing at the Si embedding plane, but this was traced to an anomaly in the construction of the potential boundary conditions due to the use of empty spheres in the substrate. By default, the program which generates the embedding potentials and boundary conditions assumes that the atomic basis in the interface is the same as the substrate, and constructs the boundary conditions accordingly. In this case the empty spheres are used in the Si substrate, but not in the interface slab, thus violating this assumption.

The density of states has been calculated at $\bar{\Gamma}$ $(0,0)$, $\bar{X}$ $(\frac{1}{2},0)$, and $\bar{M}$ $(\frac{1}{2},\frac{1}{2})$ for each atomic star, and also for the whole embedded region (Figs. 6.7-6.18). Comparison with the bulk results is facilitated using the calculated bulk band structures of Al and Si for the chosen geometry (Figs. 6.19-6.24), and remembering that the density of states is inversely proportional to $\nabla_k E$. In regions of reciprocal space where the Si has band gaps, these are predominantly filled in the interface region by bulk states from the Al leaking across the interface, and decaying into the Si. Most of the features can thus be ascribed to bulk band structure effects, with three noted exceptions. These are:

1. Fig. 6.8, $\bar{\Gamma}$, Al star 2, energy 0.42 Hartrees. This can also be seen as a shoulder in the Si density of states (Fig. 6.7).

2. Figs. 6.15-6.18, $\bar{M}$, 0.14 Hartrees.

3. Figs. 6.15-6.18, $\bar{M}$, 0.24 Hartrees.

Looking at each of these in turn, we see that the first lies in the optical gap of Si at $\bar{\Gamma}$ (Fig. 6.22), after allowing for the energy shift across the interface. However, the Al (Fig. 6.19) does not have a band gap at this energy, so the situation is probably as in the Al-Ni examples, with the interface state lying in a symmetry gap of the Al. As we do not know the symmetry of the Al bands for the given lattice, this has not yet been clarified. The charge density (Figs. 6.25 and 6.26) is in this case not helpful in determining the symmetry. The first state at $\bar{M}$ of energy 0.14 Hartrees lies in a band gap of Si (Fig. 6.24) and below the lowest valence band of Al (Fig. 6.21), so essentially is in a band gap of both materials. The charge density (Figs. 6.27 and 6.28) shows a considerable build up of charge between the Al and Si, indicating that this is associated with the bonding. The odd looking charge density of Fig. 6.27 can be discounted due to the very small charge density range present in this plane. Moving on to the second state at $\bar{M}$ of energy 0.24 Hartrees, we see that it lies in the same band gap of Si (Fig. 6.24), but is now in the valence band gap of Al (Fig. 6.21), with the charge density (Fig. 6.29 and 6.30) again concentrated between the layers.

Summary

The electronic structure of the Al-Si (001) interface correlates well with the bulk band structures for the given geometry. Localised interface states are also found to exist in band gaps of one or both materials. Comparison with other workers' results is not possible, as the calculations done to date have mainly dealt with the total density of states, rather than that at symmetry points. However, Louie and Cohen [46] and Vekilov *et al* [47] give results for the Si(111)-Al(110) interface which show interface states near the symmetry point K of the two dimensional hexagonal Brillouin zone. The nature of these states is analogous to the interface states at $\bar{M}$ in this calculation, in the sense that they exist in band gaps of both the Si and Al. The continuum of Al states is also found to decay into the Si band gaps [46].

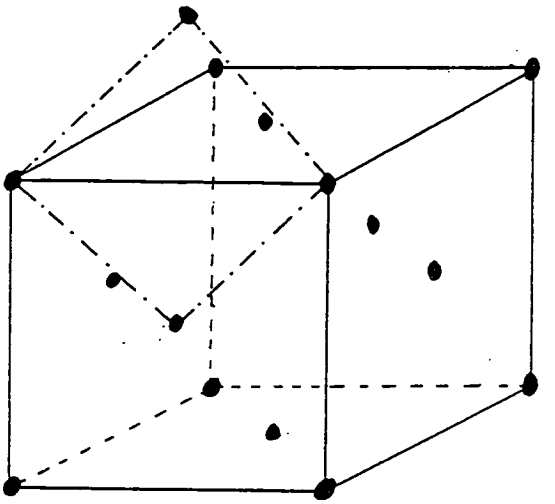

Fig. 6.1a: FCC Si unit cell (—— and- - - - -), showing only those atoms at (0,0,0), and the 2-D unit cell (–·–·–) to be used.

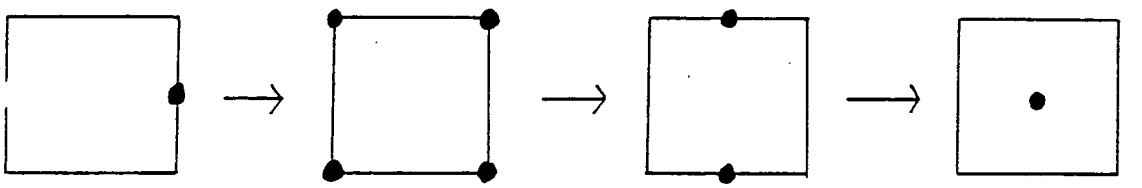

Fig. 6.1b: Repeat sequence of 2-D cells to give Si lattice.

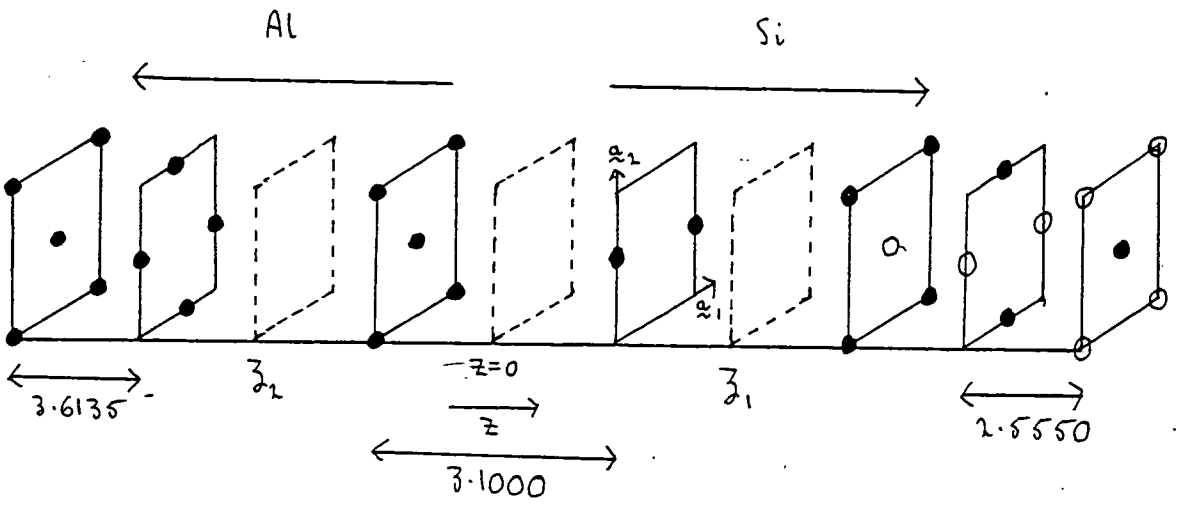

$\|\mathbf{a}_1\| = \|\mathbf{a}_2\|$	=	7.227 au
D	=	7.85845 au
$\tilde{\mathrm{D}}$	=	9.00 au
$R_{Si} = R_{es}$	=	2.21267 au
R_{Al}	=	2.54578 au
ζ_1	=	2.994055 au
ζ_2	=	-3.190195 au
Atomic star 1	=	Si at $(0, \frac{1}{2})$
Atomic star 2	=	Al at $(0,0)$
Atomic star 3	=	Al at $(\frac{1}{2}, \frac{1}{2})$
E	=	$\begin{cases} -0.1066 \rightarrow 0.3734 & \text{in Al} \\ 0.0000 \rightarrow 0.4800 & \text{in Si} \end{cases}$
		16 energy points
n for pseudo ρ expansion	=	$\begin{cases} \text{Al: } 9\ \ 8\ \ 7\ \ 6 \\ \text{Si: } 7\ \ 6\ \ 5\ \ 4 \end{cases}$

Fig. 6.2: Al-Si interface geometry and parameters.

•: Al and Si atoms, ○: empty spheres.

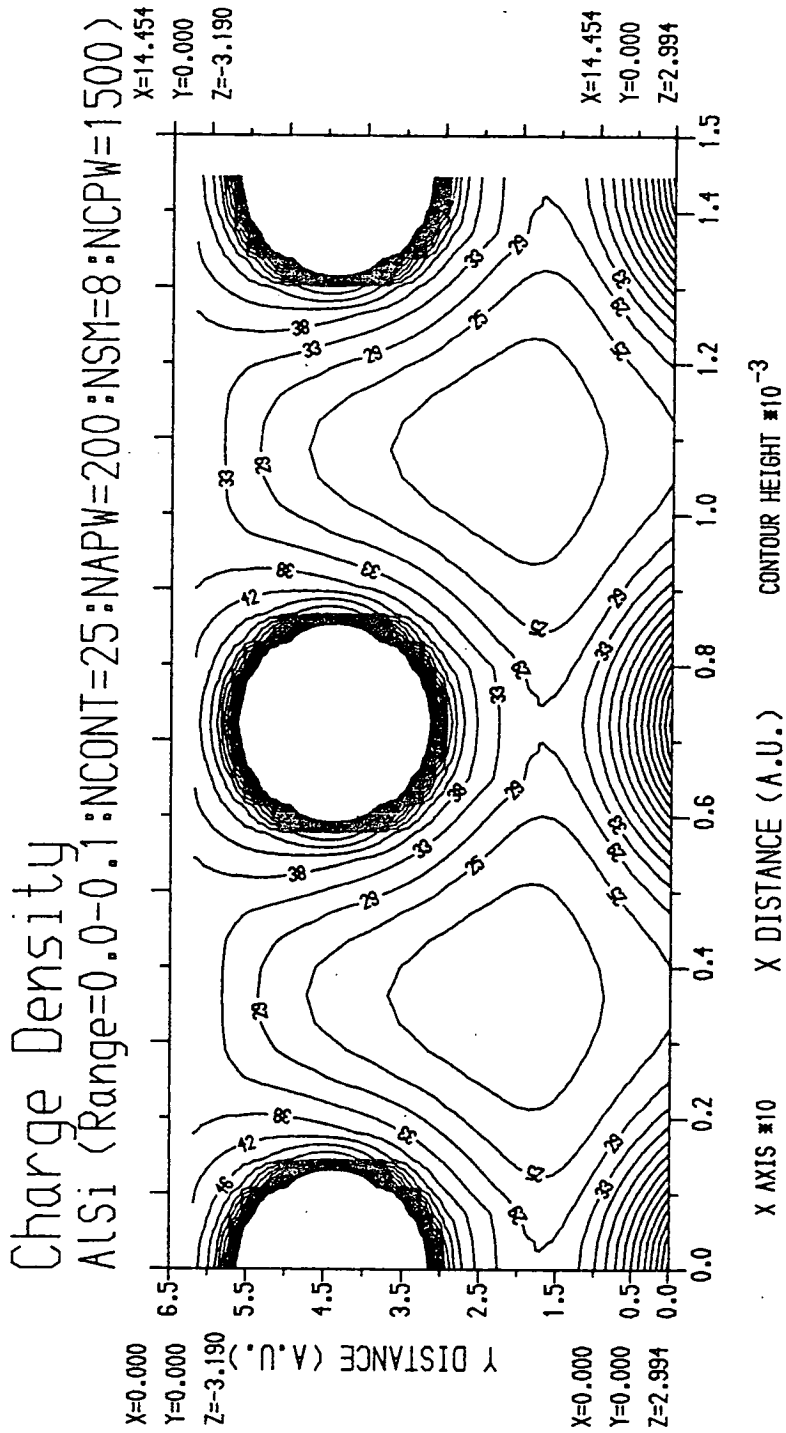

Fig.6.3: AlSi self consistent charge density in plane of Al atoms

Fig.6.4: AlSi self consistent charge density in plane of Si atoms

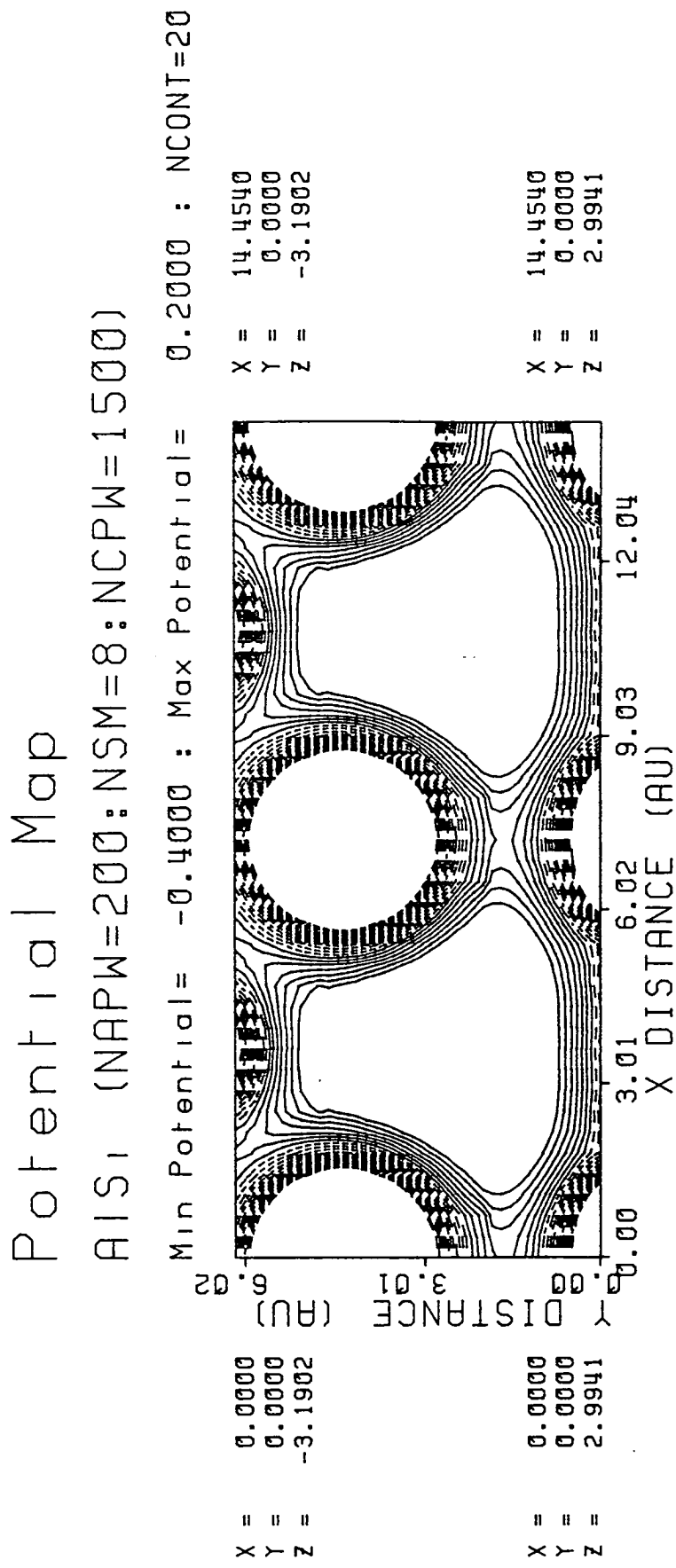

Fig.6.5: AlSi self consistent potential in plane of Al atoms

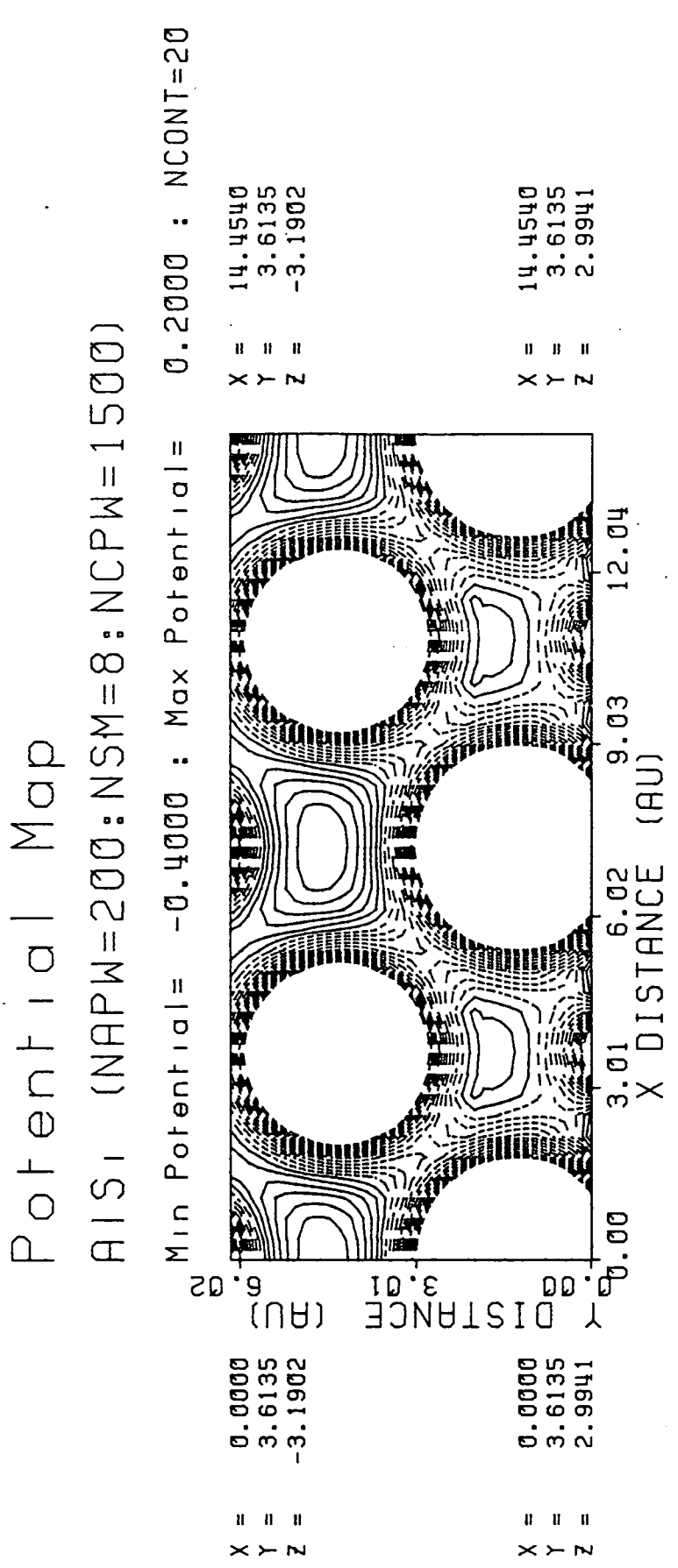

Fig.6.6: AlSi self consistent potential in plane of Si atoms

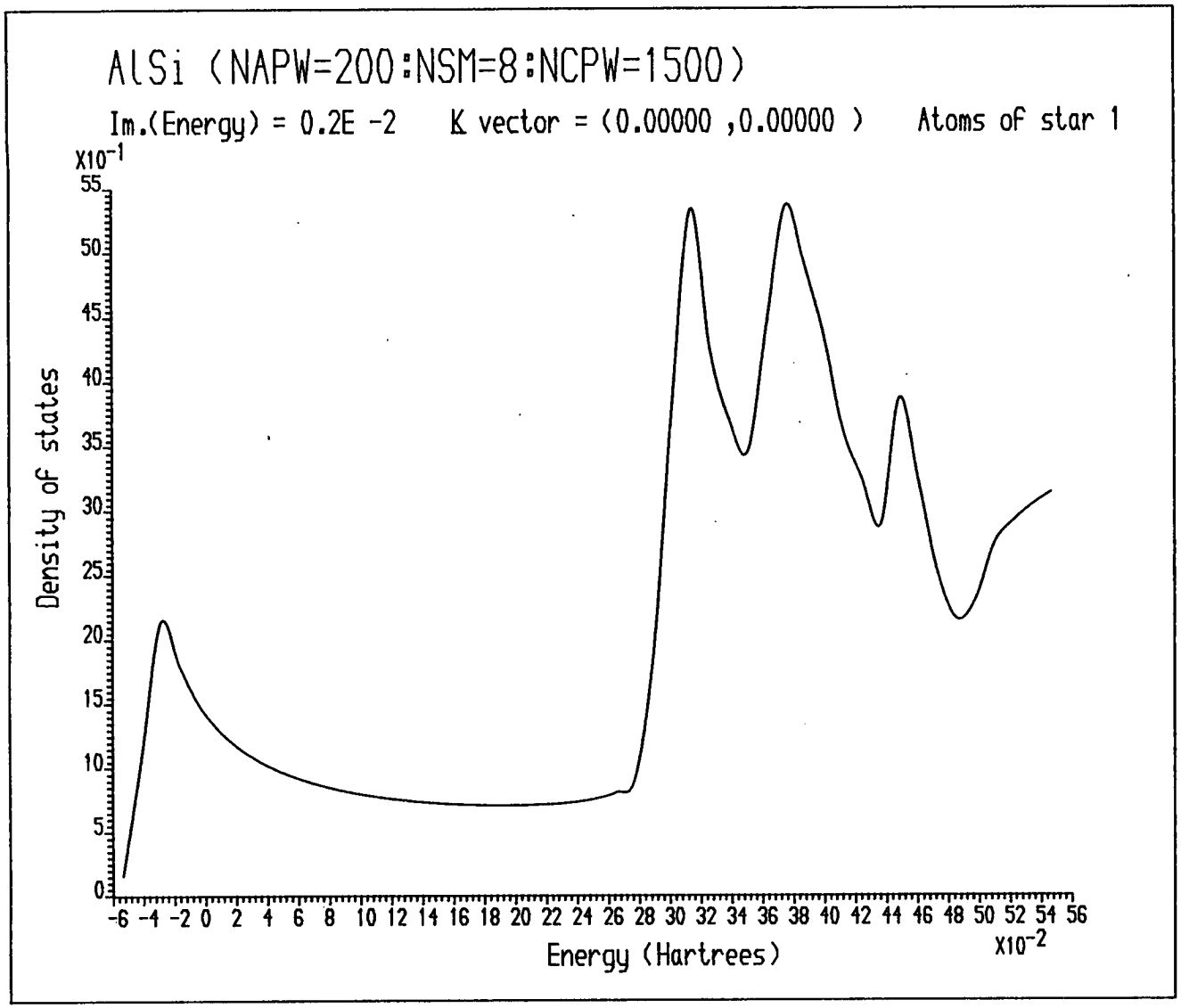

Fig.6.7: Density of states in Si muffin tin at Γ

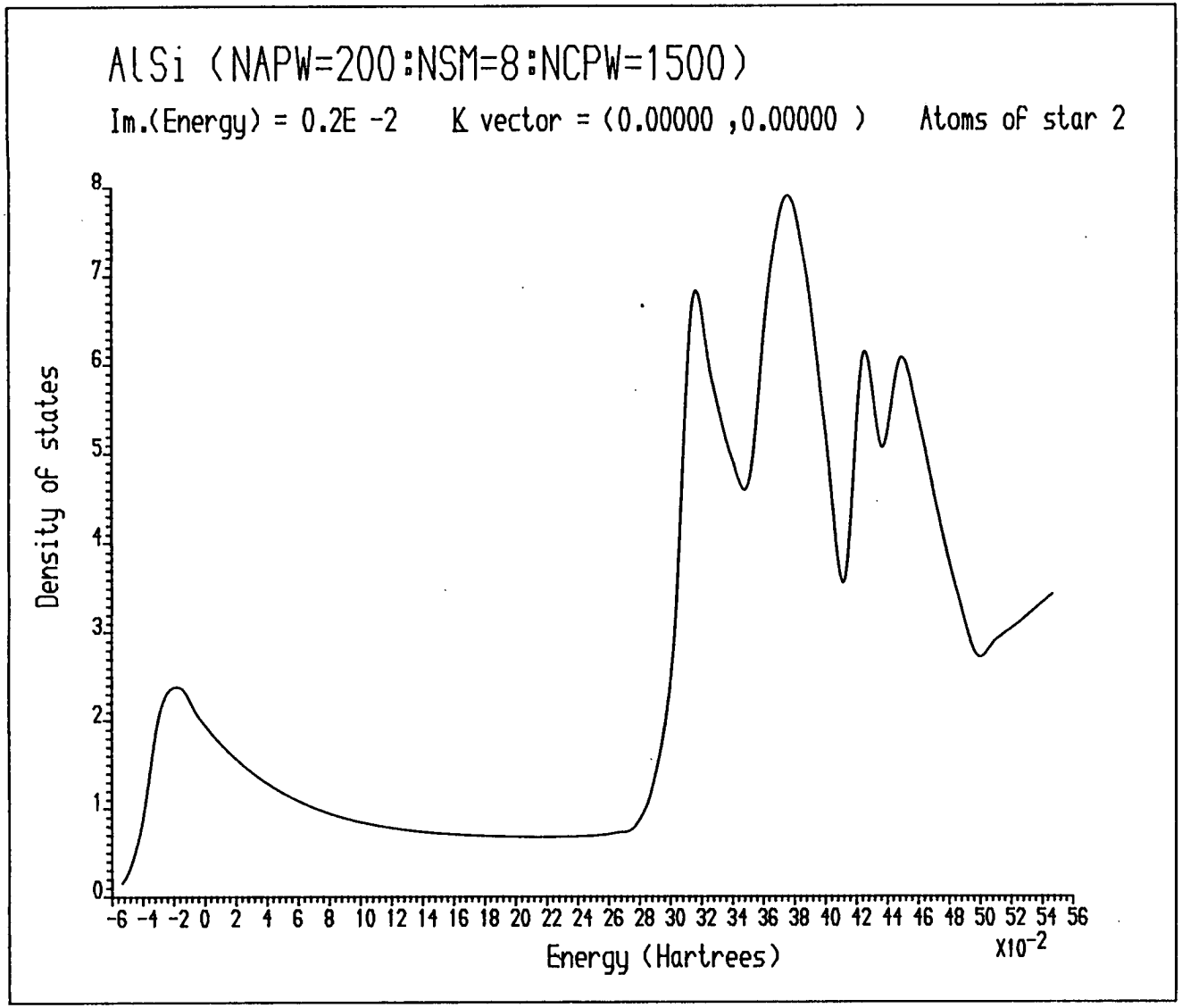

Fig.6.8: Density of states in Al muffin tin at (0,0) at $\bar{\Gamma}$

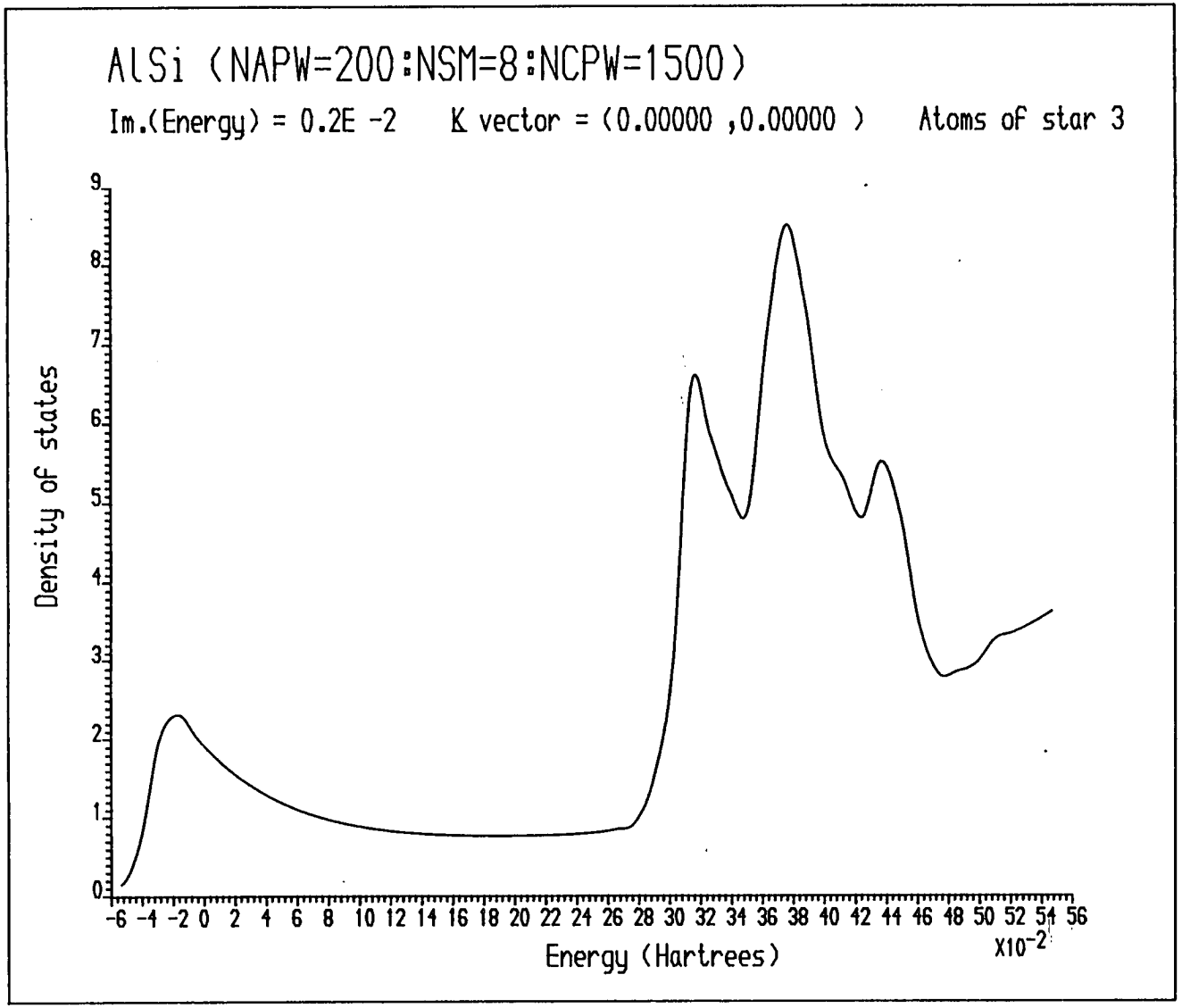

Fig.6.9: Density of states in Al muffin tin at ($\frac{1}{2}$,$\frac{1}{2}$) at

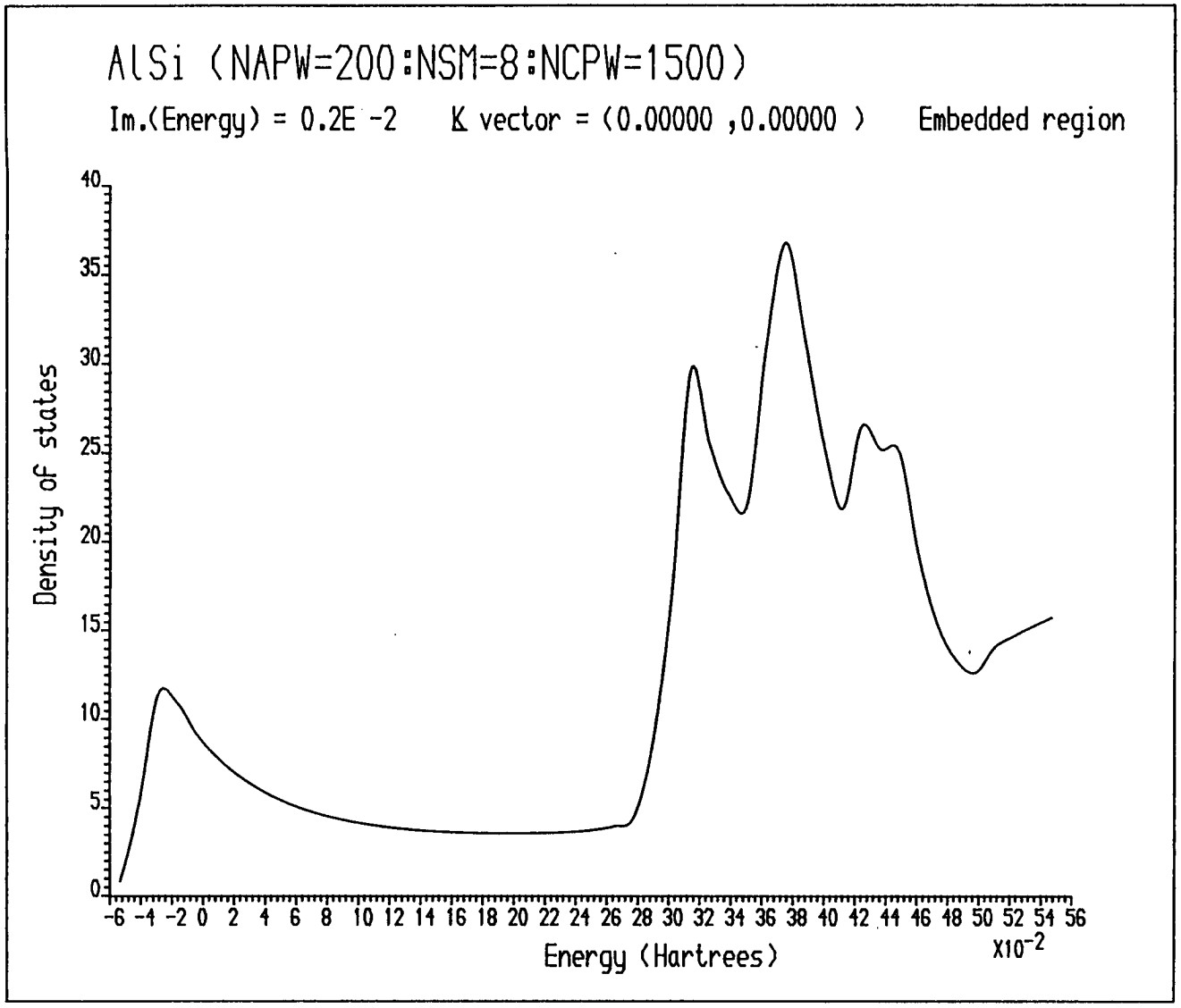

Fig.6.10: Density of states in embedded region at $\overline{\Gamma}$

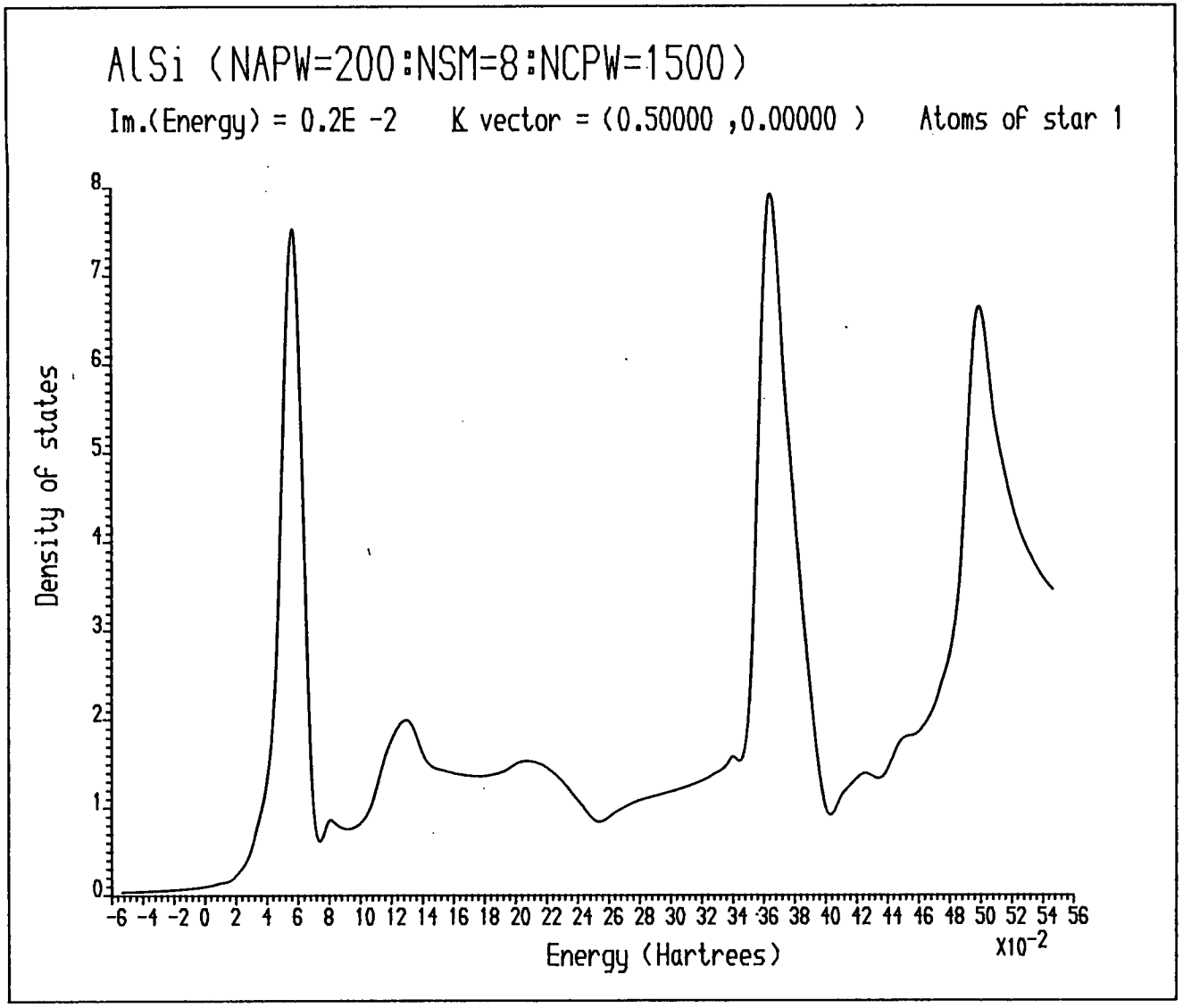

Fig.6.11: Density of states in Si muffin tin at $\overline{X}$

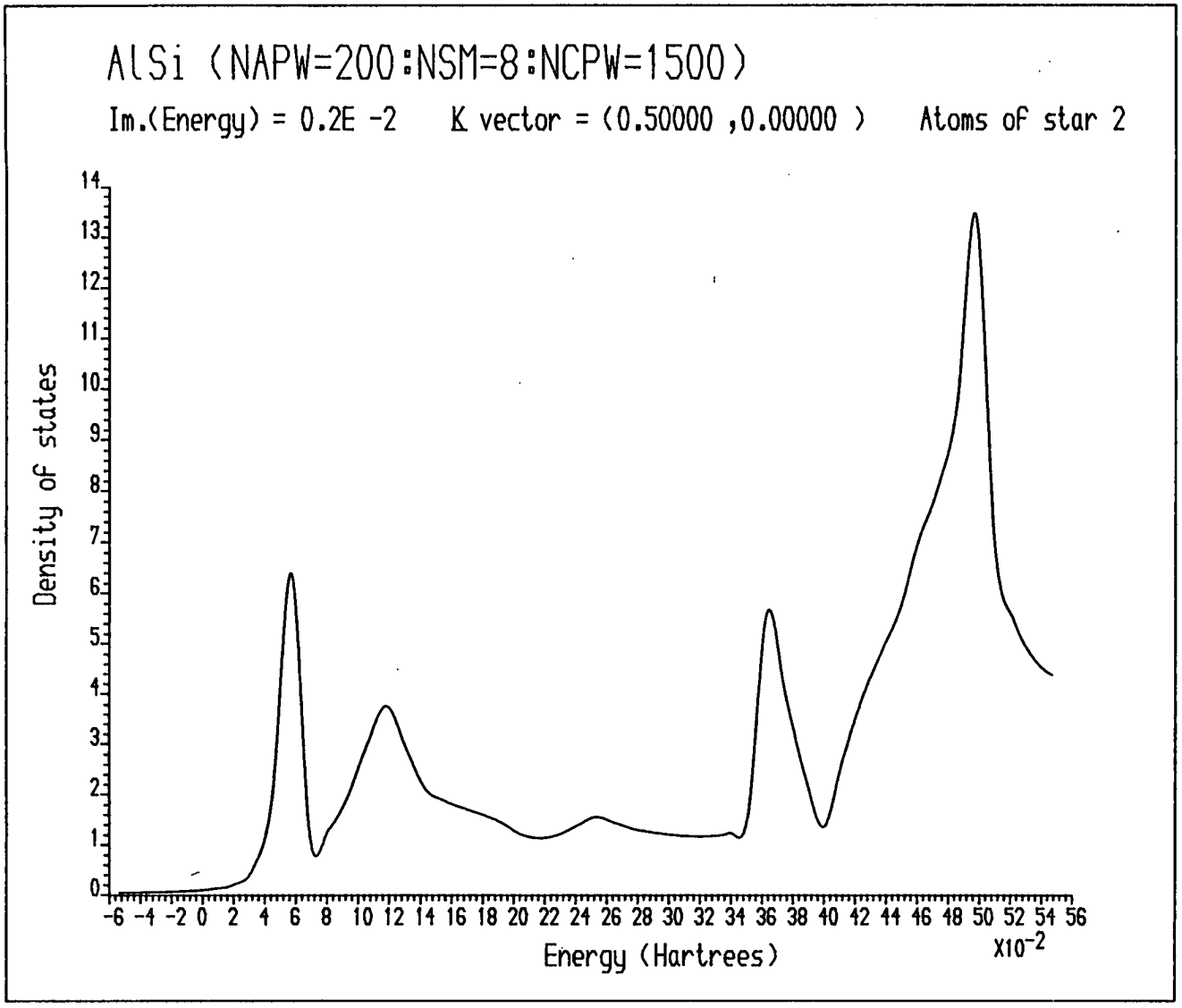

Fig.6.12: Density of states in Al muffin tin at (0,0) at $\overline{X}$

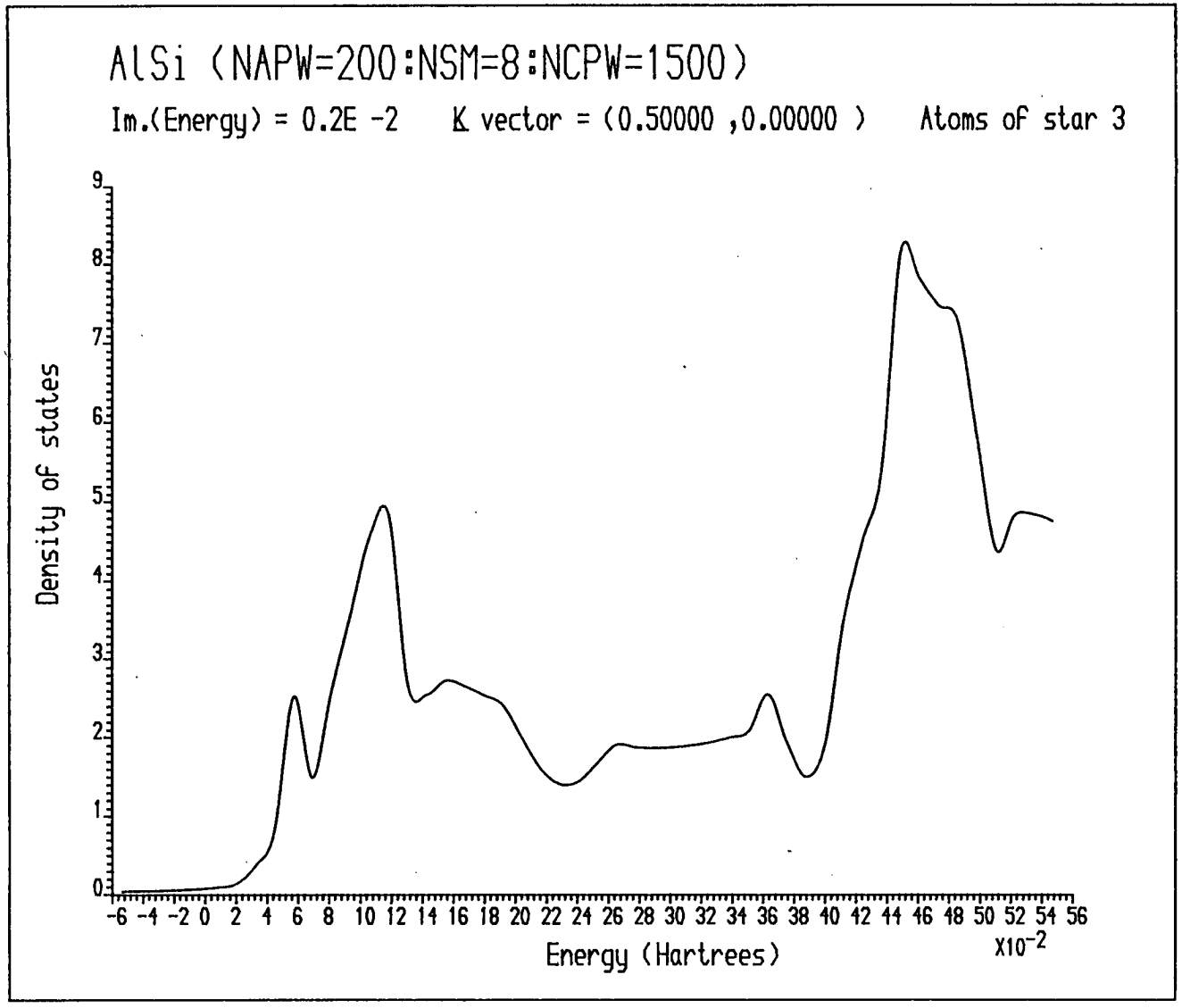

Fig.6.13: Density of states in Al muffin tin at $(\frac{1}{2},\frac{1}{2})$ at $\overline{X}$

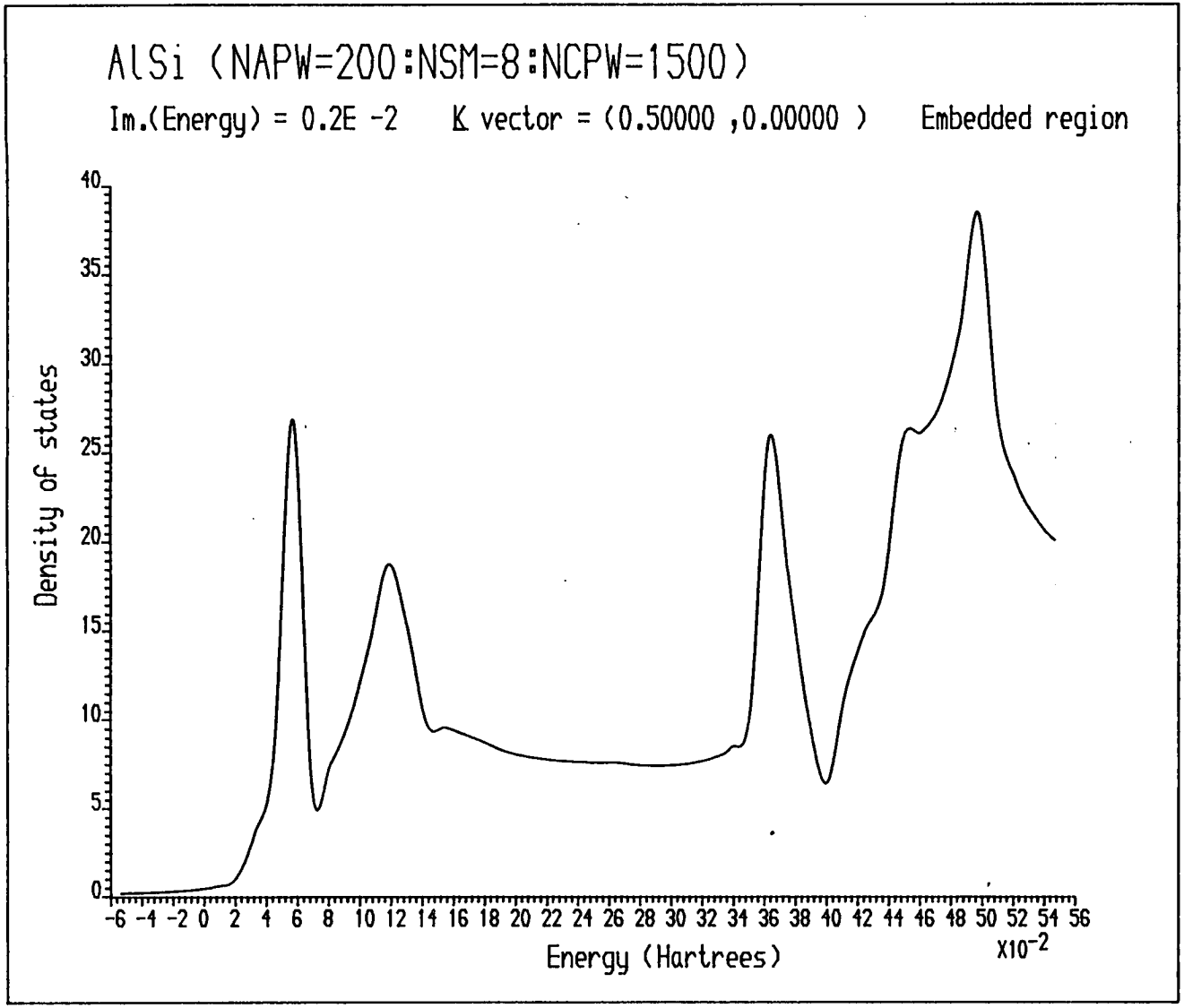

Fig.6.14: Density of states in embedded region at $\bar{X}$

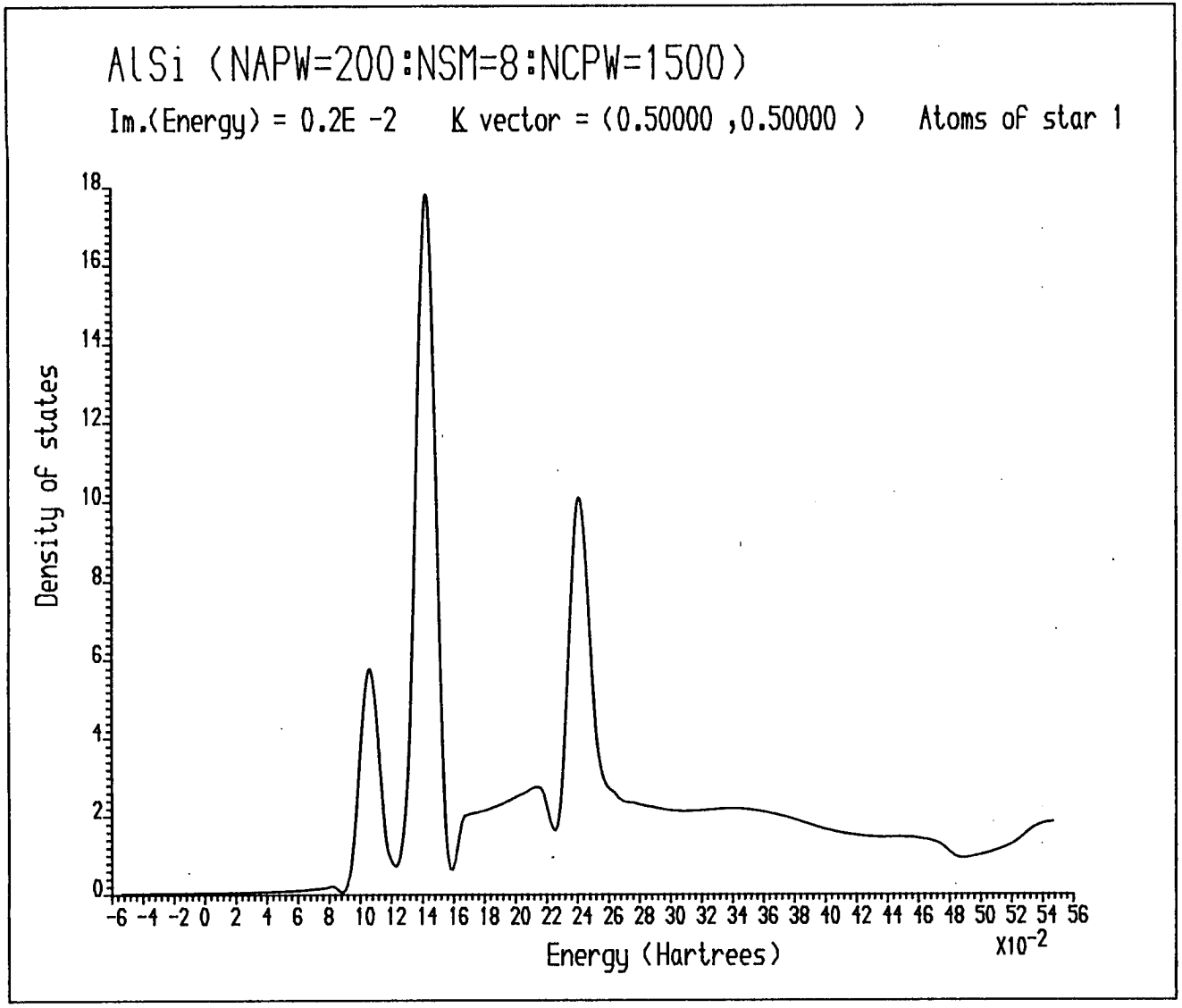

Fig.6.15: Density of states in Si muffin tin at $\overline{M}$

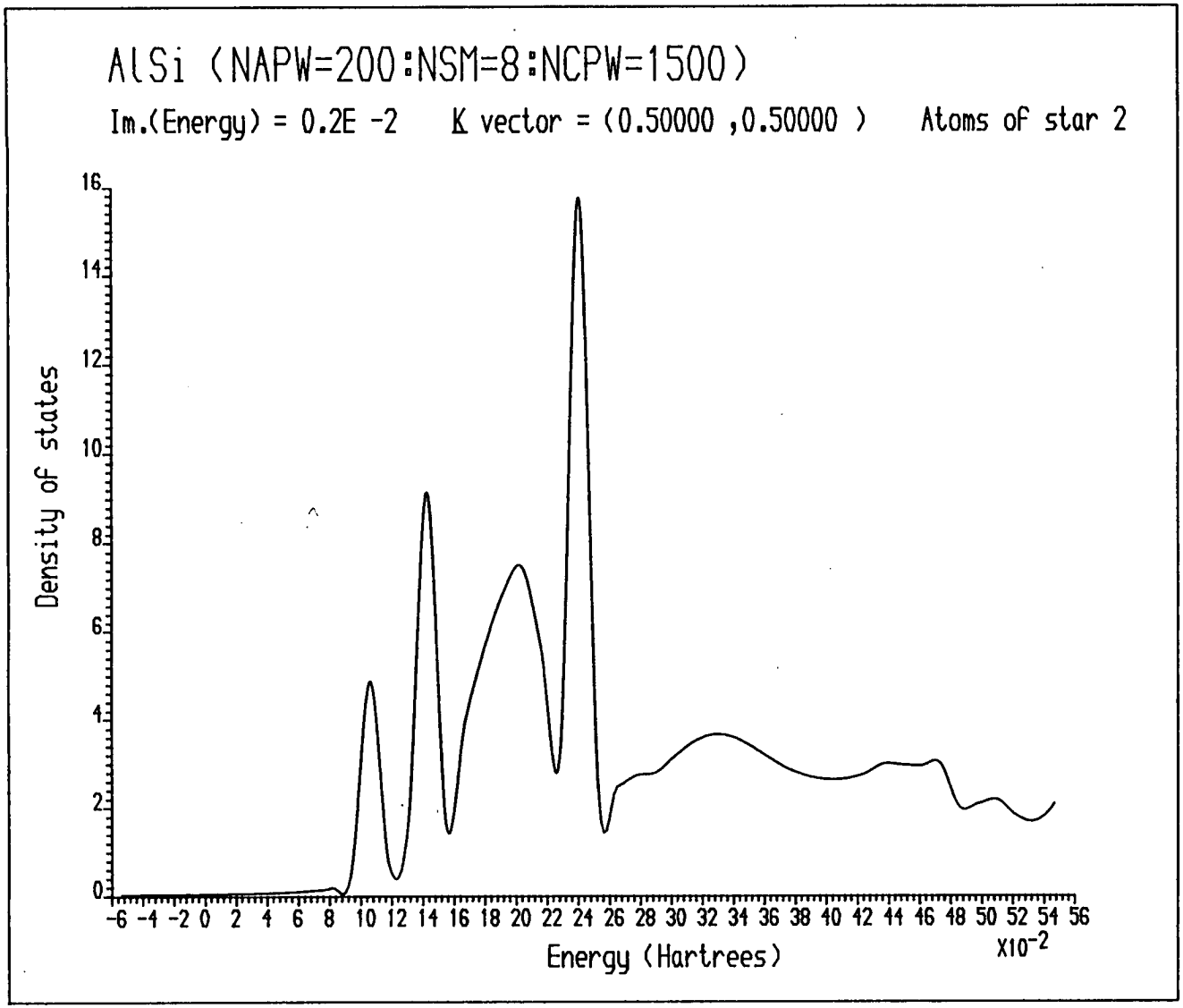

Fig.6.16: Density of states in Al muffin tin at (0,0) at $\bar{M}$

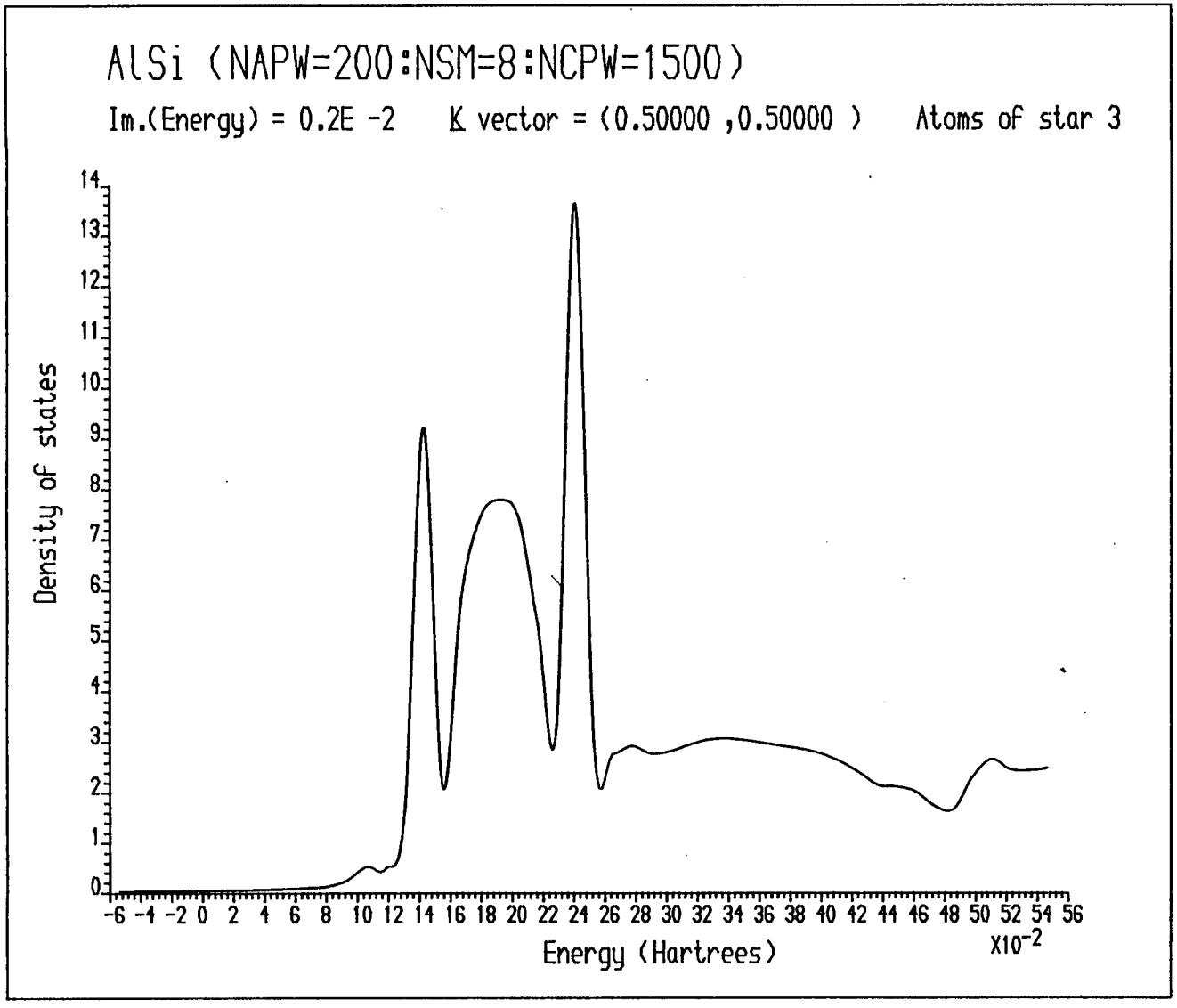

Fig.6.17: Density of states in Al muffin tin at $(\frac{1}{2},\frac{1}{2})$ at $\overline{M}$

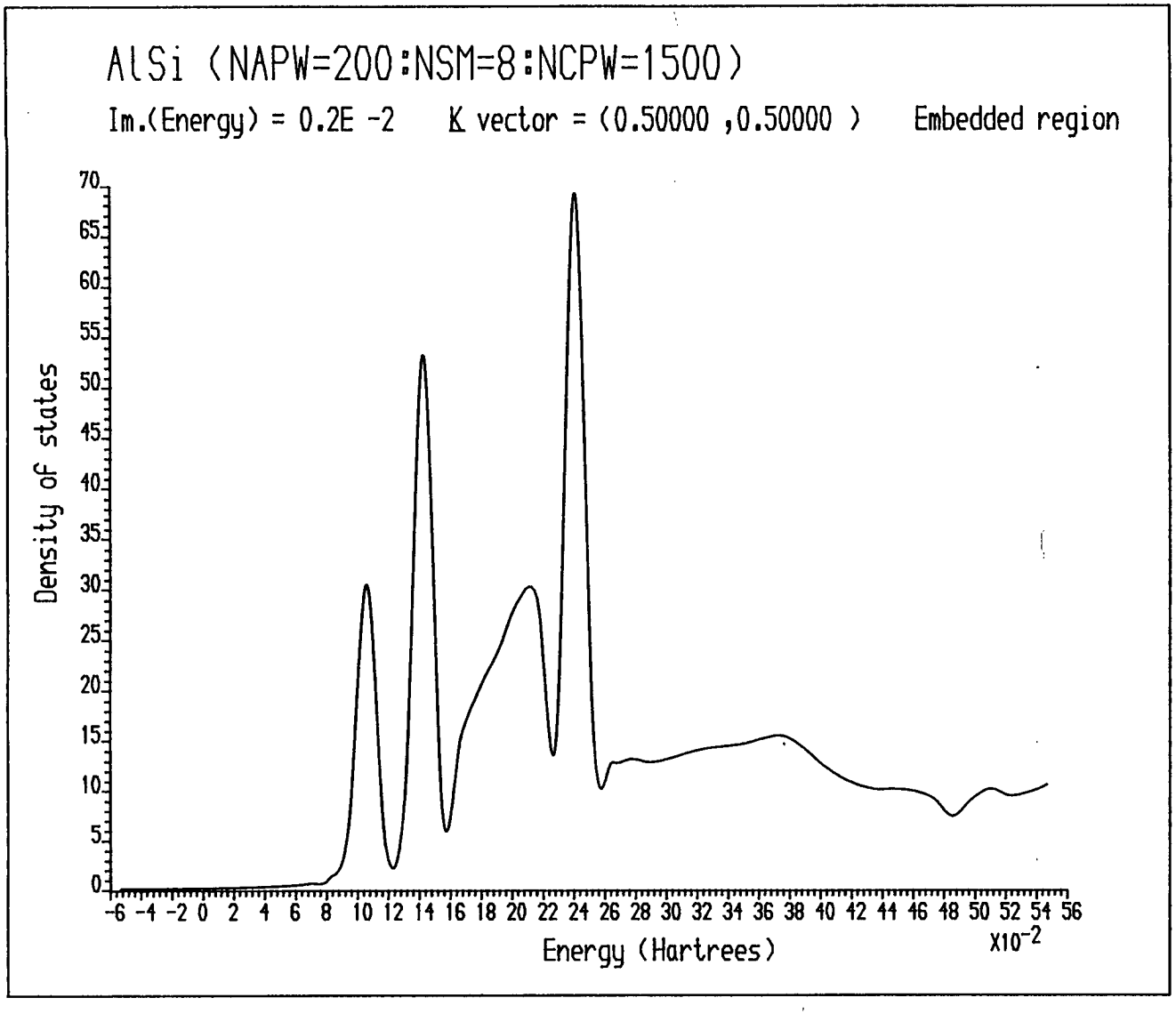

Fig.6.18: Density of states in embedded region at $\overline{M}$

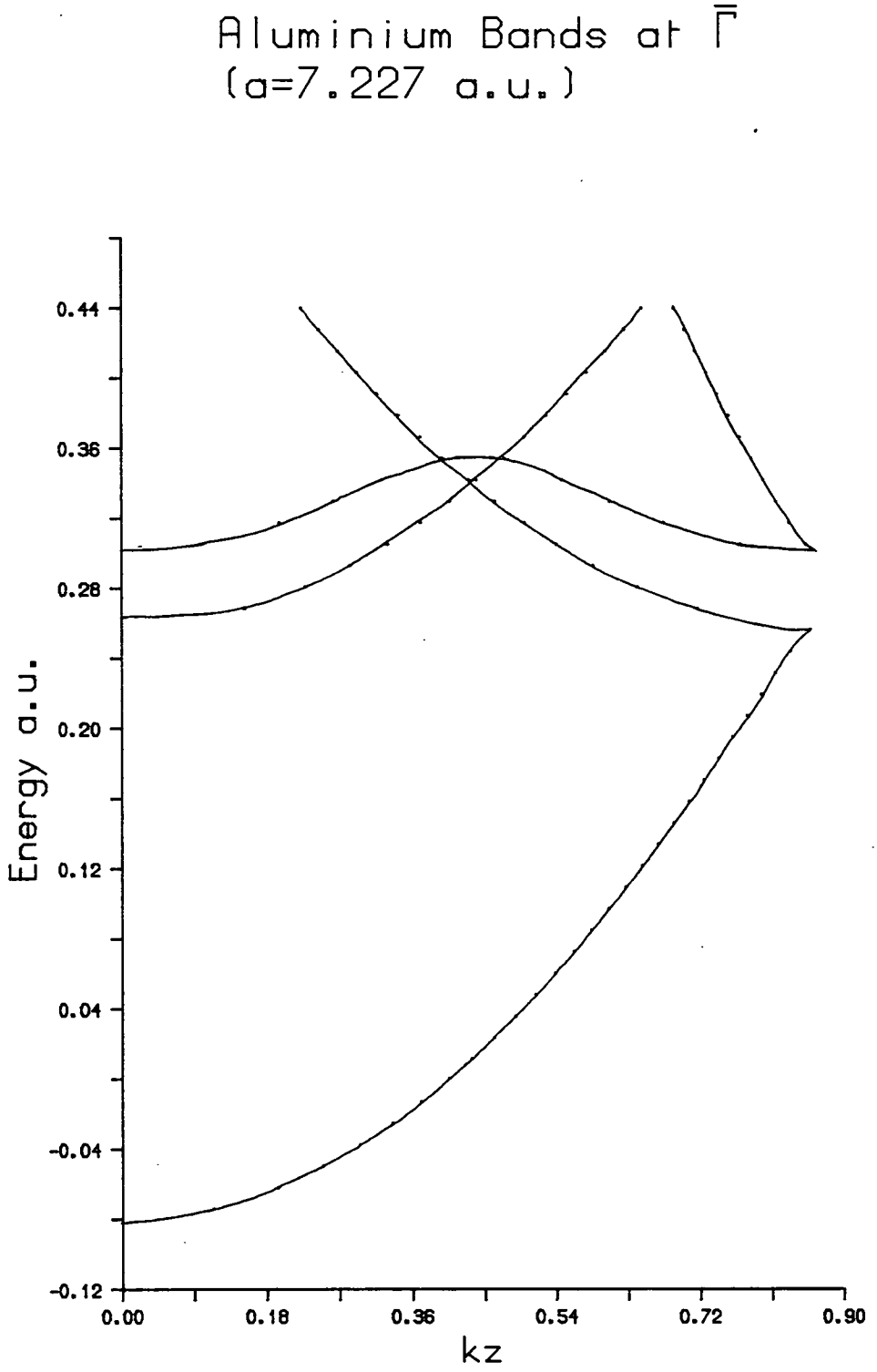

Fig.6.19: Aluminium bands at $\overline{\Gamma}$

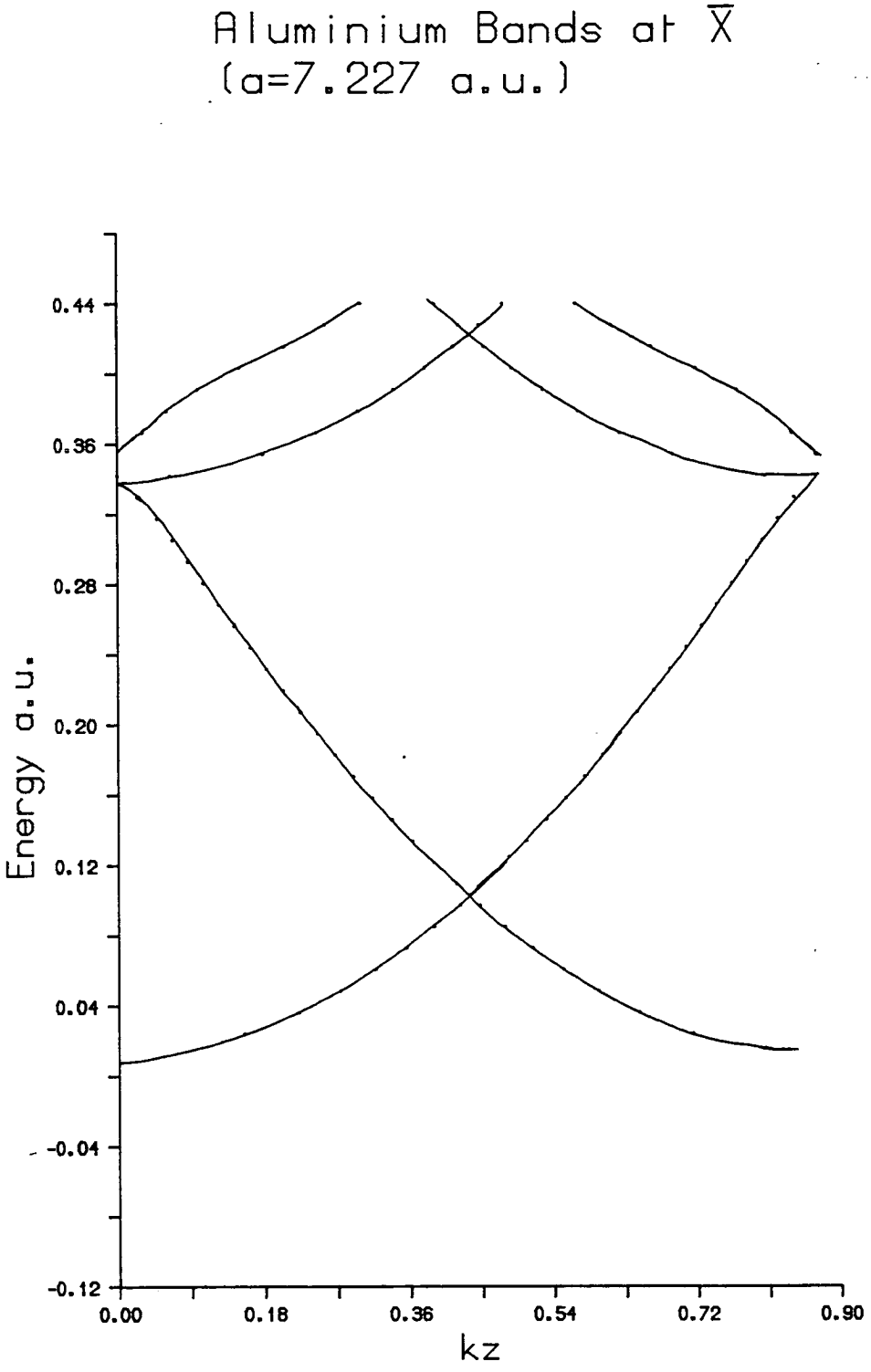

Fig.6.20: Aluminium bands at $\overline{X}$

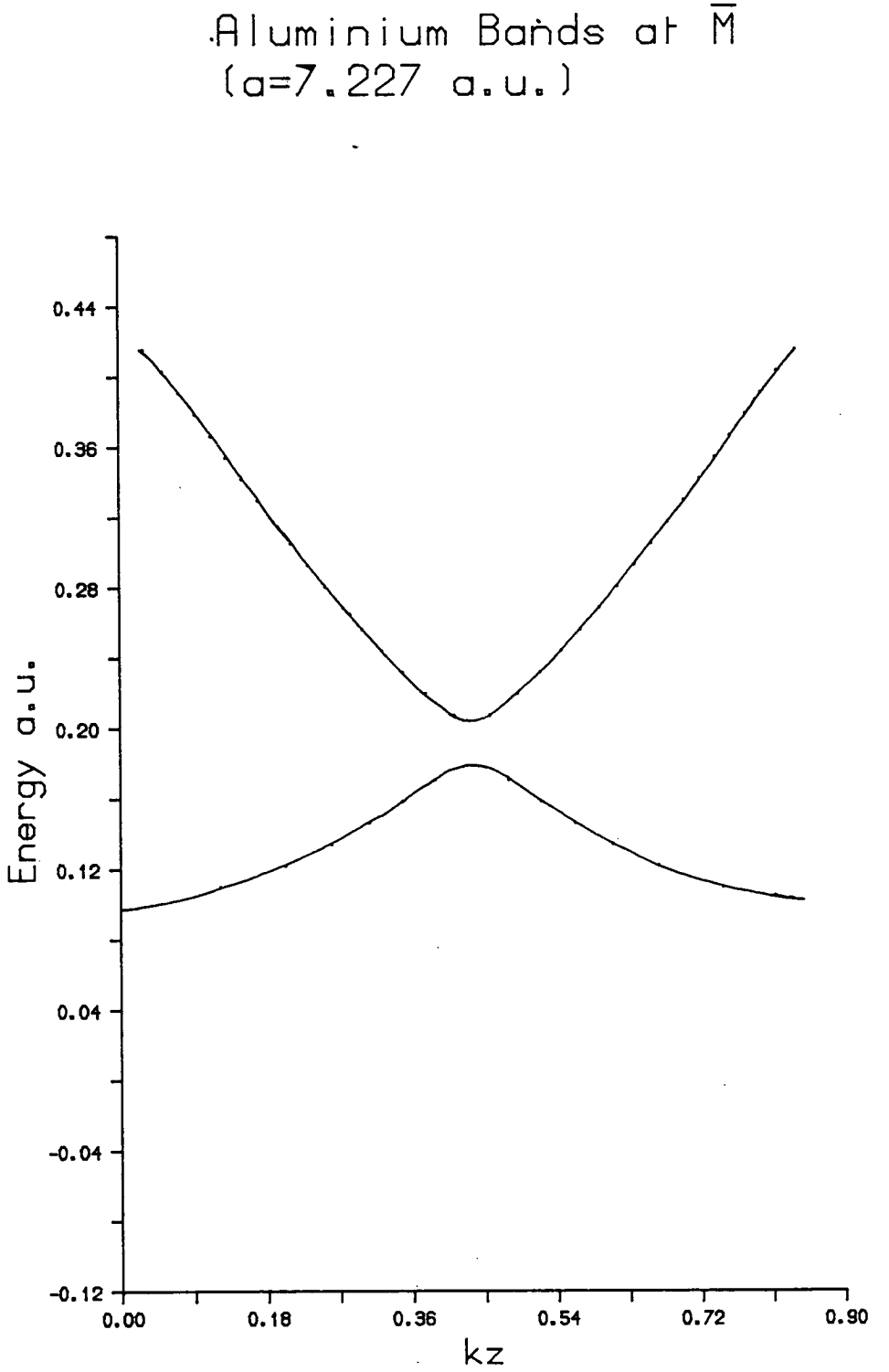

Fig.6.21: Aluminium bands at $\overline{M}$

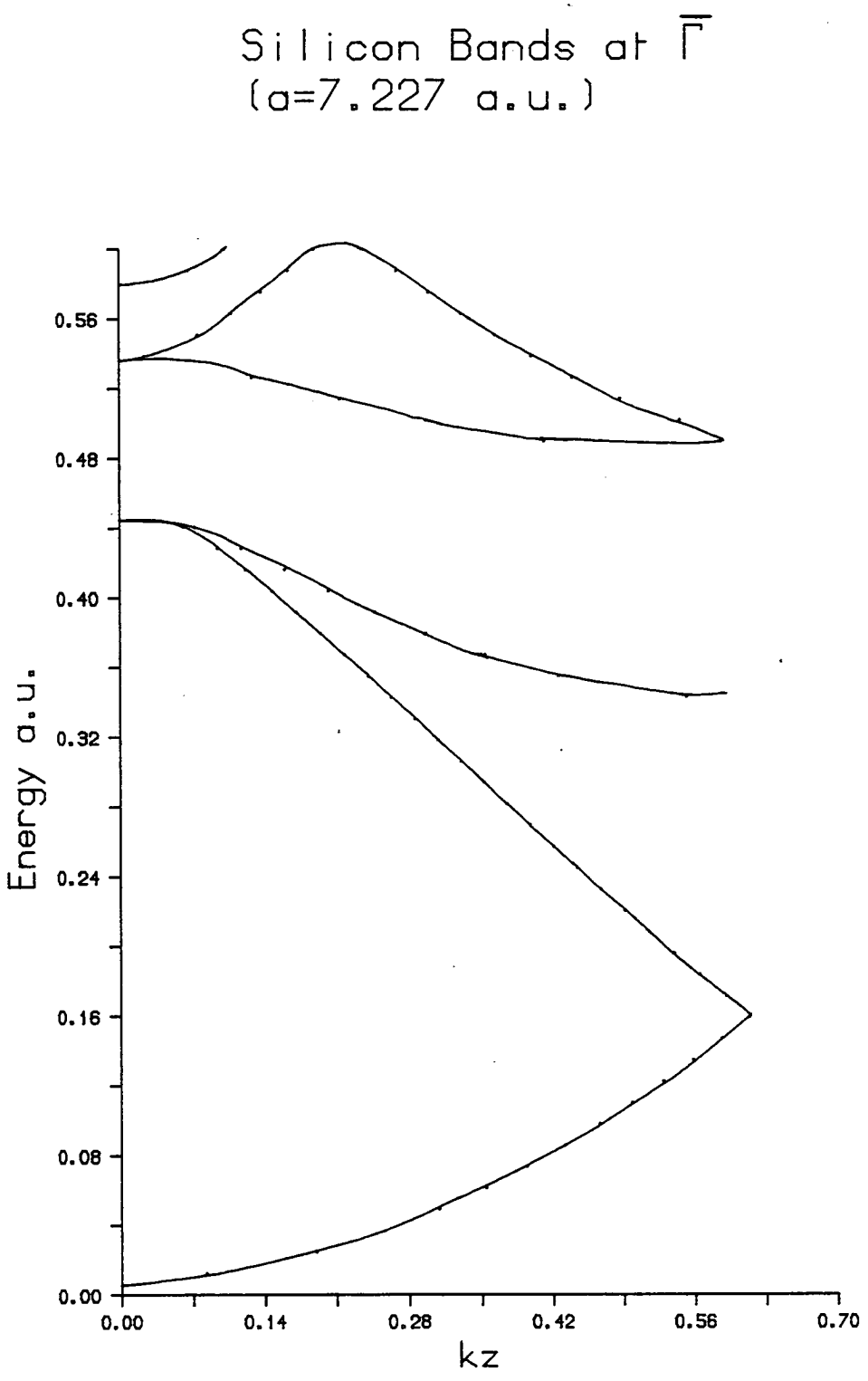

Fig.6.22: Silicon bands at $\bar{\Gamma}$

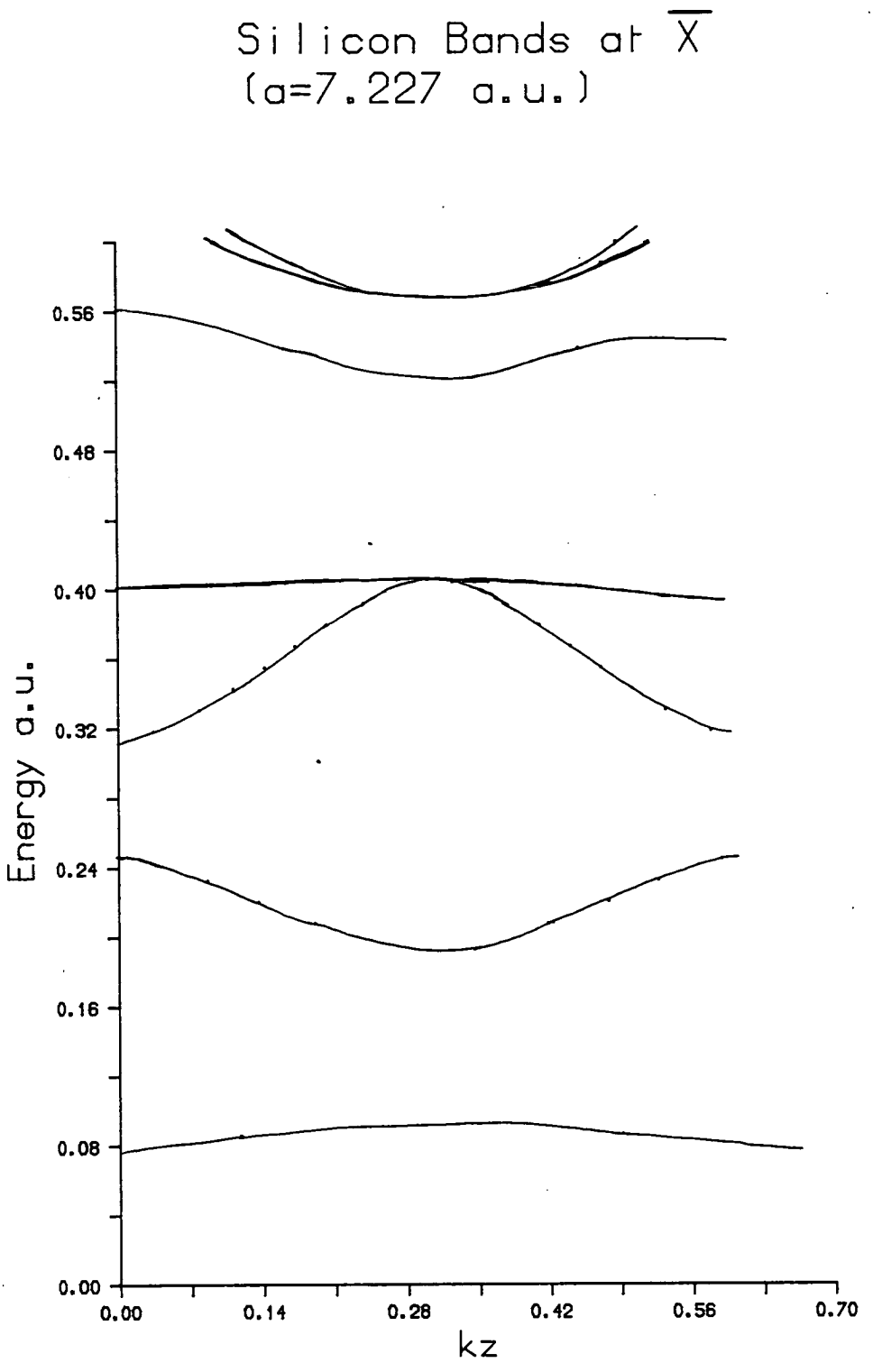

Fig.6.23: Silicon bands at $\overline{X}$

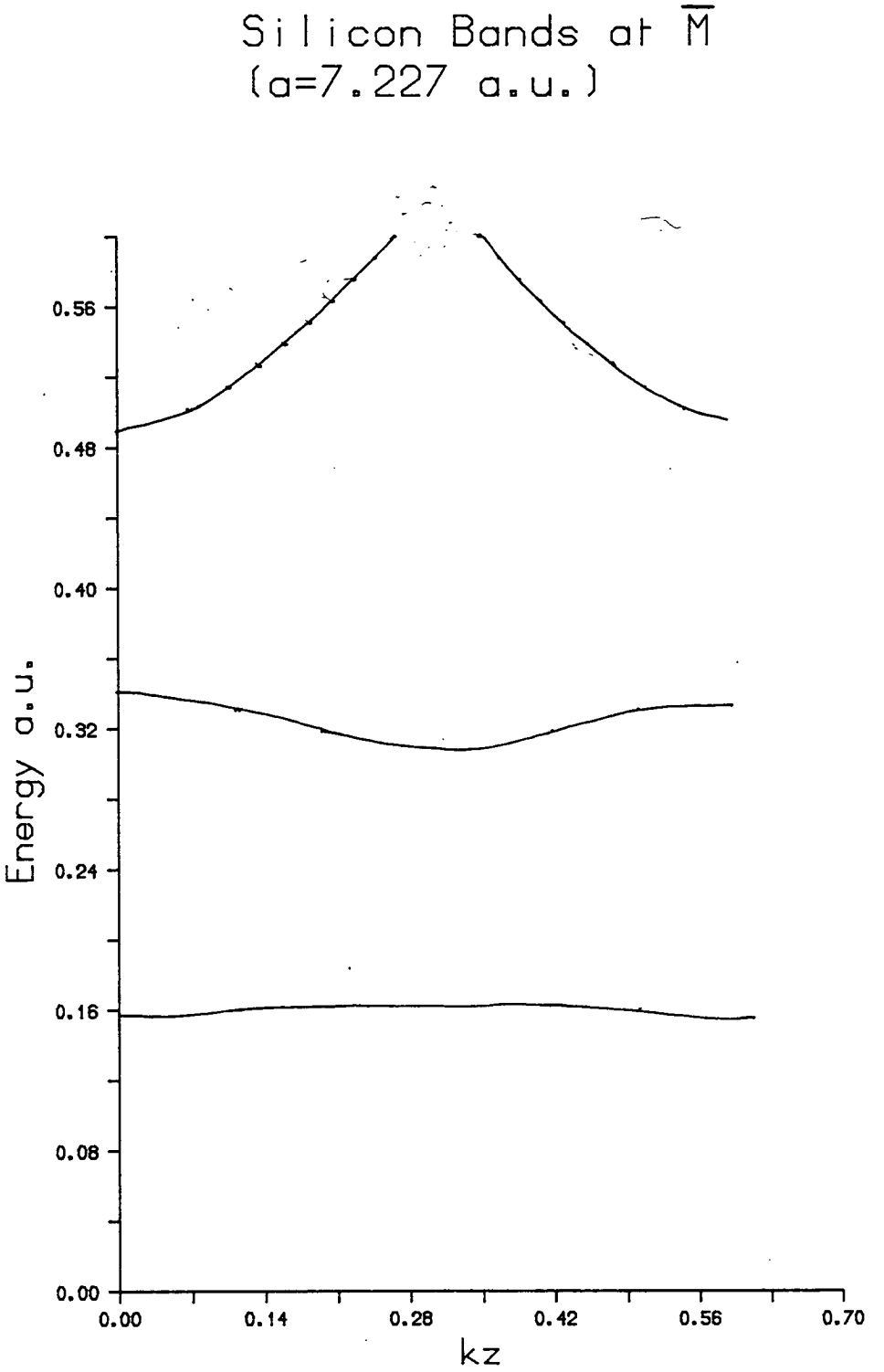

Fig.6.24: Silicon bands at $\overline{M}$

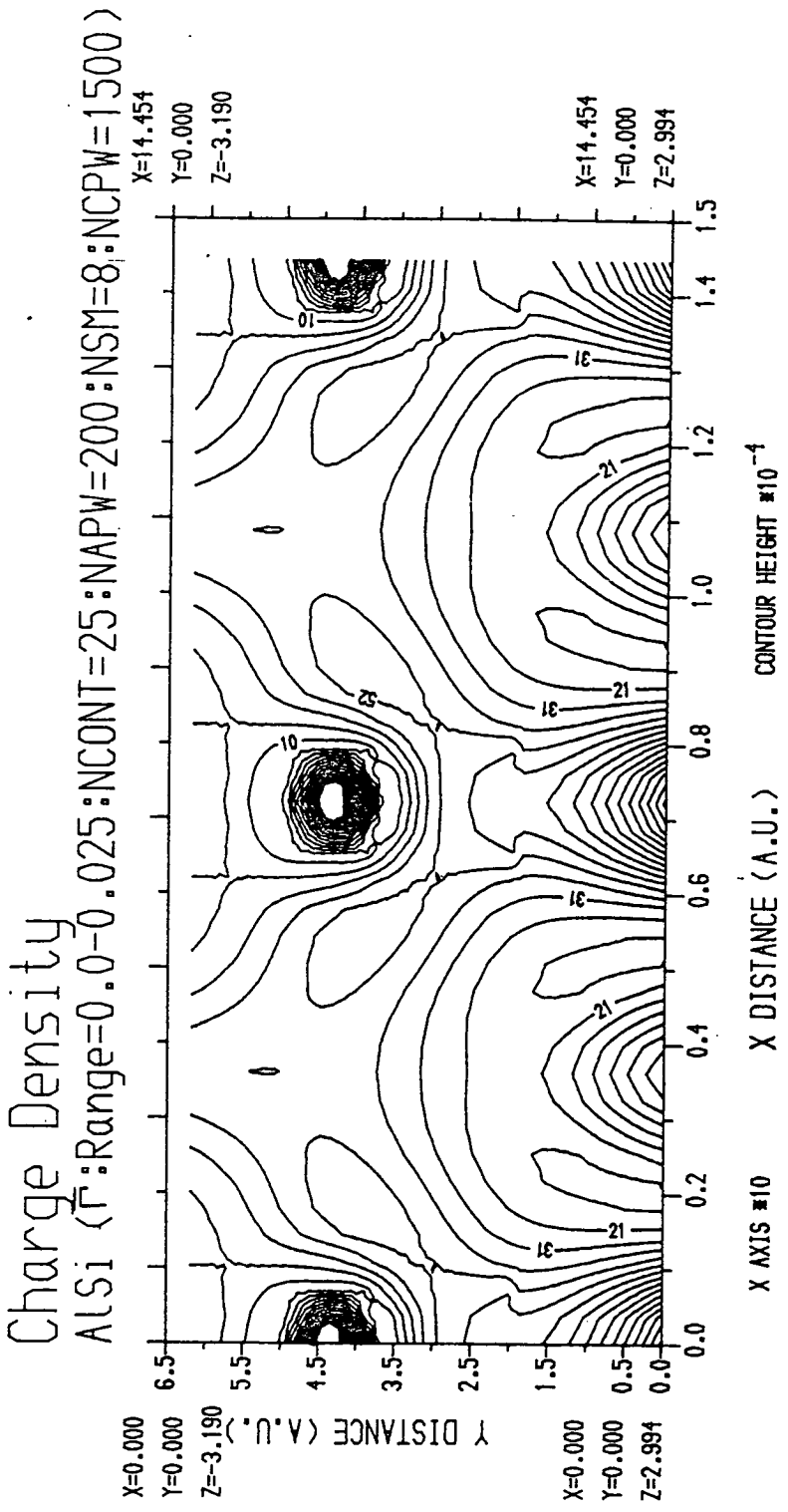

Fig.6.25: Charge density for interface state at $\bar{\Gamma}$, in plane of Al atoms

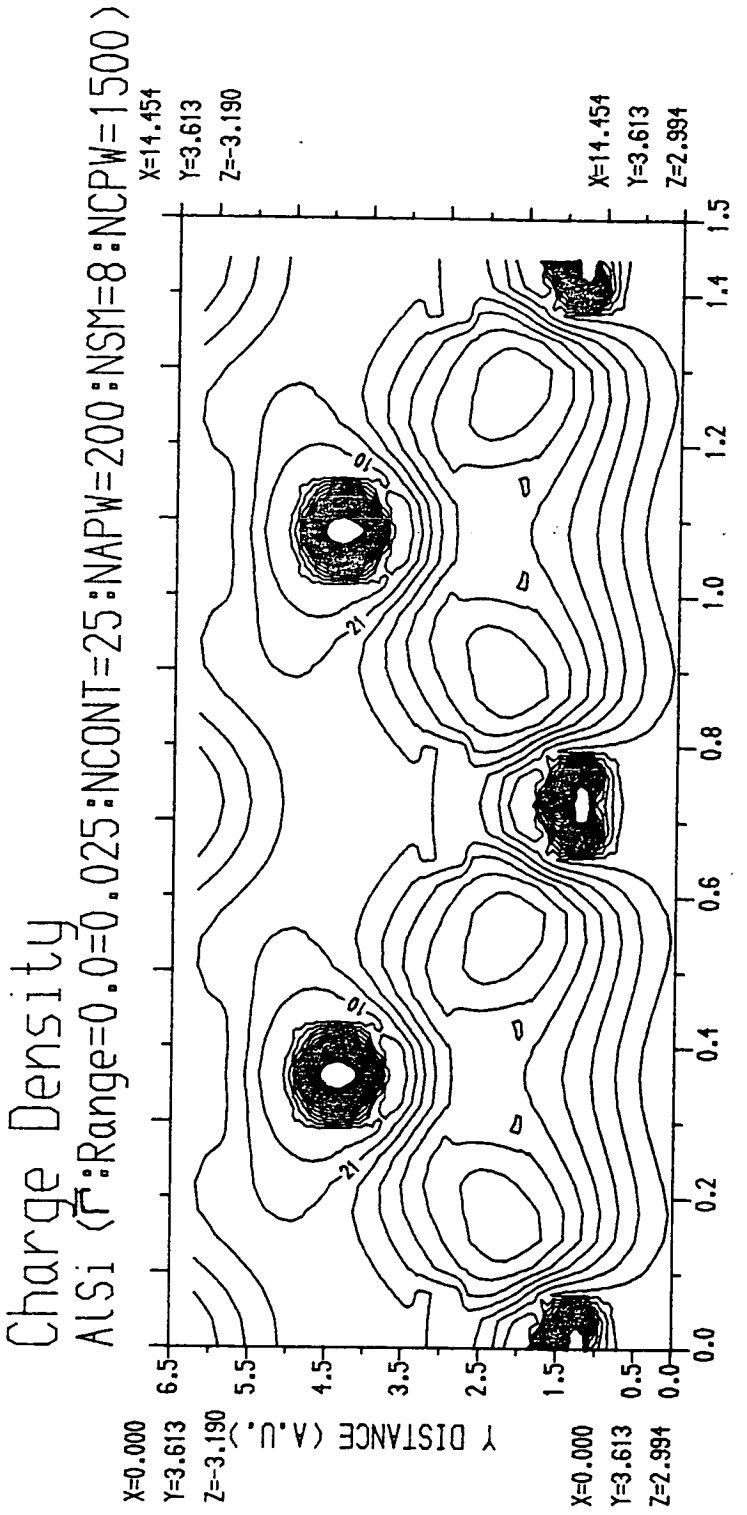

Fig.6.26: Charge density for interface state at $\bar{\Gamma}$, in plane of Si atoms

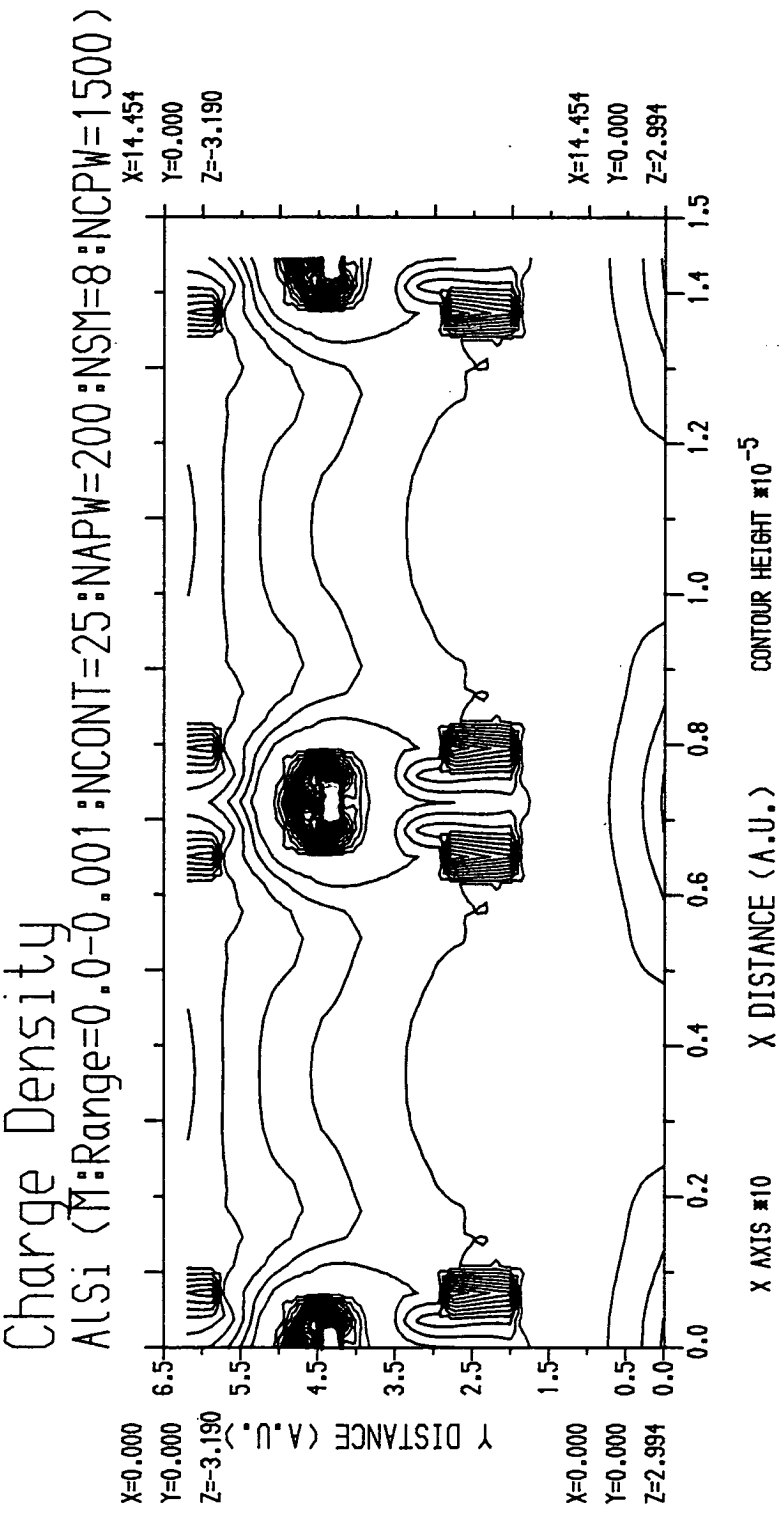

Fig.6.27: Charge density for interface state at $\bar{M}$ (Energy=0.14 Hartrees), in plane of Al atoms

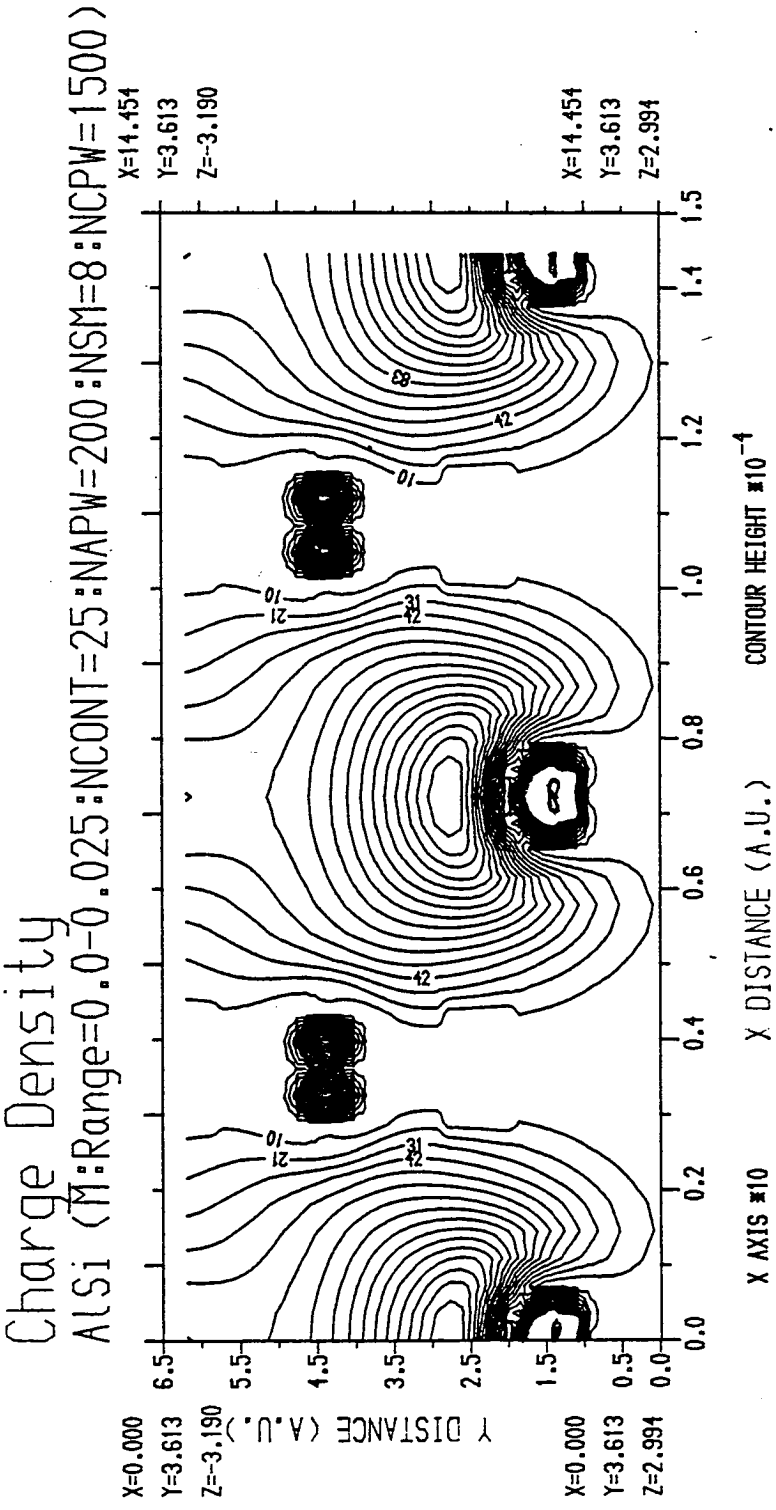

Fig.6.28: Charge density for interface state at $\overline{M}$ (Energy=0.14 Hartrees), in plane of Si atoms

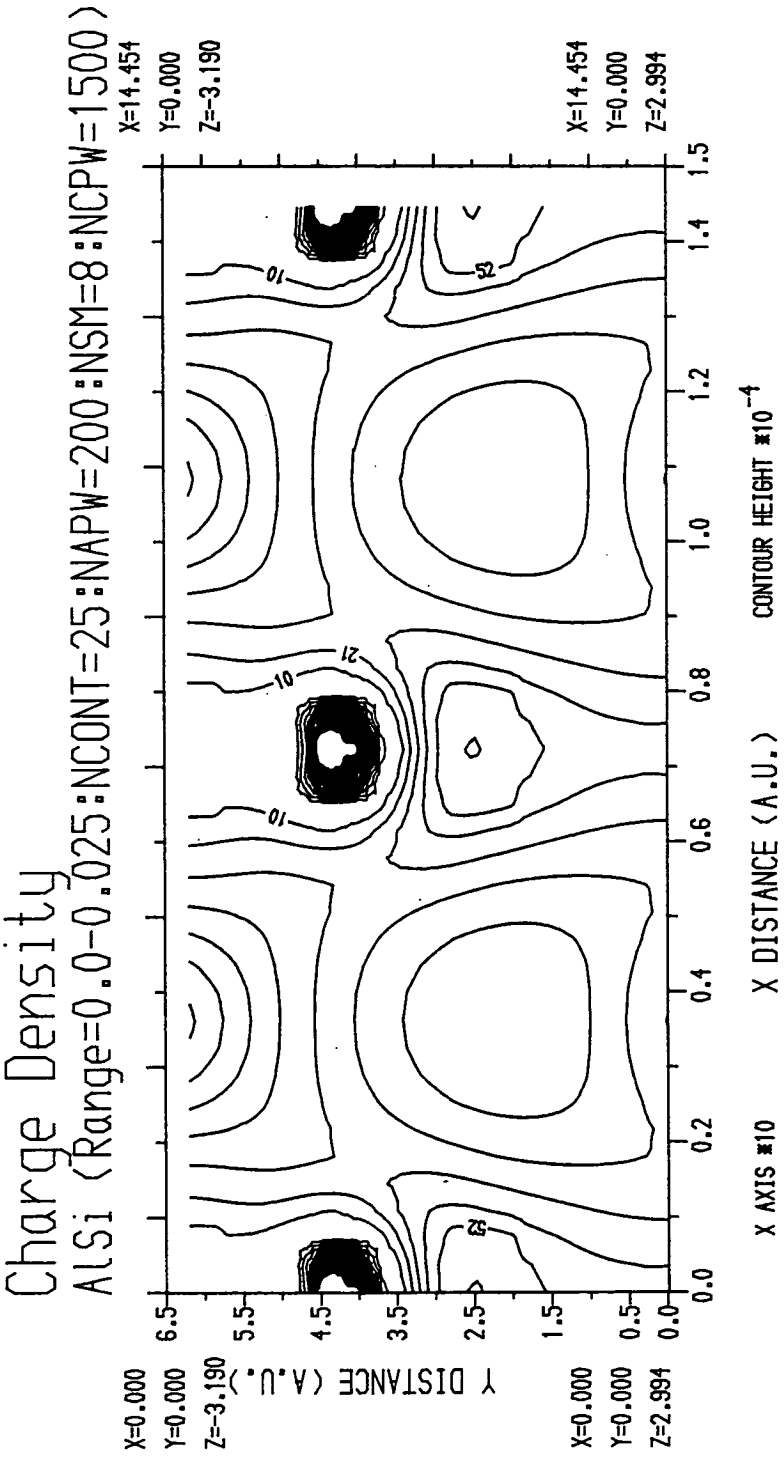

Fig.6.29: Charge density for interface state at $\bar{M}$ (Energy=0.24 Hartrees), in plane of Al atoms

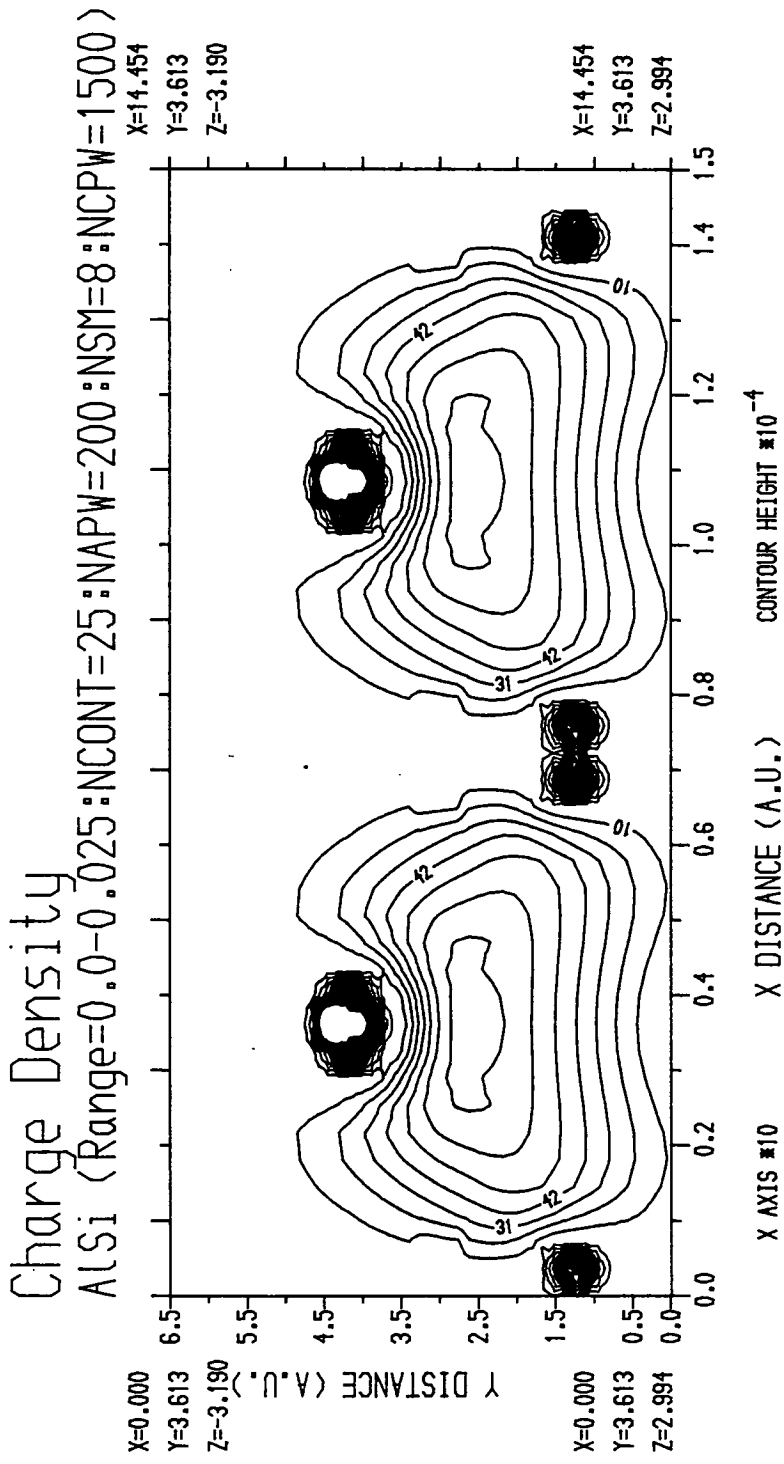

Fig.6.30: Charge density for interface state at $\overline{M}$ (Energy=0.24 Hartrees), in plane of Si atoms

Conclusion

Apart from a couple of remaining problems, the method has proved itself capable of producing useful results. There is no other technique available which correctly represents the bulk substrates in an interface calculation. The problems of discrete states in finite sized systems, and of energy level splitting due to interference have been eliminated. Thus as the results of Chapters 5 and 6 show, interface states and other interesting features can be readily identified.

As discussed in Chapter 2, the calculations are performed within the framework of density functional theory (DFT), in particular within the local density approximation (LDA). This is entirely adequate for most applications, but studies of excited states, such as unoccupied interface states, would make it desirable to move beyond the LDA, for example, by explicitly considering the self energy of the system. Much of this theory has been formulated in the recent past, so a universal picture has yet to emerge, making any such modifications somewhat specific. In some instances the correction to LDA simply involves moving the conduction and valence bands rigidly apart, but in other cases the solution is more complicated.

The major remaining problems which warrant comment are the inability to predict potential shifts across the junction, except in the case of metallic interfaces, and the instabilities which sometimes occur. At present the potential shift across the interface is essentially determined via intuition in insulator or semiconductor systems, which in an otherwise *ab initio* calculation, capable of going to self consistency, is clearly undesirable. Such shifts depend on the charge transfer across the interface, and the condition of overall charge neutrality. Since most of the charge transfer is often localised near the interface,

it is in principle possible to integrate the Green function over an energy range which gives charge neutrality in the interface region. This would require the Green function to be integrated many times, with the energy range being refined at each iteration, leading to a considerable increase in computer time. Also, varying the potential shift throughout the self consistent process would mean that one of the embedding potentials be recalculated at each iteration, somewhat defeating the purpose of using the embedding potential method. The problem of instabilities appearing with certain sizes of basis set has yet to be completely resolved. Varying the method of construction of the LAPW basis improved but did not always eliminate the problem. In retrospect, this situation is understandable, as the convergence of the embedding potential expansion will certainly depend on the material and lattice geometry studied. Thus one would expect to have to reach a compromise between basis set size and computer requirements, and as previously discussed, the solution for a given system is determined mainly via trial and error. Furthermore, the embedding potentials are calculated for the simple muffin tin potential in the substrates, but used in a full potential calculation in the interface. It would be desirable to evaluate the embedding potentials from a full potential bulk calculation, which would also allow the potential boundary conditions to be more accurately determined.

Further work on the existing embedding potential formalism remains to be done. At present the atomic positions are fixed at the outset, using an intuitive approach. This is justified in many situations, as either the lattice is known from experiment, or the interface has been grown using molecular beam epitaxy (MBE), where the underlying lattice is continuous across the junction. It would be useful to include total energy in the program, so that the lowest energy configuration of a number of options could be determined. Often one does not know the exact nature of the interface reconstruction, but does know that it is likely to be one of a finite number of possibilities. It is here that knowledge of the total energy would be useful. Also, recent experimental work by Martensson *et al* [48] has allowed interface adhesion energies to be

measured by considering the energy shifts of atomic core levels. Self consistent calculations of the total energy would be useful for comparison with this data.

It is apparent that in order to properly understand the electronic properties of interfaces, there is no substitute for both experiment and computational work of the scale presented in this thesis. There is no simple set of rules which can universally determine interface behaviour, mainly due to the detailed nature of the potential in the interface region.

References

[1] Inglesfield, J.E., J.Phys. C, **14**, 3795 (1981)

[2] Benesh, G.A., J.E. Inglesfield, J.Phys. C, **17**, 1595 (1984)

[3] Kunc, K., R.M. Martin, Phys. Rev., **B24**, 3445 (1981)

[4] Schlüter, M., J.R. Chelikowsky, S.G. Louie, M.L. Cohen, Phys. Rev., **B12**, 4200 (1975)

[5] Pendry, J.B., **Low Energy Electron Diffraction** (London, 1974)

[6] Car, R., M. Parinello, Phys. Rev. Lett., **55**, 2471 (1985)

[7] Hartree, D.R., Proc. Camb. Phil. Soc., **24**, 111 (1928)

[8] Fock, V., Z. Physik, **61**, 126 (1930)

[9] Slater, J.C., Phys. Rev., **34**, 1293 (1929)

[10] Slater, J.C., Phys. Rev., **81**, 385 (1951)

[11] Hohenberg, P., W. Kohn, Phys. Rev., **B136**, 864 (1964)

[12] Kohn, W., L.J. Sham, Phys. Rev., **A140**, 1133 (1965)

[13] Slater, J.C., **Quantum Theory of Molecules and Solids**, **1** (New York, 1963)

[14] Schwarz, K., Phys. Rev., **B5**, 2466 (1972)

[15] Hedin, L., B.I. Lundqvist, J.Phys. Chem., **4**, 2064 (1971)

[16] Pickett, W.E., Comments on Sol. Stat. Phys., **12**, No. 1 (1985) and No. 2 (1986)

[17] Sham, L.J., M. Schlüter, Phys. Rev., **B32**, 3883 (1985)

[18] Sham, L.J., M. Schlüter, Phys. Rev. Lett., **51**, 1888 (1983)

[19] Perdew, J.P., M. Levy, Phys. Rev. Lett., **51**, 1884 (1983)

[20] Pickett, W.E., C.S. Wang, Phys. Rev., **B30**, 4719 (1984)

[21] Godby, R.W., M. Schlüter, L.J. Sham, Phys. Rev. Lett., **56**, 2415 (1986)

[22] Godby, R.W., M. Schlüter, L.J. Sham, Phys. Rev., **B35**, 4170 (1987)

[23] Slater, J.C., Phys. Rev. , **51**, 846 (1937)

[24] Loucks, T.L., **Augmented Plane Wave Method**, (New York, 1967)

[25] Schlosser, H., P.M. Marcus, Phys. Rev., **131**, 2529 (1963)

[26] Andersen, O.K., Phys. Rev. ,**B12**, 3060 (1975)

[27] Koelling, D.D., G.O. Arbman, J. Phys. F, **5**, 2041 (1975)

[28] Rose, **Relativistic Electron Theory** (New York, 1961)

[29] Koelling, D.D., B.N. Harmon, J. Phys. C, **10**, 3107 (1977)

[30] Rice, J.R., **Numerical Methods, Software, and Analysis** (Singapore, 1983)

[31] Liberman, D., J.T. Waber, D.T. Cromer, Phys. Rev., **137**, A27 (1965)

[32] Baldereschi, A., Phys. Rev., **B7**, 5212 (1973)

[33] Chadi, D.J., M.L. Cohen, Phys. Rev., **B7**, 692 (1972)

[34] Chadi, D.J., M.L. Cohen, Phys. Rev., **B8**, 5747 (1973)

[35] Monkhorst, H.J., J.D. Pack, Phys. Rev., **B13**, 5188 (1974)

[36] Cunningham, S.L., Phys. Rev., **B10**, 4988 (1974)

[37] Weinert, M., J. Math. Phys., **22**, 2433 (1981)

[38] Jackson, W.D., **Classical Electrodynamics**, (New York, 1965)

[39] Hobson, E.W., **Spherical and Ellipsoidal Harmonics**, (New York, 1965)

[40] Baylis, W.E., S.J. Peel, Comp. Phys. Comm., **25**, 7 (1982)

[41] Dederichs, P.H., R. Zeller, Phys. Rev., **B28**, 5462 (1983)

[42] Moruzzi, V.L., J.F. Janak, A.R. Williams, **Calculated Electronic Properties of Metals**, (New York:Pergamon, 1978)

[43] Fargues, D., F. Vergand, C. Bonnelle, Surf. Sci., **163**, 489 (1985)

[44] Inglesfield, J.E., G.A. Benesh, Phys. Rev., **B37**, 6682 (1988)

[45] Bisi, O., L.W. Chiao, K.N. Tu, Phys. Rev., **B30**, 4664 (1984)

[46] Louie, S.G., M.L. Cohen, Phys. Rev., **B13**, 2461 (1976)

[47] Vekilov, Y.H., V.D. Verner, T.I. Egorova, Surf. Sci., **165**, L67 (1986)

[48] Martensson, N., A. Stenborg, O. Björneholm, A. Nilsson, J.N. Andersen, Phys. Rev. Lett., **60**, 1731 (1988)